THÈSE

Pour obtenir le grade de

DOCTEUR DE L'UNIVERSITÉ GRENOBLE ALPES

École doctorale : PHYS - Physique
Spécialité : Physique Théorique
Unité de recherche : PHotonique, ELectronique et Ingéniérie QuantiqueS

Excitations exotiques et transitions de phase dans des matériaux magnétiques anisotropes à deux dimensions

Exotic excitations and phase transitions in anisotropic two-dimensional magnets

Présentée par :

Anas EL MENDILI

Direction de thèse :

Mike ZHITOMIRSKY — Directeur de thèse
DIRECTEUR DE RECHERCHE, CEA CENTRE DE GRENOBLE

Rapporteurs :

FREDERIC MILA
FULL PROFESSOR, ECOLE POLYTECHNIQUE FEDERALE DE LAUSANNE
LUDOVIC JAUBERT
CHARGE DE RECHERCHE HDR, CNRS DELEGATION AQUITAINE

Thèse soutenue publiquement le **16 décembre 2025**, devant le jury composé de :

PETER HOLDSWORTH, PROFESSEUR DES UNIVERSITES, ENS DE LYON	Président
FREDERIC MILA, FULL PROFESSOR, ECOLE POLYTECHNIQUE FEDERALE DE LAUSANNE	Rapporteur
LUDOVIC JAUBERT, CHARGE DE RECHERCHE HDR, CNRS DELEGATION AQUITAINE	Rapporteur
SOPHIE DE BRION, PROFESSEURE DES UNIVERSITES, UNIVERSITE GRENOBLE ALPES	Examinatrice
ANDREW WILDES, SENIOR SCIENTIST, INSTITUT LAUE- LANGEVIN	Examinateur

Abstract

The present thesis is devoted to the theoretical description of quantum magnetic materials based on microscopic spin Hamiltonians. Two problems are addressed in this study: (i) identifying new magnetic excitations in anisotropic magnets at zero temperature, and (ii) establishing quantum-to-classical correspondence for spin Hamiltonians at finite temperature.

The first part introduces longitudinal magnons, novel quasi-particles characterized by $S^z = \pm 2S$, observed in anisotropic van der Waals antiferromagnets. These magnons appear when single-ion anisotropy (D) exceeds or equals exchange coupling (J). Their dispersion is analyzed across honeycomb, square and triangular lattices with ferro- or antiferromagnetic order for spins $S = 1,\ 3/2,\ 2$, and $5/2$, using an effective spin-$1/2$ model, multi-boson spin-wave theory, linked-cluster methods and exact two-magnon solutions. In the large J/D limit, their lifetime is limited by multi-magnon continuum interactions, notably two-magnon decay for $S = 1$. In triangular antiferromagnets at high magnetic fields, the condensation of longitudinal magnon is discussed via an exact two-particle solution, which may lead to a spin-nematic phase as suggested by recent experiments.

The second part of the study investigates the quantum-to-classical correspondence of interacting spins at finite temperatures. To this end, rescaling laws for exchange, anisotropy and Zeeman interaction terms are derived via high-temperature series expansions. Furthermore, quantum corrections to the thermodynamic quantities manifest as power series in $S(S + 1)$. Using Monte Carlo simulations with literature-based coupling constants, phase transition temperatures for ferro- and antiferromagnetic materials are calculated and validated against experimental data, unveiling complex magnetic behaviors and potential applications.

This work is dedicated to my parents, and my two brothers. A thought to my mentor.

Contents

1 Preface **1**

2 Magnetism and spin interactions **4**
2.1 A bit of history . . . 5
2.2 Electromagnetism . . . 5
2.2.1 Orbital and spin magnetic moments . . . 7
2.2.2 Multipolar expansion . . . 8
2.3 Spin Hamiltonian . . . 9
2.3.1 Exchange interaction . . . 10
2.3.2 Single-ion anisotropy . . . 13
2.4 Elementary spin excitations . . . 13
2.4.1 Semi-classical spin waves . . . 13
2.4.2 Magnons . . . 14

3 Perturbation methods **23**
3.1 Degenerate perturbation theory . . . 24
3.1.1 Effective Hamiltonian . . . 25
3.1.2 Iterative solution of the effective problem . . . 27
3.1.3 Formulae for $\hat{\mathcal{H}}_{\text{eff}}^{(i)}$ . . . 27
3.2 Series expansions . . . 29
3.2.1 $T = 0$ linked-cluster expansion . . . 29
3.2.2 High-temperature series expansion . . . 40

4 Longitudinal magnons **43**
4.1 Introduction . . . 44
4.1.1 Magnon bound-state classification . . . 44
4.1.2 Observations . . . 46
4.2 Experimental motivation . . . 46
4.2.1 van der Waals magnets $\text{FeP}\mathbf{X}_3$ . . . 47
4.2.2 $\text{Na}_2\text{BaNi}(\text{PO}_4)_2$ . . . 49
4.3 Strong-coupling expansion . . . 50
4.3.1 Presentation . . . 50
4.3.2 Effective $s = 1/2$ Hamiltonian . . . 51
4.3.3 Spin-1 magnet . . . 52
4.3.4 Spin-2 magnet . . . 55
4.3.5 Spins $S = 3/2$ and $5/2$ . . . 64

4.3.6 Conclusions . . . 65
4.4 Spin-1 square-lattice model . . . 67
4.4.1 Antiferromagnetic order . . . 67
4.4.2 Ferromagnetic order . . . 89
4.4.3 Conclusions . . . 97
4.5 Spin-1 triangular antiferromagnet at high fields . . . 98
4.5.1 Two magnon states . . . 98
4.5.2 Exact solution . . . 100
4.5.3 Effective $s = 1/2$ Hamiltonian . . . 102
4.5.4 Conclusions . . . 103
4.6 Longitudinal magnons as anti-bound states . . . 104
4.6.1 Exact solution . . . 105
4.6.2 Effective $s = 1/2$ Hamiltonian . . . 106
4.6.3 Conclusions . . . 107
4.7 Summary . . . 107

5 Quantum-to-classical correspondence at finite temperature 109
5.1 Introduction . . . 110
5.2 Quantum traces for powers of S^z . . . 111
5.3 Monte Carlo simulations of realistic spin models . . . 113
5.3.1 Thermodynamic properties . . . 113
5.3.2 Binder cumulants . . . 114
5.3.3 Phase transitions . . . 115
5.4 Conclusions . . . 121

6 Synthesis 122

Appendix A Magnetism: a cartography 123

Appendix B Matrix block diagonalization 125

1. Preface

The goal of the present work is to investigate exotic phases of matter in anisotropic magnetic materials in two dimensions. The issues explored in this dissertation stem from experimental and theoretical motivations, wherein the presence of anisotropy in conjunction with low dimensionality gives rise to unconventional phenomena. Various methods and simulations are used in this study.

The systems of interest feature magnetic interactions at the microscopic level. Interactions of this nature are described by a Hamiltonian operator, which consists of, for example, magnetic exchange, single-ion anisotropy, or external field. The electron spins, carried out by the magnetic ions of the material and defined on a lattice, are the only degrees of freedom under consideration. In the quantum-mechanical context, the spins are known to possess an integer or half-integer length, denoted by S. They are described by an angular-momentum operator $\mathbf{S}$ of magnitude $\mathbf{S}^2 = S(S+1)$. The spin interactions involved arise from a variety of effects, including electron-electron Coulomb repulsion, spin-orbital momentum interaction, or crystal field coupling. These factors may induce both individual and collective phenomena.

At zero temperature, the interacting spins commonly develop some kind of magnetic order. Standard examples include the ferromagnetic and the antiferromagnetic order, with aligned and anti-aligned spins, respectively. In this description, spins are quantum objects with discrete eigenvalues. The collective pattern in the ordered regime is characterized by an order parameter, which possesses a non-zero value and induces a correlation length in the lattice. The magnetic order may extend to a critical temperature, above which the thermal effects are significant enough to alter or destroy order. There can also be successive transitions into different magnetically-ordered phases. In addition to temperature, an external magnetic field is also prone to trigger a phase transition.

In the ordered phase, the low-energy excited states are an ensemble of elementary excitations, each with an elementary quantum number. The prototypical example is that of a transverse magnon with $|S^z| = 1$, which describes a collective precession of the spins. However, in anisotropic compounds, the interactions may energetically favor the bonding of several elementary excitations into a composite one with a larger quantum number. It is in such a context that the first signatures of $2S$-magnon bound states, for spins $S > 1$, have been observed experimentally in compounds featuring easy-axis single-ion anisotropy.

Characterizing this novel class of multipolar quasi-particles is the first problem we address in this work. We call them **longitudinal magnons**, distinctively from the ordinary transverse magnons. In order to study their energy dispersion, lifetime and interactions with other low-lying excitations, various theoretical approaches have been developed for several lattice spin models and different cases of small, moderate and large anisotropy.

Interestingly, these quasi-particles may possess infinite lifetimes in specific regions of momentum space, even close to the isotropic limit. Their condensation within a strong magnetic field may induce a spin-nematic phase, which is an exotic multipolar state, as reported in recent experiments. We present a dedicated theory, including an exact solution to the bound-state problem, in order to approach this effect. The longitudinal magnons can also exist in materials with easy-plane single-ion anisotropy, where they manifest as anti-bound states.

Upon heating an ordered magnet, the spins tend to loosen their correlation and the magnetic order is progressively suppressed. In the disordered region, the spins behave as individual *classical* vectors uniformly distributed on a sphere of radius S_c, which defines the paramagnetic phase.

The **quantum-to-classical correspondence for spin Hamiltonians** above the critical region is addressed in the second part of this work. Given a model of quantum spins, it is useful to identify the classical model that most accurately captures its thermodynamics. This is of interest for semi-classical analyses, such as classical Monte Carlo methods employed to determine the thermodynamic properties as a function of temperature. Utilizing high-temperature series expansions, we have developed rescaling relationships for the various microscopic constants in a quantum spin model. This involves quadratic and biquadratic exchange interactions, single-ion anisotropy and magnetic fields. We demonstrated that quantum corrections to the thermodynamic quantities are power series in $S(S+1)$. The findings were applied to determine the phase transition temperature in several anisotropic ferro- and antiferromagnets, using classical Monte Carlo simulations. To this end, the lattice spin models were constructed with microscopic coupling constants obtained from the literature.

In this manuscript, the systems under investigation are insulators with localized magnetic moments, and the electron charge degree of freedom is neglected. In view of the aforementioned instances, the primary objectives of the present work are outlined as follows.

Longitudinal magnons: classify the different single-ion bound states in an ordered anisotropic magnet; propose simple models to capture these magnons in the strong-coupling regime ($D \gg J$) in different lattice geometries (honeycomb, square and triangle) and spins S; describe their energy dispersion from large to small anisotropy perturbatively and non-perturbatively, in ferro- and antiferromagnets; describe their lifetime in the Born approximation for $S = 1$; obtain their exact solution in a ferromagnet and discuss their symmetry; define their energy prior to condensation in antiferromagnets at high fields; derive their dispersion as anti-bound states for easy-plane anisotropy.

Quantum-to-classical correspondence for spin Hamiltonians: obtain the form of the quantum corrections to the thermodynamic quantities at finite temperatures; derive the mapping between a quantum spin model and its classical analog and establish the relation $S_c = \sqrt{S(S+1)}$; use classical Monte Carlo simulations to obtain the critical temperature of several compounds and verify the nature of the phase transitions.

The manuscript is organized in the following manner.

Chapters 2 and **3** are introductory. The former provides a prelude to magnetism from

classical to quantum developments, and the physics leading to spin interactions in a lattice. The latter presents two analytical methods: degenerate perturbation theory and series expansions, extensively used in the subsequent chapters.
Chapter 4 presents the results on the longitudinal magnons in four sections: a strong-coupling expansion, a general solution in $S = 1$ square-lattice ferro- and antiferromagnets, an exact solution in the $S = 1$ triangular antiferromagnet in strong field, and a study of single-ion anti-bound states.
Chapter 5 presents the results on quantum-to-classical correspondence, then applied to classical Monte Carlo simulations of several anisotropic magnetic materials.
Chapter 6 synthesizes the novelty of this work.

The scientific publications associated with this thesis are:

1. F. Le Mardelé, A. El Mendili, M. E. Zhitomirsky, I. Mohelsky, D. Jana, I. Plutnarova, Z. Sofer, C. Faugeras, M. Potemski, and M. Orlita. *Transverse and longitudinal magnons in the strongly anisotropic antiferromagnet $FePSe_3$.* Phys. Rev. B **109**, 134410 (2024). DOI: https://doi.org/10.1103/PhysRevB.109.134410

2. A. El Mendili, T. Ziman, and M. E. Zhitomirsky. *Longitudinal magnons in large-S easy-axis magnets.* Phys. Rev. B **112**, 174433 (2025). DOI: https://doi.org/10.1103/gy3k-c1w3

3. A. El Mendili and M. E. Zhitomirsky. *Quantum-to-classical correspondence for spin Hamiltonians: application to classical Monte Carlo.* Manuscript edition.

4. A. El Mendili and M. E. Zhitomirsky. *Single-ion bound magnon states in strong fields.* In preparation.

2. Magnetism and spin interactions

2.1 A bit of history **5**
2.2 Electromagnetism **5**
2.2.1 Orbital and spin magnetic moments 7
2.2.2 Multipolar expansion 8
2.3 Spin Hamiltonian **9**
2.3.1 Exchange interaction 10
2.3.2 Single-ion anisotropy 13
2.4 Elementary spin excitations **13**
2.4.1 Semi-classical spin waves 13
2.4.2 Magnons 14

2.1 A bit of history

Magnetism refers to the attractive and repulsive properties exhibited by an object in the presence of an electric current or a *moment*, such as a piece of iron. It is mainly manifested through a magnetic field. The word originates from the ancient Greek term *magnetes*, referring to magnetite, a mysterious mineral stone known for attracting other minerals and first discovered in the Western Asian city of Magnesia ($\sim$ 600 BC) [1]. Since ancient times, magnetic materials, including iron-based compounds, have been extremely intriguing, particularly in medicine [2] and navigation [3].

The first scientific treatise on magnetism, written by W. Gilbert, was published in the 16th century [4]. He reported on experiments with magnetic materials, thereby establishing magnetism as a distinct physical phenomenon. Interestingly, his work connected magnetism to electricity, which developed separately for centuries. The word electricity originates from another Greek term, *electron*, also referring to a stone, amber, known to attract objects when rubbed [5]. In 1690, C. Huygens proposed the wave theory of light [6], which remained overshadowed by I. Newton's corpuscular theory until the 19th century. In 1801, T. Young conducted the famous double-slit interference experiment with light, only explicable through a wave theory [7]. In 1818, A. Fresnel corroborated the wave-like nature of light by showing its transverse property [8], then extended theoretically by D. Poisson who raised the necessary presence of white spots in diffraction experiments [9]. Concurrently, H. Ørsted demonstrated in 1820 the generation of a magnetic field from an electric current [10]. A.-M. Ampère and F. Arago in 1822 made the observation that two wires carrying antiparallel currents are repelled from each other [11]. In 1845, M. Faraday showed that an electric current is *induced* in the presence of a magnetic field [12].

The series of experiments conducted led to the establishment of a cohesive theoretical framework for electromagnetism. This development resulted in significant advancements in both the fundamental principles and the practical applications [13–23].

2.2 Electromagnetism

The classical theory of electromagnetism is based on Maxwell's equations (1865). In the presence of charge and current distributions, magnetic $\mathbf{H}$ and electric $\mathbf{E}$ fields obey [24]:

$$\begin{aligned} \nabla \cdot \mathbf{E} &= \frac{\rho}{\epsilon_0} \\ \nabla \cdot \mathbf{H} &= 0 \\ \nabla \times \mathbf{E} &= -\mu_0 \frac{\partial \mathbf{H}}{\partial t} \\ \nabla \times \mathbf{H} &= \mathbf{j} + \epsilon_0 \frac{\partial \mathbf{E}}{\partial t}\,, \end{aligned} \tag{2.1}$$

where ρ and $\mathbf{j}$ are the charge and current densities, respectively, ϵ_0 is the vacuum permittivity and μ_0 is the vacuum permeability. The first equation is Gauss's flux theorem, showing that an electric field escapes from positive to negative charges, with a net flux through a closed surface proportional to the enclosed charge. The second equation is

Gauss's law for magnetism. It reflects the solenoidal nature of the magnetic field, implying the absence of isolated magnetic charges (monopoles). The third and fourth equations are Faraday's law of induction and the Ampère-Maxwell law, respectively. In the absence of currents, these two equations describe electromagnetic waves propagating in vacuum at the speed of light $c = 1/\sqrt{\mu_0 \epsilon_0}$ [5]. Electromagnetism also constitutes the simplest form of a vector field theory in special relativity, where the quantities $c^2\mu_0^2\mathbf{H}^2 - \mathbf{E}^2$ and $\mathbf{E} \cdot \mathbf{H}$ remain invariant under the Lorentz transformation [25].

Using the Helmholtz field decomposition, the magnetic and electric fields satisfying Maxwell's equations can be expressed in terms of vector and scalar potentials $\mathbf{A}$ and Φ as[1]:

$$\mu_0 \mathbf{H} = \nabla \times \mathbf{A}\,, \qquad \mathbf{E} = -\nabla\Phi - \frac{\partial \mathbf{A}}{\partial t}\,, \tag{2.2}$$

where the choice of the potentials is determined up to a gauge. For example, for a static point charge q at distance $\mathbf{r}$, the quantity Φ is the Coulomb electrostatic potential:

$$\Phi(\mathbf{r}) = \frac{q}{4\pi\epsilon_0 r}\,, \tag{2.3}$$

responsible for the repulsion/attraction of charges of same/different signs. In a general framework, the motion of a free particle of mass m and charge q in an electromagnetic field is characterized by the classical Hamiltonian [24]:

$$\mathcal{H} = \frac{1}{2m}[\mathbf{p} - q\mathbf{A}(\mathbf{r}, t)]^2 + q\Phi(\mathbf{r}, t)\,, \tag{2.4}$$

where $\mathbf{p}$ is the momentum of the particle, and where the space and time dependencies are written explicitly for the potentials. In the quantum-mechanical picture, the position and momentum variables are operators, and the quantum Hamiltonian for the particle reads by analogy:

$$\hat{\mathcal{H}} = \frac{(\hat{\mathbf{P}} - q\mathbf{A}(\hat{\mathbf{r}}, t))^2}{2m} + q\Phi(\hat{\mathbf{r}}, t)\,. \tag{2.5}$$

The quantities denoted with a hat are operators defined over a domain in a Hilbert space. If the particle possesses a spin S, it is then described by a spin angular-momentum operator $\hat{\mathbf{S}}$, which couples to the magnetic field via an additional term in the Hamiltonian [26]:

$$\hat{\mathcal{H}}_S = -\mu_0 \frac{q}{m} \mathbf{H} \cdot \hat{\mathbf{S}} = -g\gamma \mathbf{H} \cdot \hat{\mathbf{S}}\,. \tag{2.6}$$

Here we introduced the gyromagnetic ratio $\gamma = q/(2m)$ and the Landé factor[2] g, such that

$$\hat{\mathbf{m}} = g\frac{q}{2m}\hat{\mathbf{S}} \tag{2.7}$$

is the magnetic moment. This Hamiltonian describes the tendency of the spin to align with the external field in the ground state. It is also at the root of the Zeeman effect (1896) where the energy levels of an atom are further split when it is subject to a uniform external field.

[1] The quantity $\mu_0\mathbf{H}$ is the magnetic induction, commonly denoted $\mathbf{B}$, which appears more often in the standard Maxwell equations. In a magnetic material, the induction also incorporates a local field $\mathbf{H}_0$ as $\mathbf{B} = \mu_0(\mathbf{H}_0 + \mathbf{H})$. For convenience, we will keep all explicit expressions in terms of $\mathbf{H}$.

[2] In quantum electrodynamics, the Landé factor for an electron is given as a function of the fine structure constant $\alpha = 1/137$ as $g = 2 + \alpha/\pi + O([\alpha/\pi]^2) \approx 2.0023$ [27]. For a proton, the nuclear Landé factor equals $g \approx 5.5956$ [28].

2.2.1 Orbital and spin magnetic moments

According to the Lorentz transformation of special relativity, if a magnetic field is generated by a moving charged particle, such as a proton in the reference frame of an electron, then the corresponding magnetic field reads [5]:

$$\mu_0 \mathbf{H} = \frac{1}{mc^2} \mathbf{E} \times \mathbf{p} \,. \tag{2.8}$$

$\mathbf{p}$ is assumed to be uniform, and $\mathbf{E}$ is the electrostatic field. For an electron, the proton induces an electrostatic field $\mathbf{E} = -\nabla\Phi$, where Φ is the Coulomb potential, and the magnetic field (2.8) is now proportional to the orbital angular momentum

$$\mathbf{L} = \mathbf{r} \times \mathbf{p} \,. \tag{2.9}$$

As a consequence, the Hamiltonian[3] (2.6) for an electron has the form [26]:

$$\hat{\mathcal{H}}_S = \frac{-e}{2m^2c^2r} \Phi'(\mathbf{r}) \; \mathbf{L} \cdot \mathbf{S} \,, \tag{2.10}$$

which defines the spin-orbit interaction. Its amplitude for an electrostatic potential in a given atom is $\propto \alpha^4 Z^4 (a_0/|\mathbf{r}|)^3$, where Z is the atomic number and a_0 the Bohr radius[4]. In this simple derivation, the interaction of the electron with the electrostatic field is assumed local with a point-wise charge. Other terms are however added to the Hamiltonian to account for relativistic corrections [24]. The resulting Hamiltonian induces the fine structure in atoms [26], that is the splitting of the orbital energy levels $l = 1$ (p orbital), $l = 2$ (d orbital), $l = 3$ (f orbital), etc. into levels $l \pm 1/2$. In a periodic lattice of interacting particles with spin, it is the spin-orbit interaction that links the spin space to the real (lattice) space. No wonder its energy scale, this interaction is essential in the description of collective phenomena in physical systems involving spins.

It is noteworthy that the contribution of the orbital momentum $\mathbf{L}$ to the magnetic moment $\mathbf{m}$ may contradict the alignment of this latter with an external field suggested by the Hamiltonian (2.6). This contribution arises when a charged classical particle is confined to move on an orbit. Its magnetic moment $\mathbf{m}$ is then found proportional to the orbital angular momentum $\mathbf{L}$ via the gyromagnetic ratio [29]:

$$\mathbf{m} = \gamma \mathbf{L}. \tag{2.11}$$

Whereas an external field $\mathbf{H}_e$ induces a torque on the magnetic moment as

$$\mathbf{\Gamma} = \mu_0 \mathbf{m} \times \mathbf{H}_e \,, \tag{2.12}$$

which yields the dynamical equation:

$$\frac{d\mathbf{L}}{dt} = \mathbf{\Gamma} \quad \Rightarrow \quad \frac{d\mathbf{m}}{dt} = \gamma \mu_0 \mathbf{m} \times \mathbf{H}_e. \tag{2.13}$$

[3] Here the Hamiltonian is derived in the classical picture. Note that the expression includes a 1/2 prefactor due to the Thomas precession.

[4] Its value is approximately 0.5292 Å.

Therefore, the classical magnetic moment due to orbital motion rather precesses around an external field[5]. We note that the total magnetic moment is a combination of the orbital and spin momenta as:

$$\mathbf{m}_{\text{tot}} = \mathbf{m}_L + \mathbf{m}_S = \gamma(\mathbf{L} + g\mathbf{S}). \tag{2.14}$$

Since the Landé factor g for the spin momentum is different from 1, the total magnetic moment is not parallel to the total angular momentum

$$\mathbf{J} = \mathbf{L} + \mathbf{S}. \tag{2.15}$$

2.2.2 Multipolar expansion

If the magnetic field is generated by a steady current density $\mathbf{j}$, then the vector potential is given by a contour integration [24]

$$\mathbf{A}(\mathbf{r}) = \frac{\mu_0}{4\pi} \oint_{\mathcal{C}} \frac{\mathbf{j}(\mathbf{r}')}{|\mathbf{r} - \mathbf{r}'|}\, dl' \,, \tag{2.16}$$

where $\mathcal{C}$ is tangent to the current density and contains the origin. For $|\mathbf{r}| \gg |\mathbf{r}'|$, the Legendre expansion of the denominator reads [24]:

$$\frac{1}{|\mathbf{r} - \mathbf{r}'|} = \frac{1}{r} \sum_{l=0}^{\infty} \left(\frac{r'}{r}\right)^l P_l(\cos(\hat{\mathbf{r}, \mathbf{r}'})) \,, \tag{2.17}$$

where P_l is the Legendre polynomial of order l, given in the spherical harmonics basis $\{Y_l^m\}_{l,m}$ by:

$$P_l(\cos(\hat{\mathbf{r}, \mathbf{r}'})) = \frac{4\pi}{2l+1} \sum_{m=-l}^{m=l} (-1)^{|m|} Y_l^{-m}(\theta', \varphi') Y_l^m(\theta, \varphi). \tag{2.18}$$

Here (θ, φ), resp. (θ', φ'), denote the spherical angles associated to $\mathbf{r}$, resp. $\mathbf{r}'$. Therefore, the vector potential can be written as:

$$\mathbf{A}(\mathbf{r}) = \frac{\mu_0}{4\pi} \sum_{l=0}^{\infty} \sqrt{\frac{4\pi}{2l+1}} \sum_{m=-l}^{m=l} (-1)^{|m|} \mathcal{Q}_l^{-m} \frac{1}{r^{l+1}} Y_l^m(\theta, \varphi) \tag{2.19}$$

in the form of a multipolar expansion, where $\mathcal{Q}_l^m$ is the multipolar magnetic moment of order l, given by:

$$\mathcal{Q}_l^m = \sqrt{\frac{4\pi}{2l+1}} \oint_{\mathcal{C}} r'^l Y_l^m(\theta', \varphi') \mathbf{j}(\mathbf{r}')\, dl'. \tag{2.20}$$

For the steady current, the magnetic monopole $\mathcal{Q}_0^0$ is given by trivial integration of a constant over a closed loop, which is zero, recovering the result of the Gauss's law of magnetism. Yet, effective monopoles can be realized in the quantum description of spin ice, see Ref. [30]. Otherwise, the vector potential takes the expanded form:

$$\mathbf{A}(\mathbf{r}) = \sum_{l=1}^{\infty} \mathbf{A}_l(\mathbf{r}) \tag{2.21}$$

[5] This is the Larmor precession, with frequency $\omega = -\gamma\mu_0|\mathbf{H}_e|$

where the first term is the dipolar potential, for $l = 1$. It is given explicitly by:

$$\mathbf{A}_1(\mathbf{r}) = \frac{\mu_0}{4\pi}\frac{\mathbf{m}\times\mathbf{r}}{\mathbf{r}^2}\,, \tag{2.22}$$

with $\mathbf{m}$ denoting the dipolar magnetic moment generated by the current density. Its components are a combination of the moments $\mathcal{Q}_1^m$, $m = -1,\ 0,\ 1$. By use of the gauge relation (2.2), the corresponding dipolar field reads :

$$\mathbf{H}_1 = \frac{1}{4\pi}\frac{3(\mathbf{m}\cdot\mathbf{r}) - \mathbf{m}}{r^3} + \frac{8}{3}\mathbf{m}\delta(\mathbf{r})\,. \tag{2.23}$$

where the last term accounts for the singularity at $r = 0$ in the case of a point-wise magnetic moment, with $\delta(.)$ denoting the 3D delta function. In an atom, a dipolar field couples the nuclear magnetic moment with the electron moment. This induces the hyperfine structure [26], which is responsible for the splitting of the fine structure atomic levels. Interestingly, the SI system of units defines the second (s) as a fraction of the frequency of transition between the lowest hyperfine levels in Caesium-133 (^{133}Cs) atoms[6], equal to $\nu = 9\ 192\ 631\ 770$ Hz.

On general grounds, the simplest physical dipole is a refrigerator magnet with poles S and N, and the simplest experiment to observe a dipolar field is to sprinkle iron filings on a neutral surface around the magnet, which makes the filings instantly form curved lines looping around the magnet, following field lines from the pole N to S. If a magnet is broken, the fragments become each a new dipole, impeding the existence of a classical monopole. Furthermore, a physical dipole tends to align with external magnetic fields, as is the case of a compass needle aligning with the Earth's field. In geophysics, Earth is itself approximated as a physical magnetic dipole, with Earth's dipolar field being a consequence of the motion of molten iron and nickel in its outer core.

The intrinsic magnetic moment of a quantum particle relates to its spin operator via (2.7), and the phrase *magnetic dipole* may also refer to the spin moment. Depending on the context, magnetic dipoles may allude either to the magnetic moments generated by orbital motion of charged particles, Eq. (2.11), or to the intrinsic spin. In a physical dipole such as a permanent magnet, the dipolar magnetic moment arises from the alignment of microscopic magnetic moments of either orbital or spin origin within the material. In this sense, magnetism is a pure quantum phenomenon [32].

The second non-trivial term in the multipolar expansion (2.21) arises from the quadrupolar magnetic moment $\mathcal{Q}_2^m$, $m = -2, ..., 2$, for $l = 2$. This is a second-order tensor, and the resulting quadrupolar field varies in $1/r^4$. A magnetic quadrupole can be formed by coupling two dipoles, or by the combined effect of four electric charges.

2.3 Spin Hamiltonian

Solids are characterized by a periodic arrangement of atoms in a crystal lattice. Various mechanisms lead to interaction of these different atoms via their intrinsic properties,

[6]The most recent statement dates to 2019 and reads: "The second (s) is defined by taking the fixed numerical value of the cesium frequency $\Delta\nu_{Cs}$, the unperturbed ground-state hyperfine transition frequency of the cesium-133 atom, to be 9,192,631,770 when expressed in the unit Hz, which is equal to s^{-1}" [31].

in particular their orbital or spin angular momenta. The interactions are encoded in a Hamiltonian of discrete variables, containing all degrees of freedom. If the spin is the only relevant quantity in the atomic interaction, such as in an insulator with vanishing orbital momentum $\mathbf{L}$, the Hamiltonian can be averaged over the orbital degrees of freedom. The resulting interactions are then described solely by the spin operators of the different atoms, leading to a spin Hamiltonian on a lattice.

2.3.1 Exchange interaction

The simplest form of a spin-spin interaction is the exchange [32]:

$$\mathcal{H} = \sum_{\langle i,j \rangle} J_{ij} \mathbf{S}_i \cdot \mathbf{S}_j \,, \tag{2.24}$$

with coupling J_{ij} and summation assumed over lattice bonds. The exchange coupling constants J_{ij} are given by the overlap of the atomic wavefunctions at sites i and j.

An isotropic J leads to the Heisenberg exchange interaction. In the classical picture, the ground state of a Heisenberg Hamiltonian is solely determined by the sign of J_{ij}: for a negative constant, the spins tend to align, leading to a ferromagnetic arrangement; for a negative constant, the spins are anti-aligned. Moreover, the resulting spin orientation is independent of the lattice directions. In the quantum-mechanical picture, the total spin operator $\mathbf{S}_{\text{tot}}$ commutes with the Hamiltonian, and therefore the ground state is also an eigenstate of the total spin projection S^z_{tot}. For a negative exchange, the ground state is given by maximal total spin; for a positive exchange, it is given by a vanishing total spin. A non-uniform exchange interaction or the effect of lattice geometry may lead to frustration, where the ground state is a nontrivial manifold, comprising non-equivalent spin configurations.

The spin exchange (2.24) corresponds to a dipole-dipole interaction. Other forms of multipolar interactions also exist in real materials [33, 34].

2.3.1.1 Two-spin exchange

We illustrate the isotropic exchange interaction for two spins $\mathbf{s}_1$ and $\mathbf{s}_2$, with $s = 1/2$. The Hamiltoian is determined by the bond interaction

$$\mathcal{H}_{1,2} = J \mathbf{s}_1 \cdot \mathbf{s}_2 \,. \tag{2.25}$$

Classically, this scalar product is maximized for parallel spins, with minimum and maximum energies $E_0 = -|J|s^2 = -|J|/4$ and $E_1 = |J|/4$ respectively. For negative J, the ground state is realized with aligned (ferromagnetic) spins. For positive J, it is realized with anti-aligned (antiferromagnetic) spins. Quantum-mechanically, the Hilbert space associated with each spin is spanned by the two eigenstates of the s^z_i component $|s^z = \pm 1/2\rangle$. In this basis, the spin operators are proportional to the Pauli matrices:

$$s^x = \frac{1}{2}\hat{\sigma}_1 = \frac{1}{2}\begin{pmatrix} 0 & 1 \\ 1 & 0 \end{pmatrix} \,, \quad s^y = \frac{1}{2}\hat{\sigma}_2 = \frac{1}{2}\begin{pmatrix} 0 & -i \\ i & 0 \end{pmatrix} \,, \quad s^z = \frac{1}{2}\hat{\sigma}_3 = \frac{1}{2}\begin{pmatrix} 1 & 0 \\ 0 & -1 \end{pmatrix} . \tag{2.26}$$

Accordingly, the Hamiltonian is a tensor product and possesses the matrix representation:

$$\hat{\mathcal{H}}_{1,2} = \begin{pmatrix} \frac{J}{4} & & & \\ & \frac{J}{2} & -\frac{J}{4} & \\ & -\frac{J}{4} & \frac{J}{2} & \\ & & & \frac{J}{4} \end{pmatrix}_{|s,s\rangle,|s,-s\rangle,|-s,s\rangle,|-s,-s\rangle} \tag{2.27}$$

that is diagonalized straightforwardly[7] as

$$\hat{\mathcal{H}}_{1,2} = \begin{pmatrix} 1 & & & \\ & \frac{1}{\sqrt{2}} & \frac{1}{\sqrt{2}} & \\ & \frac{1}{\sqrt{2}} & -\frac{1}{\sqrt{2}} & \\ & & & 1 \end{pmatrix} \begin{pmatrix} \frac{J}{4} & & & \\ & \frac{J}{4} & & \\ & & -\frac{3J}{4} & \\ & & & \frac{J}{4} \end{pmatrix} \begin{pmatrix} 1 & & & \\ & \frac{1}{\sqrt{2}} & \frac{1}{\sqrt{2}} & \\ & \frac{1}{\sqrt{2}} & -\frac{1}{\sqrt{2}} & \\ & & & 1 \end{pmatrix}. \tag{2.28}$$

Therefore, with

$J > 0$**:** the ground state is a singlet defined by antisymmetric superposition of antiparallel spins $(|s,-s\rangle - |-s,s\rangle)/\sqrt{2}$ with energy $E_0 = -3J/4$. This is already a departure from the classical result. The first excited level is a triplet, given by the orthogonal symmetric subspace, with excitation energy $\Delta E = J$.

$J < 0$**:** the ground-state is the symmetric triplet with the classical energy $E_0 = J/4$. The first excited state is the antisymmetric superposition of antiparallel spins, with excitation energy $\Delta E = -J$.

We will see that the classical antiferromagnetic state is not the true quantum ground state for positive J in (2.24). In contrast, the classical ferromagnetic state with fully polarized spins is identical to the quantum ferromagnetic ground state.

2.3.1.2 Order parameter

The averaged total spin defines the vector

$$\mathbf{M} = \frac{1}{N} \sum_i \langle \mathbf{S}_i \rangle \,, \tag{2.29}$$

which is proportional to the magnetic dipole moment in a solid, or magnetization[8]. In a ferromagnet, e.g. Fig. 2.1(a), a spontaneous magnetization is exhibited below a transition temperature, called the Curie temperature, T_C. Above this temperature, the total magnetization vanishes and the compound becomes paramagnetic. This is a standard example of a phase transition, and the order parameter is the magnetization vector. A strong external field also causes ferromagnetic polarization, irregardless of temperature. Examples of ferromagnetic elements are the elemental metals Gd (right at room temperature with $T_C = 292$ K), Ni ($T_C = 627$ K), Fe ($T_C = 1043$ K) and Co ($T_C = 1388$ K).

[7] By adding and subtracting the columns of the central block.

[8] Magnetization carries the unit of magnetic moment. Note that the dimensionless spin $\mathbf{S}$ here relates to the spin magnetic moment by the prefactor $\hbar$.

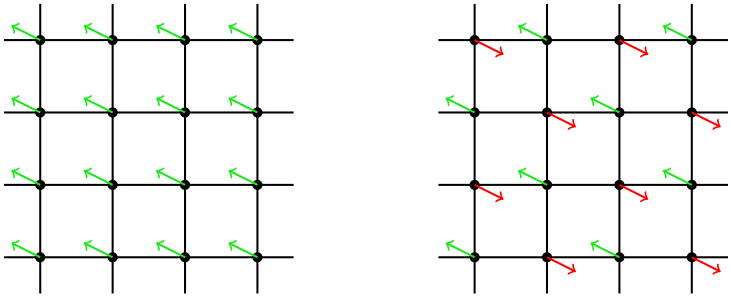

(a) Ferromagnet (b) Antiferromagnet

Figure 2.1: Two magnetically-ordered square lattices.

In an antiferromagnet, e.g. Fig. 2.1(b), the magnetization vanishes and it is useful to define the staggered magnetization vector

$$\mathbf{L} = \frac{1}{N}\sum_i (-1)^i \langle \mathbf{S}_i \rangle \,. \tag{2.30}$$

A spontaneous staggered magnetization is equally observed in an antiferromagnet below a transition temperature, called the Néel temperature, T_N. Examples of antiferromagnets in this context are Rb_2MnF_4 ($T_N = 39$ K), MnF_2 ($T_N = 68$ K) and MnTe ($T_N = 310$ K), see Chapter 5. Here, the staggered magnetization is the order parameter.

2.3.1.3 Anisotropic exchange

In a non-cubic crystal, the exchange coupling J_{ij} may depend on the space direction. In this case, the coupling coefficients form a non-trivial second-order tensor, and the exchange is said anisotropic. The case where the only non vanishing constant is J^{zz} defines the Ising interaction. On the contrary, if $J^{zz} = 0$, it is an XY interaction[9]. If $J^{xx} = J^{yy}$, this leads to an XXZ interaction, being further called *uniaxial* if $|J^{zz}| > |J^{xx}|$. Other forms of exchange anisotropy exist, such as bond-dependent exchange [35, 36], Potts exchange [37], RKKY interaction [38], etc[10]. Other forms of exchange may also be due to anisotropy, such as biquadratic exchange (where the Hamiltonian is a biquadratic form in the spin operators), arising from magneto-elastic effects [40].

In general, there are different forms of magnetic anisotropy, and the main one of interest in this work is the single-ion (or magnetocrystaline) type. In real materials, anisotropy is always present. Yet, it may be captured or omitted in the theoretical model depending on whether it is significant or not on the ground-state properties and the energy spectrum. Experimental input is essential to this regard.

We note finally that the exchange interaction may involve the total magnetic moment $\mathbf{J}$, Eq. (2.15), as in the case of rare earths. However, this is beyond the scope of our work.

[9] This is different from interacting XY spins, which are assumed to possess only two components S^x and S^y.

[10] The quadratic exchange coupling J_{ij} seen as a tensor can always be decomposed into an isotropic term, $J^{\text{iso}} = Tr\{J_{ij}\}/3$, a symmetric anisotropic term, $(J_{ij} + J_{ij}^T)/2 - J^{\text{iso}}$, referred to as the two-ion anisotropy coupling, and an antisymmetric anisotropic term, $(J_{ij} - J_{ij}^T)/2$, referring to the Dzyaloshinskii-Moriya interaction [39].

2.3.2 Single-ion anisotropy

Magnetocrystaline anisotropy is induced when the electric field from neighboring ions favors a given state of the orbital momentum of the magnetic ion. By means of the spin-orbit coupling, this effect then transits to the spin, which would favor a preferential orientation: an *easy axis* of magnetization, along which the spin aligns with a minimum energy cost, or on the opposite a *hard axis* along which the spin would align with a maximum energy cost.

A magnetic ion with an incompletely filled shell is typically surrounded by a bunch of nonmagnetic ions (creating an electric field in the case of $4f$ shells). The interplay between the LS coupling, Eq. (2.10), and the crystal field generates a perturbation to the spin-orbital levels (either to the $2L+1$ levels in a $3d$ shell or to the lowest $2J+1$ levels in a $4f$ shell). In either case of unfilled shells, the perturbation can be encoded in an effective interaction that takes the form[11]

$$\hat{\mathcal{H}}_{SI} = -D\sum_i S_i^{z2} + E\sum_i (S_i^{x2} - S_i^{y2})\,, \tag{2.31}$$

with microscopic parameters D and E, see Ref. [41]. For $D > E > 0$, the above interaction implies that the z axis is the *easy* axis, along which the spins would like to polarize (as they have the largest susceptibility), the x axis is the *hard* axis, along which the spins have the lowest susceptibility, and the y axis is the *intermediate* axis. For $|D| \gg |E|$, the single-ion anisotropy can be of several types: (i) an easy-axis anisotropy where $D > 0$, favoring a spin alignment parallel to the z axis, and (ii) an easy-plane anisotropy where $D < 0$, favoring a spin alignment perpendicular to the z direction. For non negligible E, the anisotropy is said to be bi-axial. Other complicated forms of double easy-axis anisotropies can also occur in real materials. In practice, single-ion magnets are promising compounds in both applied physics [42] and chemistry[12] [43, 44].

We will see in Chapter 4 how single-ion anisotropy occasions the appearance of exotic magnetic excitations, the longitudinal magnons.

2.4 Elementary spin excitations

2.4.1 Semi-classical spin waves

Spin interactions in magnetic media result in the propagation of spin waves, which are low-lying excitations generated by a small precession of the magnetic moments. The spin waves can be primarily obtained in a semi-classical description. For a ferromagnet, the magnetization is governed by equations analogous to the Larmor precession of a solitary magnetic moment [45, 46]:

$$\frac{\partial \mathbf{M}}{\partial t} = g\gamma \mathbf{H} \times \mathbf{M}\,, \tag{2.32}$$

where $\mathbf{H}$ here is an effective magnetic field, comprising both external and local fields. These equations are referred to as the Landau-Lifshitz equations (1935). In the absence of

[11] This form is non-trivial only for spins $S > 1/2$, by virtue of (2.26) and the property of Pauli matrices $\sigma^2 = \mathbb{I}$.

[12] The applications include existing spintronic devices and potential realization of qubits.

an external magnetic field and under the assumption of small oscillations, $\mathbf{M} = \mathbf{M}_0 + \mathbf{m}$, around a stationary direction $\mathbf{M}_0$, it can be demonstrated that the fluctuation of the magnetic moment satisfies the plane wave equation:

$$i\omega\mathbf{m} = \gamma J k^2 \mathbf{m} \times \mathbf{M}_0. \tag{2.33}$$

The resulting relation between ω and k is the spin-wave dispersion relation. In a quantum description, the lowest excited states of a magnetic compound would correspond to elementary quasi-particles, the magnons. They arise from spin exchange interactions in a lattice. Formally, a spin wave is defined as the large-k limit of a magnon [45]. The dispersion of a magnon is the object of the next subsection.

2.4.2 Magnons

We derive the magnon dispersion in two families of ordered magnets: ferromagnets and collinear antiferromagnets. In both cases, we consider anisotropic exchange interactions and include easy-axis single-ion anisotropy and an external magnetic field. The typical spin Hamiltonian of interest reads:

$$\hat{\mathcal{H}} = \sum_{\langle i,j \rangle} \sum_{\alpha,\beta} J_{ij}^{\alpha\beta} \, S_i^\alpha S_j^\beta - D \sum_i (S_i^z)^2 - H \sum_i S_i^z \,, \tag{2.34}$$

where the exchange coupling tensor $J^{\alpha\beta}$ only depends on the distance $|\delta| = |i-j|$ between the site indices i and j. Translational invariance of the lattice is implicitly satisfied here. We will consider the simple case of a diagonal tensor, with $J^{xx} = J^{yy} =: J^\perp$, and note for convenience $J^{zz} =: J^z$. The quantization is assumed along the z axis, and the coupling constants D and H are positive. We also assume $|J^\perp| \leq |J^z|$. The operators S^α, $\alpha = x, y, z$, are the Cartesian components of the spin angular momentum operator $\mathbf{S}$ of length $S \geq 1/2$. These operators satisfy the $SU(2)$ commutation rules:

$$[S_i^\alpha, S_j^\beta] = \delta_{ij} \varepsilon_{\alpha,\beta,\gamma} S_j^\gamma \,, \tag{2.35}$$

where $\delta_{l,i}$ denotes the Kronecker symbol and $\varepsilon_{\alpha,\beta,\gamma}$ is the Levi-Civita antisymmetric tensor. Below, we will make extensive use of the spin ladder operators $S^\pm = S^x \pm i S^y$, whose matrix elements in the eigenbasis of the S^z operator are [47]:

$$S^\pm \, |m\rangle = \sqrt{S(S+1) - m(m \pm 1)} \, |m \pm 1\rangle \,. \tag{2.36}$$

2.4.2.1 Ferromagnet

We consider $J^z < 0$. The fully-polarized state

$$|\mathrm{FM}\rangle = \bigotimes_i |S_i^z = S\rangle \tag{2.37}$$

is an eigenstate of both $\hat{\mathcal{H}}$ and the total spin operator S_{tot}^z. The corresponding eigenvalues are given by simple classical expressions:

$$E_0^{\mathrm{F}}/N = \left[\frac{1}{2} \sum_\delta J^z(\delta) - D \right] S^2 - HS \tag{2.38}$$

for the energy, and

$$S^z_{\text{tot}} = NS \tag{2.39}$$

for the total spin. Here N is the total number of sites, and $J(\delta)$ is a short-hand notation for J_{ij} with $\delta = i - j$. The energy is minimal with E_0^{F}, and $|\text{FM}\rangle$ is the ground state. The value of S^z remains a good quantum number for the excitations as well.

Conventional transverse magnons belong to the subsector of $S^z_{\text{tot}} = NS - 1$ and therefore each have $S^z = -1$. This is an N-dimensional subspace, which also contains the localized spin flips $|S^z_i = S - 1\rangle$. However, these latter are not eigenstates of the Hamiltonian. Instead, we can write the one-magnon wavefunction as the superposition:

$$|1\rangle = \sum_i \psi_i S_i^- \, |\text{FM}\rangle \ , \tag{2.40}$$

where the lowering S_i^- induces a single spin flip, and ψ_i are complex amplitudes. This state satisfies the Schrödinger equation:

$$\hat{\mathcal{H}} \, |1\rangle = (E_0^{\text{F}} + \varepsilon^{(1)}) \, |1\rangle \tag{2.41}$$

$$\Rightarrow \ \varepsilon^{(1)} \, |1\rangle = \sum_i \psi_i [\hat{\mathcal{H}}, S_i^-] \, |\text{FM}\rangle \ , \tag{2.42}$$

where $\varepsilon^{(1)}$ is the one-magnon energy. The rules (2.35) yield the relations:

$$\begin{aligned} [S_l^z, S_i^-] \, |\text{FM}\rangle &= -\, \delta_{l,i} S_i^- \, |\text{FM}\rangle \ , \\ [S_l^+, S_i^-] \, |\text{FM}\rangle &= 2\delta_{l,i} \ S_i^z \, |\text{FM}\rangle \ , \\ \left[(S_l^z)^2, S_i^-\right] |\text{FM}\rangle &= -\, (2S-1)\delta_{l,i} S_i^- \, |\text{FM}\rangle \, . \end{aligned} \tag{2.43}$$

For convenience, we rewrite the exchange part of the Hamiltonian as

$$\hat{\mathcal{H}}_J = \frac{1}{2} \sum_{l,\delta} \left(J^z(\delta) S_l^z S_{l+\delta}^z + J^\perp(\delta) S_l^+ S_{l+\delta}^- \right). \tag{2.44}$$

Therefore, the commutators involving the interactions in $\hat{\mathcal{H}}$ with S^- give:

$$\begin{aligned} \sum_{l,\delta} J^z(\delta) [S_l^z S_{l+\delta}^z, S_i^-] \, |\text{FM}\rangle &= -\sum_\delta J^z(\delta) \left(S_{i+\delta}^z S_i^- + S_{i-\delta}^z S_i^- \right) |\text{FM}\rangle \\ &= -\, 2S \underbrace{\sum_\delta J^z(\delta)}_{:= J_{\mathbf{0}}^z} S_i^- \, |\text{FM}\rangle \, , \end{aligned} \tag{2.45}$$

$$\begin{aligned} \sum_{l,\delta} J^\perp(\delta) [S_l^+ S_{l+\delta}^-, S_i^-] \, |\text{FM}\rangle &= \sum_\delta J^\perp(\delta) [S_i^+, S_i^-] S_{i+\delta}^- \, |\text{FM}\rangle \\ &= \sum_\delta J^\perp(\delta) (2S_i^z) S_{i+\delta}^- \, |\text{FM}\rangle \\ &= 2S \sum_\delta J^\perp(\delta) S_{i+\delta}^- \, |\text{FM}\rangle, \end{aligned} \tag{2.46}$$

$$\sum_l \left[(S_l^z)^2, S_i^-\right] |\text{FM}\rangle = -\, (2S-1) S_i^- \, |\text{FM}\rangle \, , \tag{2.47}$$

$$\sum_l \left[S_l^z, S_i^-\right] |\mathrm{FM}\rangle = -\, S_i^- \, |\mathrm{FM}\rangle \,. \tag{2.48}$$

As a consequence, Eq. (2.42) becomes:

$$\varepsilon^{(1)} \, |1\rangle = \sum_i \left(-S \sum_\delta J^z(\delta) + [2S-1]D + H \right) \psi_i S_i^- \, |\mathrm{FM}\rangle + S \sum_\delta J^\perp(\delta) \psi_i S_{i+\delta}^- \, |\mathrm{FM}\rangle. \tag{2.49}$$

This is equivalent to a linear set of equations on the wavefunction amplitudes ψ_i's:

$$\varepsilon^{(1)} \psi_i = \left(-S \sum_\delta J^z(\delta) + [2S-1]D + H \right) \psi_i + S \sum_\delta J^\perp(\delta) \psi_{i-\delta}. \tag{2.50}$$

We can invoke here the translational invariance in a Bravais lattice, to justify a Fourier transformation of the amplitudes as:

$$\psi_j = \frac{1}{N} \sum_{\mathbf{k}} e^{-i\mathbf{k}\mathbf{r}_j} \psi_{\mathbf{k}} \,, \tag{2.51}$$

to be substituted into Eq. (2.50). This yields:

$$\varepsilon^{(1)} \psi_{\mathbf{k}} = \left[-S \sum_\delta J^z(\delta) + (2S-1)D + H + S \sum_\delta J^\perp(\delta) e^{i\mathbf{k}\delta} \right] \psi_{\mathbf{k}} \,, \tag{2.52}$$

and we read out for nontrivial $\psi_{\mathbf{k}}$ the momentum-dependent one-magnon energy:

$$\varepsilon_{\mathbf{k}}^{(1)} = S(J_{\mathbf{k}}^\perp - J_{\mathbf{0}}^z) + (2S-1)D + H, \tag{2.53}$$

whose corresponding eigenstates are

$$|1_{\mathbf{k}}\rangle = \frac{1}{\sqrt{N}} \frac{1}{\sqrt{2S}} \sum_i e^{-i\mathbf{k}\mathbf{r}_i} S_i^- \, |\mathrm{FM}\rangle \,. \tag{2.54}$$

Note that we introduced the Fourier-transformed exchange couplings

$$J_{\mathbf{k}}^{z,\perp} = \sum_\delta J^{z,\perp}(\delta) e^{i\mathbf{k}\delta}. \tag{2.55}$$

As $\mathbf{k}$ belongs to a set of cardinality N, the single-flip subspace degeneracy is lifted in principle, and the one-magnon energy is minimal for $\mathbf{k}_0 = \mathrm{argmin}_{\mathbf{k}}\{J_{\mathbf{k}}^\perp\}$.

The magnon energy derived above does not assume any predefined lattice dimension or geometry, or a range for the exchange interaction. We can value it for the particular cases of a nearest-neighbor exchange as follows.

(i) **Spin chain**:

$$\varepsilon_{\mathbf{k}}^{(1)} = 2S(-J^z + J^\perp \cos k) + (2S-1)D + H \,. \tag{2.56}$$

(ii) **Square lattice**:

$$\varepsilon_{\mathbf{k}}^{(1)} = 4S(-J^z + J^\perp \gamma_{\mathbf{k}}^\square) + (2S-1)D + H \,, \tag{2.57}$$

with

$$\gamma_{\mathbf{k}}^{\square} = \frac{1}{2}(\cos k_x + \cos k_y)\,. \tag{2.58}$$

(iii) **Triangular lattice**:

$$\varepsilon_{\mathbf{k}}^{(1)} = 6S(-J^z + J^{\perp}\gamma_{\mathbf{k}}^{\triangle}) + (2S-1)D + H\,, \tag{2.59}$$

with

$$\gamma_{\mathbf{k}}^{\triangle} = \frac{1}{3}\left(\cos k_x + 2\cos\frac{k_x}{2}\cos\frac{k_y\sqrt{3}}{2}\right). \tag{2.60}$$

For all Bravais lattices (including all cases considered above), the condition $\gamma_{\mathbf{k}} = \gamma_{-\mathbf{k}}$ restores an $\lfloor (N-1)/2 \rfloor$ degeneracy of the single-flip subspace. Note that in the long-wavelength limit, *i.e.* $k \to 0$, the magnon dispersion scales $\propto \mathbf{k}^2$. This recovers the quadratic energy for spin waves seen in Eq. (2.33), which is a general result in ferromagnets [48].

We mention finally that an alternative route to obtain the one-magnon energy is to apply the harmonic spin-wave theory, which yields identically the result (2.53). This theory will be presented in the antiferromagnetic case.

2.4.2.2 Antiferromagnet

We consider now the case $J^z > 0$. In a semiclassical description, the Néel state

$$|\mathrm{AFM}\rangle = \bigotimes_i |S_i^z = (-1)^i S\rangle\,, \tag{2.61}$$

minimizes the ground-state energy with:

$$E_0^{\mathrm{AF}}/N = -\left[\frac{1}{2}\sum_{\delta} J^z(\delta) + D\right] S^2. \tag{2.62}$$

Nevertheless, it is not an eigenstate of the spin Hamiltonian. Yet, it is invariant under the $U(1)$ symmetry (of the Hamiltonian) and is also an eigenstate of the total spin operator S_{tot}^z with eigenvalue $S_{\mathrm{tot}}^z = 0$. The quantum fluctuations generated by the $U(1)$ symmetric transverse exchange terms in (2.34) reduce the ordered spin moments $\langle |S_i^z| \rangle < S$, but preserve the total spin eigenvalue $S_{\mathrm{tot}}^z = 0$ [49]. Consequently, the low-energy excitations are also described by specific values of S^z. In particular, transverse magnons have $S^z = \pm 1$.

In the general case, the lattice geometry admixed to the ratios of the exchange parameters may induce frustration [50, 51], *e.g.*, the Ising antiferromagnet on the triangular lattice, the J_1–J_2 interaction on the square lattice, the spin ice, etc. We will disregard this case and assume moderate quantum effects in the antiferromagnetic ground state. As anisotropy induces a gap in the energy spectrum, the zero-point fluctuations are significantly suppressed. Consequently, the harmonic spin-wave theory gives an accurate description of the conventional (transverse) magnons for the spin model (2.34) with $J^z > 0$. Spin-wave calculations are performed by representing spins in terms of boson operators, where magnons are created and destructed by a pair of boson operators. Accordingly,

we associate the local states $|S^z = m\rangle$, $-S \leq m \leq S$, to the boson states $|n = S - m\rangle$. Therefore, the physical space is spanned by $n = 0, .., 2S$ magnons. The matrix elements of the spin ladder operators, Eq. (2.36), can be written in terms of the boson numbers $n = S - m$ as:

$$S^+ |n\rangle = \sqrt{2S - (n-1)}\sqrt{n}\,|n-1\rangle\ , \quad S^- |n\rangle = \sqrt{n+1}\sqrt{2S-n}\,|n+1\rangle\,. \tag{2.63}$$

Whereas a pair $\{a, a^\dagger\}$ of boson operators possesses the matrix elements:

$$a\,|n\rangle = \sqrt{n}\,|n-1\rangle\ , \quad a^\dagger |n\rangle = \sqrt{n+1}\,|n+1\rangle\ , \quad a^\dagger a\,|n\rangle = n\,|n\rangle\,. \tag{2.64}$$

Therefore, we can set the following equations on operators:

$$S_i^+ = \sqrt{2S - a_i^\dagger a_i}\ a_i\,, \qquad S_i^- = a_i^\dagger \sqrt{2S - a_i^\dagger a_i}. \tag{2.65}$$

Since the same argument can apply to the diagonal S^z operator satisfying $S^z\,|n\rangle = (S - n)\,|n\rangle$, we also write:

$$S_i^z = S - a_i^\dagger a_i. \tag{2.66}$$

Eqs. (2.65) and (2.66) define the so-called Holstein-Primakoff (HP) representation of the spin operators, with the pair $\{a, a^\dagger\}$ satisfying the usual boson commutation rules:

$$[a_i, a_j] = 0\,, \quad [a_i, a_j^\dagger] = \delta_{ij}. \tag{2.67}$$

We add the remark that this representation is relevant in the low-lying spectrum with a small magnon occupation number, *i.e.* for $\langle a^\dagger a\rangle \ll 2S$. The harmonic approximation is obtained by keeping solely the linear terms in a and $a^\dagger$ appearing in the expression of $S^\pm$ above, such that the square root reduces to $\sqrt{2S}$. In a high-order spin-wave theory, the expansion of the square root yields terms in powers of $1/S$. Usually, the HP representation consists of using a single pair of boson operators. However, in the presence of an external field $H > 0$, it is technically easier to handle two pairs of operators. These two cases will be addressed separately.

2.4.2.2.1 $H = 0$

The two sublattices of the antiferromagnetic ground state, Fig. 2.1(b), are related by a π rotation around the z axis. Thus we can define a local frame (x, y, z) associated to each sublattice, and use the relative rotation matrix

$$\mathcal{R} = \begin{pmatrix} -1 & & \\ & 1 & \\ & & -1 \end{pmatrix}_{(x,y,z)}. \tag{2.68}$$

For i, j indexing spins on different sublattices and (x_0, y_0, z_0) describing coordinates in a fixed lab frame, we have:

$$\begin{aligned} J^\perp \left(S_i^{x_0} S_j^{x_0} + S_i^{y_0} S_j^{y_0}\right) + J^z S_i^{z_0} S_j^{z_0} =& J^\perp \left(-S_i^x S_j^x + S_i^y S_j^y\right) - J^z S_i^z S_j^z \\ =& -\frac{1}{2} J^\perp \left(S_i^+ S_j^+ + S_i^- S_j^-\right) - J^z S_i^z S_j^z. \end{aligned} \tag{2.69}$$

The HP transformation is then applied to spin operators in the local frame. In the harmonic approximation, we have:

$$S_i^+ = \sqrt{2S}a_i\,, \quad S_i^- = \sqrt{2S}a_i^\dagger\,, \quad S_i^z = S - a_i^\dagger a_i, \tag{2.70}$$

and the single-ion term reads:

$$(S_i^z)^2 = S^2 - (2S-1)a_i^\dagger a_i + {a_i^\dagger}^2 {a_i}^2, \tag{2.71}$$

as obtained after the normal ordering of the product $a_i^\dagger a_i a_i^\dagger a_i$. Then, we substitute the above expressions into (2.34), to obtain the boson Hamiltonian:

$$\begin{aligned}\hat{\mathcal{H}} = -\left[\frac{1}{2}\sum_\delta J^z(\delta) + D\right] S^2 + S\sum_i \Bigg[\frac{1}{2}\sum_\delta \Big(J^z(\delta)\left[a_i^\dagger a_i + a_{i+\delta}^\dagger a_{i+\delta}\right] \\ -J^\perp(\delta)\left[a_i a_{i+\delta} + a_i^\dagger a_{i+\delta}^\dagger\right]\Big) + 2D\left(1 - \frac{1}{2S}\right) a_i^\dagger a_i\Bigg] + \hat{\mathcal{H}}^{(4)}\end{aligned} \tag{2.72}$$

where $\hat{\mathcal{H}}^{(4)}$ is quartic in the boson operators (with a normal ordering) and will be neglected in the following. Note that the constant term recovers the classical energy of an antiferromagnet, Eq. (2.62). Now we invoke the translational symmetry to Fourier transform the boson operators as:

$$a_j = \frac{1}{\sqrt{N}}\sum_j e^{-i\mathbf{k}.\mathbf{r}_j} a_{\mathbf{k}}\,. \tag{2.73}$$

Accordingly, the quadratic term in (2.72) reads:

$$\hat{\mathcal{H}}^{(2)} = S\sum_{\mathbf{k}}\left[(J_{\mathbf{0}}^z + 2\bar{D})a_{\mathbf{k}}^\dagger a_{\mathbf{k}} - \frac{J_{\mathbf{k}}^\perp}{2}(a_{\mathbf{k}}a_{-\mathbf{k}} + a_{\mathbf{k}}^\dagger a_{-\mathbf{k}}^\dagger)\right] \tag{2.74}$$

where we note the renormalized single-ion coupling $\bar{D} = D[1 - 1/(2S)]$, and use the Fourier-transformed couplings (2.55). This quadratic form is not diagonal in the $\mathbf{k}$ space, and we resort to a canonical transformation of the form:

$$a_{\mathbf{k}} = u_{\mathbf{k}}\tilde{a}_{\mathbf{k}} + v_{\mathbf{k}}\tilde{a}_{-\mathbf{k}}^\dagger\,, \tag{2.75}$$

where $\{\tilde{a}, \tilde{a}^\dagger\}$ is a pair of boson operators satisfying the usual commutations rules. The constants $u_{\mathbf{k}}$ and $v_{\mathbf{k}}$ are real and satisfy subsequently:

$$u_{\mathbf{k}}^2 - v_{\mathbf{k}}^2 = 1\,, \quad u_{\mathbf{k}}v_{-\mathbf{k}} = u_{-\mathbf{k}}v_{\mathbf{k}}. \tag{2.76}$$

The relation (2.75) is the so-called canonical Bogolyubov transformation. The linear combination of $a_{\mathbf{k}}$ and $a_{-\mathbf{k}}^\dagger$ is suggested by the equations of motion on the boson operators in the Heisenberg picture: by writing $\hat{\mathcal{H}}^{(2)} = \sum_{\mathbf{k}} \hat{H}_{\mathbf{k}}$, we have $i\dot{a}_{\mathbf{k}} = [a_{\mathbf{k}}, \hat{H}_{\mathbf{k}}] = S\left([J_{\mathbf{0}}^z + 2\bar{D}]a_{\mathbf{k}} - \frac{J_{\mathbf{k}}^\perp}{2}a_{-\mathbf{k}}^\dagger\right)$, thus $a_{\mathbf{k}}$ couples to $a_{-\mathbf{k}}^\dagger$.
Upon denoting

$$A_{\mathbf{k}} = S(J_{\mathbf{0}}^z + 2\bar{D})\,, \quad B_{\mathbf{k}} = SJ_{\mathbf{k}}^\perp\,, \tag{2.77}$$

the substitution of the above transformation in (2.74) yields:

$$\hat{\mathcal{H}}^{(2)} = \frac{1}{2}\sum_{\mathbf{k}}\Bigg(\Big[\left(u_{\mathbf{k}}^2+v_{\mathbf{k}}^2\right)A_{\mathbf{k}}-2u_{\mathbf{k}}v_{\mathbf{k}}B_{\mathbf{k}}\Big]\left(\tilde{a}_{\mathbf{k}}^{\dagger}\tilde{a}_{\mathbf{k}}+\tilde{a}_{-\mathbf{k}}^{\dagger}\tilde{a}_{-\mathbf{k}}\right) + \Big[2u_{\mathbf{k}}v_{\mathbf{k}}A_{\mathbf{k}}-\left(u_{\mathbf{k}}^2+v_{\mathbf{k}}^2\right)B_{\mathbf{k}}\Big]\left(\tilde{a}_{\mathbf{k}}\tilde{a}_{-\mathbf{k}}+\tilde{a}_{\mathbf{k}}^{\dagger}\tilde{a}_{-\mathbf{k}}^{\dagger}\right)+2v_{\mathbf{k}}^2A_{\mathbf{k}}-2u_{\mathbf{k}}v_{\mathbf{k}}B_{\mathbf{k}}\Bigg) \quad (2.78)$$

Cancellation of the off-diagonal term gives an extra condition on $u_{\mathbf{k}}$ and $v_{\mathbf{k}}$:

$$2u_{\mathbf{k}}v_{\mathbf{k}}A_{\mathbf{k}}-\left(u_{\mathbf{k}}^2+v_{\mathbf{k}}^2\right)B_{\mathbf{k}}=0. \quad (2.79)$$

This equation along with (2.76) yield

$$u_{\mathbf{k}}^2+v_{\mathbf{k}}^2=\frac{A_{\mathbf{k}}}{\sqrt{A_{\mathbf{k}}^2-B_{\mathbf{k}}^2}}\,,\quad u_{\mathbf{k}}v_{\mathbf{k}}=\frac{B_{\mathbf{k}}}{2\sqrt{A_{\mathbf{k}}^2-B_{\mathbf{k}}^2}}\,, \quad (2.80)$$

and $\hat{\mathcal{H}}^{(2)}$ reads:

$$\hat{\mathcal{H}}^{(2)}=\sum_{\mathbf{k}}\left[\sqrt{A_{\mathbf{k}}^2-B_{\mathbf{k}}^2}\left(\tilde{a}_{\mathbf{k}}^{+}\tilde{a}_{\mathbf{k}}+\frac{1}{2}\right)-\frac{A_{\mathbf{k}}}{2}\right]. \quad (2.81)$$

This diagonal form encodes the one-magnon energies:

$$\varepsilon_{\mathbf{k}}^{(1)}=\sqrt{A_{\mathbf{k}}^2-B_{\mathbf{k}}^2}=S\sqrt{[J_{\mathbf{0}}^z+2\bar{D}]^2-(J_{\mathbf{k}}^{\perp})^2}. \quad (2.82)$$

Its momentum dependence lifts the degeneracy of the subspace $|S^z|=1$ only partially, since it does not discriminate the branches $S^z=1$ and $S^z=-1$. Additional degeneracies remain due to the lattice structure, for momenta satisfying $|J_{\mathbf{k}}^{\perp}|=|J_{\mathbf{p}}^{\perp}|$.
The diagonal form above also adds a quantum correction $O(S)$ to the classical energy, due to the zero-point oscillations of the one magnon:

$$\Delta E_0=\frac{1}{2}\sum_{\mathbf{k}}\left[\varepsilon_{\mathbf{k}}^{(1)}-A_{\mathbf{k}}\right]=\frac{S}{2}\sum_{\mathbf{k}}\left[\sqrt{[J_{\mathbf{0}}^z+2\bar{D}]^2-(J_{\mathbf{k}}^{\perp})^2}-(J_{\mathbf{0}}^z+2\bar{D})\right]. \quad (2.83)$$

In the particular cases of a nearest-neighbor exchange, we have the following magnon dispersion relationships.
(i) **Spin chain**:

$$\varepsilon_{\mathbf{k}}^{(1)}=2S\sqrt{[J^z+\bar{D}]^2-(J^{\perp}\cos k)^2}\,. \quad (2.84)$$

(ii) **Square lattice**:

$$\varepsilon_{\mathbf{k}}^{(1)}=4S\sqrt{[J^z+\bar{D}/2]^2-(J^{\perp}\gamma_{\mathbf{k}}^{\square})^2}\,. \quad (2.85)$$

(iii) **Triangular lattice**:

$$\varepsilon_{\mathbf{k}}^{(1)}=6S\sqrt{[J^z+\bar{D}/3]^2-(J^{\perp}\gamma_{\mathbf{k}}^{\triangle})^2}\,. \quad (2.86)$$

In the long-wavelength limit, the magnon dispersion is linear in $|\mathbf{k}|$ in the isotropic case ($J^z=J^{\perp}$ and $D=0$), and quadratic in the presence of anisotropy.

2.4.2.2.2 $H > 0$

In the presence of a field, the use of the HP representation (2.70) gives for the Zeeman energy term in the Hamiltonian:

$$-H \sum_i S_i^z = H \sum_i (-1)^i \, a_i^\dagger a_i \tag{2.87}$$

and its expression after Fourier transforming the operators is:

$$\sum_j (-1)^j \, a_j^\dagger a_j = \sum_{\mathbf{k}} a_{\mathbf{k}}^\dagger a_{\mathbf{k}+\mathbf{Q}} \tag{2.88}$$

with $\mathbf{Q} = (\pi, \pi, ..)$. The quadratic part of the Hamiltonian now has the form:

$$\hat{\mathcal{H}}^{(2)} = \sum_{\mathbf{k}} \left[A_k a_k^\dagger a_k - \frac{B_k}{2} \left(a_k^\dagger a_{-k}^\dagger + a_k a_{-k} \right) + H a_k^\dagger a_{k+Q} \right], \tag{2.89}$$

with the same factors $A_{\mathbf{k}}$ and $B_{\mathbf{k}}$ defined in (2.77), and the equations of motion on the boson operators in the Heisenberg picture would show a coupling of $a_{\mathbf{k}}$ to $a_{-\mathbf{k}}^\dagger$ and $a_{\mathbf{k}+\mathbf{Q}}$. Subsequently, a canonical transformation to diagonalize $\hat{\mathcal{H}}^{(2)}$ would involve three operators with at least three different coefficients. To circumvent this eventuality, we rather proceed with a spin representation in terms of two pairs of boson operators, associated to the two anti-aligned sublattices (positive a) and (negative b), respectively:

$$S_{a,i}^+ = \sqrt{2S} a_i \,, \quad S_{a,i}^- = \sqrt{2S} a_i^\dagger \,, \quad S_{a,i}^z = S - a_i^\dagger a_i, \tag{2.90}$$

and

$$S_{b,i}^+ = \sqrt{2S} b_i^\dagger \,, \quad S_{b,i}^- = \sqrt{2S} b_i \,, \quad S_{b,i}^z = -S + b_i^\dagger b_i. \tag{2.91}$$

In this representation, the spin operators are expressed in the global frame, since each sublattice defines a local structure with magnons in a corresponding to $S^z = -1$ and in b to $S^z = 1$. The following step is to substitute the above representation in the Hamiltonian and only keep terms up to quadratic order. Next, the Fourier transform applies to both pairs of operators $\{a, a^\dagger\}$ and $\{b, b^\dagger\}$ in a definition identical to (2.73), with $N/2$ equaling the sublattice size and appearing in the denominator. After straightforward intermediate calculation, the quadratic Hamiltonian in momentum space now reads:

$$\hat{\mathcal{H}}^{(2)} = \sum_{\mathbf{k}} \left[A_{\mathbf{k}} \left(a_{\mathbf{k}}^\dagger a_{\mathbf{k}} + b_{\mathbf{k}}^\dagger b_{\mathbf{k}} \right) + B_{\mathbf{k}} \left(a_{\mathbf{k}} b_{-\mathbf{k}} + a_{\mathbf{k}}^\dagger b_{-\mathbf{k}}^\dagger \right) + H \left(a_{\mathbf{k}}^\dagger a_{\mathbf{k}} - b_{\mathbf{k}}^\dagger b_{\mathbf{k}} \right) \right]. \tag{2.92}$$

Note that the sum runs over half the Brillouin zone. Since this form contains off-diagonal terms, which encode the coupling of $a_{\mathbf{k}}$ with $\hat{b}_{-\mathbf{k}}^\dagger$, it suggests the canonical transformation:

$$\begin{aligned} a_{\mathbf{k}} &= u_{\mathbf{k}} \tilde{a}_{\mathbf{k}} + v_{\mathbf{k}} \tilde{b}_{-\mathbf{k}}^\dagger \\ b_{\mathbf{k}} &= u_{\mathbf{k}} \tilde{b}_{\mathbf{k}} + v_{\mathbf{k}} \tilde{a}_{-\mathbf{k}}^\dagger \end{aligned} \tag{2.93}$$

to diagonalize it. The Bogolyubov boson operators $\{\tilde{a}, \tilde{a}^\dagger\}$ and $\{\tilde{b}, \tilde{b}^\dagger\}$ satisfy the usual commutation rules, which yield conditions similar to (2.76). The substitution with the new

boson operators and the cancellation of anomalous terms lead to the diagonal quadratic Hamiltonian:

$$\hat{\mathcal{H}}^{(2)} = \sum_{\mathbf{k}} \left[\left(\sqrt{A_k^2 - B_k^2} + H \right) \left(\tilde{a}_k^\dagger \tilde{a}_k + \frac{1}{2} \right) + \left(\sqrt{A_k^2 - B_k^2} - H \right) \left(\tilde{b}_k^\dagger \tilde{b}_k + \frac{1}{2} \right) - A_k \right]. \tag{2.94}$$

This diagonal form shows two magnon branches:

$$\varepsilon_{\mathbf{k}}^{\pm} = \sqrt{A_{\mathbf{k}}^2 - B_{\mathbf{k}}^2} \pm H = S\sqrt{[J_{\mathbf{0}}^z + 2\bar{D}]^2 - (J_{\mathbf{k}}^\perp)^2} \pm H. \tag{2.95}$$

Their splitting $\pm H$ manifests the Zeeman effect with the slope indicating two excitations of quantum numbers $S^z = -1$, described by bosons $\tilde{a}$, and $S^z = 1$, described by $\tilde{b}$. The quantum correction to the ground-state energy is not altered by the magnetic field, whereas the lower branch $\varepsilon_{\mathbf{k}}^-$ condenses at a critical field

$$H_c = S\sqrt{[J_{\mathbf{0}}^z + 2\bar{D}]^2 - \max_{\mathbf{k}}(J_{\mathbf{k}}^\perp)^2}\,, \tag{2.96}$$

above which the ground state acquires a canted structure.

In all the models above, the magnon dispersion is carried by the transverse exchange terms $J_{\mathbf{k}}^\perp$. For this reason, they are also termed transverse magnons. In order to clearly distinguish these ordinary magnons from the exotic longitudinal magnons presented in Chapter 4, the former will be labeled as T-magnons. The latter will be labeled accordingly as L-magnons.

3. Perturbation methods

3.1 Degenerate perturbation theory 24

3.1.1 Effective Hamiltonian 25

3.1.2 Iterative solution of the effective problem 27

3.1.3 Formulae for $\hat{\mathcal{H}}_{\text{eff}}^{(i)}$ 27

3.2 Series expansions 29

3.2.1 $T = 0$ linked-cluster expansion 29

3.2.2 High-temperature series expansion 40

This chapter introduces two perturbative methods for determining the energy spectrum of a general lattice Hamiltonian with multiple interactions. These approaches are broadly applicable across various physical systems. Specifically, we employ them to investigate quantum spin systems at both zero and finite temperatures.

3.1 Degenerate perturbation theory

The energy spectrum of a complex system with interacting degrees of freedom can be approximated by first addressing a simplified model. This consists of analyzing the dominant interaction alone and calculating its energy spectrum. Additional interactions are incorporated as perturbations, with their magnitude quantified by a small parameter, such as in the $1/S$ expansion of spin-wave theory [49], the $1/z$ expansion for spin waves in antiferromagnets, where z is the coordination number [52], the $1/Z$ expansion for atomic energy levels, where Z represents the nuclear charge [53–55], or the t/U expansion for the Hubbard model [56]. Within nondegenerate energy levels, perturbations typically result in energy renormalization without altering the associated wavefunctions. In contrast, for degenerate levels, perturbations may lift the degeneracy, fully or partially, as exemplified by the Zeeman effect and the fine and hyperfine structures discussed in the preceding chapter. Within a quasi-degenerate subspace, the action of the perturbation induces an effective interaction, truncated to a minimum order.

The perturbative approach is not exclusive to quantum mechanics and has been applied in various branches of theoretical physics. One spectacular example was the explanation of the anomalous motion of Mercury based on gravitational perturbation [57]. Another example was in determining the vibration of inhomogeneous strings [58]. The approach also served as a theoretical tool for solving partial differential equations [59]. In many other N-body problems, the energies and coupling parameters were determined only perturbatively [60–64]. Beyond physics, the principle of solving problems of big systems with interacting degrees of freedom by truncating small interactions finds applications across different fields [65–69].

In the following, we address the case of a system with discrete energy levels. We consider a Hamiltonian comprising an unperturbed term and a perturbation. The objective is to construct an effective interaction within a specified degenerate subspace. The total Hamiltonian is expressed as:

$$\hat{\mathcal{H}} = \hat{\mathcal{H}}_0 + \hat{\mathcal{V}} \tag{3.1}$$

where $\hat{\mathcal{H}}_0$ is the unperturbed Hamiltonian and $\hat{\mathcal{V}}$ represents a small perturbation. The unperturbed Hamiltonian possesses a degenerate energy level, denoted $\mathcal{E}_0$, with finite dimension d_0 and energy E_0. The goal is to derive an effective Hamiltonian within $\mathcal{E}_0$ that encodes the effects of $\hat{\mathcal{V}}$. Notably, $\mathcal{E}_0$ may represent any degenerate energy level, not necessarily the ground state. Derivation is performed in the Brillouin-Wigner framework [70–73].

3.1.1 Effective Hamiltonian

In order to construct the effective Hamiltonian, we first define the projection operator on $\mathcal{E}_0$ as follows

$$P_0 = \sum_{\mathcal{E}_0} |\alpha\rangle \langle\alpha|, \tag{3.2}$$

where $(|\alpha\rangle)_\alpha$ is an eigenbasis of $\mathcal{E}_0$. This operator satisfies the defining property:

$$P_0^2 = P_0. \tag{3.3}$$

In addition, P_0 obeys:

$$\hat{\mathcal{H}}_0 P_0 = P_0 \hat{\mathcal{H}}_0 = E_0 P_0. \tag{3.4}$$

We also define the projection on the orthogonal space to $\mathcal{E}_0$ as:

$$Q_0 = 1 - P_0 = \sum_{\mathcal{E}_n} \underbrace{|n,s\rangle \langle n,s|}_{:=P_n} \tag{3.5}$$

where $\mathcal{E}_n$ is the nth subspace of $\hat{\mathcal{H}}_0$ associated to energy $E_n \neq E_0$, and $(|n,s\rangle)_{n,s}$ is an eigenbasis of $\mathcal{E}_n$ characterized by quantum numbers n and s. Similarly, we have:

$$\hat{\mathcal{H}}_0 |n,s\rangle = E_n |n,s\rangle \tag{3.6}$$

and:

$$\hat{\mathcal{H}}_0 P_n = P_n \hat{\mathcal{H}}_0 = E_n P_n. \tag{3.7}$$

Now we consider an eigenstate $|\psi\rangle$ of the total Hamiltonian $\hat{\mathcal{H}}$ with energy E and attemp to obtain its projection on $\mathcal{E}_0$. We have

$$\hat{H} |\psi\rangle = E |\psi\rangle , \tag{3.8}$$

where E can be written as an expansion of the form:

$$E = E_0 + \Delta E^{(1)} + \Delta E^{(2)} + ... \tag{3.9}$$

Each term $\Delta E^{(i)}$ is the ith order $(i = 1, 2...)$ of the energy correction brought by $\hat{\mathcal{V}}$ to E_0. In order to obtain these corrections, we project (3.8) on $\mathcal{E}_0$ and $\mathcal{E}_n$ as follows:

$$\begin{aligned} E P_0 |\psi\rangle &= P_0(\hat{H}_0 + \hat{\mathcal{V}}) |\psi\rangle = E_0 P_0 |\psi\rangle + P_0 \hat{\mathcal{V}} |\psi\rangle \\ E P_n |\psi\rangle &= P_n(\hat{H}_0 + \hat{\mathcal{V}}) |\psi\rangle = E_n P_n |\psi\rangle + P_n \hat{\mathcal{V}} |\psi\rangle \end{aligned}$$

$$\Rightarrow \begin{cases} (E - E_0) P_0 |\psi\rangle = P_0 \hat{\mathcal{V}} \left(P_0 |\psi\rangle + \sum_m P_m |\psi\rangle \right) \\ (E - E_n) P_n |\psi\rangle = P_n \hat{\mathcal{V}} |\psi\rangle = P_n \hat{\mathcal{V}} P_0 |\psi\rangle + \sum_m P_n \hat{\mathcal{V}} P_m |\psi\rangle \end{cases}$$

which yields:

$$(E - E_0) P_0 |\psi\rangle = P_0 \hat{\mathcal{V}} \left(P_0 |\psi\rangle + \sum_m P_m |\psi\rangle \right) \tag{3.10}$$

$$P_n\hat{\mathcal{V}}P_0\left|\psi\right\rangle = \sum_m \Big([E-E_n]\delta_{nm} - P_n\hat{\mathcal{V}}P_m\Big)P_m\left|\psi\right\rangle. \tag{3.11}$$

We can introduce the diagonal matrix

$$R = \Big([E_n - E]\delta_{nm}\Big)_{nm}, \tag{3.12}$$

with δ_{nm} denoting the Kronecker symbol, and the square matrix of operators

$$\hat{S}_{nm} = \big(P_n\hat{\mathcal{V}}P_m\big)_{nm}. \tag{3.13}$$

Therefore, Eq. (3.11) can be written:

$$P_n\hat{\mathcal{V}}P_0\left|\psi\right\rangle = -\sum_m \Big(R+\hat{S}\Big)_{nm}P_m\left|\psi\right\rangle. \tag{3.14}$$

Next, we invert this equation[1] and write:

$$P_m\left|\psi\right\rangle = -\sum_n \Big(R+\hat{S}\Big)^{-1}_{mn}P_n\hat{\mathcal{V}}P_0\left|\psi\right\rangle, \tag{3.15}$$

which we then substitute in (3.10) to obtain the pseudo-eigenvalue problem[2] in $\mathcal{E}_0$:

$$(E-E_0)P_0\left|\psi\right\rangle = P_0\hat{\mathcal{V}}\left(1-\sum_{m,n}\Big[R+\hat{S}\Big]^{-1}_{mn}P_n\hat{\mathcal{V}}\right)P_0\left|\psi\right\rangle := \hat{\mathcal{H}}_{\text{eff}}P_0\left|\psi\right\rangle. \tag{3.16}$$

The effective Hamiltonian is defined as:

$$\hat{\mathcal{H}}_{\text{eff}} = P_0\hat{\mathcal{V}}\left(1-\sum_{m,n}\Big[R+\hat{S}\Big]^{-1}_{mn}P_n\hat{\mathcal{V}}\right)P_0. \tag{3.17}$$

The occurrence of P_0 on both the right- and left- hand sides of (3.17) restricts $\hat{\mathcal{H}}_{\text{eff}}$ to $\mathcal{E}_0$, such that it is fully characterized by a $d_0 \times d_0$ matrix. We note that (3.16) gives the energy corrections $\Delta E^{(i)}$ as eigenvalues of $\hat{\mathcal{H}}_{\text{eff}}$ at their respective orders: by writing

$$\hat{\mathcal{H}}_{\text{eff}} = \sum_i \hat{\mathcal{H}}^{(i)}_{\text{eff}}, \tag{3.18}$$

where $\hat{\mathcal{H}}^{(i)}_{\text{eff}}$ is of order i, we have

$$\hat{\mathcal{H}}^{(i)}_{\text{eff}}P_0\left|\psi\right\rangle = \Delta E^{(i)}P_0\left|\psi\right\rangle. \tag{3.19}$$

Therefore, the pseudo-eigenvalue problem (3.16) allows for an iterative solution in terms of the eigenvalue problems (3.19), with $i = 1, 2, ...$

[1] Under a small perturbation, we have: $\forall\, n, m,\ \left\|P_n\hat{\mathcal{V}}P_m\right\| \ll |E_n - E|$ such that $R+S$ is a diagonally-dominant matrix, thus invertible.

[2] The energy shifts $\Delta E^{(i)}$ also appear on the right-hand side of (3.16) within the matrix R.

3.1.2 Iterative solution of the effective problem

The calculation of $\hat{\mathcal{H}}_{\text{eff}}$ amounts to computing the inverse operator $(R+\hat{S})^{-1}$. For small perturbations, $\|S\| \ll \|R\|$, and this operator is represented by a geometric series:

$$(R+\hat{S})^{-1} \simeq R^{-1} - R^{-1}\hat{S}R^{-1} + R^{-1}\hat{S}R^{-1}\hat{S}R^{-1} + ... + (-1)^j R^{-1}\left(\hat{S}R^{-1}\right)^j + ..., \quad (3.20)$$

where each occurrence of $\hat{S}$ adds one more order to the perturbation. The inverse matrix R^{-1} can itself be expanded as:

$$\begin{aligned}
R^{-1} &= \left(\frac{1}{E_n - E}\delta_{nm}\right)_{nm} \\
&= \left(\frac{1}{E_n - (E_0 + \Delta E^{(1)} + \Delta E^{(2)} + ...)}\delta_{nm}\right)_{nm} \\
&= \left(\frac{1}{(E_n - E_0)\left(1 - \frac{\Delta E^{(1)} + \Delta E^{(2)} + ...}{E_n - E_0}\right)}\delta_{nm}\right)_{nm} \\
&= \left(\left[\frac{1}{E_n - E_0} + \frac{\Delta E^{(1)} + \Delta E^{(2)} + ...}{(E_n - E_0)^2} + \frac{\left(\Delta E^{(1)} + \Delta E^{(2)} + ...\right)^2}{(E_n - E_0)^3} + ...\right]\delta_{nm}\right)_{nm} \\
&= \left(\left[\underbrace{\frac{1}{E_n - E_0}}_{0^{th}\text{ order}} + \underbrace{\frac{\Delta E^{(1)}}{(E_n - E_0)^2}}_{1^{st}\text{ order}} + \underbrace{\frac{\Delta E^{(2)}}{(E_n - E_0)^2} + \frac{\left(\Delta E^{(1)}\right)^2}{(E_n - E_0)^3}}_{2^{nd}\text{ order}} + ...\right]\delta_{nm}\right)_{nm}, \quad (3.21)
\end{aligned}$$

where we list the terms in increasing order in the perturbation. Expanding R^{-1} is a distinctive step of the Brillouin-Wigner theory in comparison to the Rayleigh-Schrödinger expansion [58, 74]. This latter substitutes the perturbed energy E appearing in the denominator with the unperturbed value E_0, assuming that $|E_0 - E| \ll |E_n - E|$. Yet, the two methods give the same energy up to the second order. See Ref. [75] for a derivation of the first two orders in $\hat{\mathcal{H}}_{\text{eff}}$ in the Rayleigh-Schrödinger framework.

Using the previous expansions, we are set to obtain an explicit expression for the effective Hamiltonian $\hat{\mathcal{H}}_{\text{eff}}$ as a function solely of the perturbation, $\hat{\mathcal{V}}$, and the energy differences $E_n - E_0$, pertaining to the unperturbed Hamiltonian $\hat{\mathcal{H}}_0$. The unknown quantities of the problem are:

(i) the energy shifts $\Delta E^{(i)}$, which are determined as the discrete spectrum of $\hat{\mathcal{H}}^{(i)}_{\text{eff}}$ of cardinality d_0, and

(ii) $P_0\,|\psi\rangle$ defining the corresponding wavefunctions in $\mathcal{E}_0$.

In this sense, each correction $\Delta E^{(i)}$ admits at most d_0 values. As mentioned above, the perturbation can be carried out to several orders so as to obtain luckily d_0 energy sub-levels that lift the degeneracy of $\mathcal{E}_0$. A general spectral analysis of the convergence of perturbation series is given in Refs. [59, 76].

3.1.3 Formulae for $\hat{\mathcal{H}}^{(i)}_{\text{eff}}$

We use the results of Eqs. (3.17), (3.20) and (3.21) to write down the first few orders of $\hat{\mathcal{H}}^{(i)}_{\text{eff}}$. To the best of our knowledge, most of the results in literature give the explicit

effective Hamiltonian in the degenerate case up to second order, and none provides with the analytical result beyond fourth order.

3.1.3.1 $\underline{i=1}$:

$$\hat{\mathcal{H}}_{\text{eff}}^{(1)} = P_0\hat{\mathcal{V}}P_0 = \sum_{\alpha,\beta} |\alpha\rangle\, \hat{\mathcal{V}}_{\alpha\beta}\, \langle\beta|, \tag{3.22}$$

where $(|\alpha\rangle)_\alpha$ and $(|\beta\rangle)_\beta$ are two orthonormal bases of $\mathcal{E}_0$, and $\hat{\mathcal{V}}_{\alpha\beta} = \langle\alpha|\,\hat{\mathcal{V}}\,|\beta\rangle$.

3.1.3.2 $\underline{i=2}$:

$$\hat{\mathcal{H}}_{\text{eff}}^{(2)} = P_0\hat{\mathcal{V}}\sum_n \frac{1}{E_0-E_n}P_n\hat{\mathcal{V}}P_0 = \sum_{\alpha,\beta}|\alpha\rangle\sum_n \frac{\hat{\mathcal{V}}_{\alpha n}\hat{\mathcal{V}}_{n\beta}}{E_0-E_n}\langle\beta|\,, \tag{3.23}$$

where $(|n\rangle)_n$ is an orthonormal basis of $\mathcal{E}_n$, $n \neq 0$.

3.1.3.3 $\underline{i=3}$:

$$\begin{aligned}\hat{\mathcal{H}}_{\text{eff}}^{(3)} &= -P_0\hat{\mathcal{V}}\sum_n \frac{\Delta E^{(1)}}{(E_0-E_n)^2}P_n\hat{\mathcal{V}}P_0 + P_0\hat{\mathcal{V}}\sum_{n,m}\frac{1}{E_0-E_n}P_n\hat{\mathcal{V}}P_m\frac{1}{E_0-E_m}P_m\hat{\mathcal{V}}P_0\\ &= -\sum_{\alpha_1,\beta_1}\Delta E^{(1)}|\alpha_1\rangle\sum_n\frac{\hat{\mathcal{V}}_{\alpha_1 n}\hat{\mathcal{V}}_{n\beta_1}}{(E_0-E_n)^2}\langle\beta_1| + \sum_{\alpha,\beta}|\alpha\rangle\sum_{n,m}\frac{\hat{\mathcal{V}}_{\alpha n}\hat{\mathcal{V}}_{nm}\hat{\mathcal{V}}_{m\beta}}{(E_0-E_n)(E_0-E_m)}\langle\beta|,\end{aligned} \tag{3.24}$$

where $(|\alpha_1\rangle)_{\alpha_1}$ and $(|\beta_1\rangle)_{\beta_1}$ are two eigenbases of $\hat{\mathcal{H}}_{\text{eff}}^{(1)}$ associated to eigenvalues $\Delta E^{(1)}$, so that the first sum is well defined[3]. In the second sum $(|m\rangle)_m$ is an orthonormal basis of $\mathcal{E}_m$, $m \neq 0$.

3.1.3.4 $\underline{i=4}$:

$$\begin{aligned}\hat{\mathcal{H}}_{\text{eff}}^{(4)} &= P_0\hat{\mathcal{V}}\Bigg(\sum_n\frac{\left(\Delta E^{(1)}\right)^2}{(E_0-E_n)^3}P_n + \sum_{n,m}\frac{1}{E_0-E_n}P_n\hat{\mathcal{V}}P_m\frac{1}{E_0-E_m}\left[\frac{\Delta E^{(1)}}{E_0-E_n}+\frac{\Delta E^{(1)}}{E_0-E_m}\right]\\ &\quad -\sum_n\frac{\Delta E^{(2)}}{(E_0-E_n)^2}P_n + \sum_{n,k,m}\frac{1}{E_0-E_n}P_n\hat{\mathcal{V}}P_k\frac{1}{E_0-E_k}P_k\hat{\mathcal{V}}P_m\frac{1}{E_0-E_m}P_m\Bigg)\hat{\mathcal{V}}P_0\\ &= \sum_{\alpha_1,\beta_1}\Delta E^{(1)}|\alpha_1\rangle\sum_n\hat{\mathcal{V}}_{\alpha_1 n}\left[\frac{\Delta E^{(1)}\hat{\mathcal{V}}_{n\beta_1}}{(E_0-E_n)^3} + \sum_m\frac{\hat{\mathcal{V}}_{nm}\left(2E_0-E_n-E_m\right)\hat{\mathcal{V}}_{m\beta_1}}{(E_0-E_n)^2(E_0-E_m)^2}\right]\langle\beta_1|\\ &\quad -\sum_{\alpha_2,\beta_2}\Delta E^{(2)}|\alpha_2\rangle\sum_n\frac{\hat{\mathcal{V}}_{\alpha_2 n}\hat{\mathcal{V}}_{n\beta_2}}{(E_0-E_n)^2}\langle\beta_2|\end{aligned}$$

[3]By commutation, an eigenbasis of $\hat{\mathcal{H}}_{\text{eff}}^{(i)}$ is also an eigenbasis of P_0.

$$+\sum_{\alpha,\beta}|\alpha\rangle\sum_{n,k,m}\frac{\hat{\mathcal{V}}_{\alpha n}\hat{\mathcal{V}}_{nk}\hat{\mathcal{V}}_{km}\hat{\mathcal{V}}_{m\beta}}{(E_0-E_n)(E_0-E_k)(E_0-E_m)}\langle\beta|\,, \tag{3.25}$$

where again $(|\alpha_2\rangle)_{\alpha_2}$ and $(|\beta_2\rangle)_{\beta_2}$ are two eigenbases of $\hat{\mathcal{H}}^{(2)}_{\text{eff}}$ associated to eigenvalues $\Delta E^{(2)}$. The kets $(|k\rangle)_k$ appearing in the last sum refer to an orthonormal basis of $\mathcal{E}_k$, $k\neq 0$.

This construction can be easily computerized so as to obtain the effective Hamiltonian to a given order. A leitmotiv is that the effective Hamiltonian to order j involves the energy corrections associated to all orders up to $j-2$. We note that only the stationary case of the perturbation theory was presented here. For a review on time-dependent $\hat{\mathcal{V}}$, see Refs. [75, 77]. There also exist other variations of the degenerate perturbation theory, including the Møller-Plesset method [78] and the Goldstone expansion [79].

3.2 Series expansions

An alternative method to obtain the low-energy configuration of a complex system with a small parameter, is to perform an expansion in the real-space [80–84]. This starts with a dominant interaction that defines a ground state of finite degeneracy. But unlike the Brillouin-Wigner perturbation theory in momentum space, this expansion consists of setting up virtual processes induced by the perturbation on the lattice, and counting their amplitudes in the coordinate representation, to renormalize the wavefunction or the energy of a given state. There are different series expansion methods [85–87], and the one we use here is the linked-cluster expansion. It treats effective Hamiltonians in a low-dimensional Hilbert space. Its construction can be computerized for most of spin models.

In the following we will present two aspects of the linked-cluster expansion for a quantum system, both of use in the body of the manuscript. The first aspect considers the $T=0$ case within a small interaction parameter, with the aim of obtaining energy corrections to both the ground state and the low-lying excited state. The second aspect is an expansion in the small parameter $1/T$, with the aim of obtaining the thermodynamic properties (magnetization, susceptibility, specific heat) describing a spin system at high temperature.

3.2.1 $T=0$ linked-cluster expansion

In this approach, the energy corrections to order n, for both the ground state and the low-lying excited state, are obtained as an extensive sum of the contributions from all connected subgraphs, or linked clusters, of size up to n bonds [83]. Its consistency relies on the so-called linked-cluster theorem in the thermodynamic limit [85, 88]. The order of the processes under consideration is embodied by the dimension of the Hilbert space to span.

3.2.1.1 Ground-state energy

Consider a Hamiltonian of the form

$$\hat{\mathcal{H}}=\hat{\mathcal{H}}_0+\hat{\mathcal{V}}\,, \tag{3.26}$$

where $\hat{\mathcal{H}}_0$ is an unperturbed Hamiltonian and $\hat{\mathcal{V}}$ is a small interaction[4]. The ground state of $\hat{\mathcal{H}}$ has an energy $E_{\text{g.s.}}$ that satisfies the extensive rule:

$$E_{\text{g.s.}} = \sum_{\{\mathcal{C}\}} g(\mathcal{C})\epsilon(\mathcal{C}) \tag{3.27}$$

where the sum runs over connected clusters $\mathcal{C}$ in the lattice (monomers, dimers, trimers, ...). The quantity $g(\mathcal{C})$ is called the embedding factor of cluster $\mathcal{C}$, and equals the number of combinations of $\mathcal{C}$ in the lattice, whereas $\epsilon(\mathcal{C})$ is the cumulant energy of $\mathcal{C}$, which quantifies its proper contribution independently of its subclusters. The single counting of energies is given by the subcluster rule:

$$E(\mathcal{C}) = \sum_{\{\mathcal{C}'\subseteq\mathcal{C}\}} g(\mathcal{C}'/\mathcal{C})\epsilon(\mathcal{C}'), \tag{3.28}$$

where $E(\mathcal{C})$ is the energy of cluster $\mathcal{C}$ and $d(\mathcal{C}'/\mathcal{C})$ is the relative embedding of $\mathcal{C}'$ with respect to $\mathcal{C}$. In particular, one has the atomic identity:

$$E(\bullet) = \epsilon(\bullet), \tag{3.29}$$

where $\bullet$ denotes a monomer (single site), and the nested identity:

$$E(\bullet\!-\!\bullet) \;\; = \epsilon(\bullet\!-\!\bullet) + 2\epsilon(\bullet). \tag{3.30}$$

The cumulant energies ϵ are constructed iteratively from the atomic cluster, as will be illustrated below. We also have the inclusive relation:

$$g(\mathcal{C}/\mathcal{C}) = 1. \tag{3.31}$$

We note that for the ground-state energy, the topology of clusters is irrelevant. For example, the linked trimers $\bullet\!-\!\bullet\!-\!\bullet$,  , ... are equivalent, and so on. In the above notation, the linked-cluster theorem translates as:

$$\mathcal{C}_1 \cap \mathcal{C}_2 = \emptyset \quad \Rightarrow \quad E(\mathcal{C}_1 \cup \mathcal{C}_2) = E(\mathcal{C}_1) + E(\mathcal{C}_2). \tag{3.32}$$

The principle of the method for the ground state is to obtain the energies $E(\mathcal{C})$ by summing all virtual processes induced by the perturbation $\hat{\mathcal{V}}$ above the ground state. As the number of such processes is limited by the size of each cluster, a high-order process requires larger clusters. Conversely, the relations (3.27) and (3.28) imply that only a finite number of clusters contributes to processes of a given order. Practically, the energies $E(\mathcal{C})$ are derived using the Brillouin-Wigner perturbation theory, as shown in the previous section.

Example: $S = 1$ XXZ antiferromagnet

[4]smallness in some norm such that $\|\hat{\mathcal{V}}\| < \|\hat{\mathcal{H}}_0\|$.

We take for illustration the easy-axis $S = 1$ square-lattice antiferromagnet with single-ion anisotropy, where transverse exchange is a small perturbation. We derive the ground-state energy to the fourth order. The unperturbed Hamiltonian reads:

$$\hat{\mathcal{H}}_0 = J_{zz} \sum_{\langle i,j \rangle} S_i^z S_j^z - D \sum_j \left[(S_j^z)^2 - 1 \right] , \tag{3.33}$$

with $J_{zz}, D > 0$, and the perturbation is written:

$$\hat{\mathcal{V}} = \frac{J}{2} \sum_{\langle i,j \rangle} \left(S_i^+ S_j^- + S_i^- S_j^+ \right) . \tag{3.34}$$

The unperturbed ground state is the Néel state $|..1, -1, 1, ..\rangle$ with unperturbed energy $E_0 = 0$. Since $\hat{\mathcal{V}}$ acts on bonds, the first cluster to consider is a dimer with two spins, and the largest clusters are the open tetramer and the square with four spins. We use for the energies the formulae of Sec. 3.1.3, with the projection P_0 on the one-dimensional Néel vector. The aim is to derive the embedding energies $\epsilon(\mathcal{C})$ of each cluster, in order to compute the total ground-state energy of the lattice. In the fourth order, we need at most two virtual processes induced by $\hat{\mathcal{V}}$. This yields the following construction:
(i) the dimer •—• has an embedding factor of $g = 2N$. It includes the following virtual processes:

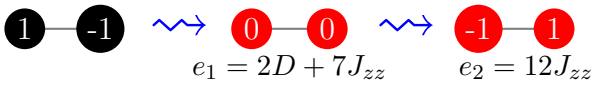

$e_1 = 2D + 7J_{zz}$ $\qquad$ $e_2 = 12J_{zz}$

where e_1 and e_2 are energies of excited subspaces, calculated using (3.33). The corresponding corrections to second and fourth orders of the energy, respectively, are:

$$\begin{aligned} E_2 &= -\frac{1}{e_1} J^2 \\ E_4/J^4 &= -\frac{1}{e_1^2 e_2} + \frac{1}{e_1^3}, \end{aligned} \tag{3.35}$$

Thus:

$$\epsilon(\bullet\!-\!\bullet) = E(\bullet\!-\!\bullet) = -\frac{1}{e_1} J^2 + \frac{1}{e_1^2} \left(\frac{1}{e_1} - \frac{1}{e_2} \right) J^4. \tag{3.36}$$

(ii) The trimer •—•—• has an embedding factor of $d = 6N$, and includes the following virtual processes:

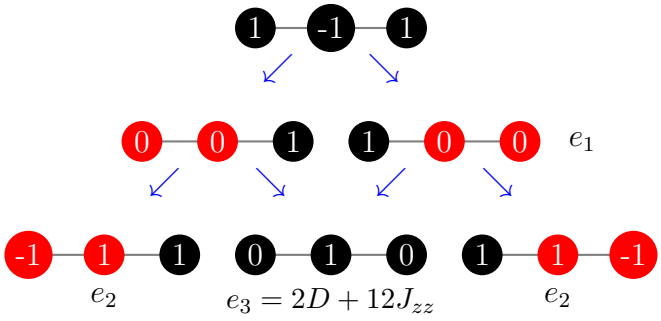

e_2 $\qquad$ $e_3 = 2D + 12J_{zz}$ $\qquad$ e_2

which now accesses a subspace of energy e_3 in the second order. This yields the energy corrections to second and fourth orders:

$$E_2 = -\frac{2}{e_1}J^2 \tag{3.37}$$

$$E_4 = \left[-\frac{1}{e_1^2}\begin{pmatrix}1 & 1\end{pmatrix}\begin{pmatrix}\frac{1}{e_2} & 0 & \frac{1}{e_3}\\ 0 & \frac{1}{e_2} & \frac{1}{e_3}\end{pmatrix}\begin{pmatrix}1 & 0\\ 0 & 1\\ 1 & 1\end{pmatrix}\begin{pmatrix}1\\ 1\end{pmatrix} + \frac{4}{e_1^3}\right] J^4 = \frac{2}{e_1^2}\left(\frac{2}{e_1} - \frac{1}{e_2} - \frac{2}{e_3}\right)J^4.$$

And

$$E(\bullet\!-\!\bullet\!-\!\bullet) = E_2 + E_4, \tag{3.38}$$

whereas we derive the cumulant energy of the trimer from the subcluster rule (3.28) as:

$$E(\bullet\!-\!\bullet\!-\!\bullet) = \epsilon\,(\bullet\!-\!\bullet\!-\!\bullet) + 2\epsilon(\bullet\!-\!\bullet). \tag{3.39}$$

Thus:

$$\epsilon\,(\bullet\!-\!\bullet\!-\!\bullet) = \frac{2}{e_1^2}\left(\frac{1}{e_1} - \frac{2}{e_3}\right)J^4. \tag{3.40}$$

(iii) The square  has an embedding $g = N$. Its virtual processes of interest are schematized as follows:

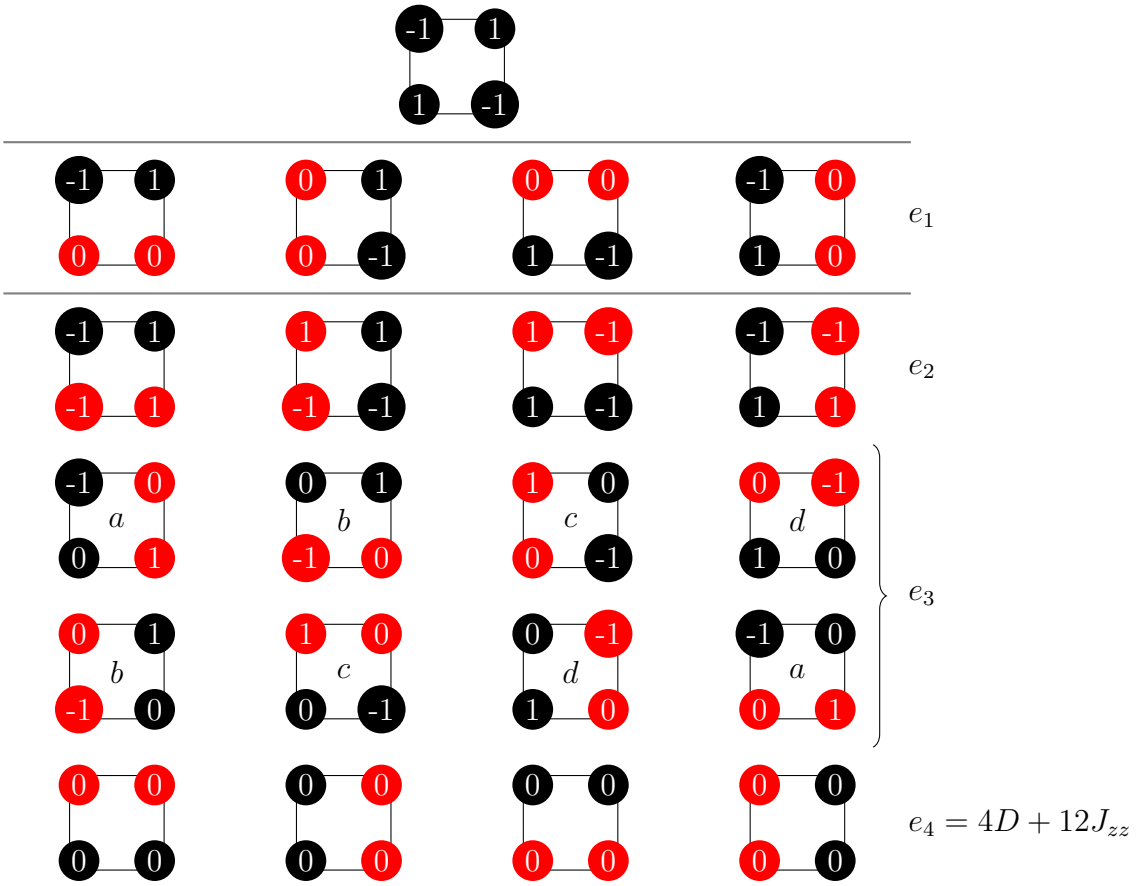

where we showed in red the active bonds at each step. The columns are independent of each other, and they trace the sequence of virtual processes in the first order (first row

with energy e_1) and in the second order (bottom part with different possible processes for each initial configuration). The letters $a-d$ label states in the subspace of energy e_3. The square cluster now accesses the excited subspace of energy e_4. As a consequence, we have the following energies to second and fourth orders:

$$
\begin{aligned}
E_2 &= -\frac{4}{e_1}J^2 \\
E_4/J^4 &= -\frac{1}{e_1^2}\begin{pmatrix}1 & 1 & 1 & 1\end{pmatrix}
\begin{pmatrix}
\frac{1}{e_2} & & & & \frac{1}{e_3} & \frac{1}{e_3} & & & \frac{1}{e_4} \\
& \frac{1}{e_2} & & & & \frac{1}{e_3} & \frac{1}{e_3} & & \frac{1}{e_4} \\
& & \frac{1}{e_2} & & & & \frac{1}{e_3} & \frac{1}{e_3} & \frac{1}{e_4} \\
& & & \frac{1}{e_2} & \frac{1}{e_3} & & & \frac{1}{e_3} & \frac{1}{e_4}
\end{pmatrix}
\begin{pmatrix}
1 & & & \\
& 1 & & \\
& & 1 & \\
& & & 1 \\
1 & & & 1 \\
1 & 1 & & \\
& 1 & 1 & \\
& & 1 & 1 \\
1 & 1 & 1 & 1
\end{pmatrix}
\begin{pmatrix}1\\1\\1\\1\end{pmatrix} \\
&\quad +\frac{16}{e_1^3} \\
&= \frac{4}{e_1^2}\left(\frac{4}{e_1}-\frac{1}{e_2}-\frac{4}{e_3}-\frac{4}{e_4}\right).
\end{aligned}
\tag{3.41}
$$

Hence, the energy of the square is

$$E\left(\square\right) = E_2 + E_4. \tag{3.42}$$

Then we use the subcluster relation:

$$E\left(\square\right) = \epsilon\left(\square\right) + 4\epsilon\left(\text{---}\right) + 4\epsilon(\text{—}) \tag{3.43}$$

in order to obtain the cumulant energy of the square:

$$\epsilon\left(\square\right) = \frac{4}{e_1^2}\left(\frac{1}{e_1}-\frac{4}{e_4}\right)J^4. \tag{3.44}$$

Note that it only contributes to the fourth order of the energy, as expected.
(iv) Finally, the open tetramer  has an embedding factor of $g = 14N$. It involves the following processes:

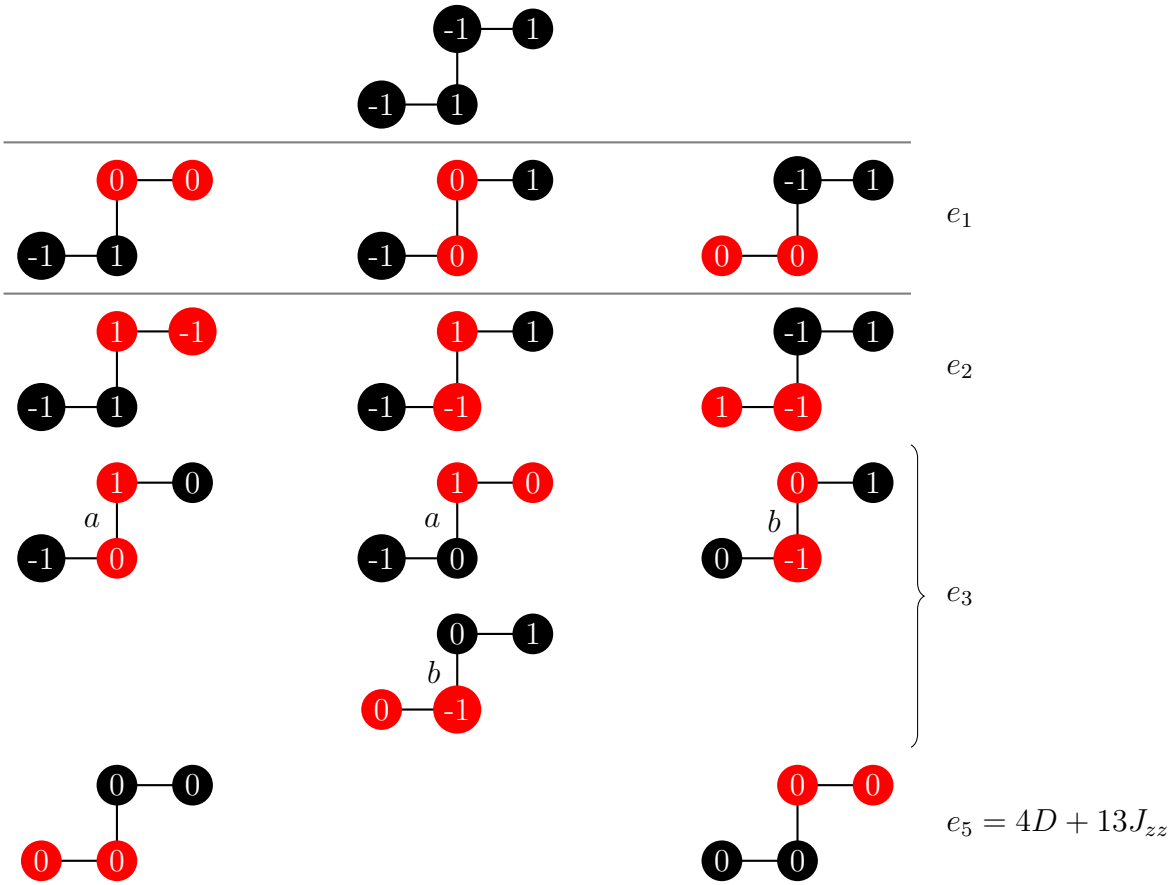

We used similar conventions as for the square. The open tetramer accesses the excited subspace of energy e_5. The resulting ground-state energies to the second and the fourth orders are:

$$\begin{aligned} E_2 &= -\frac{3}{e_1}J^2 \\ E_4/J^4 &= -\frac{1}{e_1^2}\begin{pmatrix}1 & 1 & 1\end{pmatrix}\begin{pmatrix} \frac{1}{e_2} & & & \frac{1}{e_3} & & \frac{1}{e_5} \\ & \frac{1}{e_2} & & \frac{1}{e_3} & \frac{1}{e_3} & \\ & & \frac{1}{e_2} & & \frac{1}{e_3} & \frac{1}{e_5} \end{pmatrix}\begin{pmatrix} 1 & & \\ & 1 & \\ & & 1 \\ 1 & 1 & \\ & 1 & 1 \\ 1 & & 1 \end{pmatrix}\begin{pmatrix}1\\1\\1\end{pmatrix} + \frac{9}{e_1^3} \\ &= \frac{1}{e_1^2}\left(\frac{9}{e_1} - \frac{3}{e_2} - \frac{8}{e_3} - \frac{4}{e_5}\right). \end{aligned} \tag{3.45}$$

And the energy of the tetramer is:

$$E\left(\text{ 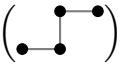 }\right) = -\frac{3}{e_1}J^2 + \frac{1}{e_1^2}\left(\frac{9}{e_1} - \frac{3}{e_2} - \frac{8}{e_3} - \frac{4}{e_5}\right), \tag{3.46}$$

whereas the subcluster relation reads:

$$E\left(\text{ 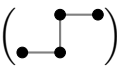 }\right) = \epsilon\left(\text{ 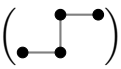 }\right) + 2\epsilon\left(\text{}\right) + 3\epsilon\left(\text{}\right). \tag{3.47}$$

Therefore, the cumulant energy of the tetramer is:

$$\epsilon\left(\text{ 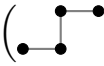 }\right) = \frac{2}{e_1^2}\left(\frac{1}{e_1} - \frac{2}{e_5}\right) J^4, \tag{3.48}$$

which only contributes to the fourth order.

In conclusion, the ground-state energy of the easy-axis antiferromagnet to fourth order is:

$$\begin{aligned}\frac{E_{\text{g.s.}}}{N} &= 2\epsilon(\text{}) + 6\epsilon\,(\text{}) + \epsilon\left(\text{  }\right) + 14\epsilon\left(\text{ 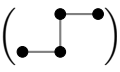 }\right) \\ &= \frac{-2}{2D+7J_{zz}}J^2 + \frac{1}{(2D+7J_{zz})^2}\left[\frac{46}{2D+7J_{zz}} - \frac{1}{6J_{zz}} - \frac{12}{D+6J_{zz}} - \frac{4}{D+3J_{zz}}\right. \\ &\quad \left. - \frac{56}{4D+13J_{zz}}\right] J^4. \end{aligned} \tag{3.49}$$

In the case of pure exchange, $D = 0$, the ground-state energy per spin is given in powers of the small anisotropy ratio $\lambda = J/J_{zz}$ as:

$$E_{\text{g.s.}}/J_{zz}/N = -\frac{2}{7}\lambda^2 - \frac{225}{8918}\lambda^4. \tag{3.50}$$

This result recovers the first two terms in the numerical series to the twelfth order given in Ref. [89].

3.2.1.2 One-particle excitation

The linked-cluster method can be also employed to obtain the energy of the lowest one-particle excitation of a lattice Hamiltonian, as powers of a small interaction parameter. This consists of counting virtual hopping processes of a single-particle excitation in the real space, starting with a small cluster. The energies to a given order are encoded in an effective Hamiltonian for each cluster, and the linked-cluster theorem applies such that only few terms are required for a fixed order in the energy. Unlike the ground-state case, the relative geometry of each cluster matters and the topology is relevant as a consequence. This would affect the embedding factors and the summation rule, *e.g.* Eq. (3.27).

Given a certain cluster, there are two quantities of interest:
(i) the reduced transition amplitudes $d(\mathbf{n})$, expressing one-particle hopping to one of the nth neighbors, without geometric distinction of clusters.
(ii) the total irreducible transition amplitudes $\Delta(\mathbf{r})$ (with $|\mathbf{r}| = n$) which distinguish the relative distance between two points matched by the same transition amplitude $d(\mathbf{n})$. For example, in a square lattice the amplitude $\Delta(\pm 2, 0)$ is solely obtained from the trimer  , the amplitude $\Delta(0, \pm 2)$ is obtained from the trimer  , whereas the square  contributes to $\Delta(\pm 1, 0)$, $\Delta(0, \pm 1)$ and $\Delta(\pm 1, \pm 1)$, and so on.

The linked-cluster theorem is applied on the auxiliary matrix:

$$\Delta_{ij}(\mathcal{C}) = \hat{H}^{\text{eff}}_{ij}(\mathcal{C}) - E_{\text{g.s.}}\delta_{ij}\,, \tag{3.51}$$

where $\hat{H}^{\text{eff}}$ is the effective Hamiltonian of the one-particle, describing hopping processes between sites i and j of a given cluster, and $E_{\text{g.s.}}$ is the ground-state energy as computed above. The theorem reads:

$$\mathcal{C}_1 \cap \mathcal{C}_2 = \emptyset \quad \Rightarrow \quad \Delta_{ij}(\mathcal{C}_1 \cup \mathcal{C}_2) = \Delta_{ij}(\mathcal{C}_1) + \Delta_{ij}(\mathcal{C}_2). \tag{3.52}$$

Practically, the irreducible amplitudes mentioned earlier are related to the auxiliary matrix Δ_{ij} by:

$$\Delta(\mathbf{r}) = \sum_{\substack{i,j \\ \mathbf{r}=\mathbf{r}_i-\mathbf{r}_j}} \Delta_{ij} \tag{3.53}$$

and the energy rule is:

$$\Delta(\mathbf{r}) = \sum_{\mathcal{C}} g(\mathcal{C}) d^{\mathcal{C}}(\mathbf{r}), \tag{3.54}$$

involving the embedding factor g and the reduced transition amplitudes $d^{\mathcal{C}}$ for cluster $\mathcal{C}$. Whereas the irreducible transition amplitudes satisfy the subcluster rule:

$$\Delta^{\mathcal{C}}(\mathbf{r}) = \sum_{\{\mathcal{C}' \subseteq \mathcal{C}\}} g(\mathcal{C}'/\mathcal{C}) d^{\mathcal{C}'}(\mathbf{r}). \tag{3.55}$$

Since the sum (3.53) also applies for $i = j$, the smallest cluster to consider for the excitation energy in the linked-cluster method is a single site. The reduced amplitudes $d^{\mathcal{C}}$ are computed iteratively, starting with the atomic cluster, similarly to the computation of the cumulant energies $\epsilon(\mathcal{C})$ for the ground state.

For a given cluster $\mathcal{C}$, we invoke its ground-state energy $E(\mathcal{C})$ and form the effective Hamiltonians in a subspace of dimension m where m is the size of $\mathcal{C}$. Then we calculate the auxiliary matrix Δ_{ij}, Eq. (3.51), and compute the irreducible amplitudes $\Delta^{\mathcal{C}}(\mathbf{r})$, Eq. (3.53) for a given relative coordinate $\mathbf{r}$. Next, we compute the reduced amplitudes $d(\mathbf{r})$, from Eqs. (3.54) and (3.55). Finally, the irreducible amplitudes are written in the coordinate representation as:

$$\Delta(\mathbf{r}) = \langle \mathbf{r_0} | \, \hat{H}^{\text{eff}} \, | \mathbf{r} + \mathbf{r_0} \rangle \tag{3.56}$$

for all position states $|\mathbf{r_0}\rangle$ in the lattice. By Fourier transforming the coordinates, *e.g.*

$$|\mathbf{r}\rangle = \frac{1}{\sqrt{N}} \sum_{\mathbf{k}} e^{-i\mathbf{k}.\mathbf{r}} \, |\mathbf{k}\rangle \ , \tag{3.57}$$

we have the momentum-dependent excitation energy:

$$\varepsilon_{\mathbf{k}} = \sum_{\mathbf{r}} e^{i\mathbf{k}\cdot\mathbf{r}} \Delta(\mathbf{r}). \tag{3.58}$$

This procedure will be illustrated in Chapter III, on the one-particle excitation consisting of a full spin reversal on a square lattice. Note that the computation of high-order effective Hamiltonians, as described in Sec. 3.1.3, may require diagonalization at intermediate steps. In such a case, we can resort to matrix block diagonalization methods; see Ref. [83].

Example: One magnon in the easy-axis $S = 1$ square-lattice antiferromagnet

We illustrate the method to obtain the magnon energy to the second order in an $S = 1$ square-lattice antiferromagnet. The unperturbed Hamiltonian has the form (3.33), along

with the perturbation (3.34). The relevant clusters here are a single site (a monomer), two sites (a dimer) and three sites (a trimer).

(i) We note the monomer $\mathcal{C}_1 =$  , with embedding factor $g(\mathcal{C}_1) = N$ (the number of sites). A single flip  defines a scalar effective Hamiltonian: $h_{\text{eff}}(\mathcal{C}_1) = 4J_{zz} + D =: g_0$. Its ground-state energy correction is zero, as shown in the previous section, and the corresponding transition amplitude for $\mathbf{r} = \mathbf{0}$ is:

$$d^{\mathcal{C}_1}(0) = \Delta^{\mathcal{C}_1}(0) = g_0. \tag{3.59}$$

(ii) We note the dimer $\mathcal{C}_2 =$  , with embedding factor $g(\mathcal{C}_1) = 2N$. The Hilbert space associated to a single spin flip is spanned by the two kets $|l\rangle =$ 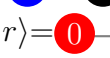 and $|r\rangle =$  . Their images by the perturbation are: $\hat{\mathcal{V}}\,|l\rangle =$ 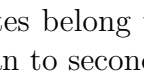 and $\hat{\mathcal{V}}\,|r\rangle =$. These resulting states belong to a subspace of energy $g_1 := 10J_{zz} + 4D$. Therefore, the effective Hamiltonian to second order:

$$h_{\text{eff}}(\mathcal{C}_2) = g_0 \begin{pmatrix} 1 & \\ & 1 \end{pmatrix} + \frac{J^2}{g_0 - g_1} \begin{pmatrix} 1 & \\ & 1 \end{pmatrix}. \tag{3.60}$$

Whereas the ground-state correction of the dimer is (see Eq. (3.36)):

$$E^{\mathcal{C}_2} = -\frac{1}{e_1} J^2\,, \tag{3.61}$$

with $e_1 = 2D + 7J$. Hence, the auxiliary matrix reads

$$\Delta^{\mathcal{C}_2} = \left[g_0 + \frac{J^2}{g_0 - g_1} - E^{\mathcal{C}_2} \right] \begin{pmatrix} 1 & \\ & 1 \end{pmatrix} \tag{3.62}$$

and the only non-vanishing irreducible transition amplitude is:

$$\Delta^{\mathcal{C}_2}(0) = Tr\left(\Delta^{\mathcal{C}_2}\right) = 2\left(g_0 + \frac{J^2}{g_0 - g_1} - E^{\mathcal{C}_2} \right) \tag{3.63}$$

whereas the subcluster rule (3.55) gives:

$$\Delta^{\mathcal{C}_2}(0) = d^{\mathcal{C}_2}(0) + 2d^{\mathcal{C}_1}(0)\,. \tag{3.64}$$

Finally, we have the reduced transition amplitudes:

$$d^{\mathcal{C}_2}(0) = 2\left(\frac{1}{e_1} + \frac{1}{g_0 - g_1} \right) J^2 \tag{3.65}$$

and

$$d^{\mathcal{C}_2}(\mathbf{1}) = \Delta^{\mathcal{C}_2}(\mathbf{1}) = 0. \tag{3.66}$$

(iii) We note the trimer $\mathcal{C}_3 =$  , with embedding factor $g(\mathcal{C}_3) = 6N$. There are three excited states, namely $\{|a\rangle\,, |b\rangle\,, |c\rangle\}$, and we have the following construction:

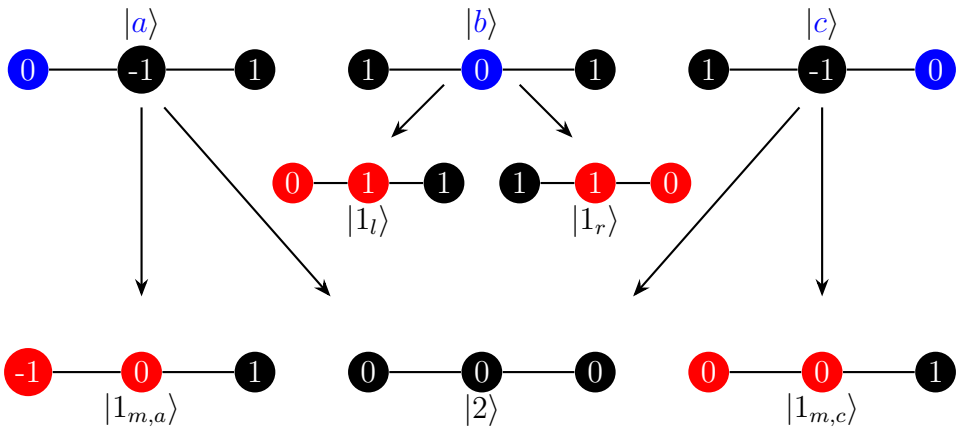

where the arrows indicate the action of perturbation $\hat{\mathcal{V}}$, with a matrix element equal to J. The states $|1_r\rangle, |1_l\rangle, |1_{m,a}\rangle$ and $|1_{m,c}\rangle$ have energy g_1 and the state $|2\rangle$ has energy $g_2 := 10J_{zz} + 3D$. The processes $|a\rangle \leftrightarrow |2\rangle \leftrightarrow |c\rangle$ induce dispersion in the second order. In view of this diagram, the effective Hamiltonians to orders 0–3 in the space spanned by kets $\{|a\rangle, |b\rangle, |c\rangle\}$, are:

$$\begin{aligned} h^{(0)}_{\text{eff}}(\mathcal{C}_3) &= g_0 \begin{pmatrix} 1 & & \\ & 1 & \\ & & 1 \end{pmatrix}, \\ h^{(1)}_{\text{eff}}(\mathcal{C}_3) &= 0, \\ h^{(2)}_{\text{eff}}(\mathcal{C}_3) &= J^2 \begin{pmatrix} \frac{1}{g_{0,1}} + \frac{1}{g_{0,2}} & \frac{2}{g_{0,1}} & \frac{1}{g_{0,2}} \\ \frac{1}{g_{0,2}} & & \frac{1}{g_{0,1}} + \frac{1}{g_{0,2}} \end{pmatrix}, \\ h^{(3)}_{\text{eff}}(\mathcal{C}_3) &= 0, \end{aligned} \tag{3.67}$$

where $g_{0,i} := g_0 - g_i,\ i = 1, 2$.
The ground-state energy associated to the trimer is given to second order by Eq. (3.37):

$$E^{\mathcal{C}_3} = -\frac{2}{e_1} J^2, \tag{3.68}$$

yielding the auxiliary matrix:

$$\Delta^{\mathcal{C}_3} = \begin{pmatrix} g_0 + \left(\frac{1}{g_{0,1}} + \frac{1}{g_{0,2}} + \frac{2}{e_1}\right) J^2 & & \frac{2}{g_{0,2}} J^2 \\ & g_0 + \left(\frac{2}{g_{0,1}} + \frac{2}{e_1}\right) J^2 & \\ \frac{2}{g_{0,2}} J^2 & & g_0 + \left(\frac{1}{g_{0,1}} + \frac{1}{g_{0,2}} + \frac{2}{e_1}\right) J^2 \end{pmatrix}. \tag{3.69}$$

The non-vanishing irreducible transition amplitudes are $\Delta^{\mathcal{C}_3}(0)$ and $\Delta^{\mathcal{C}_3}(\mathbf{2})$. And the subcluster rule gives:

$$\begin{aligned} d^{\mathcal{C}_3}(0) + 2d^{\mathcal{C}_2}(0) + 3d^{\mathcal{C}_1}(0) &= \Delta^{\mathcal{C}_3}(0) = Tr(\Delta^{\mathcal{C}_3}) \\ \Rightarrow \qquad d^{\mathcal{C}_3}(0) &= 2\left(\frac{1}{g_{0,1}} + \frac{1}{e_1}\right) J^2, \end{aligned} \tag{3.70}$$

and

$$d^{\mathcal{C}_3}(\mathbf{2}) = \Delta^{\mathcal{C}_3}(\mathbf{2}) = \frac{J^2}{g_{0,2}}. \tag{3.71}$$

Now the energy rule (3.54) yields:

$$\begin{aligned}
\Delta(0) =& d^{\mathcal{C}_1}(0) + 2d^{\mathcal{C}_2}(0) + 6d^{\mathcal{C}_3}(0) = g_0 + 4\left(\frac{4}{e_1} + \frac{1}{g_{0,1}} + \frac{3}{g_{0,2}}\right) J^2 \\
\Delta(\mathbf{1}) =& 0, \\
\Delta(\pm 2, 0) =& \Delta(0, \pm 2) = d^{\mathcal{C}_3}(\mathbf{2}) = \frac{J^2}{g_{0,2}}, \\
\Delta(\pm 1, \pm 1) =& 2d^{\mathcal{C}_3}(\mathbf{2}) = 2\frac{J^2}{g_{0,2}}.
\end{aligned} \tag{3.72}$$

Note that $\Delta(\pm 2, 0)$ gets a contribution solely from , and likewise for $\Delta(0, \pm 2)$ with  . The diagonal amplitudes $\Delta(\pm 1, \pm 1)$ get contributions from two L-shaped trimers among  , and .

Finally, the excitation energy, Eq. (3.58), is written as:

$$\begin{aligned}
\varepsilon_{\mathbf{k}} =& \Delta(0) + 4d^{\mathcal{C}_3}(\mathbf{2})(4\gamma_{\mathbf{k}}^{\square 2} - 1) \\
=& D + 4J_{zz} - 2\left(\frac{1}{3J_{zz}} + \frac{2}{D + 3J_{zz}} - \frac{8}{2D + 7J_{zz}}\right) J^2 - \frac{8}{D + 3J_{zz}} J^2 \gamma_{\mathbf{k}}^{\square 2}.
\end{aligned} \tag{3.73}$$

Figure 3.1 shows a plot of the above dispersion along high-symmetry lines of the Brillouin zone for $D = 0$, in comparison to the result of spin-wave theory, Eq. (2.85). The dispersion amplitude for the linked-cluster result may be improved by resorting to the next order in perturbation theory.

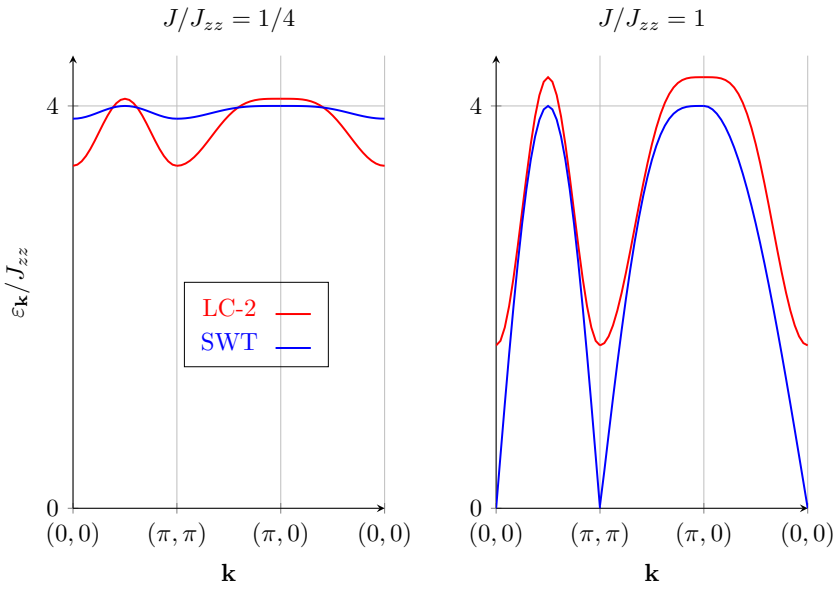

Figure 3.1: T-magnon dispersion in the spin-1 easy-axis square-lattice antiferromagnet with $D = 0$.

For a fourth-order expansion, we may use the so-called matrix block diagonalization method, see Sec. 4.4.1.1.2. This is useful as the second-order effective Hamiltonian associated to the trimer is not diagonal, whereas its eigenvalues appear in the expression of the fourth-order, Eq. (3.25), through the energies $\Delta E^{(2)}$.

3.2.2 High-temperature series expansion

The statistical mechanical description of a system of interacting degrees of freedom derives from the partition function. In the quantum picture, this function is given by

$$Z = Tr\{e^{-\beta\hat{\mathcal{H}}}\}\,, \tag{3.74}$$

where $\hat{\mathcal{H}}$ is the microscopic Hamiltonian operator, Tr denotes the trace over the accessible energy subspace and $\beta = (k_B T)^{-1}$. In a magnet with localized spins, $\hat{\mathcal{H}}$ is the spin Hamiltonian featuring the different interactions in a lattice. The computation of the partition function is important since the thermodynamic properties of the magnet (susceptibility, specific heat, entropy) are all related to Z via standard statistical mechanics' formulae [90].

3.2.2.1 Method's idea

In the high-temperature regime, the partition function Z can be evaluated as an expansion in powers of the small parameter β:

$$Z = \sum_m \frac{(-\beta)^m}{m!} Tr\{\hat{\mathcal{H}}^m\}\,, \tag{3.75}$$

with the trace considered over the paramagnetic phase. This idea follows from the early work of Thirring [91], who obtained a series expansion for the specific heat in a cubic lattice in powers of $1/T$ involving the lattice vibrational modes. A series expansion of the partition function in powers of $1/T$ was later proposed by Van Vleck [92] to study paramagnetic salts. In practice, the high-T series expansion for (3.74) amounts to tracing powers of $\hat{\mathcal{H}}$ over the lattice sites. The number of such sites grows with the range of interactions involved in the Hamiltonian. In short-range interactions as, *e.g.*, few-neighbor spin exchange, the expansion simplifies to only a finite number of lattice sites for each given order. Kramers and Opechowski devised a method to obtain few orders of the series expansion in lattice spin models by reducing the trace to finite clusters [93]. This approach was later revisited by Wortis [94] and Gelfand [82, 83]. We will give below the steps involved in this expansion with finite clusters. It will be useful for our quantum-classical correspondence in Chapter 5.

3.2.2.2 Cluster enumeration

The Hamiltonian $\hat{\mathcal{H}}$ in the most general case is a finite combination of tensor-products involving powers of the spin components on different sites:

$$\hat{\mathcal{H}} \propto \sum_{\substack{i,j,\ldots \\ \mu,\nu,\ldots \\ a,b,\ldots}} \left(S_i^\mu\right)^a \left(S_j^\nu\right)^b \ldots .$$

The indices $i, j, ..$ span the lattice sites, and $\mu, \nu, ... = x, y, z$ and $a, b, ...$ are integer powers. Therefore, tracing $\hat{\mathcal{H}}^m$ amounts to consider a series of finite clusters throughout the lattice, *i.e.*

$$Tr\{\hat{\mathcal{H}}^m\} \propto \sum_{\substack{1,2,..m \\ l_1,l_2,...l_m}} Tr\left\{\left(S^{\mu_1}\right)^{a_1}\left(S^{\nu_1}\right)^{b1}...\right\}^{l_1} \times Tr\left\{\left(S^{\mu_2}\right)^{a_2}\left(S^{\nu_2}\right)^{b_2}...\right\}^{l_2} \times ... \tag{3.76}$$

where the site indices are dropped from the trace. Instead, the exponents $l_1, l_2, ...$ appear to describe the spatial range of the terms in $\hat{\mathcal{H}}$, *e.g.* $l_i = 2$ for interactions involving at most two spins. In the case of a Heisenberg exchange between nearest-neighbors,

$$\hat{\mathcal{H}} = J \sum_{i,j} \mathbf{S}_i \cdot \mathbf{S}_j, \tag{3.77}$$

the trace is written in terms of graphs

$Tr\{\hat{\mathcal{H}}^m\} =$ 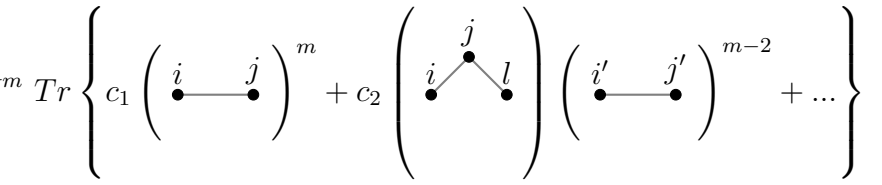

$$= J^m \sum_{\mu_1,\mu_2,...\mu_m} \Big[c_1\ Tr\{S^{\mu_1}...S^{\mu_m}\}^2 + c_2\ Tr\{S^{\mu_1}\}Tr\{S^{\mu_1}S^{\mu_2}\}Tr\{S^{\mu_2}\}Tr\{S^{\mu_3}...S^{\mu_m}\}^2 + ... \Big] \tag{3.78}$$

where c_i's are combinatorial factors resulting from $\hat{\mathcal{H}}^m$, and $\mu_i = x, y, z$. Each trace is here represented in terms of an interaction over a finite cluster of connected sites. Only a limited number of terms in the sum are non-vanishing. A more detailed description of the cluster enumeration in the high-T series expansion for the Heisenberg model is given in Ref. [95]. We also note that adding further interactions to the Hamiltonian such as biquadratic exchange, single-ion anisotropy or the Zeeman energy yield a similar construction of cluster diagrams, eventually with terms involving traces on single sites and disconnected clusters. See also Ref. [96] for an expansion with long-range dipolar interactions.

In the most general case, additional arguments of symmetry, topology and commutation can be invoked to further simply (3.78). Optimized algorithms for cluster enumeration and series convergence have also been developed [97, 98], and recent works improved the numerical complexity [99].

We note that the spin appearing in the Hamiltonian $\hat{\mathcal{H}}$ at finite temperature can be treated either classically or quantum mechanically. In the classical picture, the spin $\mathbf{S}$ is a 3D vector of length

$$|\mathbf{S}| = S_c. \tag{3.79}$$

Whereas in the quantum picture, the spin $\mathbf{S}$ is a vector operator whose components satisfy the $SU(2)$ commutation rules, with magnitude

$$\mathbf{S}^2 = S(S+1). \tag{3.80}$$

3.2.2.3 Traces of $\left(S^\mu\right)^a\left(S^\nu\right)^b...$

The sum (3.76) involves traces of the spin components on the same site. As illustrated above, the cluster enumeration allows to rearrange this sum with respect to finite clusters of connected sites. Therefore, Eq. (3.75) is fully determined by traces of the form $Tr\{\left(S^\mu\right)^a\left(S^\nu\right)^b...\}$ on a single site. Ref. [100] has tabulated different such traces to several orders for general spins S. Ref. [101] has proposed an alternative algorithm to identify the series coefficients of each trace by evaluating it for different spin values $S = 1/2, 1, ...$

An important property of use here is that, in the paramagnetic phase, all traces amount to computing $Tr\{\left(S^z\right)^n\}$ where n is an even integer [102]. This assertion can be understood from simple arguments in the quantum picture. Practically, the typical spin Hamiltonian can be written in terms of S^z and the ladder operators $S^\pm$. The only non-vanishing traces are those which conserve the S^z quantum number. Then, invoking the commutation rules, $[S^z, S^\pm] = \pm S^\pm$ and $[S^+, S^-] = 2S^z$, and the cyclic property of the trace allows one to reduce all traces into a generic term of the form $Tr\{(S^-)^p(S^+)^p(S^z)^q\}$. In the eigenbasis $|m\rangle$, $m = -S, ..., S$, of the S^z operator, the general term of this trace reads

$$\begin{aligned}
\langle m|\,(S^-)^p(S^+)^p(S^z)^q\,|m\rangle &= m^q\left\|(S^+)^p\,|m\rangle\right\|^2 \\
&= m^q\prod_{j=m}^{m+p-1}\Big[S(S+1)-j(j+1)\Big] \\
&= \mathcal{P}(m) \\
&= \langle m|\,\mathcal{P}(S^z)\,|m\rangle\ , \qquad (3.81)
\end{aligned}$$

where $\mathcal{P}$ is a polynomial of degree $2p+q$, whose coefficients are polynomials in $S(S+1)$. In the second line we used the matrix elements of S^+, Eq. (2.36). As a consequence of (3.81), all traces can be written as a finite linear combination of terms $Tr\{(S^z)^n\}$, which vanish for odd n. The coefficients of the combination carry a spin dependence in terms of powers of $S(S+1)$.

4. Longitudinal magnons

4.1 Introduction 44
4.1.1 Magnon bound-state classification 44
4.1.2 Observations 46
4.2 Experimental motivation 46
4.2.1 van der Waals magnets $FePX_3$ 47
4.2.2 $Na_2BaNi(PO_4)_2$ 49
4.3 Strong-coupling expansion 50
4.3.1 Presentation 50
4.3.2 Effective $s = 1/2$ Hamiltonian 51
4.3.3 Spin-1 magnet 52
4.3.4 Spin-2 magnet 55
4.3.5 Spins $S = 3/2$ and $5/2$ 64
4.3.6 Conclusions 65
4.4 Spin-1 square-lattice model 67
4.4.1 Antiferromagnetic order 67
4.4.2 Ferromagnetic order 89
4.4.3 Conclusions 97
4.5 Spin-1 triangular antiferromagnet at high fields 98
4.5.1 Two magnon states 98
4.5.2 Exact solution 100
4.5.3 Effective $s = 1/2$ Hamiltonian 102
4.5.4 Conclusions 103
4.6 Longitudinal magnons as anti-bound states 104
4.6.1 Exact solution 105
4.6.2 Effective $s = 1/2$ Hamiltonian 106
4.6.3 Conclusions 107
4.7 Summary 107

4.1 Introduction

Magnetic anisotropy, combined with low dimensionality or geometrical frustration, can give rise to fractional excitations. A prominent example of such fractionalization is the XXZ spin-1/2 antiferromagnetic chain, where a single magnon with $|S^z| = 1$ dissociates into two propagating domain walls, or spinons, each with $|S^z| = 1/2$ [103, 104]. Another notable instance is the emergence of magnetic monopoles in spin ice pyrochlores, where a microscopic magnetic dipole splits into two effective magnetic charges [30]. Additionally, exotic Majorana fermions can arise in the Kitaev honeycomb-lattice model with anisotropic, bond-dependent interactions [105].

Conversely, the fusion of multiple integer quasiparticles into a composite excitation represents the opposite process. The formation of bound magnon pairs in ferromagnets is a prominent example of such a phenomenon [106–109]. In the literature, these composite magnetic excitations are commonly referred to as multimagnon bound states [110–129]. However, just as fractional magnetic excitations exhibit diverse classifications, composite quasiparticles can also be categorized into distinct types.

In this study, we focus on a specific family of composite excitations: **longitudinal magnons** [130]. Unlike conventional magnons, these proposed modes possess a large angular momentum, $|S^z| = 2S$. Their emergence in collinear ferro- and antiferromagnets with $S \geq 1$ is driven by strong single-ion anisotropy of the easy-axis type[1]:

$$\hat{\mathcal{H}} = \hat{\mathcal{H}}_{\text{ex}} - D\sum_i (S_i^z)^2\,, \tag{4.1}$$

where $\hat{\mathcal{H}}_{\text{ex}}$ describes exchange interactions. The spin model (4.1) features a continuous rotation symmetry about the z axis, which leads to conservation of the z component of the total spin. As a result, for zero or weak anisotropy the low-energy excitation spectrum consists of conventional magnons with integer quantum spin numbers $S^z = -1$ for ferromagnets and $S^z = \pm 1$ for antiferromagnets [49, 131]. On the other hand, in the opposite limit $D/|J| \gg 1$ where J is the typical exchange constant, the lowest-energy excitations are spin reversals: $|\pm S\rangle \to |\mp S\rangle$. Given their quantum spin number $S^z = \pm 2S$, the longitudinal magnons can also be described as bound states of $2S$ magnons.

The theoretical prediction of new magnetic excitations in the easy-axis ferromagnets, induced by the single-ion anisotropy, dates back to the 1970's. Besides exchange bound states, a spin-S ferromagnet (4.1) exhibits an additional branch of two-magnon bound states called single-ion bound states [111, 112, 115]. The term 'two-magnon single-ion bound states' has been carried over to the experimental studies, which so far have mostly focused on the spin-1 magnetic materials [116–118, 122, 125, 129, 132]. Note that for $S = 1$ the two magnon bound states is the only possible type of single-ion excitation.

4.1.1 Magnon bound-state classification

For spins $S > 1$, the Hilbert space associated to multi-magnon bound states expands, allowing for several types of single-ion bound states. Their classification can be easily

[1] We will see in Sec. 4.6 that the longitudinal magnons may also appear in materials with easy-plane single-ion anisotropy.

understood from the large-D limit. A schematic picture of the low-energy excitations is shown in Fig. 4.1. For $D \gg |J|$, one-magnon excitations with $|S^z| = 1$ have energy $E_1 \simeq D(2S-1)$, where we keep only the largest anisotropy term contribution, and omit the dispersive part $\sim O(JS)$. Within the same accuracy, the two magnon states in the continuum are of energy $E_2 \simeq 2D(2S-1)$. A pair of magnons attracted by the exchange interactions lower their energy by $\sim O(J)$ compared to the states in the continuum but leave the anisotropic part intact: $E_2^{\mathrm{EB}} \simeq 2D(2S-1)$. In addition, there are three families of single-ion bound-states:

(i) Two magnons on the same site, Fig. 4.1(e), have $E_2^{\mathrm{SI}} \simeq 4D(S-1)$, which is lower than E_2 by $2D$. Therefore, the easy-axis anisotropy promotes creation of bound magnon pairs with $|S^z| = 2$.

(ii) A full spin flip or $2S$-magnon bound state, Fig. 4.1(f), costs no magnetic anisotropy (4.1) and acquires energy solely due to the broken exchange bonds: $E_{2S}^{\mathrm{SI}} = O(JS^2)$. These are **the longitudinal magnons**.

(iii) An $n-$magnon single-ion bound state with $|S^z| = n$ for intermediate $2 < n < 2S$ can also appear. Its energy is $E_n^{\mathrm{SI}} \simeq D(2S-n)n$, which is lower than the energy E_n of n independent magnon states in the continuum. These states are not included to Fig. 4.1.

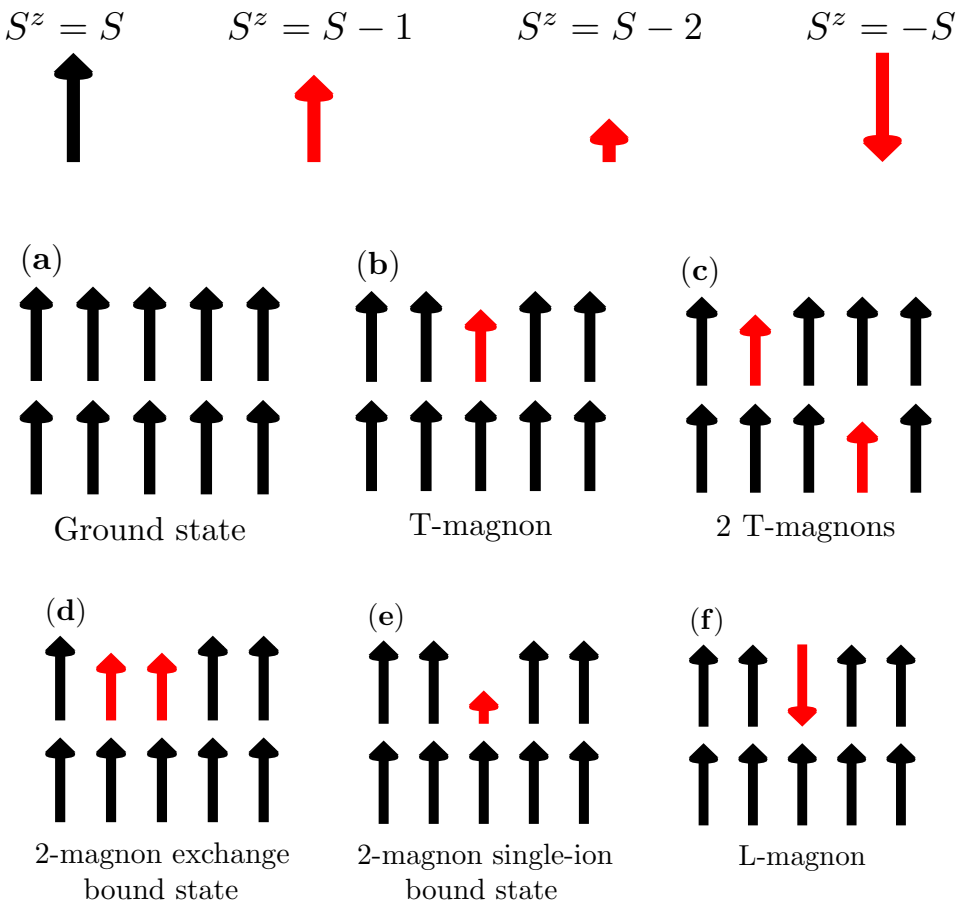

Figure 4.1: Schematic representation of the magnetic structure (a) and low-lying excitations (b-f) in the spin-S easy-axis ferromagnet. The top row shows a chart for different quantum states of a single spin.

For $S = 1$, the single-ion bound states of types I and II are the same. For $S = 3/2$, there are no states of the third type. However, for $S \geq 2$ all three types of single-ion bound states can occur. The single-ion bound states can equally appear in ferro- and antiferromagnets, whereas the exchange binding of magnons relies on the sign of the exchange interactions [106, 107, 114].

4.1.2 Observations

The two-magnon single-ion bound states have been observed experimentally in FeI_2 [116, 118, 122, 125], $FeBr_2$ [117] and $Na_2BaNi(PO_4)_2$ [129] with effective spins $S = 1$, and in CoF_2 with $S = 3/2$ [113]. The recent discovery of $|S^z| = 4$ excitations in the spin-2 antiferromagnets $FePS_3$ [123] and $FePSe_3$ [124] gives a clear evidence of the type-II single-ion bound states in the large-S magnetic materials. A signature of the 3-magnon resonances, type-III states, has been also found for $FePSe_3$ [124].

For $D \gg |J|$ and arbitrary $S \geq 1$, the type-II bound states become the lowest energy excitations across all spin subsectors. This fact, together with similarity in their theoretical description, allow us to group these excitations with a varying multipolar moment $|S^z| = 2S$ into a separate class of magnetic quasiparticles in strongly anisotropic collinear magnets. Their name stems from an observation that irrespective of the value of their angular moment S^z, the type-II single-ion bound states contribute to the longitudinal component of the dynamical structure factor $S^{zz}(\mathbf{q}, \omega)$, as we shall see in Sec. 4.3.6. To clearly distinguish the longitudinal or L-magnons from ordinary (transverse) magnons the latter are labeled as T-magnons.

In this work we develop and compare several theoretical approaches that can be used to study the L-magnons. The calculations are performed for several spin models, which allow us to check the limits of applicability for each theoretical method and determine the range of microscopic parameters where L-magnons exist as well-defined excitations. Using the multiboson representation of spins, we also compute the lifetimes of these excitations for $S = 1$, thus describing the evolution of their stability from large to weak anisotropy. The chapter is organized as follows. Section 2 elaborates briefly on some experimental measurements of the L-magnons and how they motivated our theoretical work. Section 3 describes an effective model in the strong-coupling regime, for a spin-S magnet across the honeycomb and the square lattices. Section 4 presents a general analysis in the $S = 1$ square-lattice, ferro- and antiferromagnetic. Section 5 addresses the $S = 1$ triangular antiferromagnetic case under strong magnetic field. Section 6 explores the appearance of L-magnons as anti-bound states. Section 7 provides with a summary.

4.2 Experimental motivation

Easy axis single-ion anisotropy is common in iron and nickel-based magnets and their sibling, where the $3d$ shell of metallic ions is the outer one, causing the crystal-field effect to be stronger than the LS coupling. It is particularly the case of the $S = 2$ antiferromagnets $FePS_3$ and $FePSe_3$, which host the L-magnons. These compounds belong to the van der Waals (vdW) magnets MPX_3, where M is a transition metal *e.g.* Mn, Fe, Co or Ni, and X is a chalcogene *e.g.* S, Se or Te. It is also the case of the $S = 1$ antiferromagnet $Na_2BaNi(PO_4)_2$.

4.2.1 van der Waals magnets $FePX_3$

The vdW magnets comprise insulating or semi-conducting compounds with a honeycomb lattice of spins. They feature short-range exchange interactions, with competing ferro- and antiferromagnetic bonds and dominant intra-plane couplings, in addition to a strong single-ion anisotropy [133, 134].

$FePS_3$ and $FePSe_3$ are vdW magnets with magnetic Fe^{2+} ions carrying an effective spin $S = 2$. They display antiferromagnetic order below the Néel temperatures 118 K and 106 K respectively [135]. They feature J_1–J_2–J_3 exchange interactions with negligible interplane coupling, in addition to a single-ion anisotropy of the easy-axis type. In both compounds, the ordered phase defines a zigzag structure of ferromagnetic spin chains along the a axis, which are antiparallel along the b axis with spins pointing out of the plane (along the c axis), see Fig. 4.2. In this scheme, each magnetic unit cell contains four atoms.

Interestingly, multiple high angular-momentum energy excitations with $S^z = \pm 4$ have been experimentally observed by optical spectroscopy first in $FePS_3$ and then in $FePSe_3$, Fig. 4.3, and the corresponding $k = 0$ modes lie in the high-energy range $\sim$ 55meV. In the S compound, one clear branch was observed below the four-magnon continuum at $k = 0$, with approximately a four-time larger Zeeman splitting than the standard antiferromagnetic resonance of a single magnon. In the Se compound, two such branches were observed below the $k = 0$ continuum, raising questions about their nature and the origin of their splitting.

In our published work on $FePSe_3$ [124], we have given theoretical evidence that the observed branches correspond to longitudinal magnons. This enabled an estimation of the microscopic constants J_i's and D, which have been confirmed by later experimental fits. We have also reinterpreted the single $|S^z| = 4$ magnon branch observed in $FePS_3$ [123] not as a localized excitation, but as the lowest branch of a split pair, the upper branch of which overlaps with the four-magnon continuum.

Both compounds feature the low-energy Hamiltonian

$$\hat{\mathcal{H}} = \sum_{n=1}^{3} J_n \sum_{\langle i,j \rangle_n} \mathbf{S}_i \cdot \mathbf{S}_j - D \sum_i S_i^{z2} - H \sum_i S_i^z \,, \tag{4.2}$$

with exchange interaction up to the third neighbors, and $D > 0$.

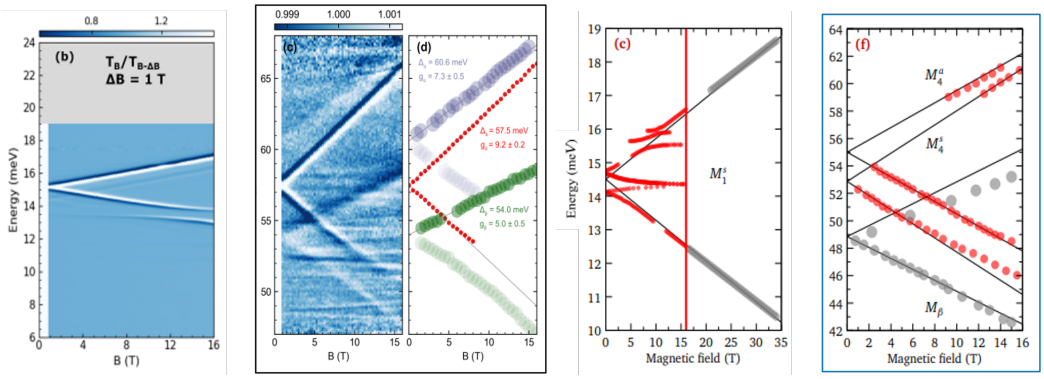

Figure 4.3: Magneto-transmission measurements at $k = 0$ of $FePS_3$ (left) [123] and $FePSe_3$ (right) [124].

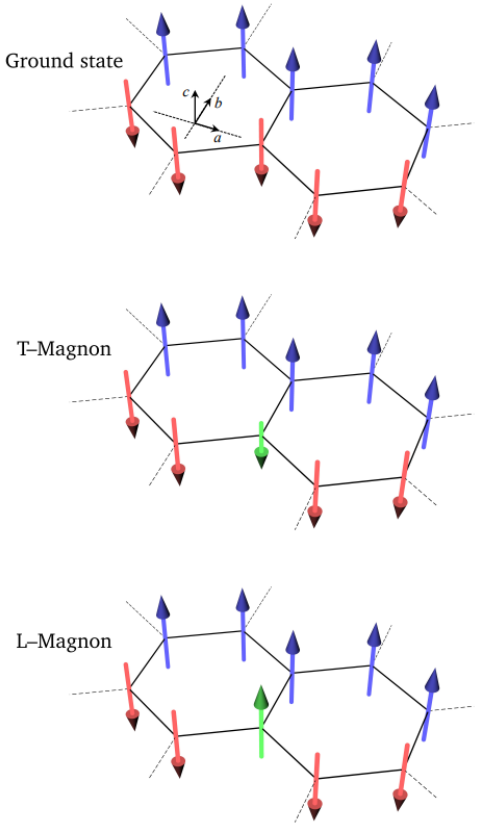

Figure 4.2: Cartoon representation of T- and L-magnons localized on a single lattice site (green arrow). Top panel: a collinear zigzag antiferromagnetic structure in $FePSe_3$ and $FePS_3$ materials. Middle panel: an ordinary transverse or T-magnon with $|\Delta S^z| = 1$. Bottom panel: a longitudinal or L-magnon with $|\Delta S^z| = 2S$ ($= 4$ for $S = 2$ of Fe^{2+} ions). Extracted from Ref. [124].

4.2.1.1 $FePS_3$

$FePS_3$ has a richer literature with a relatively better-known microscopic parameters and spectra from preceding spectroscopic experiments [40, 136, 137]. The magnetic iron ions form honeycomb layers stacked following the monoclinic crystalline arrangement [138]. Accordingly, the coupling constants in this compound are [40]:

$$J_1 = -2.92 \text{ meV}\,, \quad J_2 = 0.44 \text{ meV}\,, \quad J_3 = 1.1 \text{ meV}\,, \quad D = 3.28 \text{ meV}. \tag{4.3}$$

We note that this set of parameters is obtained by further including a biquadratic exchange in the Hamiltonian (4.2), in order to fit the magnon dispersion [40]. The recent experiments of magneto-transmission (IR transmission spectroscopy in high magnetic field) observed the conventional semi-classical antiferromagnetic resonances ω_{AFM} at $\sim$ 15.1 meV and $\sim$ 39.6 meV, respectively, of a single magnon at $k = 0$. Under magnetic field H, these resonances split into two branches by the Zeeman effect as

$$\omega = \omega_{\text{AFM}} \pm HS^z. \tag{4.4}$$

Moreover, a high-energy mode at $\sim$ 57.5 meV appears to exhibit a four-time larger Zeeman splitting, approximately. This indicates a four-time larger g factor , thus an excitation

carrying $S^z = \pm 4$ in contrast to $S^z = \pm 1$ for the conventional magnons. The first interpretation of such high angular-momentum mode argued in favor of a classical Ising excitation of broken exchange bonds, led by a localized spin reversal $|2\rangle \to |-2\rangle$. A first estimate of its energy could be given by the classical energy of a reversed spin:

$$\Delta_4 = 2S^2(-J_1 + 2J_2 + 3J_3) = 56.8 \text{ meV} \tag{4.5}$$

in zero field, in good agreement with the observation. The reanalysis of the experimental data from Ref. [123] showed the presence of a second line at 60.6 meV that exhibits about a four-time splitting. Whereas the four-magnon level lies at energies $\sim 4 \times 15.1 = 60.4$ meV, such a resonance overlaps with the onset of the four-magnon continuum, explaining its weak signal.

4.2.1.2 $FePSe_3$

Similar observations were made in the spectrum of the sister compound $FePSe_3$, which exhibits a rhombohedral stacking of the honeycomb layers [138]. The $k = 0$ spectrum showed the conventional antiferromagentic resonances ω_{AFM} at ~ 14.5 meV and 34.6 meV, and two high angular-moementum modes at ~ 52.6 meV and 55 meV, respectively. These latter modes show a four-time larger Zeeman splitting in comparison to one magnons, and are distinctively located below the four-magnon continuum, estimated at ~ 58 meV.

There is need to overcome the classical picture of a localized spin reversal in order to explain the two distinct modes at $k = 0$. The microscopic parameters were also unknown for this compound by the time Ref. [124] was being edited [2].

The first route to treat this problem starts from the so-called *strong-coupling* picture, where we assume a large D. In such a regime, the exchange interactions are a perturbation to the single-ion anisotropy. This latter defines an unperturbed subspace of fully polarized spins $|\pm 2\rangle$, where spin reversals $S^z \to -S^z$ do not cost any energy. The degeneracy of this free reversal is lifted by the transverse exchange interaction terms. Therefore, the energy associated to the spin reversal can be determined from an expansion in powers of the small parameters $|J_i|/D$. This will be tackled in Sec. 4.3.

4.2.2 $Na_2BaNi(PO_4)_2$

A recent work evidenced the appearance of longitudinal magnons in the easy-axis spin-1 triangular antiferromagnet $Na_2BaNi(PO_4)_2$, with dominant easy-axis single-ion anisotropy [129, 132]. The interesting feature in the experimental data is the signature of a spin-nematic phase below a saturation field of $\sim 2T$. Such a phase is brought about by the condensation of a 2-magnon single-ion bound-state. This represents the first experimental proof of a spin nematic and opens the route for new exotic phases in classically-ordered magnets. Section 4.5 of this chapter will address the energy and condensation of the L-magnons. We will present preliminary results that would allow to characterize this exotic phase systematically, using the theoretical apparatus elaborated in Sec.4.4.

[2] A concurrent work by Chen *et al.*, based on a fit of neutron scattering data, obtained another set of microscopic parameters for $FePSe_3$ [139]

4.3 Strong-coupling expansion

4.3.1 Presentation

The strong-coupling regime describes the spin model (4.2) with large $D/|J_i|$. Practically, the Hamiltonian is split into an unperturbed part $\hat{\mathcal{H}}_0$ and a perturbation $\hat{\mathcal{V}}$ as:

$$\begin{aligned} \hat{\mathcal{H}} &= \hat{\mathcal{H}}_0 + \hat{\mathcal{V}} \quad , \\ \hat{\mathcal{H}}_0 \ &= -D\sum_i (S_i^z)^2 \quad , \quad \hat{\mathcal{V}} \ = \sum_{\langle i,j\rangle} \sum_{\alpha,\beta} J_{\alpha\beta}\ S_i^\alpha S_j^\beta, \end{aligned} \tag{4.6}$$

where we assume exchange interactions involving nearest neighbors only. The situation of second, third, ... neighbors will be discussed in the next subsection. Yet for the exchange coupling $J_{\alpha\beta}$ we allow for an anisotropic XXZ type, where we assume non-vanishing $J_{xx} = J_{yy} =: J$ and J_{zz} . The purpose is to determine the dispersion of the longitudinal magnons in the low-lying energy spectrum of $\hat{\mathcal{H}}$ for small $|J_i|/D$.

We first rewrite the perturbation as:

$$\hat{\mathcal{V}} = \sum_{\langle i,j\rangle} \Big[J_{xy}(S_i^x S_j^x + S_i^y S_j^y) + J S_i^z S_j^z \Big] = \sum_{\langle i,j\rangle} \left[\frac{J_{xy}}{2}\big(S_i^+ S_j^- + S_i^- S_j^+\big) + J S_i^z S_j^z \right]. \tag{4.7}$$

Here, the unperturbed ground state pertaining to $\hat{\mathcal{H}}_0$ is determined by the factorized form

$$|\mathrm{GS}_0\rangle = \bigotimes_i |S_i^z = \pm S\rangle\,, \tag{4.8}$$

with a degeneracy of 2^N for N lattice sites, and the unperturbed energy reads:

$$E_0 = -NDS^2. \tag{4.9}$$

Introducing the exchange interactions as a perturbation conserves the $U(1)$ rotation symmetry with respect to the z axis. As we will see, it induces an effective interaction that allows us to lift the ground-state degeneracy and classify the energy levels with respect to the quantum number $S^z_{\mathrm{tot}} = \sum_i S_i^z$, irregardless of the sign of exchange couplings.

We deploy the perturbation theory in the Brillouin-Wigner framework, as presented in Sec. 3.1. Since the interaction $\hat{\mathcal{V}}$ is quadratic in the spin operators, in the first few orders it only acts on nearest-neighbor bonds $|\pm S, \pm S\rangle$. Therefore, we start with the bond basis $\mathcal{B}_0 = \{|\pm S, \pm S\rangle\}$, where we have

$$\langle \mathrm{GS}_0|\,\hat{\mathcal{V}}\,|\mathrm{GS}_0\rangle = J_{zz}S^2 \begin{pmatrix} 1 & & & \\ & -1 & & \\ & & -1 & \\ & & & 1 \end{pmatrix}_{|S,S\rangle,|S,-S\rangle,|-S,S\rangle,|-S,-S\rangle} \tag{4.10}$$

which clearly favors a specific alignment of adjacent spins as a function of the sign of J_{zz}:

(i) for $J_{zz} > 0$, the spins pick up a negative alignment to minimize the energy, yielding a Néel order: $|GS\rangle = \bigotimes_n |S_n^z = e^{in\pi}S\rangle$,

(ii) for $J_{zz} < 0$, they pick up a positive alignment, giving the fully polarized ferromagnetic state: $|GS\rangle = \bigotimes_n |S_n^z = S\rangle$ with fixed $\epsilon = 0$ or 1 for the lattice.

In either case, the perturbation to the first order reduces the degeneracy from 2^N to 2. A subsequent application of a finite magnetic field is sufficient to obtain a unique ground state. The matrix (4.10) defines the first-order effective interaction in the unperturbed space generated by $\mathcal{B}_0$. Its diagonal form only encodes the potential energy. Off-diagonal elements in the effective interaction only appear in the $2S^{\text{th}}$ order in the case of quadratic exchange. Intermediate orders $1, .., 2S-1$, solely renormalize the ground-state energy without level splitting.

4.3.2 Effective $s = 1/2$ Hamiltonian

The polarized spins $|S_i^z = \pm S\rangle$ define the lowest-energy states of the easy-axis anisotropy. This space is isomorphic to the spin-1/2 up-down space:

$$\left(|S\rangle, |-S\rangle\right)_i \to \left(|\uparrow\rangle, |\downarrow\rangle\right)_i . \tag{4.11}$$

Therefore, the problem of lifting the degeneracy for the lowest energy subspace of spins S amounts to solving an effective Hamiltonian in terms of spins $s = 1/2$. The correspondence between the different operators is defined by:

$$s_i^z \leftrightarrow (2S)^{-1} S_i^z , \qquad s_i^{\pm} \leftrightarrow (S_i^{\pm})^{2S} \tag{4.12}$$

where the operators s^α, $\alpha = x,\ y,\ z$ are defined in (2.26), with $s_i^{\pm} = s_i^x \pm s_i^y$. Subsequently, the effective Hamiltonian we search for can be expressed exclusively in the spin-1/2 algebra. Extended to the lattice, this describes an *effective exchange* interaction of pseudo-spins of the form:

$$\hat{\mathcal{H}}_{\text{eff}} = \sum_{\langle ij \rangle} \Big[J_{\parallel} s_i^z s_j^z + J_{\perp} \left(s_i^x s_j^x + s_i^y s_j^y \right) \Big] \tag{4.13}$$

where the $U(1)$ rotation symmetry around the z-axis is conserved by virtue of (4.12). The effective constants $J_{\parallel,\perp}$ are power series of J/D.

Effective spin-1/2 Hamiltonians similar to the above expression have been previously derived for a number of specific models and spin values, see, for example, [124, 140, 141].

In the following, we construct the effective Hamiltonian, due to quadratic exchange, in the particular case of $S = 1$, and obtain the lowest energy levels. We then duplicate this approach for the spin values $S = 3/2,\ 2$ and $5/2$. To this aim, we use the energy differences $E_n - E_0$ between the degenerate subspace and intermediate spaces.

We will also make use of the matrix expression of the bilinear forms of spin-1/2 operators:

$$s_i^z s_j^z = \frac{1}{4} \begin{pmatrix} 1 & & & \\ & -1 & & \\ & & -1 & \\ & & & 1 \end{pmatrix} , \qquad s_i^x s_j^x + s_i^y s_j^y = \frac{1}{2} \begin{pmatrix} 0 & .. & .. & 0 \\ : & 0 & 1 & : \\ : & 1 & 0 & : \\ 0 & .. & .. & 0 \end{pmatrix} . \tag{4.14}$$

Additionally, for simplification, we distinguish longitudinal and transverse exchanges by writing the perturbation (4.7) as:

$$\hat{\mathcal{V}} = \sum_{\langle i,j \rangle} (\hat{V}_1 + \hat{V}_2),$$

$$\hat{V}_1 = \frac{1}{2} J \left(S_i^+ S_j^- + S_i^- S_j^+ \right), \qquad \hat{V}_2 = J_{zz} S_i^z S_j^z , \tag{4.15}$$

where site indices are skipped in the notation of $\hat{V}_1$ and $\hat{V}_2$.

The lowest order that produces off-diagonal terms is the $2S^{\text{th}}$ one. If we intend to include all bond effects, we may however go beyond that limit. This is true for the $(2S+1)^{\text{th}}$ order for instance. But in the $(2S+2)^{\text{th}}$ order, second-neighbor effects get involved, which generates multi-site off-diagonal terms in the Hamiltonian. There are also multi-spin terms contributing to the diagonal elements in the effective subspace. One such example is the biquadratic interaction term $(s_1^z s_2^z)(s_2^z s_3^z)$ for three spins on a trimer. As these generally depend on the specific lattice geometry, they will be omitted in our simple spin-1/2 model. The results we will obtain hold subsequently for all sorts of lattices.

4.3.3 Spin-1 magnet

4.3.3.1 Third-order Hamiltonian

In the particular case of spins $S = 1$, the longitudinal magnons can be viewed as two-magnon single-ion bound states. They are described by a second-order spin-flip process. In view of the previous remarks, we derive the effective Hamiltonians to the third order in the strong-coupling expansion based on the interaction (4.6). Using the degenerate perturbation theory as presented in Chapter 2, the partial effective Hamiltonians to orders 1–3 are given respectively by:

$$\hat{\mathcal{H}}_{\text{eff}}^{(1)} = P_0 \hat{V}_2 P_0 = J_{zz} \begin{pmatrix} 1 & & & \\ & -1 & & \\ & & -1 & \\ & & & 1 \end{pmatrix} = 4 J_{zz} s_i^z s_j^z , \tag{4.16}$$

thus $\Delta E^{(1)} = \pm J_{zz}$,

$$\begin{aligned} \hat{\mathcal{H}}_{\text{eff}}^{(2)} = P_0 \hat{V}_1 \sum_n \frac{1}{E_0 - E_n} P_n \hat{V}_1 P_0 \quad &= J \frac{1}{-2D} J \begin{pmatrix} 0 & .. & .. & 0 \\ : & 1 & 1 & : \\ : & 1 & 1 & : \\ 0 & .. & .. & 0 \end{pmatrix} \\ &= -\frac{1}{2} \frac{J^2}{D} \left(\frac{1}{2} I_4 + 2 \left[s_i^x s_j^x + s_i^y s_j^y - s_i^z s_j^z \right] \right), \end{aligned} \tag{4.17}$$

where I_4 denotes the unit matrix. And:

$$\begin{aligned} \hat{\mathcal{H}}_{\text{eff}}^{(3)} &= -P_0 \hat{V}_1 \sum_n \frac{\Delta E^{(1)}}{(E_0 - E_n)^2} P_n \hat{V}_1 P_0 + P_0 \hat{V}_1 \sum_{n,m} \frac{1}{E_0 - E_n} P_n \hat{V}_2 P_m \frac{1}{E_0 - E_m} P_m \hat{V}_1 P_0 \\ &= -J \frac{-J_{zz}}{(-2D)^2} J \begin{pmatrix} 0 & .. & .. & 0 \\ : & 1 & 1 & : \\ : & 1 & 1 & : \\ 0 & .. & .. & 0 \end{pmatrix} + 0 \\ &= \frac{J^2 J_{zz}}{4D^2} \left(\frac{1}{2} I_4 + 2 \left[s_i^x s_j^x + s_i^y s_j^y - s_i^z s_j^z \right] \right). \end{aligned} \tag{4.18}$$

For all orders we used the matrix elements of the ladder operators, Eq. (2.36).

4.3.3.2 Effective bond interaction

Although we are interested in coherent modes defined throughout the lattice, we can examine the effective Hamiltonian for two spins (a bond) in the 4×4 matrix representation:

$$\hat{\mathcal{H}}^{S=1}_{\text{eff},,\langle i,j\rangle} = \begin{pmatrix} J_{zz} & & & \\ & -J_{zz} - \frac{J^2}{2D} + \frac{J^2 J_{zz}}{4D^2} & -\frac{J^2}{2D} + \frac{J^2 J_{zz}}{4D^2} & \\ & -\frac{J^2}{2D} + \frac{J^2 J_{zz}}{4D^2} & -J_{zz} - \frac{J^2}{2D} + \frac{J^2 J_{zz}}{4D^2} & \\ & & & J_{zz} \end{pmatrix}, \tag{4.19}$$

which is diagonalized similarly to (2.28):

$$\hat{\mathcal{H}}^{S=1}_{\text{eff},\langle i,j\rangle} = \begin{pmatrix} 1 & & & \\ & \frac{1}{\sqrt{2}} & \frac{1}{\sqrt{2}} & \\ & \frac{1}{\sqrt{2}} & -\frac{1}{\sqrt{2}} & \\ & & & 1 \end{pmatrix} \begin{pmatrix} J_{zz} & & & \\ & -J_{zz} - \frac{J^2}{D} + \frac{J^2 J_{zz}}{2D^2} & & \\ & & -J_{zz} & \\ & & & J_{zz} \end{pmatrix} \begin{pmatrix} 1 & & & \\ & \frac{1}{\sqrt{2}} & \frac{1}{\sqrt{2}} & \\ & \frac{1}{\sqrt{2}} & -\frac{1}{\sqrt{2}} & \\ & & & 1 \end{pmatrix}. \tag{4.20}$$

Thus, at the bond level, this effective interaction further splits the degeneracy of the unperturbed ground state defined in (4.8), in function of the sign of J_{zz}.

(i) $J_{zz} > 0$: the ground state is a singlet defined by a symmetric superposition of antiparallel spins $|GS\rangle = (|1,-1\rangle + |-1,1\rangle)/\sqrt{2}$, with energy $E_0 = -J_{zz} - J^2/D + J^2 J_{zz}/(2D^2)$. The first excited level is the antisymmetric state $(|1,-1\rangle - |-1,1\rangle)/\sqrt{2}$ with energy $E_1 = -J_{zz}$. Above these levels lays a doubly-degenerate excited state of parallel spins, with energy $E_2 = J_{zz}$.

(ii) $J_{zz} < 0$: the ground-state is the doubly-degenerate ferromagnetic state, with energy $E_0 = J_{zz}$. The first excited state is the symmetric superposition of antiparallel spins, with energy $E_1 = -J_{zz} - J^2/D + J^2 J_{zz}/(2D^2)$, assuming $J \sim J_{zz}$. The second excited state is the antisymmetric superposition of parallel spins, with energy $E_2 = -J_{zz}$.

In either case, the perturbation to the second order is sufficient to lift the degeneracy of the subspace of antiparallel spins. Nonetheless, the double degeneracy of the ferromagnetic state sustains. This is a remnant of the $U(1)$ symmetry of the total Hamiltonian. One should resort to another interaction that breaks such a symmetry in order to fully discriminate this level, *e.g.* by switching on a small magnetic field.
Note that all energies above should be augmented by the unperturbed energy due to the single-ion Hamiltonian: $E_0^{(0)} = -ND$.

4.3.3.3 Effective Hamiltonian

Back to the level of the lattice, the effective Hamiltonian to the third order for $S = 1$ reads:

$$\hat{\mathcal{H}}^{S=1}_{\text{eff}} = -N_z \left(\frac{J^2}{4D} - \frac{J^2 J_{zz}}{8D^2}\right) + \sum_{\langle i,j\rangle} \left[\left(\frac{-J^2}{D} + \frac{J^2 J_{zz}}{2D^2}\right)\left(s_i^x s_j^x + s_i^y s_j^y\right) + \left(4J_{zz} + \frac{J^2}{D} - \frac{J^2 J_{zz}}{2D^2}\right) s_i^z s_j^z \right], \tag{4.21}$$

where N_z is the number of bonds in the lattice. The lowest energy levels of this effective interaction can be determined using the harmonic spin-wave theory applied to the lattice of pseudo-spins $s = 1/2$. The first excited state corresponds to transverse magnons in this lattice with $|\Delta s^z| = 1$, which describe longitudinal magnons in the original lattice of

spins $S = 1$ with $|\Delta S^z| = 2$. As seen in Sec. (2.4.2), both the ground-state energy and the magnon dispersion depend on the sign of J_{zz}, the lattice geometry and the underlying magnetic structure.

4.3.3.3.1 $J_{zz} > 0$

The entangled antiferromagnetic state $(|..,\uparrow,\downarrow,\uparrow,..\rangle + |..,\downarrow,\uparrow,\downarrow,..\rangle)/\sqrt{2}$ arising in the bond Hamiltonian is not an eigenstate of the effective lattice Hamiltonian (4.21). With the antiferromagnetic sign of J_{zz}, we approach the problem assuming a Néel state $|..,\uparrow,\downarrow,\uparrow,..\rangle$, as a classical ground state, and elaborate the spin-wave theory for a spin-1/2 antiferromagnet.

The routine use of the Holstein-Primakoff representation, followed by a Fourier transformation to momentum space and then a canonical Bogolyubov transformation, yield the energy spectrum for the transverse magnons in the lattice of pseudospins 1/2 – that are the longitudinal magnons in the $S = 1$ lattice:

$$\varepsilon^L_{\mathbf{k}} = 2\sqrt{\left(4J_{zz}+\frac{J^2}{D}-\frac{J^2J_{zz}}{2D^2}\right)^2 - \left(\frac{-J^2}{D}+\frac{J^2J_{zz}}{2D^2}\right)^2 (\gamma^{\square}_{\mathbf{k}})^2}\,, \tag{4.22}$$

where $\gamma^{\square}_{\mathbf{k}}$ is given in (2.58). The estimation of the ground-state energy is given by the constant term in (4.21), with $N_z = 2N$, shifted by the contribution $O(s^2)$ of the longitudinal exchange and the zero-point magnon oscillations. These three terms are then added to the unperturbed energy of the single-ion Hamiltonian (4.9). This gives the energy per spin:

$$\begin{aligned} E^{\mathrm{AF}}_{\mathrm{gs}} &= -D - 2\left(\frac{J^2}{4D}-\frac{J^2J_{zz}}{8D^2}\right) - \frac{1}{2}\left(4J_{zz}+\frac{J^2}{D}-\frac{J^2J_{zz}}{2D^2}\right) \\ &\quad + \frac{1}{2N}\sum_{\mathbf{k}}\left(\varepsilon^L_{\mathbf{k}} - \left[8J_{zz}+\frac{2J^2}{D}-\frac{J^2J_{zz}}{D^2}\right]\right) \\ &= -D - 6J_{zz} - \frac{2J^2}{D} + \frac{J^2J_{zz}}{D^2} + \frac{1}{2N}\sum_{\mathbf{k}}\varepsilon^L_{\mathbf{k}}. \end{aligned} \tag{4.23}$$

Graphical representations of the L-magnon energy and the ground-state energy are shown in Sec. , where they are compared to other analytical methods.

4.3.3.3.2 $J_{zz} < 0$

In the case of ferromagnetic exchange, we start with the fully polarized ground state of pseudo-spins $|..,\uparrow,\uparrow,..\rangle$. The low-lying excitation is again the transverse magnon for this pseudo-spins, which is the longitudinal magnon for $S = 1$ spins. Its energy dispersion is obtained exactly (see Chapter II) as:

$$\varepsilon^L_{\mathbf{k}} = 2\left(\left|4J_{zz}+\frac{J^2}{D}-\frac{J^2J_{zz}}{2D^2}\right| + \left[\frac{-J^2}{D}+\frac{J^2J_{zz}}{2D^2}\right]\gamma^{\square}_{\mathbf{k}}\right), \tag{4.24}$$

with the same definition of $\gamma^{\square}_{\mathbf{k}}$, Eq. (2.58). The ground-state energy is the sum of the unperturbed energy (4.9) with the constant term in (4.21) and the contribution $O(s^2)$ of

the longitudinal exchange:

$$\begin{aligned} E_{\text{gs}}^{\text{F}} &= -D - 2\left(\frac{J^2}{4D} - \frac{J^2 J_{zz}}{8D^2}\right) + \frac{1}{2}\left(4J_{zz} + \frac{J^2}{D} - \frac{J^2 J_{zz}}{2D^2}\right) \\ &= -D + 2J_{zz}\,, \end{aligned} \tag{4.25}$$

which is identically the exact ground-state energy for a ferromagnet.
Note that the above results are obtained in the nearest-neighbor model. In the case of several exchanges as, *e.g*, a spin Hamiltonian with the form (4.2), the strong-coupling expansion applies to each of the exchange bonds (J_i) separately. This approach will be thoroughly explored in the next section.

4.3.4 Spin-2 magnet

After a theoretical detour, we have constructed so far an effective simple model for the appearance of L-magnons in a spin-S compound in the large-D limit. We illustrated this approach for the $S = 1$ square lattice. Now, we would like to complete on the experimental motivation discussed in Sec. 4.2.1.2. Practically, we address the spin Hamiltonian of $FePSe_3$, Eq. (4.2), and obtain the L-magnon energy at $k = 0$ in the strong-coupling expansion. This will enable us to interpret the high-angular momentum modes spotted at ~ 52.6 meV and 55 meV.

4.3.4.1 Fifth-order Hamiltonian

We consider here the case of interacting spins $S = 2$. The longitudinal magnons are four-magnon single-ion bound states, described by a fourth-order hopping process. Similarly to the case of $S = 1$, we derive the following partial effective Hamiltonians to orders 1–5, based on the total Hamiltonian (4.6) and a perturbation of the additive form (4.15). In order to further simplify the derivation and comply with the real model of $FePSe_3$, we assume $J = J_{zz}$ such that the exchange interaction is isotropic.
We investigate a perturbation given by the exchange interaction of two spins, in the unperturbed bond space $(|\pm S, \pm S\rangle\,, |\mp S, \pm S\rangle)$. Given the permanent degeneracy of the ferromagnetic states $|S, S\rangle\,, |-S, -S\rangle$ as seen in the case $S = 1$, the only states of interest for the propagation of the L-magnons are the antiferromagnetic dimers $|\pm S, \mp S\rangle$, and the only matrix elements of interest for the dispersion of the magnons are the off-diagonal terms. Therefore, we restrict the derivation of the effective Hamiltonians here to the subspace generated by $(|2, -2\rangle\,, |-2, 2\rangle)$ as follows:

$$\hat{\mathcal{H}}_{\text{eff}}^{(1)} = P_0 \hat{V}_2 P_0 = \begin{pmatrix} -4J & 0 \\ 0 & -4J \end{pmatrix}\,, \tag{4.26}$$

thus $\Delta E^{(1)} = -4J$;

$$\hat{\mathcal{H}}_{\text{eff}}^{(2)} = P_0 \hat{V}_1 \sum_n \frac{1}{E_0 - E_n} P_n \hat{V}_1 P_0 = \begin{pmatrix} 2J & 0 \\ 0 & 2J \end{pmatrix} \frac{1}{-6D} \begin{pmatrix} 2J & 0 \\ 0 & 2J \end{pmatrix} = -\frac{2}{3}\frac{J^2}{D} \begin{pmatrix} 1 & 0 \\ 0 & 1 \end{pmatrix}\,, \tag{4.27}$$

thus $\Delta E^{(2)} = -\frac{2}{3}\frac{J^2}{D}$;

$$\begin{aligned}
\hat{\mathcal{H}}^{(3)}_{\text{eff}} &= -P_0\hat{V}_1\sum_n \frac{\Delta E^{(1)}}{(E_0-E_n)^2}P_n\hat{V}_1P_0 + P_0\hat{V}_1\sum_{n,m}\frac{1}{E_0-E_n}P_n\hat{V}_2P_m\frac{1}{E_0-E_m}P_m\hat{V}_1P_0 \\
&= -\begin{pmatrix}2J & 0\\ 0 & 2J\end{pmatrix}\frac{-4J}{(-6D)^2}\begin{pmatrix}2J & 0\\ 0 & 2J\end{pmatrix} \\
&\quad + \begin{pmatrix}2J & 0\\ 0 & 2J\end{pmatrix}\frac{1}{-6D}\begin{pmatrix}-J & 0\\ 0 & -J\end{pmatrix}\frac{1}{-6D}\begin{pmatrix}2J & 0\\ 0 & 2J\end{pmatrix} \\
&= \frac{1}{3}\frac{J^3}{D^2}\begin{pmatrix}1 & 0\\ 0 & 1\end{pmatrix}, \qquad (4.28)
\end{aligned}$$

$$\begin{aligned}
\hat{\mathcal{H}}^{(4)}_{\text{eff}} &= P_0\hat{V}_1\sum_{n,k,m}\frac{1}{E_0-E_n}P_n\hat{V}_1P_k\frac{1}{E_0-E_k}P_k\hat{V}_1P_m\frac{1}{E_0-E_m}P_m\hat{V}_1P_0 \\
&\quad + P_0\hat{V}_1\Bigg(\sum_{n,m}\frac{1}{E_0-E_n}P_n\hat{V}_2P_m\frac{1}{E_0-E_m}\left[\frac{\Delta E^{(1)}}{E_0-E_n}+\frac{\Delta E^{(1)}}{E_0-E_m}\right] \\
&\qquad -\sum_n\frac{\Delta E^{(2)}}{(E_0-E_n)^2}P_n \quad +\sum_n\frac{\left(\Delta E^{(1)}\right)^2}{(E_0-E_n)^3}P_n\Bigg)\hat{V}_1P_0 \\
&= \begin{pmatrix}2J & 0\\ 0 & 2J\end{pmatrix}\frac{1}{-6D}\begin{pmatrix}3J\\ 3J\end{pmatrix}\frac{1}{-8D}\begin{pmatrix}3J & 3J\end{pmatrix}\frac{1}{-6D}\begin{pmatrix}2J & 0\\ 0 & 2J\end{pmatrix} \\
&\quad + \begin{pmatrix}2J & 0\\ 0 & 2J\end{pmatrix}\frac{1}{-6D}(2(-4J)\frac{1}{-6D})\begin{pmatrix}-J_{zz} & 0\\ 0 & -J_{zz}\end{pmatrix}\frac{1}{-6D}\begin{pmatrix}2J & 0\\ 0 & 2J\end{pmatrix} \\
&\quad - \begin{pmatrix}2J & 0\\ 0 & 2J\end{pmatrix}\left(\frac{-2}{3}\frac{J^2}{D}\frac{1}{(-6D)^2}\right)\begin{pmatrix}2J & 0\\ 0 & 2J\end{pmatrix} \\
&\quad + \begin{pmatrix}2J & 0\\ 0 & 2J\end{pmatrix}\frac{(-4J)^2}{(-6D)^3}\begin{pmatrix}2J & 0\\ 0 & 2J\end{pmatrix} \\
&= -\frac{3^2.2^2}{6^2.8}\frac{J^4}{D^3}\underbrace{\begin{pmatrix}0 & 1\\ 1 & 0\end{pmatrix}}_{s_i^+s_j^- + s_i^-s_k^+} + \left(-\frac{3^2.2^2}{6^2.8}-\frac{2^5}{6^3}+\frac{2^3}{3.6^2}-\frac{2^6}{6^3}\right)\frac{J^4}{D^3}\begin{pmatrix}1 & 0\\ 0 & 1\end{pmatrix} \\
&= -\frac{1}{8}\frac{J^4}{D^3}\left(s_i^+s_j^- + s_i^-s_j^+\right) - \left(\frac{107}{216}\right)\frac{J^4}{D^3}\begin{pmatrix}1 & 0\\ 0 & 1\end{pmatrix}. \qquad (4.29)
\end{aligned}$$

In the fifth order, we count the process

$$|2,-2\rangle \xrightarrow{\hat{V}_1} |1,-1\rangle \xrightarrow{\hat{V}_2} |1,-1\rangle \xrightarrow{\hat{V}_1} |0,0\rangle \xrightarrow{\hat{V}_1} |-1,1\rangle \xrightarrow{\hat{V}_1} |-2,2\rangle$$

and its hermitian conjugate process, in addition to a correction from the fourth order. For simplicity, we will lump together all diagonal terms:

$$\hat{\mathcal{H}}^{(5)}_{\text{eff}} = P_0\hat{V}\sum_{n,k,m,l}\frac{1}{E_0-E_n}P_n\hat{V}P_k\frac{1}{E_0-E_k}P_k\hat{V}P_m\frac{1}{E_0-E_m}P_m\hat{V}P_l\frac{1}{E_0-E_l}P_l\hat{V}P_0$$

$$
\begin{aligned}
&-P_0\hat{V}_1\sum_{n,k,m}\left(\sum_{j=n,k,m}\frac{\Delta E^{(1)}}{E_0-E_j}\right)\frac{1}{E_0-E_n}P_n\hat{V}_1P_k\frac{1}{E_0-E_k}P_k\hat{V}_1P_m\frac{1}{E_0-E_m}P_m\hat{V}_1P_0\\
&+\text{diagonal terms.}\\
&=2\begin{pmatrix}2J&0\\0&2J\end{pmatrix}\frac{1}{-6D}\begin{pmatrix}-J&0\\0&-J\end{pmatrix}\frac{1}{-6D}\begin{pmatrix}3J\\3J\end{pmatrix}\frac{1}{-8D}\begin{pmatrix}3J&3J\end{pmatrix}\frac{1}{-6D}\begin{pmatrix}2J&0\\0&2J\end{pmatrix}\\
&-(-4J)\left(2\frac{1}{-6D}+\frac{1}{-8D}\right)\begin{pmatrix}2J&0\\0&2J\end{pmatrix}\frac{1}{-6D}\begin{pmatrix}3J\\3J\end{pmatrix}\frac{1}{-8D}\begin{pmatrix}3J&3J\end{pmatrix}\frac{1}{-6D}\begin{pmatrix}2J&0\\0&2J\end{pmatrix}\\
&+\beta\begin{pmatrix}1&0\\0&1\end{pmatrix}\qquad(\beta\text{ real})\\
&=\left(-\frac{2^3.3^2}{6^3.8}+\frac{4.11.2^2.3^2}{24.6^2.8}\right)\frac{J^5}{D^4}\begin{pmatrix}0&1\\1&0\end{pmatrix}+\beta'\begin{pmatrix}1&0\\0&1\end{pmatrix}\qquad(\beta'\text{ real})\\
&=\frac{3}{16}\frac{J^5}{D^4}\left(s_i^+s_j^-+s_i^-s_j^+\right)+\beta'\begin{pmatrix}1&0\\0&1\end{pmatrix}.
\end{aligned}
\tag{4.30}
$$

Therefore, one has the effective Hamiltonian to the fifth order in the 2×2 dimer space spanned by $(|\pm 2,\pm 2\rangle)$:

$$
\hat{\mathcal{H}}^{S=2}_{\text{eff},,\langle i,j\rangle}=E_0+\left(-\frac{1}{4}\frac{J^4}{D^3}+\frac{3}{8}\frac{J^5}{D^4}\right)\left(S_i^xS_j^x+S_i^yS_j^y\right)+\left(16J+\frac{4}{3}\frac{J^2}{D}-\frac{2}{3}\frac{J^3}{D^2}\right)S_i^zS_j^z. \tag{4.31}
$$

We ignore the constant energy E_0 and show only three leading terms in the effective longitudinal exchange.

4.3.4.2 Spin model for $FePX_3$ materials

In the following, we consider a single-ion $S=2$ antiferromagnet with first, second and third neighbor exchanges, described by the couplings constants $J_{1,2,3}$ respectively. In this case, the above derivation of the effective exchange couplings applies to each of the original exchange interactions mediated by J_i. The effective lattice Hamiltonian is thus described by an XXZ exchange for the three families of neighbors. For simplification, we introduce the notation for the effective couplings:

$$
\tilde{J}_n^{\perp}=-\frac{J_n^4}{4D^3}+\frac{3J_n^5}{8D^4}\,,\qquad \tilde{J}_n^z=16J_n+\frac{4J_n^2}{3D}-\frac{2}{3}\frac{J_n^3}{D^2} \tag{4.32}
$$

with $n=1,2,3$. Accordingly, the effective Hamiltonian reads:

$$
\hat{\mathcal{H}}_{\text{eff}}=\sum_{n=1}^{3}\sum_{\langle i,j\rangle_n}\left[\tilde{J}_n^{\perp}\left(S_i^xS_j^x+S_i^yS_j^y\right)+\tilde{J}_n^z\;S_i^zS_j^z\right] \tag{4.33}
$$

where $\langle i,j\rangle_n$ defines bond summation involving n^{th} neighbors. Alike the original spin Hamiltonian, the same ratio of the longitudinal exchange couplings $\tilde{J}_2^z/\tilde{J}_1^z\approx J_2/J_1$ and $\tilde{J}_3^z/\tilde{J}_1^z\approx J_3/J_1$ to leading order suggests a zigzag antiferromagnetic structure for the ground state of (4.33) in the lattice of pseudo-spins 1/2. Therefore, we will apply spin-wave theory in this stationary state, in order to obtain the dispersion of the L-magnons.

The lattice is described by antiparallel ferromagnetic chains AB ($\uparrow$) and CD($\downarrow$), Fig. 4.4. The magnetic unit cell contains four sites: A, B, C and D. Accordingly, we define

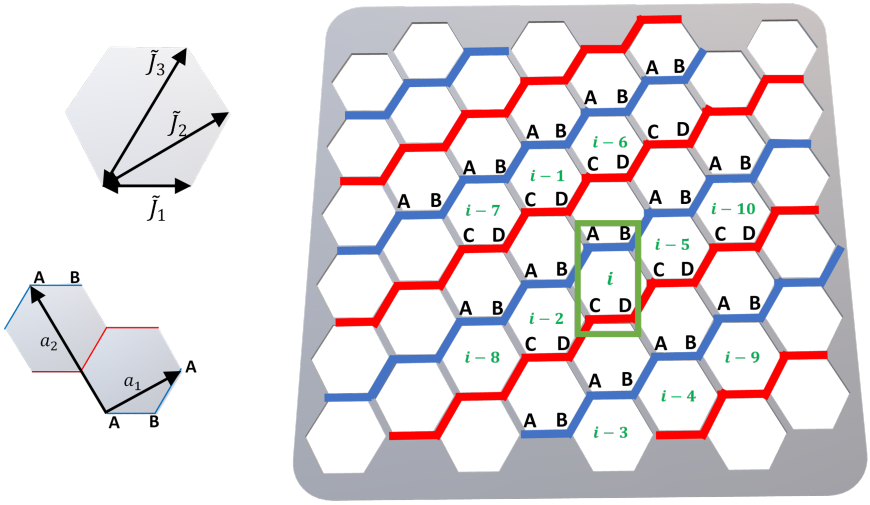
$\tilde{J}_3$
$\tilde{J}_2$
$\tilde{J}_1$
A B
a_2
a_1
A
A B
A B
A B

the general product rule in the local frame for parallel or antiparallel spins, in the harmonic approximation:

$$\underset{i\,j}{\uparrow\uparrow}:\ \tilde{J}\,\mathbf{S}_i\cdot\mathbf{S}_j=\tilde{J}^z S_i^z S_j^z+\frac{\tilde{J}^\perp}{2}(S_i^+ S_j^-+S_i^- S_j^+)=\tilde{J}^z S^2+S\left(-\tilde{J}^z[\alpha_i^\dagger\alpha_i+\beta_j^\dagger\beta_j]+\tilde{J}^\perp[\alpha_i^\dagger\beta_j+\beta_j^\dagger\alpha_i]\right)$$

$$\underset{i\,j}{\uparrow\downarrow}:\ \tilde{J}\,\mathbf{S}_i\cdot\mathbf{S}_j=-\tilde{J}^z S_i^z S_j^z-\frac{\tilde{J}^\perp}{2}(S_i^+ S_j^++S_i^- S_j^-)=-\tilde{J}^z S^2+S\left(\tilde{J}^z[\alpha_i^\dagger\alpha_i+\beta_j^\dagger\beta_j]-\tilde{J}^\perp[\alpha_i\beta_j+\alpha_i^\dagger\beta_j^\dagger]\right)$$

where the pairs of boson operators α and β are associated to sublattices i and j, respectively.

The second step is to perform Fourier transformation of the boson operators:

$$\alpha_i\ =\frac{1}{\sqrt{N}}\sum_{\mathbf{k}} e^{i\mathbf{k}.(\mathbf{r}_i+\mathbf{R}_\alpha)}\alpha_{\mathbf{k}}\,,\qquad \alpha=a,b,c,d \tag{4.38}$$

with the relative coordinate vectors:

$$\mathbf{R}_a=(0,0)\,,\quad \mathbf{R}_b=(1,0)\,,\quad \mathbf{R}_c=\left(0,-\sqrt{3}\right),\quad \mathbf{R}_d=\left(1,-\sqrt{3}\right). \tag{4.39}$$

Following these considerations, the effective Hamiltonian (4.33) is arranged in the matrix form, up to a constant term:

$$\hat{\mathcal{H}}_{\text{eff}}=\frac{S}{2}\sum_{\mathbf{k}}\underline{X}_{\mathbf{k}}^\dagger\hat{H}_{\mathbf{k}}\underline{X}_{\mathbf{k}}\,,\qquad {}^t\underline{X}_{\mathbf{k}}=(a_{\mathbf{k}},..,d_{\mathbf{k}},a_{-\mathbf{k}}^\dagger,..,d_{-\mathbf{k}}^\dagger)\,, \tag{4.40}$$

with the matrix Hamiltonian:

$$\hat{H}_{\mathbf{k}}=\begin{pmatrix} A & B_0 & & & & & -B_2 & -B_1\\ B_0^* & A & & & & & -B_1^* & -B_2\\ & & A & B_0 & -B_2 & -B_1 & & \\ & & B_0^* & A & -B_1^* & -B_2 & & \\ & & -B_2 & -B_1 & A & B_0 & & \\ & & -B_1^* & -B_2 & B_0^* & A & & \\ -B_2 & -B_1 & & & & & A & B_0\\ -B_1^* & -B_2 & & & & & B_0^* & A \end{pmatrix}:=\begin{pmatrix} M_{\mathbf{k}} & -N_{\mathbf{k}}\\ -N_{\mathbf{k}} & M_{\mathbf{k}}\end{pmatrix} \tag{4.41}$$

hermitian of dimension 8. The matrices $M_{\mathbf{k}}$ and $N_{\mathbf{k}}$ thus defined are, respectively, block diagonal and anti-diagonal. The matrix elements above are:

$$\begin{aligned} &A=3\tilde{J}_3^z-\tilde{J}_1^z+2[\tilde{J}_2^z+\tilde{J}_2^\perp\,\mathrm{Re}\,(\gamma_1\gamma_3^*)],\\ &B_0=(\gamma_1+\gamma_3)\tilde{J}_1^\perp\,,\quad B_1=\mathrm{Re}[\gamma_2^*(\gamma_1+\gamma_3)]\tilde{J}_2^\perp,\\ &B_2=\gamma_2\tilde{J}_1^\perp+\left(\gamma_1^{*2}+\gamma_2^{*2}+\gamma_3^{*2}\right)\tilde{J}_3^\perp,\\ &\gamma_1=e^{ik_x},\quad \gamma_2=e^{i(-k_x+\sqrt{3}k_y)/2},\quad \gamma_3=e^{-i(k_x+\sqrt{3}k_y)/2}, \end{aligned} \tag{4.42}$$

and a star, *e.g* f^*, is used to denote the complex conjugate of a c-number f.
The above Hamiltonian $\hat{H}_{\mathbf{k}}$ can be diagonalized by means of a canonical Bogolyubov transformation, which has now a matrix form, in contrast to the usual 2×2 transformation presented in Sec. (2.4.2.2).

4.3.4.2.1 Matrix Bogolyubov transformation

We first introduce a Bogolyubov basis of boson operators, encoded in an eigenvector:

$$\underline{Y}_{\mathbf{k}} = {}^t(\tilde{a}_{\mathbf{k}}, .., \tilde{d}_{\mathbf{k}}, \tilde{a}^\dagger_{-\mathbf{k}}, .., \tilde{d}^\dagger_{-\mathbf{k}}) \,. \tag{4.43}$$

This is related to $\underline{X}_{\mathbf{k}}$ via the transfer relationship

$$\underline{X}_{\mathbf{k}} = P\underline{Y}_{\mathbf{k}} \,, \tag{4.44}$$

with P a real transfer matrix. The diagonalization of $\hat{H}_{\mathbf{k}}$ is written as

$$\underline{X}^\dagger_{\mathbf{k}} \hat{H}_{\mathbf{k}} \underline{X}_{\mathbf{k}} = \underline{Y}^\dagger_{\mathbf{k}} \Omega_{\mathbf{k}} \underline{Y}_{\mathbf{k}} \,, \tag{4.45}$$

where $\Omega_{\mathbf{k}} = \mathrm{diag}(\omega_1, .., \omega_4, \omega_1, .., \omega_4)$ is a diagonal matrix giving the magnon energies ω_i. Substitution of (4.44) in (4.45) implies:

$$\underline{Y}^\dagger_{\mathbf{k}} \big(P^\dagger \hat{H}_{\mathbf{k}} P - \Omega_{\mathbf{k}} \big) \underline{Y}_{\mathbf{k}} = 0 \,, \tag{4.46}$$

which holds for the basis of eigenstates $\underline{Y}^\dagger_{\mathbf{k}}$. Therefore, $P^\dagger \hat{H}_{\mathbf{k}} P - \Omega_{\mathbf{k}}$ has a zero rank, *i.e.*

$$P^\dagger \hat{H}_{\mathbf{k}} P = \Omega_{\mathbf{k}}. \tag{4.47}$$

However, P is not a unitary matrix in general. Therefore, this is not an eigenvalue problem. In order to obtain one, we further invoke the condition of the boson commutation rules on the pairs of Bogolyubov operators:

$$\underline{Y}_{\mathbf{k}} \underline{Y}^\dagger_{\mathbf{k}} - {}^t\underline{Y}^\dagger_{\mathbf{k}} \, {}^t\underline{Y}_{\mathbf{k}} = \begin{pmatrix} I_4 & \\ & -I_4 \end{pmatrix} =: G. \tag{4.48}$$

The commutation matrix G thus defined satisfies $G^2 = I_8$. The original Holstein-Primakoff boson operators satisfy the same rule:

$$\underline{X}_{\mathbf{k}} \underline{X}^\dagger_{\mathbf{k}} - {}^t\underline{X}^\dagger_{\mathbf{k}} \, {}^t\underline{X}_{\mathbf{k}} = G. \tag{4.49}$$

Therefore, using the real property of P, we have:

$$PGP^\dagger = G \,. \tag{4.50}$$

Finally, we have:

$$\begin{aligned} & \Omega_{\mathbf{k}} = P^\dagger \hat{H}_{\mathbf{k}} = GP^{-1} G \hat{H}_{\mathbf{k}} P \\ \Longrightarrow \quad & G\Omega_{\mathbf{k}} = P^{-1} G \hat{H}_{\mathbf{k}} P. \end{aligned} \tag{4.51}$$

Since $G\Omega_{\mathbf{k}} = \mathrm{diag}(\omega_1, .., \omega_4, -\omega_1, .., -\omega_4)$ is a diagonal matrix, this is an admissible eigenvalue problem. The matrix to diagonalize following the Bogolyubov transformation is therefore $G\hat{H}_{\mathbf{k}}$.

4.3.4.2.2 Matrix diagonalization

The matrix to diagonalize has the 2×2 block form

$$G\hat{H}_{\mathbf{k}} = \begin{pmatrix} M_{\mathbf{k}} & -N_{\mathbf{k}} \\ N_{\mathbf{k}} & -M_{\mathbf{k}} \end{pmatrix}. \tag{4.52}$$

Besides numerical diagonalization algorithms, we can simplify the problem using the special symmetry properties of the $G\hat{H}_{\mathbf{k}}$. With straightforward algebra we show that if ω is an eigenvalue of $G\hat{H}_{\mathbf{k}}$ with an eigenvector of the form ${}^t(U, V)$, then ω^2 is an eigenvalue of the 4×4 matrix:

$$O_{\mathbf{k}} = (M_{\mathbf{k}} - N_{\mathbf{k}})(M_{\mathbf{k}} + N_{\mathbf{k}}) \tag{4.53}$$

with eigenvector ${}^t(U - V)$. In our case, the matrix $O_{\mathbf{k}}$ is block symmetric as it reads:

$$O_{\mathbf{k}} = \begin{pmatrix} x & y & z & \\ y^* & x & & -z \\ z & & x & y \\ & -z & y^* & x \end{pmatrix} =: \begin{pmatrix} C_{\mathbf{k}} & D_{\mathbf{k}} \\ D_{\mathbf{k}} & C_{\mathbf{k}} \end{pmatrix}, \tag{4.54}$$

with:

$$\begin{aligned} x = &\ A^2 + |B_0|^2 - B_1^2 - |B_2|^2 \\ y = &\ 2(AB_0 - B_1 B_2) \\ z = &\ 2i\ \mathrm{Im}(B_0 B_1^*). \end{aligned} \tag{4.55}$$

It is immediate to show that the spectrum of $O_{\mathbf{k}}$ is included in the spectrum of the 2×2 matrices $C_{\mathbf{k}} + D_{\mathbf{k}}$ and $C_{\mathbf{k}} - D_{\mathbf{k}}$, with $C_{\mathbf{k}}$ and $D_{\mathbf{k}}$ as defined in (4.54). And we have:

$$C_{\mathbf{k}} + D_{\mathbf{k}} = \begin{pmatrix} x + z & y \\ y^* & x - z \end{pmatrix}, \tag{4.56}$$

whose spectrum is simply $x \pm \sqrt{|y|^2 + z^2}$. The same expression is obtained for the spectrum of $C_{\mathbf{k}} - D_{\mathbf{k}}$.

4.3.4.2.3 L-magnon energy

Using the previous results, the magnon energies in the effective spin-1/2 model, on the honeycomb lattice within the zigzag structure, are given by the doubly-degenerate branches:

$$E_{\mathbf{k}}^{\pm 2} = \frac{1}{4}\left(A^2 + |B_0|^2 - B_1^2 - |B_2|^2\right) \pm \frac{1}{2}\sqrt{|AB_0 - B_1 B_2|^2 - [\mathrm{Im}(B_0 B_1^*)]^2},$$

where the different constants involved are defined in function of the microscopic parameters, as in (4.42). The existence of two branches is inherent to the zigzag magnetic structure defining two ferromagnetic chains, prone to oscillate in phase or out of phase. An illustration of this dispersion is presented below in Fig. 4.5, where we use a set of microscopic parameters obtained by fitting experimental data.

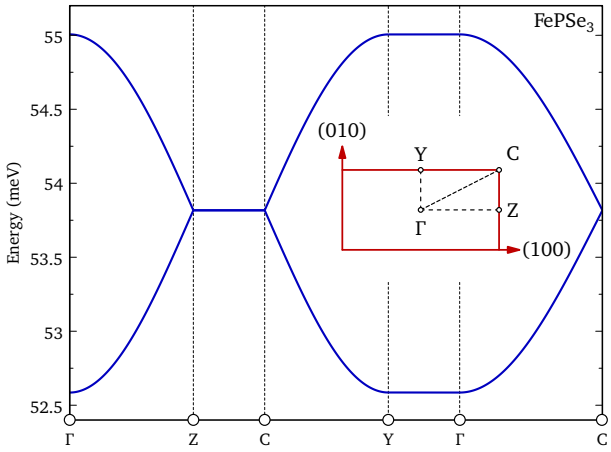

Figure 4.5: Computed dispersion of longitudinal magnons using the microscopic parameters of $FePSe_3$; see the text.

Interestingly, the L-magnons have almost quasi-one-dimensional bands with a strongly dispersive direction parallel to the ferromagnetic chains of the zigzag structure. This property follows naturally from small $\tilde{J}_n^{\perp} \ll \tilde{J}_n^z$. The energy gaps for the symmetric and antisymmetric L-magnons with $k = 0$ measured in the optical experiments are expressed as

$$\Delta_4^{s,a} = \Delta_4 - \frac{2J_1^2 - 4J_2^2 - 6J_3^2}{3D} + \tilde{J}_2{}^{\perp} \mp |\tilde{J}_1^{\perp}|\,, \tag{4.57}$$

where Δ_4 is given by Eq. (4.5) with $S = 2$. The splitting of the two modes provides with a mechanism to interpret the two pairs of four-magnon resonances discussed in Sec. 4.2.1.2. This is further detailed below.

4.3.4.3 Fitting experimental data

We have mentioned in 4.2.1.2 the observation of two transverse modes (antiferromagnetic resonances), in addition to high-energy modes with a four-time Zeeman splitting. The former are transverse magnons, carrying the quantum number $S^z = \pm 1$, whereas the latter modes are the longitudinal magnons, carrying the quantum number $S^z = \pm 4$. The energy of the former modes can be obtained using harmonic spin-wave theory for the lattice of spins $S = 2$, whereas the energy of the latter has been derived within an effective spin-1/2 model, Eq. (4.57).

4.3.4.3.1 T-magnon energy

The $k = 0$ transverse-magnon modes can be obtained by means of a simplified spin-wave theory. Starting with a spin model similarly to Sec. 4.3.4.2 with isotropic exchange constants, we first add the single-ion interaction. Then, we introduce a Holstein-Primakoff representation with boson pair operators a, b, c and d. The single-ion term only induces diagonal terms in the boson Hamiltonian. Then we drop the momentum dependence from the boson operators and diagonalize a 4×4 Hamiltonian. The resulting resonances of of T-magnons, corresponding to symmetric (s) and antisymmetric (a) oscillations of parallel

spins in ferromagnetic zigzag chains, are:

$$\Delta_1^s = 2S\sqrt{\bar{D}(\bar{D} + J_1 + 4J_2 + 3J_3)} \pm H \tag{4.58}$$

and

$$\Delta_1^a = 2S\sqrt{(\bar{D} - 2J_1 + 4J_2)(\bar{D} - J_1 + 3J_3)} \pm H\,. \tag{4.59}$$

In these expressions we have included the renormalized constant $\bar{D} = D[1 - 1/(2S)]$ [120, 142, 143], which reflects the absence of single-ion anisotropy for $S = 1/2$; see the associated remark in Chapter 2.

4.3.4.3.2 Microscopic constants

The set of equations (4.57), (4.58) and (4.59) provides with four conditions, which depend on four parameters J_{1-3} and D. An additional constraint is induced by the zigzag structure in the ground state of the FePSe3 compound; see Fig. 4.6(a). The problem is solvable at this stage, and its solutions read:

$$J_1 = -2.47 \text{ meV}\,, \quad J_2 = 1.39 \text{ meV}\,, \quad J_3 = 0.5 \text{ meV}\,, \quad D = 2.66 \text{ meV}. \tag{4.60}$$

Alternatively, it is useful to obtain a large uncertainty interval in each of the microscopic constants. This is obtained by including the loss of accuracy in the strong-coupling expansion giving the L-magnon energy gaps $\Delta_4^{s,a}$. This loss is expected for $J_n \sim D$. Still, from comparison of the first two contributions into the effective interaction parameters (4.32) we can conclude that the "center-of-mass" position of two modes $(\Delta_4^s + \Delta_4^a)/2$ is given by Eq. (4.57) with a higher accuracy compared to the gap splitting $(\Delta_4^a - \Delta_4^s)$. Subsequently, we fit the data using the center-of-mass position of the two L-magnon modes, in addition to the transverse-magnon modes and the constraint of the magnetic order. The solutions are depicted in Fig. 4.6, where the selected parameter is the renormalized single-ion coupling $\bar{D}$. The relaxed solutions then read:

$$J_1 = -2.5 \pm 0.2 \text{ meV}\,, \quad J_2 = 0.5 \pm 1.0 \text{ meV}\,, \quad J_3 = 1.0 \pm 0.7 \text{ meV}\,, \quad D = 3.7 \pm 1.2 \text{ meV}. \tag{4.61}$$

And we obtain for the splitting $\Delta_4^a - \Delta_4^s \in (0.2 - 7.7)$ meV. The experimentally observed value of 2.4 meV lies within this interval, thus corroborating the physical interpretation. These solutions agree to a large extent (except for J_3) with recent values proposed in Ref. [139]: $J_1 = -2.3$ meV, $J_2 = -0.23$ meV, $J_3 = 2.01$ meV and $D = 3.65$ meV [3].

4.3.4.4 On $FePS_3$

In the sister compound $FePS_3$, only one longitudinal magnon was clearly identified, at 57.5 meV, below the four-magnon continuum (at $\sim$ 60.4 meV). Reanalysis of the experimental data showed a weak signal of a second mode at $\sim$ 60.6 meV. Most likely, this mode merges with the onset of the four-magnon continuum and, therefore, decays quickly due to magnon-magnon interaction. Using retrospectively the set of microscopic

[3] The single-ion constant given in Ref. [139] is the renormalized quantity $\bar{D} = 2.74$ meV, as obtained by using linear spin-wave theory, and not the bare constant D.

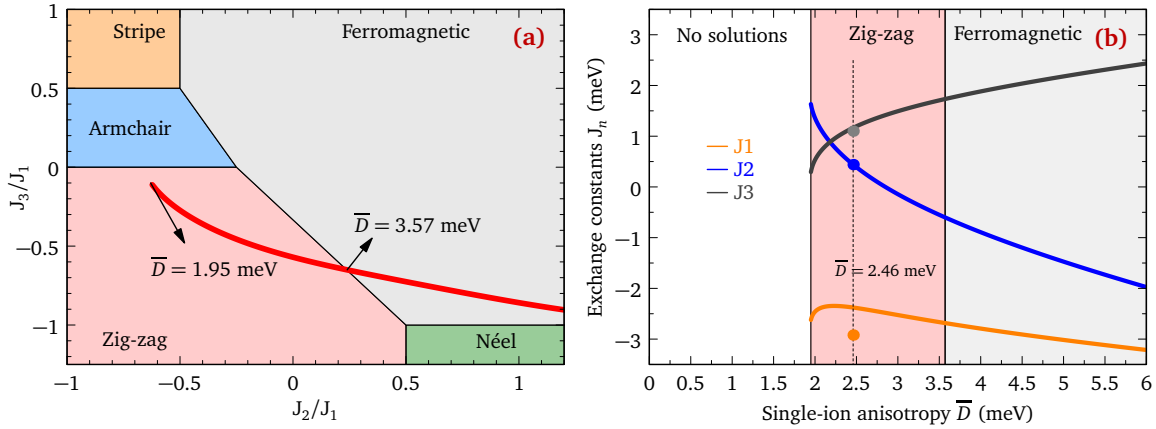

Figure 4.6: (a) Phase diagram of the J_1–J_2–J_3 honeycomb antiferromagnet with strong easy-axis anisotropy, see the main text and Ref. [144]. The red curve represents solutions of Eqs. (4.58)–(4.59). The zigzag antiferromagnetic structure appears for $1.9 < \bar{D}(\text{meV}) < 3.6$. (b) Exchange coupling constants corresponding to the experimental gaps as functions of $\bar{D}$. Full circles in (b) show values of exchange constants in $FePS_3$ consistent with the L-magnon gap in this material [123]. See Ref. [124] for further details on the fit.

parameters provided for $FePS_3$ in (4.3), we estimate from Eq. (4.57) the gap splitting as $\Delta_4^a - \Delta_4^s \approx 2.4$ meV. This value is sufficient to make Δ_4^a approach the 4-magnon continuum boundary and, thus, may explain its poor intensity.
This differential behavior in comparison to $FePSe_3$ is due to the higher ratio $|J_1|/D$ (0.89 versus 0.67 as obtained from (4.61)). The longitudinal magnon would then require a higher energy to break the surrounding bonds in $FePS_3$, which only undermines its stability as a bound state with respect to the four-magnon continuum.

4.3.4.5 Synthesis

The use of a strong-coupling expansion in spin-2 honeycomb-lattice zigzag antiferromagnets allowed us to theoretically compute the energy dispersion of the longitudinal magnons, in the limit of $D > J_n$. The aim of this study has been to fit the experimental $k = 0$ modes, observed in $FePSe_3$, and subsequently determine the microscopic couplings featured in the compound.
Comparison of the theoretical findings and the experimental data enabled us to achieve this purpose. Moreover, we reinterpreted the signal in the previously studied antiferromagnet $FePSe_3$, and identified a longitudinal magnon that overlaps with the onset of the four-magnon continuum.
The strong-coupling approach is a first route to understand the appearance of the longitudinal magnons, and to characterize their energy. For quantitative purposes beyond the limit of small $|J|$, other methods should be employed. This will be the object of Part II.

4.3.5 Spins $S = 3/2$ and $5/2$

We can mimic the derivations of the previous sections for other spin values $S > 1$. In a Hamiltonian of the form (4.6), we present in Table 4.1 the results of the effective

coupling parameters $J_\parallel$ and $J_\perp$ for four values of spin $S = 1$, $3/2$, 2, and $5/2$. For each S we include the two and three leading contributions for $J_\perp$ and $J_\parallel$, respectively. Note that in all expressions J can be positive or negative depending on the initial spin model. We also added the Zeeman contribution, using the results of Sec. 2.4.2 and the mapping (4.12).

S	$J_\parallel$	$J_\perp$	L-magnon energy	
			Ferromagnet	Antiferromagnet
1	$4J + \frac{J^2}{D} - \frac{1}{2}\frac{J^3}{D^2}$	$-\frac{J^2}{D} + \frac{1}{2}\frac{J^3}{D^2}$	$\varepsilon^L_{\mathbf{k}} = \frac{z}{2}\big[-J_\parallel + J_\perp f(\mathbf{k})\big] + 2SH$	$\varepsilon^{L,\pm}_{\mathbf{k}} = \frac{z}{2}\sqrt{J_\parallel^2 - J_\perp^2 f(\mathbf{k})^2} \pm 2SH$
$\frac{3}{2}$	$9J + \frac{9}{8}\frac{J^2}{D} - \frac{9}{32}\frac{J^3}{D^2}$	$\frac{9}{16}\frac{J^3}{D^2} + \frac{45}{64}\frac{J^4}{D^3}$		
2	$16J + \frac{4}{3}\frac{J^2}{D} - \frac{2}{3}\frac{J^3}{D^2}$	$-\frac{1}{4}\frac{J^4}{D^3} + \frac{3}{8}\frac{J^5}{D^4}$		
$\frac{5}{2}$	$25J + \frac{25}{16}\frac{J^2}{D} - \frac{25}{32}\frac{J^3}{D^2}$	$\frac{25}{256}\frac{J^5}{D^4} + \frac{12925}{24576}\frac{J^6}{D^5}$		

Table 4.1: Exchange parameters in the effective spin Hamiltonian obtained in powers of J/D for different values of S. Expressions for the L-magnon energy $\varepsilon^L_{\mathbf{k}}$ for ferro- and antiferromagnetic states are computed in the harmonic spin-wave approximation for the effective spin-1/2 model. For the spin chain: $z = 2$ and $f(\mathbf{k}) = \cos k$. For the square lattice: $z = 4$ and $f(\mathbf{k}) = \gamma^{\square}_{\mathbf{k}}$. For the triangular lattice: $z = 6$ and $f(\mathbf{k}) = \gamma^{\triangle}_{\mathbf{k}}$.

4.3.6 Conclusions

In the strong-coupling regime, the dominant Ising effective coupling $J_\parallel$ establishes the same ferro- or antiferromagnetic structure of pseudospins $\langle s^z_i \rangle$ as the magnetic ground state of the original spin-S Hamiltonian (4.6). However, the pseudospin excitations described by the effective Hamiltonian (4.13) correspond to full flips of the original spins rather than to ordinary magnons. These coherently propagating multipolar modes are nothing else than the longitudinal magnons introduced in Sec. 4.1. One can use harmonic spin-wave theory for the $s = 1/2$ model (4.13) to derive their dispersion $\varepsilon^L_{\mathbf{k}}$.

The L-magnon energy $\varepsilon^L_{\mathbf{k}}$ has a minimum at $\mathbf{k} = 0$ for both signs of J. To leading order, the corresponding gap $\Delta_L = \varepsilon^L_0$ is given by the classical energy of a reversed spin $\Delta_L \approx 8|J|S^2$ for both states. In contrast, the L-magnon bandwidth differs substantially between the two magnetic structures: it is larger for a ferromagnet, $\Delta\varepsilon_L = 2J_\perp$, than for an antiferromagnet, $\Delta\varepsilon_L \approx J_\perp^2/J_\parallel$.

For $J/D \to 0$, the L-magnons are the lowest energy excitations and have infinite life times. They contribute in a standard way to the pseudospin correlation function

$$s^{\alpha\beta}(\mathbf{q},\omega) = \int_{-\infty}^{\infty} \mathrm{d}t\, e^{i\omega t} \langle s^\alpha_{\mathbf{q}}(t) s^\beta_{-\mathbf{q}} \rangle \,. \tag{4.62}$$

To be specific, the transverse spin correlator displays quasiparticle delta peaks $s^\perp(\mathbf{q},\omega) \simeq \delta(\omega - \varepsilon^L_{\mathbf{q}})$ for both ferro- and antiferromagnetic states. The longitudinal structure factor for an antiferromagnet also includes a two-magnon contribution

$$s^{zz}(\mathbf{q},\omega) = \pi \sum_{\mathbf{k}} (u_{\mathbf{k}} v_{\mathbf{k}-\mathbf{q}} + v_{\mathbf{k}} u_{\mathbf{k}-\mathbf{q}})^2 \delta(\omega - \varepsilon^L_{\mathbf{k}} - \varepsilon^L_{\mathbf{k}-\mathbf{q}}), \tag{4.63}$$

where $u_{\mathbf{k}}$, $v_{\mathbf{k}}$ are the Bogolyubov coefficients [145–147]. Because of the operator relation (4.12), the longitudinal dynamical structure factor of original spins $S^{zz}(\mathbf{q},\omega)$ features the same L-magnon continuum (4.63). The spin selection rules do not restrict the L-magnon response in $S^{zz}(\mathbf{q},\omega)$ for any $S \geq 1$ since the two-particle states in the continuum (4.63) have $S^z_{\rm tot} = 0$. Spin dependence appears indirectly via $J_\perp \sim (J/D)^{2S}$. Since $v_{\mathbf{k}} \sim J_\perp/J_\parallel$, the continuum intensity (4.63) decreases with increasing S, but remains finite as long as the longitudinal magnons are coherently propagating excitations.

In contrast, the presence of L-magnon peaks in $S^{\perp}(\mathbf{q},\omega)$ is forbidden by the dipole selection rules. However, additional weak spin-orbit terms in real materials that break the $U(1)$ rotation symmetry of the Hamiltonian will mix magnetic excitations with different S^z allowing for *weak* L-magnon peaks in $S^{\perp}(\mathbf{q},\omega)$. Such a mechanism explains the observation of L-magnons in ESR and inelastic neutron-scattering experiments on the $S = 1$ antiferromagnet FeI_2 [116, 118, 122, 125] and in the ESR experiments on the $S = 2$ antiferromagnets $FePS_3$ and $FePSe_3$ [123, 124].

As J/D increases, the energies of transverse magnons decrease and they rapidly become the excitations of lowest energy. The corresponding level crossing takes place for a value $(|J|/D)_{c1}$ that can be estimated from $\Delta_L = \Delta_T$. Approximating the energy gap for ordinary magnons by $\Delta_T \approx 2\bar{D}S$ and the L-magnon gap by $\Delta_L \approx 8|J|S^2$ as seen above, we obtain

$$(|J|/D)_{c1} \simeq 1/(4S)\,. \tag{4.64}$$

The L-magnons persist as well-defined excitations for a range of values of J/D, before eventually disappearing for a particular value $(|J|/D)_{c2}$. Indeed, for $D = 0$ the Heisenberg ferro- and antiferromagnets have no sharp excitations with $S^z = 2S$ [148]. The destruction of L-magnons with $S^z = 2S$ proceeds as a decay into low-energy excitations with smaller S^z values. The corresponding decay processes are not explicitly included in the effective Hamiltonian. We treat the L-magnon decay in the following Section for the $S = 1$ model by employing the multiboson representation of spin operators. Nevertheless, a threshold value $(|J|/D)_{c2}$, above which L-magnons acquire a finite life time upon entering the $2S$-magnon continuum, can be estimated from $\Delta_L = 2S\Delta_T$. This yields

$$(|J|/D)_{c2} \simeq 1/2 \tag{4.65}$$

for the square lattice model. For more precise estimates of $(J/D)_{c1}$ and $(J/D)_{c2}$ we need to take into account the dispersion of both types of magnon.

We conclude this section by commenting on the sign alternation of $J_\perp$ for integer and half-integer spins of the original model with $J > 0$, see Tab. 4.1. This sign alternation is related to the even or odd powers of the perturbation expansion, where the full spin-flip processes initially occur for each value of S. The sign of the transverse coupling plays no role in zero field in the Ising antiferromagnetic state, where the excitation energy is quadratic in $J_\perp$ (last column, Table 4.1). However, it becomes important in the polarized state above the saturation magnetic field H_s, where the sign of $J_\perp$ determines the gap position ($\mathbf{k}_0$) in the excitation energy $\varepsilon^L_{\mathbf{k}}$ of longitudinal magnons. At $H = H_s$, the gap closes and L-magnons with $\mathbf{k} = \mathbf{k}_0$ begin to condense. This transition has been recently observed in the $S = 1$ triangular antiferromagnet $Na_2BaNi(PO_4)_2$ [129]. Independently of the lattice structure, the multipolar state at $H < H_s$ has $\mathbf{k}_0 = 0$ for integer spins ($J_\perp < 0$). For half-integer spins ($J_\perp > 0$), the high-field multipolar state is instead modulated with a finite $\mathbf{k}_0$, which is equal to (π,π) for the square-lattice model considered here. The

ordering wavevector variation with S is an interesting example of the spin-parity effect in two-dimensional quantum magnetism.

4.4 Spin-1 square-lattice model

We would like to study longitudinal magnons in the simple model of a spin-1 square-lattice ferro- or antiferromagnet. In the previous section, we tackled the strong-coupling regime for small J/D, via an effective pseudospin-1/2 model. Here, we present other approaches for the energy dispersion of the longitudinal magnons. The spin model studied is defined by the Hamiltonian

$$\hat{\mathcal{H}} = J \sum_{\langle i,j \rangle} \mathbf{S}_i \cdot \mathbf{S}_j - D \sum_i (S_i^z)^2, \tag{4.66}$$

with $D > 0$.

4.4.1 Antiferromagnetic order

We discuss in the following two alternative theoretical approaches that complement the effective Hamiltonian method of Sec. 4.3. The first is the linked-cluster expansion, and the second is the multi-boson spin-wave theory. In principle, both methods can be used for an arbitrary spin S. However, the analytical calculations are most tractable for small spin values. We shall therefore set $S = 1$ from now on. Furthermore, in this section we treat only the antiferromagnetic model (4.66), with $J > 0$. The results for the excitation spectra obtained with the use of different methods are illustrated in Figs. 4.7 and 4.8, and further discussed in Sec. 4.4.1.3.

4.4.1.1 Linked-cluster expansion

The linked-cluster expansion for quantum spin systems at $T = 0$ is a variant of real-space perturbation theory, as seen in Sec. 3.2.1. For our problem, selected properties of the spin-1 square-lattice antiferromagnet with the easy-axis single-ion anisotropy have been previously computed to the twelfth order of the linked cluster expansion in J/D [120]. Here we obtain analytical expressions for the ground-state and the T- and L-magnon excitation energies to the fourth order, which can be used for comparison with other approaches.

To construct the J/D expansion we split the spin Hamiltonian (4.66) into an unperturbed part

$$\hat{H}_0 = J \sum_{\langle ij \rangle} S_i^z S_j^z - D \sum_i (S_i^z)^2 \tag{4.67}$$

diagonal in S_i^z, and the transverse coupling, considered as a perturbation

$$\hat{V} = \frac{J}{2} \sum_{\langle ij \rangle} (S_i^+ S_j^- + S_i^- S_j^+). \tag{4.68}$$

The ground state is the Néel state $|.., 1, -1, ...\rangle$ with the unperturbed energy per spin:

$$E_0 = -2J - D. \tag{4.69}$$

The L-magnon in this real-space framework is a single-particle excitation formed by a reversed spin $|\pm 1\rangle \to |\mp 1\rangle$. In the Néel state, a reversed spin causes its adjoining bonds to saturate. Therefore, the first hopping process for the spin reversal involves second-nearest neighbors, and is therefore of fourth order. Accordingly, the leading order of the L-magnon dispersion is obtained by considering processes in clusters with up to four connected bonds. These are dimers, trimers, open tetramers, and squares.

As described in Sec. 3.2.1, the preliminary step in this approach is to compute the ground-state energy $E_{\text{g.s.}}$ to the same order, using the same clusters. This is summarized in Tab. 4.2, where the ground-state energy of each cluster is given by the composition rule (3.28). Defining the small parameter $j = J/D$, we recall the result of Eq. (3.49):

$$\frac{E_{\text{g.s.}} - E_0}{D} = -\frac{2j^2}{2+7j} - \frac{j^4}{(2+7j)^2}\left(\frac{1}{6j} + \frac{4}{1+3j} + \frac{12}{1+6j} - \frac{46}{2+7j} + \frac{56}{4+13j}\right). \quad (4.70)$$

This expansion compares well with the twelfth-order expansion of Ref. [120], showing no more than 1.2% error for $j = 1$.

4.4.1.1.1 L-magnon dispersion

Above the ground state, we obtain the L-magnon energy $\varepsilon^L_{\mathbf{k}}$ from the sum of all transition amplitudes involving a reversed spin that propagates to its next-nearest neighbors. These amplitudes are read out straightforwardly from the effective Hamiltonian associated to each cluster, starting with a single site. For convenience, we shift the ground-state energy to zero by considering $\hat{H}_0 \to \hat{H}_0 - E_0$, which does not affect the results obtained. The construction follows the case study of Sec. 3.2.1.2.

(i) We note the monomer $\mathcal{C}_1 =$ 

, with embedding $g(\mathcal{C}_1) = N$. A single reversed spin 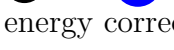

defines a scalar effective Hamiltonian: $h_{\text{eff}}(\mathcal{C}_1) = 8J =: f_0$. Its ground-state energy correction is zero, and the corresponding transition amplitude for $\mathbf{r} = \mathbf{0}$ is:

$$d^{\mathcal{C}_1}(0) = \Delta^{\mathcal{C}_1}(0) = f_0. \quad (4.71)$$

(ii) We note the dimer $\mathcal{C}_2 =$ 

, with embedding factor $g(\mathcal{C}_1) = 2N$. The Hilbert space of the reversed-spin excitation is spanned by the two kets $|l\rangle =$ 

and $|r\rangle =$ 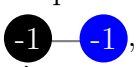

, and we have $\hat{\mathcal{V}}|l\rangle = 0 = \hat{\mathcal{V}}|r\rangle$. Therefore, the effective Hamiltonian of the dimer is:

$$h_{\text{eff}}(\mathcal{C}_2) = f_0 \begin{pmatrix} 1 & \\ & 1 \end{pmatrix}. \quad (4.72)$$

Whereas the ground-state correction of the dimer is (see Eq. (3.36)):

$$E^{\mathcal{C}_2} = -\frac{1}{e_1}J^2 + \frac{1}{e_1^2}\left(\frac{1}{e_1} - \frac{1}{e_2}\right)J^4, \quad (4.73)$$

with $e_1 = 2D + 7J$ and $e_2 = 12J$. Hence, the auxiliary matrix reads

$$\Delta^{\mathcal{C}_2} = \left[f_0 - E^{\mathcal{C}_2}\right]\begin{pmatrix} 1 & \\ & 1 \end{pmatrix} \quad (4.74)$$

and the only non-trivial irreducible transition amplitude is:

$$\Delta^{\mathcal{C}_2}(0) = Tr\left(\Delta^{\mathcal{C}_2}\right) = 2\left(f_0 - E^{\mathcal{C}_2}\right) \tag{4.75}$$

whereas the subcluster rule (3.55) yields:

$$\Delta^{\mathcal{C}_2}(0) = d^{\mathcal{C}_2}(0) + 2d^{\mathcal{C}_1}(0)\,. \tag{4.76}$$

Then we have the reduced transition amplitudes:

$$d^{\mathcal{C}_2}(0) = \frac{2}{e_1}J^2 - \frac{2}{e_1^2}\left(\frac{1}{e_1} - \frac{1}{e_2}\right)J^4 \tag{4.77}$$

and

$$d^{\mathcal{C}_2}(\mathbf{1}) = \Delta^{\mathcal{C}_2}(\mathbf{1}) = 0. \tag{4.78}$$

(iii) We note the trimer $\mathcal{C}_3 =$ 

, with embedding factor $g(\mathcal{C}_3) = 6N$. There are three excited states, namely $\{|a\rangle, |b\rangle, |c\rangle\}$, and we have the following construction:

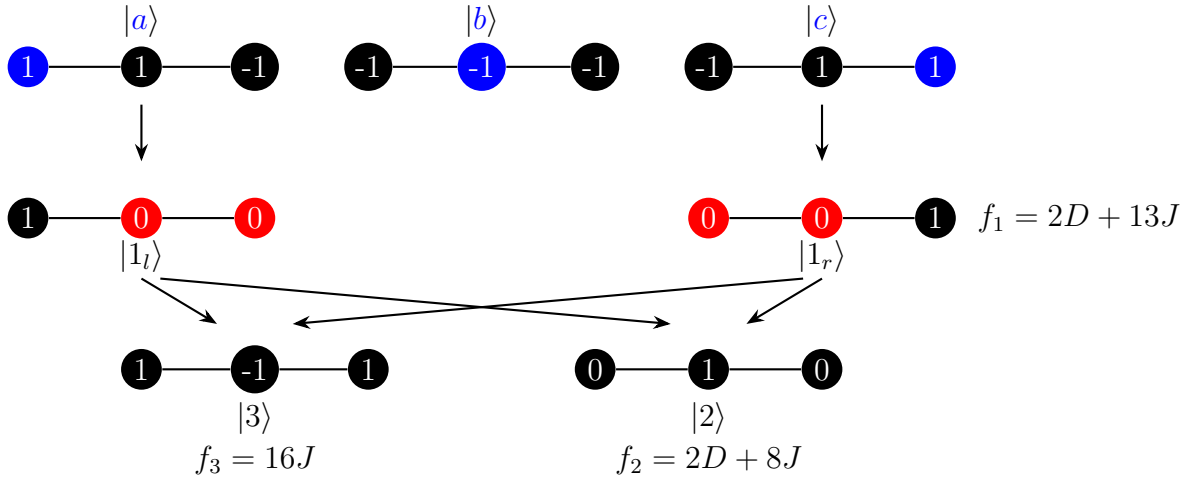

where the arrows indicate the action of perturbation $\hat{\mathcal{V}}$. The middle ket in the first row is saturated, and its image is zero. The energies are indicated for each intermediate state. In view of the above diagram, the effective Hamiltonians to orders 0–4 in the space spanned by kets $\{|a\rangle, |b\rangle, |c\rangle\}$, are:

$$\begin{aligned}
h_{\text{eff}}^{(0)}(\mathcal{C}_3) &= f_0 \begin{pmatrix} 1 & & \\ & 1 & \\ & & 1 \end{pmatrix}, \\
h_{\text{eff}}^{(1)}(\mathcal{C}_3) &= 0, \\
h_{\text{eff}}^{(2)}(\mathcal{C}_3) &= J^2 \begin{pmatrix} \frac{1}{f_{0,1}} & & \\ 0 & 0 & \\ & & \frac{1}{f_{0,1}} \end{pmatrix} \begin{pmatrix} 1 & 0 & \\ 0 & 1 & \end{pmatrix} = \frac{J^2}{f_{0,1}} \begin{pmatrix} 1 & & \\ & 0 & \\ & & 1 \end{pmatrix}, \\
h_{\text{eff}}^{(3)}(\mathcal{C}_3) &= 0,
\end{aligned}$$

$$\begin{aligned}\frac{1}{J^4}h^{(4)}_{\text{eff}}(\mathcal{C}_3) &= \begin{pmatrix}\frac{1}{f_{0,1}} & & \\ 0 & 0 & \\ & \frac{1}{f_{0,1}} & \end{pmatrix}\begin{pmatrix}\frac{1}{f_{0,2}} & \frac{1}{f_{0,3}} \\ \frac{1}{f_{0,2}} & \frac{1}{f_{0,3}}\end{pmatrix}\begin{pmatrix}1 & 1\\ 1 & 1\end{pmatrix}\begin{pmatrix}\frac{1}{f_{0,1}} & 0 & \\ & 0 & \frac{1}{f_{0,1}}\end{pmatrix} \\ &\quad -\frac{1}{f_{0,1}}\begin{pmatrix}\frac{1}{f^2_{0,1}} & & \\ 0 & 0 & \\ & \frac{1}{f^2_{0,1}} & \end{pmatrix}\begin{pmatrix}1 & 0 & \\ & 0 & 1\end{pmatrix} \\ &= \frac{1}{f^2_{0,1}}\begin{pmatrix}-\frac{1}{f_{0,1}}+\frac{1}{f_{0,2}}+\frac{1}{f_{0,3}} & 0 & \frac{1}{f_{0,2}}+\frac{1}{f_{0,3}} \\ 0 & 0 & 0 \\ \frac{1}{f_{0,2}}+\frac{1}{f_{0,3}} & 0 & -\frac{1}{f_{0,1}}+\frac{1}{f_{0,2}}+\frac{1}{f_{0,3}}\end{pmatrix},\end{aligned} \tag{4.79}$$

where $f_{0,i} := f_0 - f_i,\ i = 1,2,3$. Therefore, the resulting effective Hamiltonian to the fourth order for the trimer is:

$$h_{\text{eff}}(\mathcal{C}_3) = \begin{pmatrix} f_0+\frac{1}{f_{0,1}}J^2+\frac{1}{f^2_{0,1}}\left(\frac{-1}{f_{0,1}}+\frac{1}{f_{0,2}}+\frac{1}{f_{0,3}}\right)J^4 & 0 & \frac{1}{f^2_{0,1}}\left(\frac{1}{f_{0,2}}+\frac{1}{f_{0,3}}\right)J^4 \\ 0 & f_0 & 0 \\ \frac{1}{f^2_{0,1}}\left(\frac{1}{f_{0,2}}+\frac{1}{f_{0,3}}\right)J^4 & 0 & f_0+\frac{1}{f_{0,1}}J^2+\frac{1}{f^2_{0,1}}\left(\frac{-1}{f_{0,1}}+\frac{1}{f_{0,2}}+\frac{1}{f_{0,3}}\right)J^4 \end{pmatrix}. \tag{4.80}$$

Whereas, from Eq. (3.38), the ground-state energy of the trimer is:

$$E^{\mathcal{C}_3} = -\frac{2}{e_1}J^2 + \frac{2}{e_1^2}\left(\frac{2}{e_1}-\frac{1}{e_2}-\frac{2}{e_3}\right)J^4, \tag{4.81}$$

with $e_3 = 2D + 12J$. Thus

$$3d^{\mathcal{C}_1}(0) + 2d^{\mathcal{C}_2}(0) + d^{\mathcal{C}_3}(0) = \Delta^{\mathcal{C}_3}(0) = Tr\left(h_{\text{eff}}(\mathcal{C}_3) - E^{\mathcal{C}_3}I_3\right). \tag{4.82}$$

Therefore:

$$d^{\mathcal{C}_3}(0) = \left(\frac{2}{f_{0,1}}+\frac{2}{e_1}\right)J^2 + \left(\frac{2}{f^2_{0,1}}\left[\frac{-1}{f_{0,1}}+\frac{1}{f_{0,2}}+\frac{1}{f_{0,3}}\right]+\frac{2}{e_1^2}\left[\frac{-4}{e_1}-\frac{1}{e_2}+\frac{6}{e_3}\right]\right)J^4, \tag{4.83}$$

and

$$\begin{aligned} d^{\mathcal{C}_3}(\mathbf{1}) &= \Delta^{\mathcal{C}_3}(\mathbf{1}) = 0, \\ d^{\mathcal{C}_3}(\mathbf{2}) &= \Delta^{\mathcal{C}_3}(\mathbf{2}) = \frac{1}{f^2_{0,1}}\left(\frac{1}{f_{0,2}}+\frac{1}{f_{0,3}}\right)J^4. \end{aligned} \tag{4.84}$$

(iv) We note the square $\mathcal{C}_4 =$ 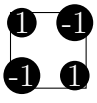

with embedding factor $g(\mathcal{C}_4) = N$, and we construct the following processes:

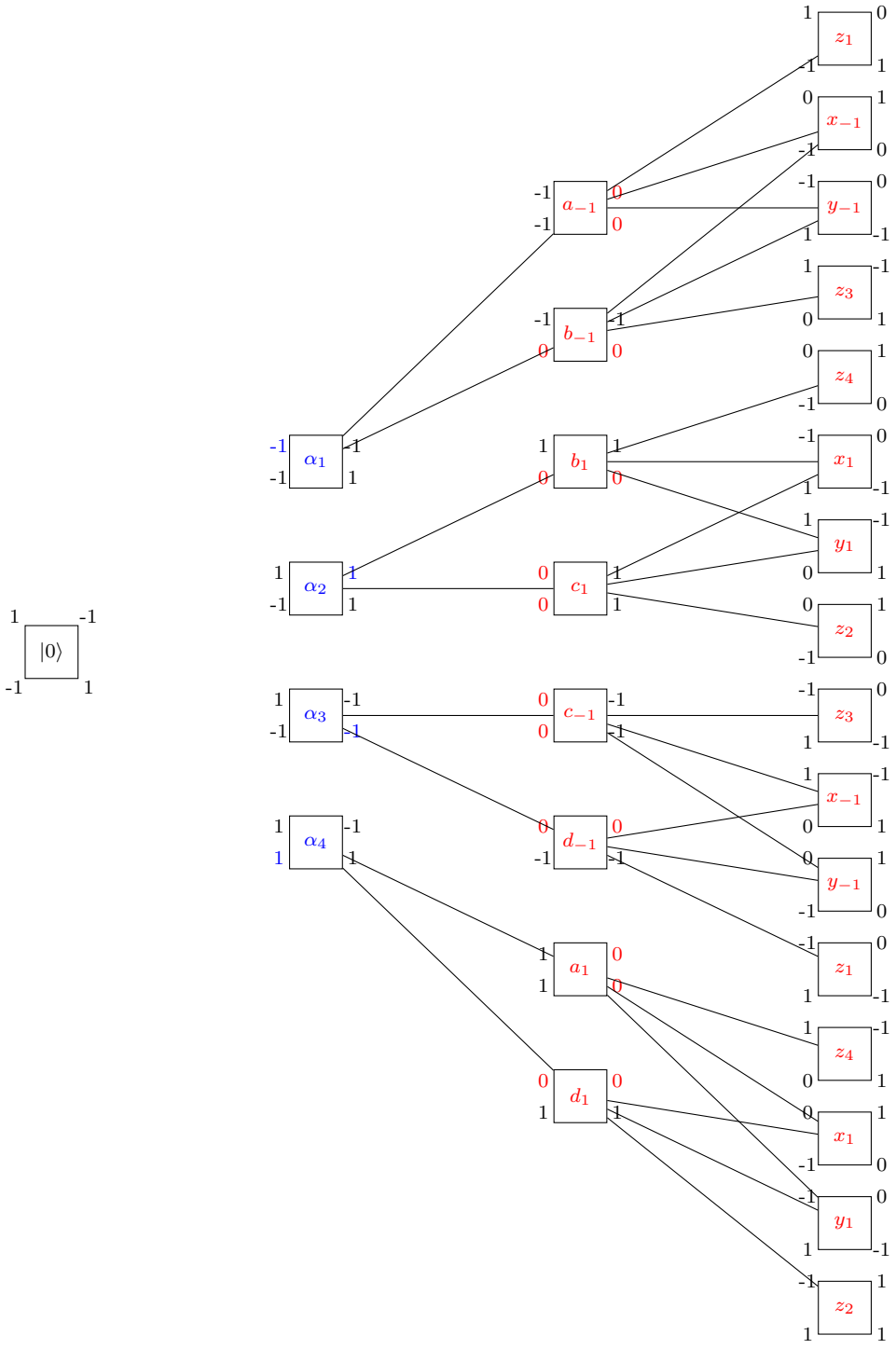

The arrows from left to right indicate a single action of the perturbation. The states α_i, $i = 1, .., 4$, describe the different configurations of a reversed spin. The states obtained in the first order (third column above) correspond to energy $f_1 = 2D + 13J$. In the second order (fourth column), the states labeled as x_1 and x_{-1} correspond to energy

$f_2 = 2D + 8J$; the states labeled as z_i, $i = 1, .., 4$ correspond to energy $f_3 = 16J$, and the states labeled as y_1 and y_{-1} correspond to energy $f_4 = 2D + 16J$. We note that each arrow matching two states contributes with a matrix element equal to J. Moreover, the shortest path between two states from the subspace of a reversed spin is four arrows long. Therefore the first dispersive term is of the fourth order. Subsequently, we proceed with the construction of the effective Hamiltonian as specified in Sec. 3.1.3 without using matrix block diagonalization. Accordingly, we write the following:

$$\begin{aligned} h_{\text{eff}}^{(0)}(\mathcal{C}_4) =& f_0 I_4, \\ h_{\text{eff}}^{(1)}(\mathcal{C}_4) =& 0, \\ h_{\text{eff}}^{(2)}(\mathcal{C}_4)/J^2 =& \frac{2}{f_{0,1}} I_4, \\ h_{\text{eff}}^{(3)}(\mathcal{C}_4) =& 0, \end{aligned} \tag{4.85}$$

$$h_{\text{eff}}^{(4)}(\mathcal{C}_4)/J^4 = \frac{-2}{f_{0,1}^3} I_4 + \frac{2}{f_{0,1}^2}\left[\frac{2}{f_{0,2}} + \frac{1}{f_{0,3}} + \frac{2}{f_{0,4}}\right] \begin{pmatrix} 1 & & 1 & \\ & 1 & & 1 \\ 1 & & 1 & \\ & 1 & & 1 \end{pmatrix}. \tag{4.86}$$

Whereas the ground-state energy of the square is given by Eq. (3.42) with $e_4 = 4D + 12J$. Thus

$$4d^{\mathcal{C}_1}(0) + 4d^{\mathcal{C}_2}(0) + 4d^{\mathcal{C}_3}(0) + d^{\mathcal{C}_4}(0) = \Delta^{\mathcal{C}_4}(0) = Tr\left(h_{\text{eff}}(\mathcal{C}_4) - E^{\mathcal{C}_4} I_4\right). \tag{4.87}$$

Therefore:

$$d^{\mathcal{C}_4}(0) = 8\left(\frac{1}{f_{0,1}^2}\left[\frac{1}{f_{0,2}} + \frac{2}{f_{0,4}}\right] + \frac{1}{e_1^2}\left[\frac{-3}{e_1} + \frac{2}{e_3} + \frac{8}{e_4}\right]\right) J^4, \tag{4.88}$$

$$d^{\mathcal{C}_3}(\mathbf{1}) = \Delta^{\mathcal{C}_3}(\mathbf{1}) = 0, \tag{4.89}$$

and

$$\begin{aligned} 2d^{\mathcal{C}_3}(\pm 1, \pm 1) + d^{\mathcal{C}_4}(\pm 1, \pm 1) =& \Delta^{\mathcal{C}_4}(\pm 1, \pm 1) = \frac{2}{f_{0,1}^2}\left[\frac{2}{f_{0,2}} + \frac{1}{f_{0,3}} + \frac{2}{f_{0,4}}\right] J^4 \\ \Longrightarrow \qquad d^{\mathcal{C}_4}(\pm 1, \pm 1) =& \frac{2}{f_{0,1}^2}\left[\frac{1}{f_{0,2}} + \frac{2}{f_{0,4}}\right] J^4. \end{aligned} \tag{4.90}$$

(v) We note equally the open tetramer $\mathcal{C}_5 =$ 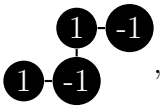

, with embedding factor $g(\mathcal{C}_5) = 14N$, and we construct the following processes:

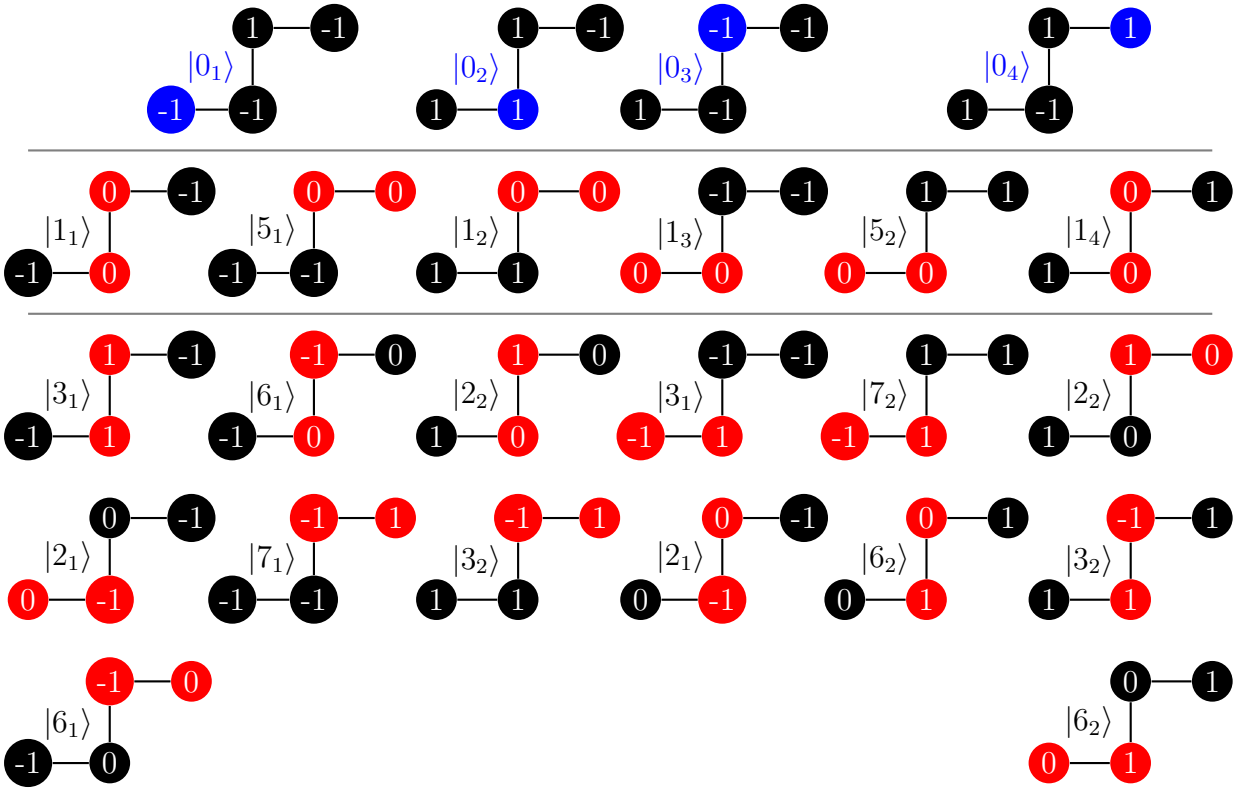

Here, the Hilbert space is spanned by states of reversed spins $|0_i\rangle$, i =1-4, of energy f_0 (first row above). In the first order of perturbation we have the following mapping:

$$\hat{\mathcal{V}}\,|0_1\rangle = |1_1\rangle + |5_1\rangle\ , \quad \hat{\mathcal{V}}\,|0_2\rangle = |1_2\rangle\ , \quad \hat{\mathcal{V}}\,|0_3\rangle = |1_3\rangle\ , \quad \hat{\mathcal{V}}\,|0_1\rangle\,|0_4\rangle = |5_2\rangle + |1_4\rangle \tag{4.91}$$

Then each of the resulting virtual states from the second row above is mapped in the second order of perturbation to the states shown in the same column:

$$\hat{\mathcal{V}}\,|1_1\rangle = |3_1\rangle + |2_1\rangle + |6_1\rangle\ , \quad \hat{\mathcal{V}}\,|5_1\rangle = |6_1\rangle + |7_1\rangle\ , \quad \hat{\mathcal{V}}\,|1_2\rangle = |2_2\rangle + |3_2\rangle\ , \tag{4.92}$$

$$\hat{\mathcal{V}}\,|1_3\rangle = |3_1\rangle + |2_1\rangle\ , \quad \hat{\mathcal{V}}\,|5_2\rangle = |7_2\rangle + |6_2\rangle\ , \quad \hat{\mathcal{V}}\,|1_4\rangle = |2_2\rangle + |3_2\rangle + |6_2\rangle\ . \tag{4.93}$$

In this notation, each state $|n_j\rangle$ belongs to a subspace of energy f_n, with:

$$\begin{aligned} f_1 = 2D + 13J\,, \quad f_2 = 2D + 8J\,, \quad f_3 = 16J\,, \quad f_5 = 2D + 15J \\ f_6 = 2D + 18J\,, \quad f_7 = 20J\,. \end{aligned} \tag{4.94}$$

The effective Hamiltonians are then:

$$\begin{aligned} h^{(0)}_{\text{eff}}(\mathcal{C}_5) &= f_0 I_4, \\ h^{(1)}_{\text{eff}}(\mathcal{C}_5) &= 0, \\ h^{(2)}_{\text{eff}}(\mathcal{C}_5) &= J^2 \begin{pmatrix} \frac{1}{f_{0,1}} & & & & \frac{1}{f_{0,5}} \\ & \frac{1}{f_{0,1}} & & & \\ & & \frac{1}{f_{0,1}} & & \\ & & & \frac{1}{f_{0,1}} & \\ & & & & \frac{1}{f_{0,5}} \end{pmatrix} \begin{pmatrix} 1 & & & & \\ & 1 & & & \\ & & 1 & & \\ & & & 1 & \\ 1 & & & & \\ & & & & 1 \end{pmatrix} \end{aligned}$$

$$= J^2 \begin{pmatrix} \frac{1}{f_{0,1}} + \frac{1}{f_{0,5}} & & & \\ & \frac{1}{f_{0,1}} & & \\ & & \frac{1}{f_{0,1}} & \\ & & & \frac{1}{f_{0,1}} + \frac{1}{f_{0,5}} \end{pmatrix} \tag{4.95}$$

$$\begin{aligned} h_{\text{eff}}^{(3)}(\mathcal{C}_5) &= 0, \\ h_{\text{eff}}^{(4)}(\mathcal{C}_5) &= h_{\text{eff}}^{(4),1}(\mathcal{C}_5) + h_{\text{eff}}^{(4),2}(\mathcal{C}_5) \end{aligned}$$

where

$$h_{\text{eff}}^{(4),1}(\mathcal{C}_5) = M_1 \begin{pmatrix} \frac{1}{f_{0,2}} & & \frac{1}{f_{0,3}} & & \frac{1}{f_{0,6}} & & \\ & \frac{1}{f_{0,2}} & & \frac{1}{f_{0,3}} & & & \\ \frac{1}{f_{0,2}} & & \frac{1}{f_{0,3}} & & & & \\ & \frac{1}{f_{0,2}} & & \frac{1}{f_{0,3}} & & \frac{1}{f_{0,6}} & \\ & & & & \frac{1}{f_{0,6}} & & \frac{1}{f_{0,7}} \\ & & & & & \frac{1}{f_{0,6}} & \end{pmatrix} \begin{pmatrix} 1 & & 1 & & & \\ & 1 & & 1 & & \\ 1 & & 1 & & & \\ & 1 & & 1 & & \\ 1 & & & & 1 & \\ & & & 1 & & 1 \\ & & & & 1 & \\ & & & & & 1 \end{pmatrix} M_1^T \tag{4.96}$$

with the matrix M_1 defined as

$$M_1 = \begin{pmatrix} \frac{1}{f_{0,1}} & & & \frac{1}{f_{0,5}} \\ & \frac{1}{f_{0,1}} & & \\ & & \frac{1}{f_{0,1}} & \\ & & \frac{1}{f_{0,1}} & \\ & & & \frac{1}{f_{0,5}} \end{pmatrix}, \tag{4.97}$$

and

$$h_{\text{eff}}^{(4),2}(\mathcal{C}_5) = -J^4 \begin{pmatrix} \frac{1}{f_{0,1}} + \frac{1}{f_{0,5}} & & & \frac{1}{f_{0,1}} + \frac{1}{f_{0,5}} & \\ & \frac{1}{f_{0,1}} & & & \\ & & \frac{1}{f_{0,1}} & & \\ & & \frac{1}{f_{0,1}} + \frac{1}{f_{0,5}} & & \frac{1}{f_{0,1}} + \frac{1}{f_{0,5}} \end{pmatrix} \begin{pmatrix} \frac{1}{f_{0,1}^2} & & & & \\ & \frac{1}{f_{0,1}^2} & & & \\ & & \frac{1}{f_{0,1}^2} & & \\ \frac{1}{f_{0,5}^2} & & & \frac{1}{f_{0,1}^2} & \\ & & & & \frac{1}{f_{0,5}^2} \end{pmatrix}. \tag{4.98}$$

The matrix products yield this form for the fourth-order effective Hamiltonian:

$$h_{\text{eff}}^{(4)}(\mathcal{C}_5) = \begin{pmatrix} h_{11} & & h_{13} & \\ & h_{22} & & h_{24} \\ h_{13} & & h_{33} & \\ & h_{24} & & h_{44} \end{pmatrix}, \tag{4.99}$$

with

$$h_{11} = h_{44} = \frac{1}{f_{0,1}^2}\Big(\frac{1}{f_{0,2}} + \frac{1}{f_{0,3}}\Big) + \Big(\frac{1}{f_{0,1}} + \frac{1}{f_{0,5}}\Big)\Big(\frac{1}{f_{0,6}}\Big[\frac{1}{f_{0,1}} + \frac{1}{f_{0,5}}\Big] - \frac{1}{f_{0,1}^2} - \frac{1}{f_{0,5}^2}\Big) + \frac{1}{f_{0,5}^2}\frac{1}{f_{0,7}}$$

$$h_{13} = h_{24} = \frac{1}{f_{0,1}^2}\Big(\frac{1}{f_{0,2}} + \frac{1}{f_{0,3}}\Big) \tag{4.100}$$
$$h_{22} = h_{33} = \frac{1}{f_{0,1}^2}\Big(-\frac{1}{f_{0,1}} + \frac{1}{f_{0,2}} + \frac{1}{f_{0,3}}\Big).$$

Note that we keep using the notation of the previous paragraph: $f_{0,i} = f_0 - f_i$. The ground-state energy $E^{\mathcal{C}_5}$ of the open tetramer is given by Eq. (3.46). Thus we write the subcluster rule for the reduced transition amplitudes:

$$4d^{\mathcal{C}_1}(0) + 3d^{\mathcal{C}_2}(0) + 2d^{\mathcal{C}_3}(0) + d^{\mathcal{C}_5}(0) = Tr\left(h_{\text{eff}}(\mathcal{C}_5) - E^{\mathcal{C}_5} I_4\right) \tag{4.101}$$

to extract

$$d^{\mathcal{C}_5}(0) = \left[\frac{2}{f_{0,1}^2}\left(\frac{-1}{e_1} + \frac{1}{f_{0,2}} + \frac{1}{f_{0,3}} + \frac{1}{f_{0,6}}\right) + \frac{2}{e_1^2}\left(\frac{-6}{e_1} + \frac{8}{e_5} + \frac{1}{f_{0,6}}\right) - \frac{4}{e_1 f_{0,1} f_{0,6}}\right] J^4. \tag{4.102}$$

Note that we also used $e_1 = 2D + 7J = -f_{0,5}$ to simplify this expression. Similarly, we have:

$$d^{\mathcal{C}_5}(\mathbf{1}) = 0, \tag{4.103}$$

and

$$d^{\mathcal{C}_5}(\mathbf{2}) = 2h_{13} - 2d^{\mathcal{C}_3}(\mathbf{2}) = 0. \tag{4.104}$$

Thus the open tetramer only contributes to the constant energy term.

Now we summarize all the above results to obtain the L-magnon dispersion to the fourth order. We first have the energy rule, Eq. (3.54) on the irreducible transition amplitudes:

$$\begin{aligned} \Delta(0) =& d^{\mathcal{C}_1}(0) + 2d^{\mathcal{C}_2}(0) + 6d^{\mathcal{C}_3}(0) + d^{\mathcal{C}_4}(0) + 14d^{\mathcal{C}_5}(0) \\ \Delta(\mathbf{1}) =& 0, \\ \Delta(\pm 2, 0) =& \Delta(0, \pm 2) = d^{\mathcal{C}_3}(\mathbf{2}), \\ \Delta(\pm 1, \pm 1) =& 2d^{\mathcal{C}_3} + 2d^{\mathcal{C}_4}(\mathbf{2}). \end{aligned} \tag{4.105}$$

Subsequently, the dispersion relationship is:

$$\begin{aligned} \varepsilon_{\mathbf{k}}^L =& \sum_{\mathbf{r}} e^{i\mathbf{k}\cdot\mathbf{r}} \Delta(\mathbf{r}) \\ \Rightarrow \frac{\varepsilon_{\mathbf{k}}^L - \varepsilon_0}{D} =& -\frac{2j^3}{(2+5j)^2}\left[(1+4j)\gamma_{\mathbf{k}}^2 + 4j\,\frac{3+4j}{1+4j}\cos k_x \cos k_y\right], \end{aligned} \tag{4.106}$$

where

$$\begin{aligned} \frac{\varepsilon_0}{4D} =& 2j + \frac{4j^2}{2+7j} - \frac{3j^2}{2+5j} - \frac{j^4}{(2+5j)^2}\left(\frac{9}{8j} + \frac{11}{2} + \frac{2}{1+4j} - \frac{3}{2+5j} + \frac{7}{2+7j} + \frac{7}{2+10j}\right) \\ &+ \frac{j^4}{(2+7j)^2}\left(\frac{1}{3j} + \frac{4}{1+3j} + \frac{11}{1+6j} - \frac{61}{2+7j} - \frac{7}{2+10j} + \frac{56}{4+13j}\right) \\ &- \frac{7j^4}{(1+5j)(2+5j)(2+7j)}. \end{aligned} \tag{4.107}$$

We note that the term $\propto \cos k_x \cos k_y$ stems from the effect of a closed loop in a square. We also note that $\varepsilon_{\mathbf{k}}^L$ is minimal at $k = 0$.

	Embedding	Embedding energy	L-magnon transition amplitudes	T-magnon transition amplitudes
	1	0	$d(\mathbf{0}) = f_0$	$d(\mathbf{0}) = g_0$
	2	$\frac{-1}{e_1}\lambda^2 + \frac{1}{e_1^2}\left(\frac{1}{e_1} - \frac{1}{e_2}\right)\lambda^4$	$d(\mathbf{0}) = \frac{2}{e_1}\lambda^2 - \frac{2}{e_1^2}\left(\frac{1}{e_1} - \frac{1}{e_2}\right)\lambda^4,$ $d(\mathbf{1}) = 0.$	$d(\mathbf{0}) = 2\left(\frac{1}{g_{0,1}} + \frac{1}{e_1}\right)\lambda^2 - 2\left(\frac{1}{g_{0,1}^3} + \frac{1}{e_1^2}\left[\frac{1}{e_1} - \frac{1}{e_2}\right]\right)\lambda^4,$ $d(\mathbf{1}) = 0.$
	6	$\frac{1}{e_1^2}\left(\frac{2}{e_1} - \frac{4}{e_3}\right)\lambda^4$	$d(\mathbf{0}) = \left(\frac{2}{f_{0,1}} + \frac{2}{e_1}\right)\lambda^2 + \left[\frac{2}{f_{0,1}^2}\left(\frac{-1}{f_{0,1}} + \frac{1}{f_{0,2}} + \frac{1}{f_{0,3}}\right) + \frac{2}{e_1^2}\left(\frac{-4}{e_1} + \frac{1}{e_2} + \frac{6}{e_3}\right)\right]\lambda^4.$ $d(\mathbf{1}) = 0,$ $d(\mathbf{2}) = \frac{1}{f_{0,1}^2}\left(\frac{1}{f_{0,2}} + \frac{1}{f_{0,3}}\right)\lambda^4.$	$d(\mathbf{0}) = \left(\frac{2}{g_{0,2}} + \frac{2}{e_1}\right)\lambda^2 + \left(\frac{-2}{g_{0,1}^3} - \frac{4}{g_{0,2}^3} - \frac{2}{g_{0,1}^2 g_{0,2}} - \frac{2}{g_{0,1}g_{0,2}^2} + \frac{2}{g_{0,1}^2 g_{0,3}} + \frac{4}{g_{0,2}^2 g_{0,3}} + \frac{4}{g_{0,1}g_{0,2}g_{0,3}} - \frac{2}{e_1^2}\left(\frac{4}{e_1} + \frac{1}{e_2} + \frac{6}{e_3}\right)\right)\lambda^4,$ $d(\mathbf{1}) = 0,$ $d(\mathbf{2}) = \frac{1}{g_{0,2}^2}\lambda^2 - \left(\frac{2}{g_{0,2}^3} + \frac{1}{g_{0,1}^2 g_{0,2}} + \frac{1}{g_{0,1}g_{0,2}^2} - \frac{2}{g_{0,2}^2 g_{0,3}} - \frac{2}{g_{0,1}g_{0,2}g_{0,3}}\right)\lambda^4.$
	1	$\frac{4}{e_1^2}\left(\frac{1}{e_1} - \frac{4}{e_4}\right)\lambda^4$	$d(\mathbf{0}) = \left[\frac{8}{f_{0,1}^2}\left(\frac{1}{f_{0,2}} + \frac{2}{f_{0,4}}\right) + \frac{8}{e_1^2}\left(\frac{-3}{e_1} + \frac{2}{e_3} + \frac{8}{e_4}\right)\right]\lambda^4,$ $d(\mathbf{1}) = 0,$ $d(\mathbf{2}) = \frac{2}{f_{0,1}^2}\left(\frac{1}{f_{0,2}} + \frac{2}{f_{0,4}}\right)\lambda^4.$	
	14	$\frac{1}{e_1^2}\left(\frac{2}{e_1} - \frac{4}{e_5}\right)\lambda^4$	$d(\mathbf{0}) = \left[\frac{2}{f_{0,1}^2}\left(\frac{-1}{e_1} + \frac{1}{f_{0,2}} + \frac{1}{f_{0,3}} + \frac{1}{f_{0,6}}\right) + \frac{2}{e_1^2}\left(\frac{-6}{e_1} + \frac{8}{e_5} + \frac{1}{f_{0,6}}\right) - \frac{4}{e_1 f_{0,1} f_{0,6}}\right]\lambda^4,$ $d(\mathbf{1}) = 0,$ $d(\mathbf{2}) = 0.$	

Table 4.2: Clusters involved in the 4th-order correction to the ground-state energy and the L-magnon spectrum in the $S = 1$ square-lattice antiferromagnet. Energies e_i read: $e_1 = 2D + 7J$, $e_2 = 12J$, $e_3 = 2D + 12J$, $e_4 = 4D + 12J$, $e_5 = 4D + 13J$. Energies f_i read: $f_0 = 8J$, $f_1 = 2D + 13J$, $f_2 = 2D + 8J$, $f_3 = 16J$, $f_4 = 2D + 16J$, $f_5 = 2D + 18J$ and $f_{0,i} = f_0 - f_i$. And energies g_i read: $g_0 = D + 4J$, $g_1 = 4D + 10J$, $g_2 = 3D + 10J$, $g_3 = D + 14J$, with $g_{0,i} = g_0 - g_i$. The first column gathers all topologically equivalent clusters sharing the same reduced transition amplitudes $d(\mathbf{n})$, although they contribute to different irreducible amplitudes $\Delta(\mathbf{r})$, see the text. Bold characters $\mathbf{n}$ indicate vectors of L^1-norm n.

4.4.1.1.2 T-magnon dispersion

The calculation of the T-magnon energy to the fourth order follows from similar arguments. Here we consider a single spin flip, $|\pm 1\rangle \to |0\rangle$, hopping on dimers and trimers. We derived in Sec. 3.2.1.2 the T-magnon dispersion to the second order in J/D. Here we attempt to obtain the fourth order from additional hopping processes in trimers. The results are summarized in Tab. 4.2. Accordingly, we list the following clusters:

$\mathcal{C}_1 =$ (1) has an embedding factor $g(\mathcal{C}_1) = N$, and encodes an effective Hamiltonian:

$$h_{\text{eff}}(\mathcal{C}_1) = 4J + D =: g_0. \tag{4.108}$$

$\mathcal{C}_2 =$ (-1)—(1) has an embedding factor $g(\mathcal{C}_1) = 2N$, and encodes the effective Hamiltonian, Eq. (3.60):

$$h_{\text{eff}}(\mathcal{C}_2) = g_0 \begin{pmatrix} 1 & \\ & 1 \end{pmatrix} + \frac{J^2}{g_0 - g_1} \begin{pmatrix} 1 & \\ & 1 \end{pmatrix}, \tag{4.109}$$

with $g_1 := 10J + 4D$.

$\mathcal{C}_3 =$ (1)—(-1)—(1) has an embedding factor $g(\mathcal{C}_3) = 6N$, and encodes the following processes for a single flip:

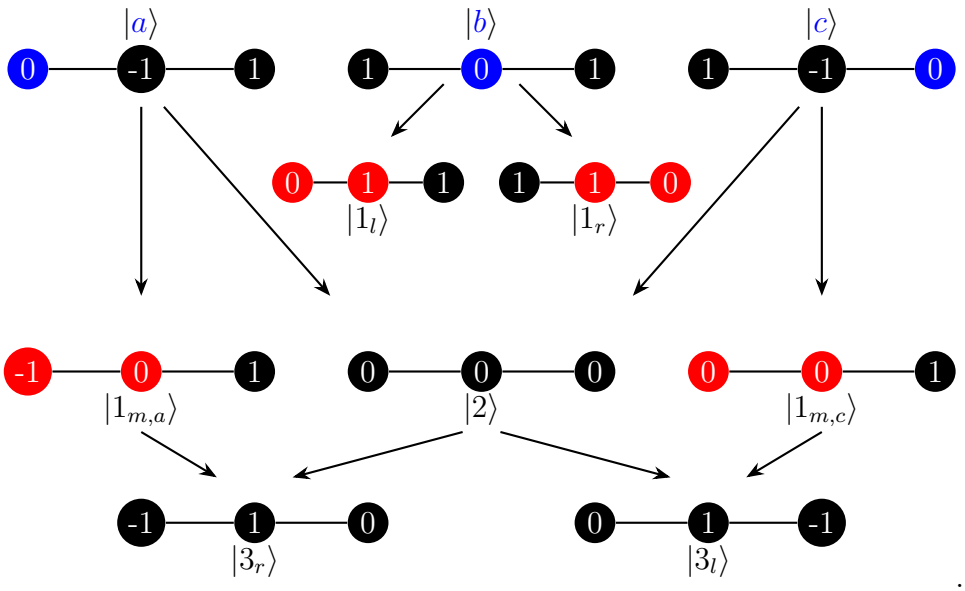

The arrows indicate the action of perturbation $\hat{\mathcal{V}}$. Each arrows has magnitude (matrix element) J. The states $|1_r\rangle, |1_l\rangle, |1_{m,a}\rangle$ and $|1_{m,c}\rangle$ have energy g_1, the state $|2\rangle$ has energy $g_2 := 10J+3D$, and the states $|3_r\rangle$ and $|3_l\rangle$ have energy $g_3 := 14J+D$. The processes $|a\rangle \leftrightarrow |2\rangle \leftrightarrow |c\rangle$ induce dispersion in the second order, as obtained in Eq. (3.73). As the second-order effective Hamiltonian associated to the trimer is non-diagonal, we employ matrix block diagonalization [83] to obtain the fourth-order effective Hamiltonian. Appendix B gives further details on this method. It consists of deriving one by one the effective Hamiltonians $h_{\text{eff}}^{(i)}$ and matrices $O^{(i)}$,

$i = 0$–4, where $O = O^{(0)} + O^{(1)} + ...$ is orthogonal and satisfies $Oh_{\text{eff}} = \hat{\mathcal{H}}O$. We have therefore:

$$h_{\text{eff}}^{(0)} = g_0 I_3\,, \quad O^{(0)} = I_3$$

$$h_{\text{eff}}^{(1)} = 0\,, \quad O^{(1)} = J \left(\begin{array}{ccc} \multicolumn{3}{c}{0_{3\times 3}} \\ \hline \frac{1}{g_{0,1}} & 0 & 0 \\ 0 & 0 & \frac{1}{g_{0,1}} \\ 0 & \frac{1}{g_{0,1}} & 0 \\ 0 & \frac{1}{g_{0,1}} & 0 \\ \frac{1}{g_{0,2}} & 0 & \frac{1}{g_{0,2}} \\ 0 & 0 & 0 \\ 0 & 0 & 0 \end{array}\right)$$

$$h_{\text{eff}}^{(2)} = \left(\sum_l \frac{\hat{\mathcal{V}}_{il}\hat{\mathcal{V}}_{lj}}{g_{0,l}}\right) = J^2 \begin{pmatrix} \frac{1}{g_{0,1}} + \frac{1}{g_{0,2}} & & \frac{1}{g_{0,2}} \\ & \frac{2}{g_{0,1}} & \\ \frac{1}{g_{0,2}} & & \frac{1}{g_{0,1}} + \frac{1}{g_{0,2}} \end{pmatrix}$$

$$e_i = e_j = g_0: \; O_{ij}^{(2)} = \frac{-J^2}{2} O^{(1)T} O^{(1)} = \frac{-1}{2} \begin{pmatrix} \frac{1}{g_{0,1}^2} + \frac{1}{g_{0,2}^2} & & \frac{1}{g_{0,2}^2} \\ & \frac{2}{g_{0,1}^2} & \\ \frac{1}{g_{0,2}^2} & & \frac{1}{g_{0,1}^2} + \frac{1}{g_{0,2}^2} \end{pmatrix}$$

$$e_i \neq e_j = g_0: \; O_{ij}^{(2)} = \left(\sum_l \frac{\hat{\mathcal{V}}_{il} O_{lj}^{(1)}}{g_0 - e_i}\right) = \left(\begin{array}{ccc} \multicolumn{3}{c}{0_{4\times 3}} \\ \hline \frac{1}{g_{0,3}}\left(\frac{1}{g_{0,1}} + \frac{1}{g_{0,2}}\right) & 0 & \frac{1}{g_{0,2}g_{0,3}} \\ \frac{1}{g_{0,2}g_{0,3}} & 0 & \frac{1}{g_{0,3}}\left(\frac{1}{g_{0,1}} + \frac{1}{g_{0,2}}\right) \end{array}\right)$$

$$h_{\text{eff}}^{(3)} = 0,$$

$$\begin{aligned} e_i = e_j = g_0: \; O_{ij}^{(3)} =& \frac{-J^3}{2}\left(O^{(1)T} O^{(2)} + O^{(2)T} O^{(1)}\right) \\ =& \frac{-J^3}{2}\left[\left(0 \;\middle|\; X \;\middle|\; 0\right) \begin{pmatrix} X \\ \hline 0 \\ \hline X \end{pmatrix} + \left(X \;\middle|\; 0 \;\middle|\; X\right) \begin{pmatrix} 0 \\ \hline X \\ \hline 0 \end{pmatrix}\right] \\ =& 0\,, \end{aligned}$$

$$e_i \neq e_j = g_0: \; O_{ij}^{(3)} = \left(\sum_l \frac{\hat{\mathcal{V}}_{il} O_{lj}^{(2)} - O_{il}^{(1)} h_{\text{eff}\,lj}^{(2)}}{g_0 - e_i}\right)$$

$$
\begin{aligned}
&= J^3 \left(\begin{array}{ccc|ccccc|cc}
\frac{1}{g_{0,1}} & 0 & 0 & & & & & & \frac{1}{g_{0,1}} & 0 \\
0 & 0 & \frac{1}{g_{0,1}} & & & & & & & \frac{1}{g_{0,1}} \\
0 & \frac{1}{g_{0,1}} & 0 & & & \mathbf{0}_{5\times 5} & & & 0 & 0 \\
0 & \frac{1}{g_{0,1}} & 0 & & & & & & 0 & 0 \\
\frac{1}{g_{0,2}} & 0 & \frac{1}{g_{0,2}} & & & & & & \frac{1}{g_{0,2}} & \frac{1}{g_{0,2}} \\
\hline
\frac{1}{g_{0,3}}\left(\frac{1}{g_{0,1}}+\frac{1}{g_{0,2}}\right) & 0 & \frac{1}{g_{0,2}g_{0,3}} & \frac{1}{g_{0,3}} & 0 & 0 & 0 & \frac{1}{g_{0,3}} & 0 & 0 \\
\frac{1}{g_{0,2}g_{0,3}} & 0 & \frac{1}{g_{0,3}}\left(\frac{1}{g_{0,1}}+\frac{1}{g_{0,2}}\right) & 0 & \frac{1}{g_{0,3}} & 0 & 0 & \frac{1}{g_{0,3}} & 0 & 0
\end{array}\right)
\left(\begin{array}{ccc}
\frac{-1}{2}\left(\frac{1}{g_{0,1}^2}+\frac{1}{g_{0,2}^2}\right) & 0 & \frac{-1}{2g_{0,2}^2} \\
0 & \frac{1}{g_{0,2}^2} & 0 \\
\frac{-1}{2g_{0,2}^2} & 0 & \frac{-1}{2}\left(\frac{1}{g_{0,1}^2}+\frac{1}{g_{0,2}^2}\right) \\
\hline
 & \mathbf{0}_{5\times 3} & \\
\hline
\frac{1}{g_{0,3}}\left(\frac{1}{g_{0,1}}+\frac{1}{g_{0,2}}\right) & 0 & \frac{1}{g_{0,2}g_{0,3}} \\
\frac{1}{g_{0,2}g_{0,3}} & 0 & \frac{1}{g_{0,3}}\left(\frac{1}{g_{0,1}}+\frac{1}{g_{0,2}}\right)
\end{array}\right) \\
&\quad - J^3 \left(\begin{array}{ccc}
\frac{1}{g_{0,1}^2} & 0 & 0 \\
0 & 0 & \frac{1}{g_{0,1}^2} \\
0 & \frac{1}{g_{0,1}^2} & 0 \\
0 & \frac{1}{g_{0,1}^2} & 0 \\
\frac{1}{g_{0,2}^2} & 0 & \frac{1}{g_{0,2}^2} \\
\hline
 & \mathbf{0}_{3\times 2} &
\end{array}\right)
\begin{pmatrix}
\frac{1}{g_{0,1}}+\frac{1}{g_{0,2}} & & \frac{1}{g_{0,2}} \\
 & \frac{2}{g_{0,1}} & \\
\frac{1}{g_{0,2}} & & \frac{1}{g_{0,1}}+\frac{1}{g_{0,2}}
\end{pmatrix} \\
&= J^3 \left(\begin{array}{ccc}
\frac{-3}{2g_{0,1}^3}-\frac{1}{2g_{0,1}g_{0,2}^2}-\frac{1}{g_{0,1}^2g_{0,2}}+\frac{1}{g_{0,1}^2g_{0,3}}+\frac{1}{g_{0,1}g_{0,2}g_{0,3}} & 0 & \frac{-2}{g_{0,1}g_{0,2}^2}-\frac{1}{g_{0,1}^2g_{0,2}}+\frac{1}{g_{0,1}g_{0,2}g_{0,3}} \\
\frac{-1}{g_{0,1}^2}-\frac{1}{2g_{0,1}g_{0,2}^2}+\frac{1}{g_{0,1}g_{0,2}g_{0,3}} & 0 & \frac{-3}{2g_{0,1}^3}-\frac{1}{2g_{0,1}g_{0,2}^2}-\frac{1}{g_{0,1}^2g_{0,2}}+\frac{1}{g_{0,1}^2g_{0,3}}+\frac{1}{g_{0,1}g_{0,2}g_{0,3}} \\
0 & \frac{-3}{g_{0,1}^3} & 0 \\
0 & \frac{-3}{g_{0,1}^3} & 0 \\
\frac{-3}{g_{0,2}^3}-\frac{1}{2g_{0,1}^2g_{0,2}}-\frac{1}{g_{0,1}g_{0,2}^2}+\frac{2}{g_{0,2}^2g_{0,3}}+\frac{1}{g_{0,1}g_{0,2}g_{0,3}} & 0 & \frac{-3}{g_{0,2}^3}-\frac{1}{2g_{0,1}^2g_{0,2}}-\frac{1}{g_{0,1}g_{0,2}^2}+\frac{2}{g_{0,2}^2g_{0,3}}+\frac{1}{g_{0,1}g_{0,2}g_{0,3}} \\
\hline
 & \mathbf{0}_{3\times 2} &
\end{array}\right)
\end{aligned}
\tag{4.110}
$$

And without showing intermediate matrix products, we have

$$h_{\text{eff}}^{(4)} = \hat{\mathcal{V}} O^{(3)} - O^{(2)} h_{\text{eff}}^{(2)} = \begin{pmatrix} h_{11}^{(4)} & & h_{13}^{(4)} \\ & h_{22}^{(4)} & \\ h_{13}^{(4)} & & h_{33}^{(4)} \end{pmatrix} \tag{4.111}$$

with:

$$\begin{aligned} h_{11}^{(4)}/J^4 = h_{33}^{(4)}/J^4 &= \frac{-1}{g_{0,1}^3} - \frac{2}{g_{0,2}^3} - \frac{1}{g_{0,1}^2 g_{0,2}} - \frac{1}{g_{0,1} g_{0,2}^2} + \frac{1}{g_{0,1}^2 g_{0,3}} + \frac{2}{g_{0,2}^2 g_{0,3}} + \frac{2}{g_{0,1} g_{0,2} g_{0,3}} \\ h_{13}^{(4)}/J^4 &= \frac{-2}{g_{0,2}^3} - \frac{1}{g_{0,1}^2 g_{0,2}} - \frac{1}{g_{0,1} g_{0,2}^2} + \frac{2}{g_{0,2}^2 g_{0,3}} + \frac{2}{g_{0,1} g_{0,2} g_{0,3}} \\ h_{22}^{(4)}/J^4 &= \frac{-4}{g_{0,1}^3}. \end{aligned} \tag{4.112}$$

Whereas the ground-state energy associated to the trimer is given in Eq. (3.38). Therefore, we write the subcluster rule:

$$\begin{aligned} & d^{\mathcal{C}_3}(0) + 2d^{\mathcal{C}_2}(0) + 3d^{\mathcal{C}_1}(0) = Tr(h_{\text{eff}}(\mathcal{C}_3) - E^{\mathcal{C}_3}) \\ \Rightarrow \quad & d^{\mathcal{C}_3}(0) = 2\left(\frac{1}{g_{0,1}} + \frac{1}{e_1}\right) J^2 + 2h_{11}^{(4)} + h_{22}^{(4)} + 2\left(\frac{2}{g_{0,1}} - \frac{4}{e_1^3} + \frac{1}{e_1^2 e_2} + \frac{6}{e_1^2 e^3}\right) J^4, \end{aligned} \tag{4.113}$$

and

$$d^{\mathcal{C}_3}(\mathbf{2}) = \frac{J^2}{g_{0,2}} + h_{13}^{(4)}. \tag{4.114}$$

Now, the energy rule (3.54) yields, similarly to Eq. (3.72):

$$\begin{aligned} \Delta(0) &= d^{\mathcal{C}_1}(0) + 2d^{\mathcal{C}_2}(0) + 6d^{\mathcal{C}_3}(0) \\ \Delta(\mathbf{1}) &= 0, \\ \Delta(\pm 2, 0) &= \Delta(0, \pm 2) = d^{\mathcal{C}_3}(\mathbf{2}), \\ \Delta(\pm 1, \pm 1) &= 2d^{\mathcal{C}_3}(\mathbf{2}). \end{aligned} \tag{4.115}$$

Finally, the T-magnon energy to the fourth order is

$$\begin{aligned} \varepsilon_{\mathbf{k}}^T &= \sum_{\mathbf{r}} e^{i\mathbf{k}\cdot\mathbf{r}} \Delta(\mathbf{r}) \\ \Rightarrow \frac{\varepsilon_{\mathbf{k}}^T - \tilde{\varepsilon}_0}{D} &= -\frac{8j^2}{1+3j}\left[1 + \frac{j}{60(1+3j)}\left(j + \frac{4-33j}{3(1+3j)}\right)\right]\gamma_{\mathbf{k}}^2, \end{aligned} \tag{4.116}$$

where

$$\frac{\tilde{\varepsilon}_0}{D} = 1 + \frac{911j}{270} + j^2\left(\frac{16}{2+7j} - \frac{181}{45(1+3j)}\right) + \frac{4j^3}{3}\left(\frac{1}{(2+7j)^2} - \frac{1}{20(1+3j)^2}\right) + \frac{j^4}{2(1+3j)^3}$$

$$+\frac{j^4}{(2+7j)^2}\left(\frac{9}{1+6j}-\frac{13}{2+7j}\right). \tag{4.117}$$

With these results we may refine the estimates (4.64) and (4.65). The L-magnons here are the lowest one-particle excitation for $J/D \leq (J/D)_{c1} \simeq 0.18$. They enter the onset of the two-particle continuum for $(J/D)_{c2} \simeq 0.62$. Further analyses of the results are given in Sec. 4.4.1.3.

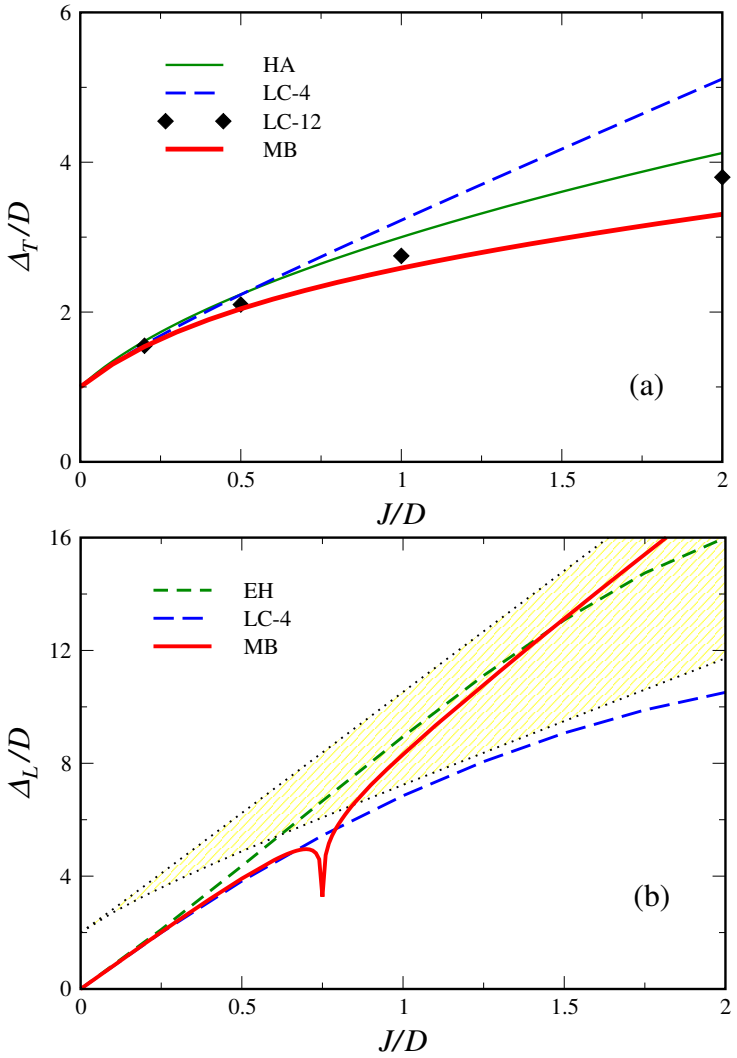

Figure 4.7: The $k = 0$ energy gaps for T-magnons (a) and L-magnons (b) in the spin-1 easy-axis square-lattice antiferromagnet as a function of J/D. We use the acronyms HA for the harmonic approximation of spin-wave theory, EH for the effective-Hamiltonian method, LC-4 for the linked-cluster expansion to the fourth order, LC-12 for the linked-cluster expansion to the twelfth order of Ref. [120], and MB for the multi-boson spin-wave theory within a self-consistent harmonic approximation. The lightly-shaded region in (b) shows the two-magnon continuum $\{\varepsilon^b_{\mathbf{q}} + \varepsilon^b_{-\mathbf{q}}\}$.

4.4.1.2 Multi-boson spin-wave theory

Several versions of the multi-boson representation of spin operators have been used in the past for different problems in quantum magnetism. These include the spin-dimer singlets [149–151], magnets with the dominant single-ion anisotropy [152–154], and the $SU(N)$ spin models [155]. The basic idea of all these approaches comes from Hubbard's work on narrow electron bands in solids [156]. The objective is to construct the solution of a lattice problem from the basis states, which take into account strong local correlations. In our case, the eigenstates of the single-ion anisotropy term are states with different $S^z = \pm 1, 0$. Accordingly, we assign $|+1\rangle$, $|0\rangle$, and $|-1\rangle$ to a single-occupant states for three species of bosons a, b and c, respectively. The single-ion anisotropy is then expressed as

$$\hat{\mathcal{H}}_D = -D \sum_i \left(a_i^\dagger a_i + c_i^\dagger c_i \right) . \tag{4.118}$$

The boson representation of spin operators is constructed so as to reproduce the matrix elements between the eigenstates of $\hat{\mathcal{H}}_D$:

$$S_i^z = a_i^\dagger a_i - c_i^\dagger c_i \,, \quad S_i^+ = \sqrt{2}(a_i^\dagger b_i + b_i^\dagger c_i) \,, \tag{4.119}$$

and $S_i^- = (S_i^+)^\dagger$. To match the Hilbert space of the physical model, the boson operators must satisfy the local constraint

$$a_i^\dagger a_i + b_i^\dagger b_i + c_i^\dagger c_i = 1 \,. \tag{4.120}$$

The above representation of $S = 1$ operators is more complicated than the conventional Holstein-Primakoff representation. Nevertheless, the multiboson representation correctly reproduces the energy spacings between the crystal-field levels on the same site even within the harmonic approximation (see below).

4.4.1.2.1 Boson Hamiltonian

The representation (4.119) is used to express the exchange interactions via the boson operators. Presence of the antiferromagnetic order is taken into account by applying the multiboson representation in the rotated (staggered) local frame with the propagation wave-vector $\mathbf{Q} = (\pi, \pi)$. Following Ref. [150], the constraint (4.120) is enforced via Lagrange multipliers, by adding to the boson Hamiltonian $\hat{\mathcal{H}}_b$ an extra term

$$\hat{\mathcal{H}}_L = \sum_i \mu_i \left(a_i^\dagger a_i + b_i^\dagger b_i + c_i^\dagger c_i - 1 \right) . \tag{4.121}$$

and imposing $\langle \psi | \, \partial \hat{\mathcal{H}}_b / \partial \mu_i \, | \psi \rangle = 0$ for any boson state $|\psi\rangle$. Furthermore, the translational symmetry allows for a substitution $\mu_i \to \mu$, which replaces a set of N constraints with a single global one. In the rotated local frame, the antiferromagnetic ground state corresponds to a uniform condensate of a_i bosons:

$$\langle a_i \rangle = \langle a_i^\dagger \rangle = \bar{s} \,. \tag{4.122}$$

The variational parameter $\bar{s}$ is chosen to minimize the ground-state energy. Together with the constraint on the boson occupation numbers, this yields a set of saddle-point

equations on μ and $\bar{s}$:

$$\frac{\partial E_{\text{g.s.}}}{\partial \mu} = 0\,, \qquad \frac{\partial E_{\text{g.s.}}}{\partial \bar{s}} = 0\,. \tag{4.123}$$

The non-condensed b_i and c_i bosons describe transverse and longitudinal magnons with $S^z = \pm 1$ and $S^z = \pm 2$, respectively. Regrouping terms according to the number of b_i and c_i operators, we obtain the boson Hamiltonian as

$$\hat{\mathcal{H}}_b = \hat{\mathcal{H}}_0 + \hat{\mathcal{H}}_2 + \hat{\mathcal{H}}_3 + \hat{\mathcal{H}}_4\,. \tag{4.124}$$

Here, the constant term is

$$\hat{\mathcal{H}}_0 = -N\left[2J\bar{s}^4 - \mu(\bar{s}^2 - 1) + D\bar{s}^2\right] \tag{4.125}$$

The quadratic, cubic, and quartic terms are given by, respectively,

$$\begin{aligned}
\hat{\mathcal{H}}_2 &= \sum_i \left[\mu b_i^\dagger b_i + (4J\bar{s}^2 + \mu - D)\, c_i^\dagger c_i\right] \\
&\qquad - J\bar{s}^2 \sum_{\langle ij\rangle} (b_i b_j + b_i^\dagger b_j^\dagger)\,, \\
\hat{\mathcal{H}}_3 &= -2J\bar{s} \sum_{\langle ij\rangle} b_i^\dagger (c_j^\dagger + c_i) b_j\,, \\
\hat{\mathcal{H}}_4 &= -J \sum_{\langle ij\rangle} \left[\left(b_i^\dagger b_j^\dagger c_i c_j + c_i^\dagger c_j^\dagger b_i b_j\right) + c_i^\dagger c_j^\dagger c_i c_j\right].
\end{aligned} \tag{4.126}$$

A lack of small parameter for Eq. (4.126) and similar multiboson Hamiltonians [149–154] poses a problem for any perturbative treatment of magnon interactions described by $\hat{\mathcal{H}}_3$ and $\hat{\mathcal{H}}_4$. In our case, the quantum ground state exhibits a classical Néel order. Therefore, we follow a similar sequence of successive approximations to that in a standard spin-wave expansion. An analog of the $1/S$ small parameter for our problem is $1-\bar{s}^2$, which measures the strength of zero-point motion in the ground state.

4.4.1.2.2 Harmonic approximation

We start with the classical energy $\hat{\mathcal{H}}_0$ and obtain, with the help of (4.123), the classical values

$$\mu_0 = D + 4J\,, \qquad \bar{s}_0 = 1\,. \tag{4.127}$$

The quadratic Hamiltonian $\hat{\mathcal{H}}_2$ can be now straightforwardly diagonalized by using Fourier transformation followed by the canonical Bogolyubov transformation $b_{\mathbf{k}} = u_{\mathbf{k}} \tilde{b}_{\mathbf{k}} + v_{\mathbf{k}} \tilde{b}_{-\mathbf{k}}^\dagger$, see (2.75). The ordinary transverse magnons are described by the $\tilde{b}_{\mathbf{k}}$ boson branch and their excitation energy is

$$\varepsilon_{\mathbf{k}}^b = \sqrt{\mu^2 - (4J\bar{s}^2\gamma_{\mathbf{k}})^2}\,. \tag{4.128}$$

With the classical μ_0 and $\bar{s}_0$, the above expression coincides with the linear spin-wave result (2.85) for $S = 1$ with the renormalized $\bar{D} = D/2$. Thus, the conventional and the multi-boson spin wave theories have the same harmonic spectra and the same description of quantum zero-point oscillations in the semiclassical ground state.

The longitudinal magnons are described by the $c_{\mathbf{k}}$ boson branch and have energy

$$\varepsilon^{c}_{\mathbf{k}} = \mu - D + 4J\bar{s}^2 \,. \tag{4.129}$$

They remain fully localized in this approximation and their classical energy $\varepsilon^{c}_{0\mathbf{k}} = 8J$ is determined by four broken exchange bonds created by a fully reversed spin. We note that the harmonic multiboson spin-wave theory has been applied for a theoretical description of the excitation spectra in FeI_2 [122].

4.4.1.2.3 Quantum corrections

In the standard spin-wave theory, quantum corrections to the classical harmonic spectra are determined by two contributions: (i) the renormalization of the ground state and (ii) the anharmonic terms in the boson Hamiltonian. Such calculations have been performed using the $1/S$ expansion, for example for the Heisenberg square-lattice antiferromagnet in an applied field [147, 157] and for the Heisenberg helimagnet with strong quantum fluctuations [158–160].

In our case the leading quantum correction to the ground state energy comes from the zero-point oscillations obtained after diagonalization of $\hat{\mathcal{H}}_2$:

$$\Delta E_{\text{g.s.}} = \frac{1}{2N}\sum_{\mathbf{k}}\Big[\sqrt{\mu^2 - (4J\bar{s}^2\gamma_{\mathbf{k}})^2} - \mu\Big]. \tag{4.130}$$

Adding this contribution to the classical energy, we obtain from the saddle point condition (4.123) the equations for the renormalized $\bar{s}$ and μ:

$$\begin{aligned} 1-\bar{s}^2 &= \frac{1}{2N}\sum_{\mathbf{k}}\Big[\frac{\mu}{\sqrt{\mu^2-(4J\bar{s}^2\gamma_{\mathbf{k}})^2}} - 1\Big], \\ \mu-\mu_0 &= 4J(\bar{s}^2-1) + \frac{1}{2N}\sum_{\mathbf{k}}\frac{\left(4J\bar{s}\gamma_{\mathbf{k}}\right)^2}{\sqrt{\mu^2-(4J\bar{s}^2\gamma_{\mathbf{k}})^2}} \,. \end{aligned} \tag{4.131}$$

The above equations have to be solved either perturbatively in the spirit of the $1/S$ expansion or self-consistently. We find that a self-consistent harmonic approach (SCHA) is more practical, providing physical solutions over a wider range of J/D. For example, for $J = D$ we obtain $\bar{s} = 0.98$ and $\mu/D = 5.26$ ($\mu_0/D = 5$).

The new $\bar{s}$ and μ are used to compute modified $\varepsilon^{b,c}_{\mathbf{k}}$ according to Eqs. (4.128) and (4.129). However, these are not yet the final magnon energies, since the interaction terms $\hat{\mathcal{H}}_3$ and $\hat{\mathcal{H}}_4$ generate extra contributions that are generally of the same order in the small parameter $1 - \bar{s}^2$.

Cubic Interaction: The cubic boson terms $\hat{\mathcal{H}}_3$ are represented in the momentum space as

$$\begin{aligned} \hat{\mathcal{H}}_3 =& \frac{1}{2\sqrt{N}}\sum_{\mathbf{k},\mathbf{q}} V_3^{(1)}(\mathbf{k},\mathbf{q})(\tilde{b}_{\mathbf{k}}\tilde{b}_{\mathbf{q}}c_{-\mathbf{k}-\mathbf{q}} + \text{h.c.}) + \frac{1}{\sqrt{N}}\sum_{\mathbf{k},\mathbf{q}} V_3^{(2)}(\mathbf{k},\mathbf{q})(\tilde{b}^{\dagger}_{\mathbf{k}}\tilde{b}_{\mathbf{q}}c_{\mathbf{k}-\mathbf{q}} + \text{h.c.}) \\ &+ \frac{1}{2\sqrt{N}}\sum_{\mathbf{k},\mathbf{q}} V_3^{(3)}(\mathbf{k},\mathbf{q})(c^{\dagger}_{\mathbf{k}}\tilde{b}_{\mathbf{q}}\tilde{b}_{\mathbf{k}-\mathbf{q}} + \text{h.c.}) \end{aligned} \tag{4.132}$$

where h.c. denotes harmonic conjugate terms. The three cubic vertices are expressed by

$$\begin{aligned} V_3^{(1)}(\mathbf{k},\mathbf{q}) &= -4J\bar{s}\big(\gamma_{\mathbf{k}}u_{\mathbf{k}}v_{\mathbf{q}}+\gamma_{\mathbf{q}}u_{\mathbf{q}}v_{\mathbf{k}}\big)\,, \\ V_3^{(2)}(\mathbf{k},\mathbf{q}) &= -4J\bar{s}\big(\gamma_{\mathbf{k}}v_{\mathbf{k}}v_{\mathbf{q}}+\gamma_{\mathbf{q}}u_{\mathbf{k}}u_{\mathbf{q}}\big)\,, \\ V_3^{(3)}(\mathbf{k},\mathbf{q}) &= -4J\bar{s}\big(\gamma_{\mathbf{k}-\mathbf{q}}u_{\mathbf{q}}v_{\mathbf{k}-\mathbf{q}}+\gamma_{\mathbf{q}}u_{\mathbf{k}-\mathbf{q}}v_{\mathbf{q}}\big)\,. \end{aligned} \tag{4.133}$$

Here $V_3^{(1)}$ represents the vacuum source vertex, while $V_3^{(2,3)}$ describe scattering processes. Treating the cubic terms as a perturbation to the harmonic theory we obtain in the second order the following magnon self energies:

$$\Sigma_b(\omega,\mathbf{k}) = \frac{1}{N}\sum_{\mathbf{q}}\left[\frac{\big|V_3^{(2)}(\mathbf{k},\mathbf{q})\big|^2}{\omega-\varepsilon^b_{\mathbf{q}}-\varepsilon^c_{\mathbf{k}-\mathbf{q}}+i0}-\frac{\big|V_3^{(1)}(\mathbf{k},\mathbf{q})\big|^2}{\omega+\varepsilon^b_{\mathbf{q}}+\varepsilon^c_{\mathbf{k}+\mathbf{q}}}\right],$$

$$\Sigma_c(\omega,\mathbf{k}) = \frac{1}{2N}\sum_{\mathbf{q}}\left[\frac{\big|V_3^{(3)}(\mathbf{k},\mathbf{q})\big|^2}{\omega-\varepsilon^b_{\mathbf{q}}-\varepsilon^b_{\mathbf{k}-\mathbf{q}}+i0}-\frac{\big|V_3^{(1)}(\mathbf{k},\mathbf{q})\big|^2}{\omega+\varepsilon^b_{\mathbf{q}}+\varepsilon^b_{\mathbf{k}+\mathbf{q}}}\right],$$

where $\varepsilon^b_{\mathbf{k}}$ and $\varepsilon^c_{\mathbf{k}}$ are the harmonic magnon energies. In the Born approximation, the correction to the energy of b magnons comes from the cubic processes alone and is expressed as

$$\delta\varepsilon^b_{\mathbf{k}} = \Sigma_b(\varepsilon^b_{\mathbf{k}},\mathbf{k}) = \frac{1}{N}\sum_{\mathbf{q}}\left[\frac{\big|V_3^{(2)}(\mathbf{k},\mathbf{q})\big|^2}{\varepsilon^b_{\mathbf{k}}-\varepsilon^b_{\mathbf{q}}-\varepsilon^c_{\mathbf{k}-\mathbf{q}}}-\frac{\big|V_3^{(1)}(\mathbf{k},\mathbf{q})\big|^2}{\varepsilon^b_{\mathbf{k}}+\varepsilon^b_{\mathbf{q}}+\varepsilon^c_{\mathbf{k}+\mathbf{q}}}\right]. \tag{4.134}$$

The cubic processes also produce momentum-dependent corrections to the energy of longitudinal magnons:

$$\delta\varepsilon^{c\,\prime}_{\mathbf{k}} = \Sigma_c(\varepsilon^c_{\mathbf{k}},\mathbf{k}) = \frac{1}{2}\frac{1}{N}\sum_{\mathbf{q}}\left[\frac{\big|V_3^{(3)}(\mathbf{k},\mathbf{q})\big|^2}{\varepsilon^c_{\mathbf{k}}-\varepsilon^b_{\mathbf{q}}-\varepsilon^b_{\mathbf{k}-\mathbf{q}}}-\frac{\big|V_3^{(1)}(\mathbf{k},\mathbf{q})\big|^2}{\varepsilon^c_{\mathbf{k}}+\varepsilon^b_{\mathbf{q}}+\varepsilon^b_{\mathbf{k}+\mathbf{q}}}\right]. \tag{4.135}$$

For J exceeding the critical ratio $(J/D)_{c2}\simeq 0.75$, the c-magnon branch crosses into the two-magnon continuum and the self-energy $\Sigma_c(\varepsilon^c_{\mathbf{k}},\mathbf{k})$ acquires a finite imaginary part. This is further discussed below. Note that the b-magnon self energy never has an imaginary part on the mass surface $\omega=\varepsilon^b_{\mathbf{k}}$.

Quartic Interaction: The Hamiltonian $\hat{\mathcal{H}}_4$ is treated in the mean-field approximation with Hartree-Fock decoupling of the boson operators. The subsequent energy contribution is on the same footing as the one obtained from the cubic Hamiltonian $\hat{\mathcal{H}}_3$ treated perturbatively above. Around the harmonic state, the only non-zero average is $\langle b_i b_j\rangle$, given by

$$\Delta_b = \langle b_i b_j\rangle = \frac{1}{2N}\sum_{\mathbf{k}}\frac{4\bar{s}^2J\gamma^2_{\mathbf{k}}}{\sqrt{\mu^2-(4J\bar{s}^2\gamma_{\mathbf{k}})^2}}\,. \tag{4.136}$$

The decoupling yields a non-diagonal quadratic Hamiltonian in the c bosons. After applying a Fourier transformation, we obtain

$$\hat{\mathcal{H}}_4^{\mathrm{MF}} = -2J\Delta_b\sum_{\mathbf{k}}\gamma_{\mathbf{k}}\,(c_{\mathbf{k}}c_{-\mathbf{k}}+\mathrm{h.c.}). \tag{4.137}$$

As the b magnon spectrum is intact in this procedure we only write the total mean-field Hamiltonian in the c bosons

$$\hat{\mathcal{H}}^{\mathrm{MF}} = \sum_{\mathbf{k}} \left[(4J\bar{s}^2+\mu-D) c^{\dagger}_{\mathbf{k}} c_{\mathbf{k}} - 2J\Delta_b \gamma_{\mathbf{k}} \left(c_{\mathbf{k}} c_{-\mathbf{k}} + \mathrm{h.c.} \right) \right] \tag{4.138}$$

where we include the diagonal part that appears in the Fourier transformation of $\hat{\mathcal{H}}_2$. We diagonalize $\hat{\mathcal{H}}^{\mathrm{MF}}$ by means of a canonical Bogolyubov transformation

$$c_{\mathbf{k}} = w_{\mathbf{k}} \tilde{c}_{\mathbf{k}} + x_{\mathbf{k}} \tilde{c}^{\dagger}_{-\mathbf{k}} \tag{4.139}$$

where $w_{\mathbf{k}}$ and $x_{\mathbf{k}}$ are defined in a way similar to (2.75). The resulting spectrum of $\hat{\mathcal{H}}^{\mathrm{MF}}$ encodes the renormalized energy in the mean-field processing:

$$\varepsilon^c_{\mathbf{k}} + \delta\varepsilon^{c\,\prime\prime}_{\mathbf{k}} = \sqrt{(4J\bar{s}^2 + \mu - D)^2 - (4J\Delta_b\gamma_{\mathbf{k}})^2}. \tag{4.140}$$

In the leading order, the correction $\delta\varepsilon^{c\,\prime\prime}_{\mathbf{k}}$ is given by

$$\delta\varepsilon^{c\,\prime\prime}_{\mathbf{k}} = -\frac{8(J\Delta_b\gamma_{\mathbf{k}})^2}{\varepsilon^c_{\mathbf{k}}}\,, \tag{4.141}$$

In total, the magnon spectra in the multiboson spin-wave theory are $\varepsilon^b_{\mathbf{k}} + \delta\varepsilon^{b\,\prime}_{\mathbf{k}}$ for the T-magnons and $\varepsilon^c_{\mathbf{k}} + \delta\varepsilon^{c\,\prime}_{\mathbf{k}} + \delta\varepsilon^{c\,\prime\prime}_{\mathbf{k}}$ for the L-magnons. Results for the magnon spectra obtained by numerical evaluation of the analytical expressions (4.134), (4.135), and (4.136) are presented and discussed in the following.

The renormalized magnon energies can be used to improve on the general estimates of the critical couplings (4.64) and (4.65), which signify qualitative transformations in the excitation spectrum for our model. Specifically, for $J/D \leq (J/D)_{c1} = 0.18$ the L-magnons lie below the conventional T-magnon branch and represent the lowest-energy excitations. For $(J/D)_{c2} \simeq 0.75$, the L-magnon band starts to overlap with the two-magnon continuum. As a result, the longitudinal magnons acquire a finite lifetime $\tau_{\mathbf{k}}$ determined by two-magnon decay processees. In the Born approximation, the decay rate $\Gamma_{\mathbf{k}} = 1/\tau_{\mathbf{k}}$ is expressed as

$$\Gamma_{\mathbf{k}} = \frac{\pi}{2N} \sum_{\mathbf{q}} \left[V^{(3)}_3(\mathbf{k},\mathbf{q}) \right]^2 \delta\left(\varepsilon^c_{\mathbf{k}} - \varepsilon^b_{\mathbf{q}} - \varepsilon^b_{\mathbf{k}-\mathbf{q}} \right). \tag{4.142}$$

The two magnon decays are responsible for various singularities in the magnon spectra for low-dimensional quantum antiferromagnets [161, 162]. Specifically, in the present case the singularity develops near the crossing point denoted by $\mathbf{k}^*$. Expanding the denominator of the decay contribution given by the first term in (4.135) near the bottom of the two magnon continuum corresponding to b magnons with the momenta $\mathbf{q}^*$ and $\mathbf{k}^* - \mathbf{q}^*$, we get:

$$\varepsilon^c_{\mathbf{k}} - \varepsilon^b_{\mathbf{q}} - \varepsilon^b_{\mathbf{k}-\mathbf{q}} \approx -\mathbf{v}\cdot\Delta\mathbf{k} - Aq^2\,, \tag{4.143}$$

where $\mathbf{v} = \nabla\varepsilon^b_{\mathbf{k}^*-\mathbf{q}^*}$ and $\mathbf{q} \to \mathbf{q}^* + \mathbf{q}$. Therefore, the on-shell magnon self energy can be approximated by

$$\Sigma_c(\mathbf{k}) \approx \int \frac{d^2q}{-v\Delta k - Aq^2 + i0} \simeq \ln\frac{\Lambda}{\Delta k} - i\pi\Theta(\Delta k)\,. \tag{4.144}$$

Here Λ is a high-energy cut-off and $\Theta(x)$ is the step function. The logarithmic divergence is very pronounced in $\delta\varepsilon^{c\,\prime}_{\mathbf{k}}$ obtained using Eq. (4.135) for $J/D > 0.75$. Corresponding results are further analyzed below.

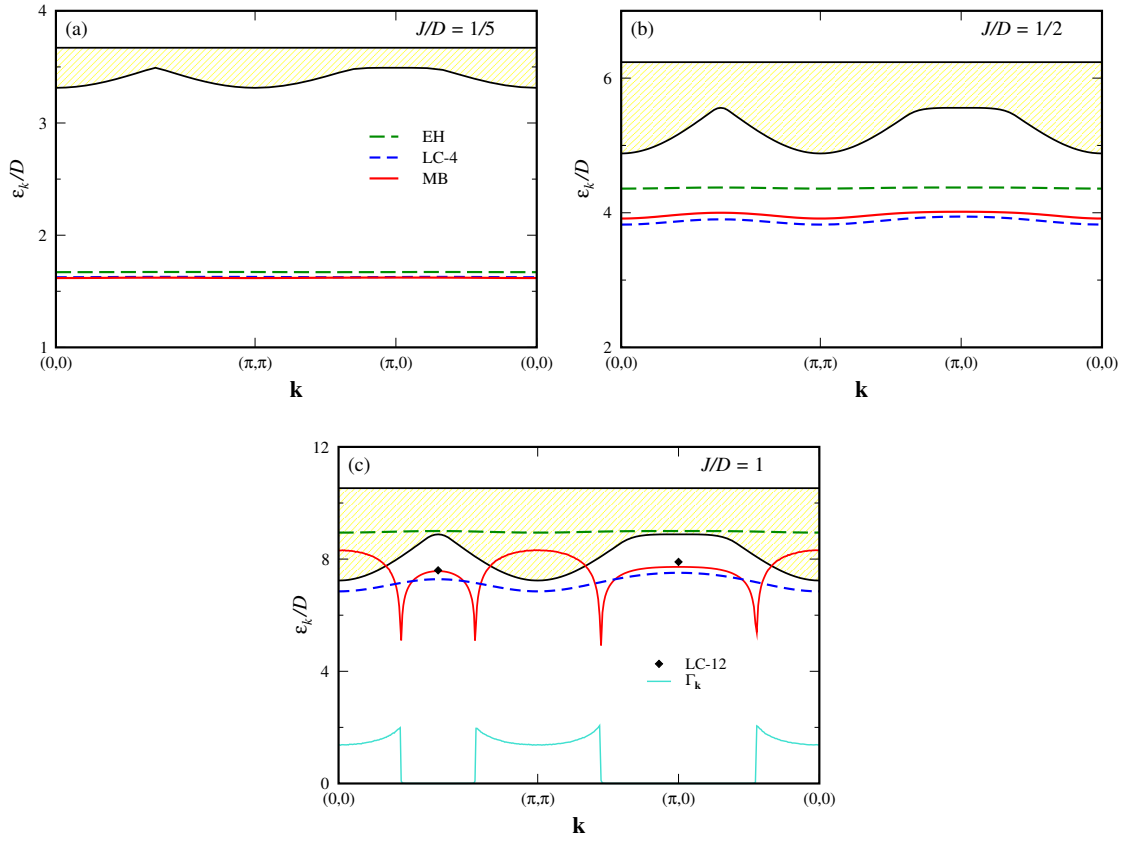

Figure 4.8: The longitudinal magnon spectra computed by different methods for the antiferromagnet with $J/D = 1/5$ (a), $1/2$ (b), and 1 (c). Acronyms in the legend are the same as in Fig. 4.7. Lightly shadowed regions denote the two-magnon continuum as obtained in the self-consistent harmonic approximation. Panel (c) includes the L-magnon decay rate $\Gamma_{\mathbf{k}}$ (4.142).

4.4.1.3 Comparison of results

In the following we discuss the excitation spectra obtained using the different theoretical methods. The ground-state energy, Fig. 4.9, comes out comparatively well for all approaches except for the effective Hamiltonian method. That approach loses accuracy at $J/D \gtrsim 0.3$, in the parameter range where transverse magnons become the lowest energy excitations and determine the zero-point vacuum fluctuations.

The excitation gap for ordinary (T) magnons Δ_T is shown as a function of J/D in Fig. 4.7(a). The twelfth-order linked-cluster expansion results LC-12 computed by Oitmaa and Hamer for selected values of J/D [120] can be used as accurate reference values. The analytical methods agree with the numerical reference values for small values of $J/D \lesssim 0.5$. The fourth-order linked-cluster expansion data, LC-4, start to deviate from the accurate LC-12 values for $J/D = 1$. The harmonic approximation HA, which does not depend on whether the Holstein-Primakoff or the multi-boson representation

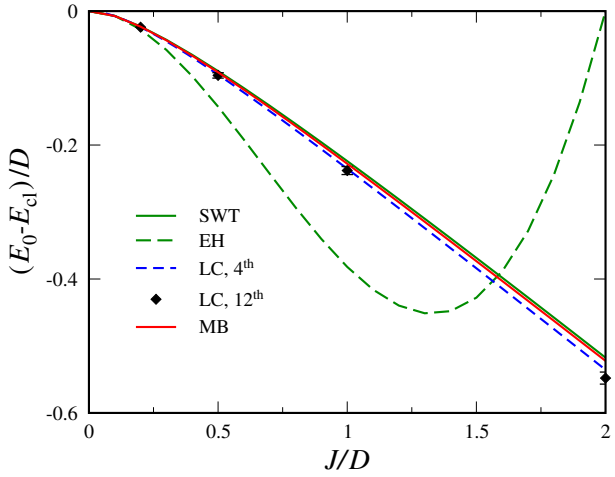

Figure 4.9: Ground-state energy of the $S = 1$ square-lattice antiferromagnet, obtained with different analytical methods, in comparison to the classical energy $E_{\rm cl} = -2J - D$. The notation follows from Figs. 4.7 and 4.8. The curves denoted SWT gives the zero-point energy in the standard spin-wave theory (2.83).

of spin operators is applied, works better than LC-4 for all $J/D \lesssim 1$. The nonlinear quantum corrections to the harmonic approximation, obtained within the multi-boson spin wave theory MB, improve on the agreement with the reference result for $J/D = 1/2$. In summary, the harmonic theory can give a semi-quantitative description for all $0 < J/D < \infty$, whereas the more elaborate approaches, that take into account nonlinear effects, work reasonably well only for $J/D < 1$.

Figure 4.7(b) presents results for the L-magnon gap Δ_L. Because of the lack of accurate numerical results, we use our lower-order linked-cluster expansion results LC-4 for comparison with the analytical approaches for $J/D \lesssim 0.75$. For small values $J/D \lesssim 0.25$, the three approaches agree with one other quantitatively. The effective Hamiltonian results (EH) become less accurate when J/D exceeds 0.3. The harmonic theory yields the dispersionless band of longitudinal magnons corresponding to a straight line in Fig. 4.7(b): $\Delta_L/D = 8J/D$. The MB results include nonlinear quantum effects and show a better agreement with LC-4 theory up to $J/D \sim 0.5$–0.6. A lightly shaded region in Fig. 4.7(b) corresponds to the extension of the two-magnon continuum for each value of J/D. It is constructed using the self-consistent harmonic approximation (SCHA), which in our case is only marginally different from the HA results. The crossing point of the unperturbed SCHA branch with the continuum takes place at $J/D \sim 0.75$. The MB theory displays a sharp dip for the respective value of J/D, reflecting the corresponding logarithmic singularity in the real part of the self-energy (4.144).

Finally, Fig. 4.8 shows the momentum dependence of the L-magnon excitation energy for representative values of J/D. Overall, the longitudinal magnons have a weak dispersion, which is, nonetheless, noticeable for $J/D \sim 1/2$. The multi-boson spin wave theory is in good quantitative agreement with the LC-4 results for small $J/D \lesssim 0.5$. The effective Hamiltonian approach gives in this coupling range somewhat overestimated energy $\varepsilon^L_{\mathbf{k}}$. For larger $J/D \gtrsim 0.75$, the longitudinal magnon branch enters the two-magnon continuum. The multi-boson theory is the only analytical approach that can predict finite life times for the L-magnons in this regime.

Close to the crossing point with the continuum the second-order correction (4.135) develops a logarithmic singularity as a function of momentum described by Eq. (4.144). Such a behavior is an artifact of the Born approximation in conjunction with the low dimensionality of the spin model [161]. The quantum correction $\delta\varepsilon^L_{\mathbf{k}}$ is regularized by higher-order processes. Specifically, the singularity from the two-particle decays is treated by taking into account the vertex corrections via a resummation of most divergent diagrams [45, 161]. Analysis of the analytical properties of the magnon self-energy $\Sigma_c(\omega, \mathbf{k})$ suggests that in two dimensions the single-particle branch $\varepsilon^L_{\mathbf{k}}$ enters the continuum tangentially with vanishing quasiparticle weight towards the crossing point [162].

In the bottom panel, Fig. 4.8(c), corresponding to $J/D = 1$, we also include two points corresponding to longitudinal magnons with $\mathbf{k} = (\pi/2, \pi/2)$ and $\mathbf{k} = (\pi, 0)$ obtained with the help of the high-order linked cluster expansion LC-12 [120]. As one can see from the comparison with the MB curve, the interacting multi-boson approach remains in agreement with the numerical results for relatively large J/D as long as the L-magnon branch lies outside of the continuum. The inverse lifetime of longitudinal magnons $\Gamma_{\mathbf{k}}$ (in units of D) is also included to this plot. The ratio $\Gamma_{\mathbf{k}}/\varepsilon_{\mathbf{k}}$ does not exceed ~ 0.3 for this value of J/D, implying that the longitudinal magnons remain as well-defined resonances inside the continuum. The decay rates of the longitudinal magnons rapidly grow upon further increase of the coupling constant. Their transformation into short-lived excitations throughout the whole Brillouin zone takes place for

$$(J/D)_{c3} \simeq 1.55\,. \tag{4.145}$$

4.4.2 Ferromagnetic order

We now consider the ferromagnetic model (4.66) with $J < 0$. Presence of the exact ground state with a parallel spin alignment along $\pm z$ direction allows for the exact solution of the two-particle problem. Besides the two-magnon continuum, the corresponding eigenstates include the exchange and the single-ion bound states. For $S = 1$, the latter states are identical to the longitudinal magnons. In the following we obtain the exact dispersion of L-magnons by solving the two-particle Schrödinger equation and compare it to results of two approximate methods: the effective spin Hamiltonian and the multiboson spin-wave theory.

We denote the fully polarized ferromagnetic state with spins pointing in the $+z$ direction by $|\mathrm{FM}\rangle$. A general state in the two-magnon subsector with $S^z = -2$ can be represented as

$$|2\rangle = \sum_{i,j} \psi_{ij}\, S_i^- S_j^- \,|\mathrm{FM}\rangle \tag{4.146}$$

with site summation implied and $\psi_{ij} = \psi_{ji}$. The eigenstate condition for the state $|2\rangle$ yields

$$\varepsilon_2\,|2\rangle = \sum_{i,j} \psi_{ij}[\hat{\mathcal{H}}, S_i^- S_j^-]\,|\mathrm{FM}\rangle\ , \tag{4.147}$$

where $\varepsilon_2 = E_2 - E_{\mathrm{g.s.}}$ is the excitation energy.

Investigation of bound magnon states in ferromagnets based on the Schrödinger equation (4.147) have been performed in Refs. [106–109, 111]. This approach allows to track a real-space structure of the bound-state wave function as well as its symmetry. Below,

we revisit this method and formulate Eq. (4.147) as a linear eigenvalue problem for the binding energy. Other approaches to the same problem include the Bethe ansatz method used for the anisotropic spin chains [163, 164] and the Green's function calculations [112].

The single-ion bound states (L-magnons) are distinguished from the exchange bound states (EBS) by amplitude ratios: $|\psi_{ii}| \gtrsim |\psi_{i,i+\boldsymbol{\delta}}|$ for the former and $|\psi_{ii}| \lesssim |\psi_{i,i+\boldsymbol{\delta}}|$ for the latter, where $\boldsymbol{\delta}$ is the bond vector. In particular, the single-ion bound states always correspond to the eigenstates with the s-wave symmetry, whereas the exchange bound states depending on the model may have various symmetries.

4.4.2.1 Exact solution

The operator commutators in Eq. (4.147) are computed separately for $i = j$ and for $i \neq j$. For commodity of the calculation, we give the results as a side note for a general spin $S \geq 1$ and isotropic exchange J.

For $i = j$:

$$\begin{aligned}
\sum_{l,\delta} J(\delta)\left[S_l^z S_{l+\delta}^z, S_i^{-2}\right]|\mathrm{FM}\rangle &= \sum_{\delta} J(\delta)\left(\left[S_i^z S_{i+\delta}^z, S_i^{-2}\right] + \left[S_{i-\delta}^z S_i^z, S_i^{-2}\right]\right)|\mathrm{FM}\rangle \\
&= 2\sum_{\delta} J(\delta) S(S-2-S) S_i^{-2}|\mathrm{FM}\rangle \\
&= -4SJ_{\mathbf{0}} S_i^{-2}|\mathrm{FM}\rangle\,, \qquad (4.148)\\
\sum_{l,\delta} J(\delta)\left[S_l^+ S_{l+\delta}^-, S_i^{-2}\right]|\mathrm{FM}\rangle &= \sum_{\delta} J(\delta) S_{i+\delta}^- \left[S_i^+, S_i^{-2}\right]|\mathrm{FM}\rangle \\
&= (4S-2)\sum_{\delta} J(\delta) S_{i+\delta}^- S_i^-|\mathrm{FM}\rangle, \qquad (4.149)
\end{aligned}$$

$$\left(\underline{\text{as}}\ S_i^+ S_i^{-2}|\mathrm{FM}\rangle = (4S-2)S_i^-|\mathrm{FM}\rangle\ \ \underline{\text{and}}\ S_i^+|\mathrm{FM}\rangle = 0\right)$$

$$\begin{aligned}
\sum_{l}\left[S_l^{z\,2}, S_i^{-2}\right]|\mathrm{FM}\rangle &= \left[S_i^{z\,2}, S_i^{-2}\right]|\mathrm{FM}\rangle \\
&= \left((S-2)^2 - S^2\right) S_i^{-2}|\mathrm{FM}\rangle \\
&= -4(S-1) S_i^{-2}|\mathrm{FM}\rangle\,. \qquad (4.150)
\end{aligned}$$

Therefore,

$$\left[\hat{\mathcal{H}}, S_i^{-2}\right]|\mathrm{FM}\rangle = \left(-2SJ_{\mathbf{0}}^z + 4(S-1)D\right) S_i^{-2}|\mathrm{FM}\rangle + (2S-1)\sum_{\delta} J^{\perp}(\delta) S_i^- S_{i+\delta}^-|\mathrm{FM}\rangle. \qquad (4.151)$$

Note the notation $J_{\mathbf{k}} = \sum_{\delta} J(\delta) e^{-i\mathbf{k}\delta}$.

For $i \neq j$:

$$\begin{aligned}
\sum_{l,\delta} J(\delta)\left[S_l^z S_{l+\delta}^z, S_i^- S_j^-\right]|\mathrm{FM}\rangle &= \sum_{l,\delta} J(\delta)\left(\delta_{l,i}\delta_{l+\delta,j} + \delta_{l,j}\delta_{l+\delta,i}\right)\left[S_l^z S_{l+\delta}^z, S_i^- S_j^-\right]|\mathrm{FM}\rangle \\
&+ \sum_{\substack{l=i \\ \delta\neq j-l}} J(\delta)\left[S_l^z S_{l+\delta}^z, S_i^- S_j^-\right]|\mathrm{FM}\rangle + \sum_{\substack{l=j \\ \delta\neq i-l}} J(\delta)\left[S_l^z S_{l+\delta}^z, S_i^- S_j^-\right]|\mathrm{FM}\rangle
\end{aligned}$$

$$
\begin{aligned}
&+\sum_{\substack{l+\delta=i\\ l\neq j}} J(\delta)\left[S_l^z S_{l+\delta}^z, S_i^- S_j^-\right]|\mathrm{FM}\rangle+\sum_{\substack{l+\delta=j\\ l\neq i}} J(\delta)\left[S_l^z S_{l+\delta}^z, S_i^- S_j^-\right]|\mathrm{FM}\rangle\\
=&2J_{ij}\left[S_i^z S_j^z, S_i^- S_j^-\right]|\mathrm{FM}\rangle+\sum_{\delta\neq j-i} J(\delta)\left[S_i^z S_{i+\delta}^z, S_i^- S_j^-\right]|\mathrm{FM}\rangle\\
&+\sum_{\delta\neq i-j} J(\delta)\left[S_j^z S_{j+\delta}^z, S_i^- S_j^-\right]|\mathrm{FM}\rangle+\sum_{l\neq j} J_{i,l}\left[S_l^z S_i^z, S_i^- S_j^-\right]|\mathrm{FM}\rangle\\
&+\sum_{l\neq i} J_{j,l}\left[S_l^z S_j^z, S_i^- S_j^-\right]|\mathrm{FM}\rangle\\
=&\Bigg[2\left[(S-1)^2-S^2\right]J_{ij}+S\,(S-1-S)\Big(\sum_{\delta\neq j-i} J(\delta)+\sum_{\delta\neq i-j} J(\delta)\\
&+\sum_{l\neq j} J_{il}+\sum_{l\neq i} J_{jl}\Big)\Bigg] S_i^- S_j^-|\mathrm{FM}\rangle\\
=&\left(2J_{ij}-4SJ_{\mathbf{0}}\right)S_i^- S_j^-|\mathrm{FM}\rangle\,,
\end{aligned}
\tag{4.152}
$$

$$
\begin{aligned}
\sum_{l,\delta} J(\delta)[S_l^+ S_{l+\delta}^-, S_i^- S_j^-]|\mathrm{FM}\rangle=&\sum_{\delta} J(\delta)\left([S_i^+, S_i^-]S_{i+\delta}^- S_j^- + [S_j^+, S_j^-]S_{j+\delta}^- S_i^-\right)|\mathrm{FM}\rangle\\
=&\sum_{\delta} J(\delta)\left(2S_i^z S_{i+\delta}^- S_j^-|\mathrm{FM}\rangle+2S_j^z S_{j+\delta}^- S_i^-|\mathrm{FM}\rangle\right)\\
=&2S\sum_{\delta} J(\delta)\left(S_{i+\delta}^- S_j^-|\mathrm{FM}\rangle+S_{j+\delta}^- S_i^-|\mathrm{FM}\rangle\right),
\end{aligned}
\tag{4.153}
$$

$$
\begin{aligned}
\sum_{l}\left[S_l^{z2}, S_i^- S_j^-\right]|\mathrm{FM}\rangle=&\left[S_i^{z2}, S_i^-\right]S_j^-|\mathrm{FM}\rangle+S_i^-\left[S_j^{z2}, S_j^-\right]|\mathrm{FM}\rangle\\
=&2\left((S-1)^2-S^2\right)S_i^- S_j^-|\mathrm{FM}\rangle\\
=&-2(2S-1)S_i^- S_j^-|\mathrm{FM}\rangle\,.
\end{aligned}
\tag{4.154}
$$

Therefore,

$$
\begin{aligned}
[\hat{\mathcal{H}}, S_i^- S_j^-]|\mathrm{FM}\rangle=&\Big(-2SJ_{\mathbf{0}}+2(2S-1)D+J_{ij}\Big)S_i^- S_j^-|\mathrm{FM}\rangle\\
&+S\sum_{\delta} J(\delta)\left(S_{i+\delta}^- S_j^-|\mathrm{FM}\rangle+S_{j+\delta}^- S_i^-|\mathrm{FM}\rangle\right).
\end{aligned}
\tag{4.155}
$$

Thus the expanded form of (4.147):

$$
\begin{aligned}
\varepsilon^{(2)}\sum_{i,j}\psi_{ij}|2_{ij}\rangle=&\sum_i \psi_{ii}\left(\Big(-2SJ_{\mathbf{0}}+4(S-1)D\Big)|2_{ii}\rangle+(2S-1)\sum_{\delta} J(\delta)|2_{i,i+\delta}\rangle\right)\\
&+\sum_{i\neq j}\psi_{ij}\left(\Big(-2SJ_{\mathbf{0}}+2(2S-1)D+J_{ij}\Big)|2_{ij}\rangle+S\sum_{\delta} J(\delta)\Big(|2_{i+\delta,j}\rangle+|2_{i,j+\delta}\rangle\Big)\right).
\end{aligned}
\tag{4.156}
$$

We used here the short-hand notation $|2_{ij}\rangle = S_i^- S_j^-|\mathrm{FM}\rangle$. Henceforth, we project (4.156) on $|2_{ij}\rangle$ in order to obtain a scalar equation in $(\psi_{ij})_{i,j}$. The family $(|2_{ij}\rangle)_{ij}$ is not normalized, as:

$$
\langle 2_{ij}|2_{ij}\rangle = 2S\delta_{i\neq j}+2\sqrt{S(2S-1)}\delta_{ij}.
\tag{4.157}
$$

We obtain accordingly from (4.151):

$$
\varepsilon^{(2)}\psi_{ii}=\Big(-2SJ_{\mathbf{0}}+4(S-1)D\Big)\psi_{ii}+S\sum_{\delta} J(\delta)\Big(\psi_{i-\delta,i}+\psi_{i,i-\delta}\Big).
\tag{4.158}
$$

and from (4.156):

$$\varepsilon^{(2)}\psi_{ij} = -\frac{1}{2}J_{ij}\big(\psi_{ii}+\psi_{jj}\big) + \Big(-2SJ_{\mathbf{0}} + 2(2S-1)D + J_{ij}\Big)\psi_{ij} + S\sum_{\delta} J(\delta)\big(\psi_{i-\delta,j}+\psi_{i,j-\delta}\big). \quad (4.159)$$

The obtained linear equations for ψ_{ij} are expressed in momentum space with the help of the double Fourier transformation:

$$\psi_{ij} = \frac{1}{N}\sum_{\mathbf{k}} e^{i\mathbf{k}(\mathbf{r}_i+\mathbf{r}_j)/2}\,\psi_{\mathbf{k}}(\mathbf{r})\ , \quad (4.160)$$

with amplitudes

$$\psi_{\mathbf{k}}(\mathbf{r}) = \frac{1}{N}\sum_{\mathbf{q}} e^{i\mathbf{q}\mathbf{r}}\psi_{\mathbf{k},\mathbf{q}}\ , \quad (4.161)$$

where $\mathbf{r} = \mathbf{r}_j - \mathbf{r}_i$ is a relative distance between two lattice sites and $\mathbf{k}$ is a total momentum of the magnon pair. As a result, we obtain a system of two equations, the first of which stems from the inter-site hopping of two spin flips,

$$\big[\varepsilon_2 - \varepsilon^T_{\mathbf{k}/2+\mathbf{q}} - \varepsilon^T_{\mathbf{k}/2-\mathbf{q}}\big]\psi_{\mathbf{k},\mathbf{q}} = \frac{2J}{N}\sum_{\mathbf{p}}\Big[\cos q_x\big(\cos p_x - \cos\frac{k_x}{2}\big) + \cos q_y\big(\cos p_y - \cos\frac{k_y}{2}\big)\Big]\psi_{\mathbf{k},\mathbf{p}}\ , \quad (4.162)$$

and the second describes a constraint on the same-site amplitude,

$$\frac{1}{N}\sum_{\mathbf{p}}\Big[\varepsilon_2 - \varepsilon^T_{\mathbf{k}/2+\mathbf{p}} - \varepsilon^T_{\mathbf{k}/2-\mathbf{p}} + 2D\Big]\psi_{\mathbf{k},\mathbf{p}} = 0\ . \quad (4.163)$$

Here $\varepsilon^T_{\mathbf{k}}$ is the one-magnon excitation energy for $S=1$, and

$$\varepsilon^T_{\mathbf{k}/2+\mathbf{p}} + \varepsilon^T_{\mathbf{k}/2-\mathbf{p}} = -8J + 2D + 4J\Big[\cos\frac{k_x}{2}\cos q_x + \cos\frac{k_y}{2}\cos q_y\Big] \quad (4.164)$$

gives the energy of the two-magnon continuum. For $D=0$, the second equation, (4.163), automatically follows from the first, (4.162). One therefore recovers the same eigenstate problem as for the exchange bound states in the Heisenberg ferromagnet [109]. For $D>0$, the attractive single-ion term in Eq. (4.163) creates an 'impurity potential'. This breaks translational invariance for the relative motion of two spin flips and, therefore, precludes solution of the two-magnon problem by an expansion in a few lattice harmonics.

Below, we solve the eigenstate problem in the mixed momentum/real-space representation of the wave function $\psi_{\mathbf{k}}(\mathbf{r})$, which is appropriate for bound two-magnon pairs. We further use the short-hand notations $c_{x,y} = 4\cos k_{x,y}/2$ and define dimensionless parameters

$$d = D/|J|\,, \quad e_b = \varepsilon_2/J + 8 + 2d - c_x - c_y\,. \quad (4.165)$$

Here e_b denotes the dimensionless binding energy, measured from the bottom of the two-magnon continuum. The momentum resummation in Eqs. (4.162) and (4.163) yields

$$\big(e_b + c_x + c_y - c_x\cos q_x - c_y\cos q_y\big)\psi_{\mathbf{k},\mathbf{q}} = 2\cos q_x\big[\psi_{\mathbf{k}}(\boldsymbol{a}) - \tfrac{1}{4}c_x\psi_{\mathbf{k}}(0)\big]$$

$$+ 2\cos q_y\big[\psi_{\mathbf{k}}(\boldsymbol{b}) - \tfrac{1}{4}c_y\psi_{\mathbf{k}}(0)\big]\ , \tag{4.166}$$

$$\big(e_b + c_x + c_y - 2d\big)\psi_{\mathbf{k}}(0) = c_x\psi_{\mathbf{k}}(\boldsymbol{a}) + c_y\psi_{\mathbf{k}}(\boldsymbol{b})\ , \tag{4.167}$$

where $\boldsymbol{a} = (1,0)$ and $\boldsymbol{b} = (0,1)$.

Next, we specify $\mathbf{r} \neq \mathbf{0}$ and convolute both sides of Eq. (4.166) with $\cos(\mathbf{q}.\mathbf{r})$, summing up over $\mathbf{q}$ in the first Brillouin zone. This yields

$$\begin{aligned}(e_b + c_x + c_y)\psi_{\mathbf{k}}(\mathbf{r}) - \frac{c_x}{2}\big[\psi_{\mathbf{k}}(\mathbf{r}+\boldsymbol{a}) + \psi_{\mathbf{k}}(\mathbf{r}-\boldsymbol{a})\big] - \frac{c_y}{2}\big[\psi_{\mathbf{k}}(\mathbf{r}+\boldsymbol{b}) + \psi_{\mathbf{k}}(\mathbf{r}-\boldsymbol{b})\big]\\ = \delta(\mathbf{r}-\boldsymbol{a})\big[\psi_{\mathbf{k}}(\boldsymbol{a}) - \frac{c_x}{4}\psi_{\mathbf{k}}(0)\big] + \delta(\mathbf{r}-\boldsymbol{b})\big[\psi_{\mathbf{k}}(\boldsymbol{b}) - \frac{c_y}{4}\psi_{\mathbf{k}}(0)\big]\end{aligned} \tag{4.168}$$

with $\delta(.)$ denoting the Kronecker delta function. This equation can be simplified by rearranging amplitudes from a two-dimensional $N_L \times N_L$ plane on a one-dimensional array of length $N = N_L \times N_L$:

$$\Psi_{\mathbf{k}} = {}^t\big(\{\psi_{\mathbf{k}}(-N_0, n)\}, ..., \{\psi_{\mathbf{k}}(0, n)\}, ..., \{\psi_{\mathbf{k}}(N_0, n)\}\big). \tag{4.169}$$

Note that for convenience we set $N_L = 2N_0 + 1$. The two equations Eqs. (4.167) and (4.168) can now be represented in the centrosymmetric matrix form

$$\begin{pmatrix}
\mathbb{P}_0 & \mathbb{J} & & & & & & & \\
\mathbb{J} & \mathbb{P}_0 & \mathbb{J} & & & & & & \\
 & & .. & & & & & & \\
 & & \mathbb{J} & \mathbb{P}_0 & \mathbb{J} & & & & \\
 & & & \mathbb{J} & \mathbb{P}_1 & \mathbb{Q} & & & \\
 & & & & \mathbb{J} & \mathbb{P}_2 & \mathbb{J} & & \\
 & & & & & \mathbb{Q} & \mathbb{P}_1 & \mathbb{J} & \\
 & & & & & & \mathbb{J} & \mathbb{P}_0 & \mathbb{J} \\
 & & & & & & & .. & \\
 & & & & & & & \mathbb{J} & \mathbb{P}_0 \quad \mathbb{J} \\
 & & & & & & & & \mathbb{J} \quad \mathbb{P}_0
\end{pmatrix} \Psi_{\mathbf{k}} = 0. \tag{4.170}$$

Here, $\mathbb{J} = (-c_x/2)\mathbb{I}$ with $\mathbb{I}$ the unit matrix, $\mathbb{Q}$ is a diagonal matrix defined as

$$\mathbb{Q}(N_0+1, N_0+1) = -c_x/4\,, \quad \mathbb{Q}(i,i) = -c_x/2\,,\ i \neq N_0+1, \tag{4.171}$$

and $\mathbb{P}_l$, $l = 0, 1, 2$ are symmetric centrosymmetric tridiagonal matrices specified by

$$\begin{aligned}\mathbb{P}_0(1,1) &= e_b + c_x + c_y\,, \\ \mathbb{P}_0(i, i\pm 1) = -c_y/2\,, &\quad \mathbb{P}_0(i,i) = e_b + c_x + c_y\,,\ i \geq 2\,.\end{aligned} \tag{4.172}$$

$$\begin{aligned}\mathbb{P}_1(i,j) &= \mathbb{P}_0(i,j)\,, \qquad (i,j) \neq (N_0+1, N_0+1)\,, \\ \mathbb{P}_1(N_0+1, N_0+1) &= e_b + c_x + c_y - 1\,.\end{aligned} \tag{4.173}$$

$$\begin{aligned}\mathbb{P}_2(i, i\pm 1) &= -c_y/2\,, \\ \mathbb{P}_2(j,j) &= e_b + c_x + c_y\,, \quad |j - N_0 - 1| > 1\,,\end{aligned}$$

$$\begin{aligned}\mathbb{P}_2(N_0, N_0) &= e_b + c_x + c_y - 1\,,\\ \mathbb{P}_2(N_0+1, N_0+1) &= e_b + c_x + c_y - 2d\,,\\ \mathbb{P}_2(N_0+2, N_0+2) &= e_b + c_x + c_y - 1\,,\\ \mathbb{P}_2(N_0+1\pm 1, N_0+1) &= -c_y/4\,.\end{aligned} \tag{4.174}$$

Above, we used the property $\psi_{\mathbf{k}}(\mathbf{r}) = \psi_{\mathbf{k}}(-\mathbf{r})$ as a consequence of the definition $\psi_{ij} = \psi_{ji}$ in Eq. (4.146). The resulting eigenvalue problem can be solved for e_b with the help of standard numerical algorithms. Practically, we use the Lapack routines to directly diagonalize the above matrix over a finite $N = N_L \times N_L$ lattice. The method exhibits a fast convergence with increasing system size providing a sufficient accuracy for $N_L^{\max} = 35$. The figure of merit used for convergence is the relative error $|\varepsilon_{\mathbf{k}}^{(N_L+1)} - \varepsilon_{\mathbf{k}}^{(N_L)}|/\varepsilon_{\mathbf{k}}^{(N_L)}$ with tolerance 10^{-3}, where $\varepsilon_{\mathbf{k}}^{(N_L)}$ denotes a computed bound-state solution for a given N_L. Note that we set open boundary conditions in this problem, consistent with the rapid decrease of the wavefunction amplitude with increasing $|\mathbf{r}|$.

For all values of $\mathbf{k}$ there are at most three solutions with $e_b > 0$, which can be associated with the single-ion (L-magnon) and two exchange bound states. Using the Gershgorin circle theorem on eigenvalue bounds for square matrices [165], we obtain:

$$-2(c_x + c_y) \leq e_b \leq \max\{2d, 1\}. \tag{4.175}$$

Since the width of the continuum is exactly $2(c_x + c_y)$, there are no anti-bound states above the continuum. The right-hand side of the previous inequality sets a lower bound for the two-magnon energy:

$$\varepsilon_2/|J| \geq 8 + 2d - c_x - c_y - \max\{2d, 1\}. \tag{4.176}$$

The matrix in (4.170) has a centrosymmetric structure, which leads to special symmetry properties of its eigenstates. Specifically, the eigenstates of a centrosymmetric matrix are classified into centro-symmetric and skew-symmetric vectors [166]. The former correspond to the s-wave bound-state wavefunctions, whereas the latter describe the d-wave bound states.

For $k_x = \pi$, the matrix (4.170) acquires a block-diagonal form leading to independent secular equations:

$$\det(\mathbb{P}_l) = 0\,, \quad l = 0, 1, 2\,. \tag{4.177}$$

Given the centrosymmetric form of $\mathbb{P}_l$'s and the property $\psi_{\mathbf{k}}(\mathbf{r}) = \psi_{\mathbf{k}}(-\mathbf{r})$, it is sufficient here to look for eigenvectors in the positive quadrant $\{\mathbf{r} = (m, n);\ m, n \geq 0\}$ only. The Gershgorin theorem can be separately applied for matrix $\mathbb{P}_0$ to show that it has only negative eigenvalues, corresponding to states within the continuum. The matrix structure is further simplified at $\mathbf{k}_0 = (\pi, \pi)$, for which all matrices $\mathbb{P}_l$ become diagonal. In this case, the block $\mathbb{P}_2$ provides two solutions with positive e_b:

(i) $e_b = 2d$, which has $\psi_{\mathbf{k}_0}(0) \neq 0$ and $\psi_{\mathbf{k}_0}(n\boldsymbol{b}) = 0$ for $n \geq 1$;

(ii) $e_b = 1$, which has $\psi_{\mathbf{k}_0}(\boldsymbol{b}) \neq 0$ and $\psi_{\mathbf{k}_0}(0) = \psi_{\mathbf{k}_0}(n\boldsymbol{b}) = 0$ for $n \geq 2$.

The former corresponds to the single-ion bound state (L-magnon), whereas the latter is the exchange bound state. The second equation for $l = 1$ has another bound state solution with $e_b = 1$, and $\psi_{\mathbf{k}_0}(\boldsymbol{a}) \neq 0$ and $\psi_{\mathbf{k}_0}(0) = \psi_{\mathbf{k}_0}(n\boldsymbol{a}) = 0$ for $n \geq 2$. Hence, the anisotropic square-lattice ferromagnet has three bound states with the total momentum $\mathbf{k}_0$, one single ion and two degenerate exchange states.

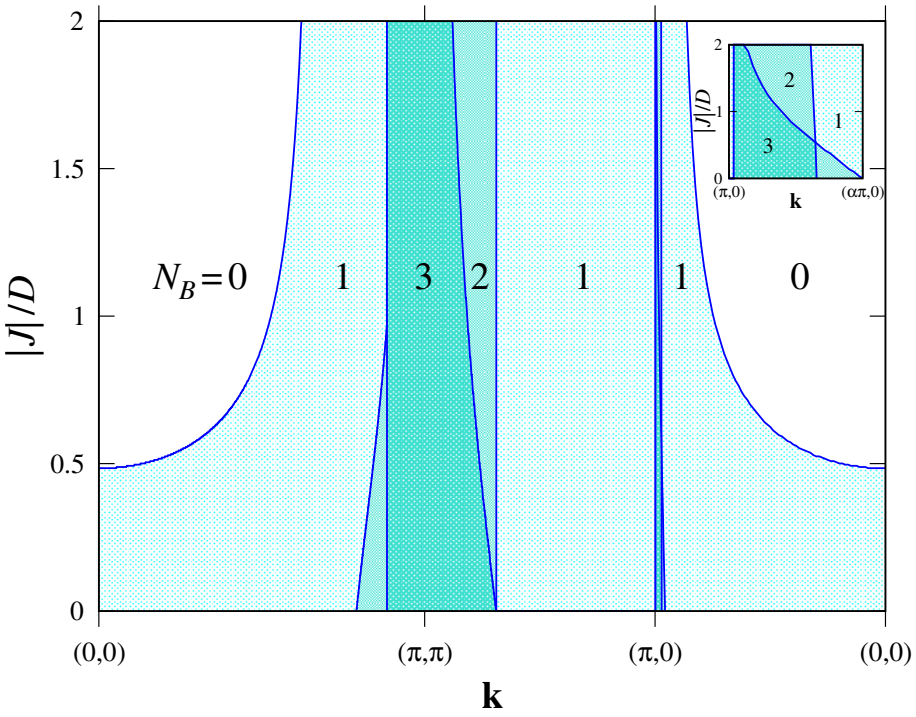

Figure 4.10: Diagram for the number of two-magnon bound states for the anisotropic square-lattice ferromagnet. The horizontal line represents a path along symmetry directions in the Brillouin zone. The vertical line spans a range of $|J|/D$ values. The number of bound states below the continuum is indicated by N_B for each of the differently shaded regions. The inset figure is a zoom on the path around $\mathbf{k} = (\pi, 0)$ with $\alpha \simeq 0.986$.

The diagram in Fig. 4.10 illustrates how the number of bound states changes upon moving away from the (π, π) point depending on the ratio $|J|/D$. The single-ion bound states (L-magnon branch) can easily be distinguished from the exchange bound states, as the latter do not exist for zero total momentum of a magnon pair $\mathbf{k} = 0$ for any value of J. The L-magnon dispersion curve has a minimum at $\mathbf{k} = 0$ and a maximum $\varepsilon = 8|J|$ at $\mathbf{k} = \mathbf{k}_0$. The L-magnon branch lies below the one-magnon excitations up to a threshold $(|J|/D)_{c1} \simeq 0.14$. It starts to overlap with the two-magnon continuum when $(|J|/D)_{c2} \simeq 0.5$.

Finally, we briefly comment on the question of the number of bound states for a ferromagnet in $\mathcal{D}$ dimensions, as raised in previous studies [106, 112]. Within our approach, the wavefunction amplitudes $\psi_{\mathbf{k}}(\mathbf{r})$ defined on a $\mathcal{D}$-dimensional cubic lattice are arranged into a one-dimensional array as in Eq. (4.195). By setting $\mathbf{k}_0 = (\pi, \pi, ...)$ we again obtain a fully diagonal matrix. For $D > 0$, it has $\mathcal{D} + 1$ positive eigenvalues $e_b > 0$ corresponding to bound states. One of them, with $e_b = 2D$, corresponds to the single-ion bound state (L-magnon). The other $\mathcal{D}$ exchange bound states, with $e_b = |J|$, are degenerate for this value of $\mathbf{k}$. By using the extended Gershgorin theorem [165], it can be shown that there are no additional bound state solutions of the secular equation for other values of $\mathbf{k}$. Note that this analysis applies only for the hypercubic-lattice models with the number of nearest-neighbor bonds equal to twice the number of momentum components. Extension to other lattices is an interesting open problem.

4.4.2.2 Comparison of results

The strong-coupling expansion in terms of the effective Hamiltonian approach, Sec. 4.3.3, yields for L-magnons in the anisotropic ferromagnet (4.66):

$$\varepsilon^L_{\mathbf{k}} = \varepsilon_0 - \left(\frac{2J^2}{D} - \frac{J^3}{D^2}\right)(1+\gamma_{\mathbf{k}})\,, \tag{4.178}$$

where $\varepsilon_0 = 8|J|$ is the classical energy of a fully reversed spin. For $\mathbf{k}_0 = (\pi,\pi)$ this yields $\varepsilon^L_{\mathbf{k}_0} = \varepsilon_0$, which is lower by $2D$ than the energy of two T-magnons: $\varepsilon_0 + 2D$, see Eq. (4.164). Thus, the effective spin-1/2 model reproduces the correct binding energy of $e_b = 2D$ for L-magnons at the Brillouin zone corner.

We can also obtain the L-magnon dispersion with the help of the multi-boson spin-wave theory, see Sec. 4.4.1.2. This approach is more simple for a ferromagnet than for an antiferromagnet since there are no zero-point fluctuations in the ground state and one-magnon excitations are also obtained exactly. The only cubic vertex present for a ferromagnet couples a longitudinal magnon (c boson) with two transverse magnons (b bosons). Contributions of the quartic terms vanish in the mean-field approximation. We skip straightforward intermediate steps and give the final result:

$$\varepsilon^c_{\mathbf{k}} = \varepsilon_0 + \frac{(4J)^2}{2N}\sum_{\mathbf{q}} \frac{(\gamma_{\mathbf{q}}+\gamma_{\mathbf{k}-\mathbf{q}})^2}{\varepsilon_0 - \varepsilon^b_{\mathbf{q}} - \varepsilon^b_{\mathbf{k}-\mathbf{q}}}\,. \tag{4.179}$$

The above expression also yields $\varepsilon^c_{\mathbf{k}_0} = \varepsilon_0$ corresponding to the correct binding energy once the longitudinal magnon wavefunction is completely localized. In the multiboson theory we can also compute the L-magnon decay rate from the imaginary part of the self-energy:

$$\Gamma_{\mathbf{k}} = \pi\frac{(4J)^2}{2N}\sum_{\mathbf{q}}(\gamma_{\mathbf{q}}+\gamma_{\mathbf{k}-\mathbf{q}})^2\,\delta\big(\varepsilon_0 - \varepsilon^b_{\mathbf{q}} - \varepsilon^b_{\mathbf{k}-\mathbf{q}}\big). \tag{4.180}$$

This expression vanishes at $\mathbf{k}_0$, recovering the long-lived character of the L-magnon at the zone corner.

Figure 4.11 presents the two magnon excitation spectra for the anisotropic ferromagnet along high-symmetry lines in the Brillouin zone. Different panels correspond to three characteristic values of J/D. Besides the single ion (SIBS) and the exchange bound states (EBS) obtained from the exact solution of the two magnon problem, we also show the exact two-magnon continuum and the results for the L-magnons from the effective Hamiltonian approach (EH) and by the multi-boson spin-wave theory (MB). For $J/D = -1/5$, panel (a), the L-magnon branch lies below the two-magnon continuum for all wave-vectors.

The exact solution shows that the binding energy vanishes smoothly at the onset of the two-magnon continuum. This recovers the known property of exponentially-vanishing binding energy of the two-magnon exchange bound states in isotropic ferromagnets [167]. The effective spin-1/2 model (EH) is in very good agreement with the exact solution, as long as the L-magnons are outside the continuum.

The multi-boson theory (MB) also agrees with the exact solution over a significant region around the zone corner, which extends towards $k = 0$ as D increases. An inaccurate reproduction of the precise position where longitudinal magnons overlap with the continuum, visible in both the excitation energy and the decay rate in Figs. 4.11(b) and

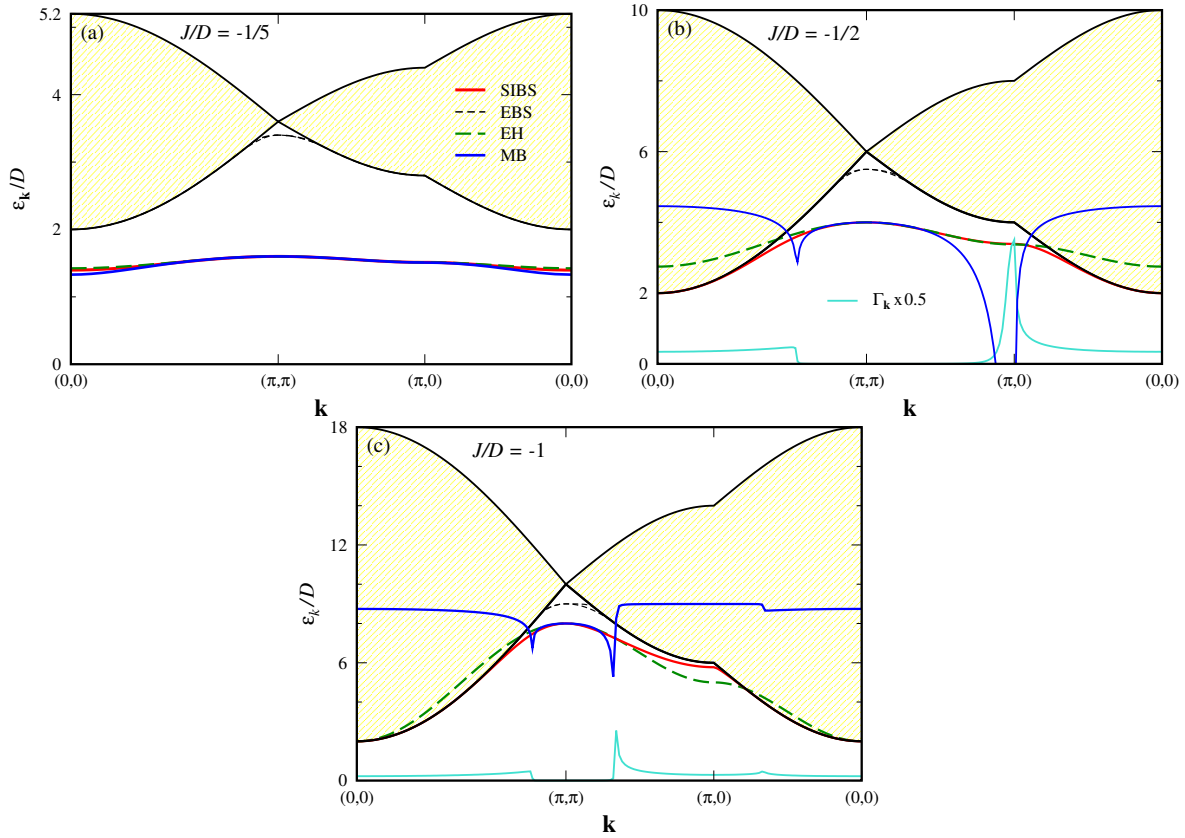

Figure 4.11: The two-magnon spectrum in the spin-1 easy-axis square-lattice ferromagnet. The acronyms used are: SIBS for the single-ion bound-state solution (L-magnon), EBS for the exchange bound-state solutions, EH for the effective Hamiltonian method and MB for the multi-boson theory. Panels (b) and (c) show also the L-magnon decay rate $\Gamma_{\mathbf{k}}$, Eq. (4.180).

(c), is due to the Born approximation used to evaluate the magnon self-energy correction. An alternative to this approximation would be to solve the Dyson equation [168]. Similarly to the antiferromagnetic case, the vertex function in (4.179) yields logarithmic singularities at its poles, describing strong repulsion from the continuum. However, these singularities would be suppressed by a regularized treatment involving higher orders.

4.4.3 Conclusions

We have presented in this section the results of various approximate methods for the $S = 1$ anisotropic square-lattice model (4.66). For antiferromagnetic coupling, $J > 0$, we used the numerical linked-cluster calculations and the multiboson spin-wave theory. Whereas for the ferromagnetic case $J < 0$, we use the exact solution of the two-magnon problem. These approaches follow up the mapping to an effective spin-1/2 model, presented in the previous section. Both the effective spin-1/2 model and the multi-boson spin-wave theory predict the dispersion of L-magnons with reasonably good accuracy up to moderate values of $|J|/D \simeq 0.75$. For the antiferromagnetic coupling, the multi-boson theory is somewhat more accurate, whereas for the ferromagnet the effective spin-1/2

Hamiltonian gives better results when compared to the exact solution.

Using the multi-boson framework, we have performed the calculations for two-magnon decays of the L-magnons in the $S = 1$ model, for ferromagnetic and antiferromagnetic exchange couplings. The second-order Born approximation leads to singularities both in the real and the imaginary parts of the longitudinal magnon self-energy in line with their general appearance for two-dimensional bosonic models. Such singularities disappear, however, once higher-order renormalization processes are taken into account [161]. The finite lifetime calculations enable us to trace the fate of the multipolar crystal-field excitations up to the limit of weak anisotropy, where no such excitations are generally present.

Apart from the experimental examples cited in the prelude to this work, we should mention another compound, $S = 1$ antiferromagnetic $Ni(NCS)_2(pyzdo)_2$ polymer [169], which has a square lattice geometry, close to the spin model studied in this section. The moderate value of $D/J \lesssim 1$ suggests that longitudinal magnons should exist at finite momenta in certain regions of the Brillouin zone.

4.5 Spin-1 triangular antiferromagnet at high fields

The study of L-magnons in zero magnetic field can be extended to the triangular lattice with large easy-axis single-ion anisotropy. The apparatus of the linked-cluster expansion and the multi-boson spin-wave theory developed above can still be used here. However, the problem can be approached differently in the presence of magnetic field above saturation. If the L-magnon branch appears below the two-particle continuum, the Zeeman effect leads to its condensation prior to the one-magnon branch. This may cause the appearance of a multi-polar ground-state. Since the phase is ferromagnetic above saturation, the L-magnon energy can be obtained exactly, by solving the two-magnon bound-state problem in the mixed real space-Fourier space representation, similarly to the previous section. We will examine this problem below.

4.5.1 Two magnon states

The Hamiltonian of interest reads:

$$\hat{\mathcal{H}} = \sum_{\langle ij \rangle} \left[J^{\perp}(S_i^x S_j^x + S_i^y S_j^y) + J^z S_i^z S_j^z \right] - D \sum_i (S_i^z)^2 - H \sum_j S_j^z \tag{4.181}$$

with $J^z > J^{\perp} > 0$. For $H \geq H_s$ the saturation field, the spins are aligned along the $+z$ direction. In this ferromagnetic phase, the exact ground-state energy for general spins S is given by the classical value:

$$E_0/N = (3J^z - D)S^2 - HS\,. \tag{4.182}$$

Before proceeding with the exact solution, let us briefly comment on the multi-magnon energies in the semi-classical limit, for $H, D \gg J^{z,\perp}$:
(i) A one-magnon state possesses $S^z = -1$ and has energy $E_1 \simeq H + D(2S-1) - 6J^z$, omitting the dispersive part $\sim O(J^{\perp}S)$. Because of positive J^z, the exchange favors localized spin flips.

(ii) Two-magnon states in the continuum have energy $E_2 \simeq 2H + 2D(2S-1) - 12J^z$ within the same accuracy.
(iii) A pair of magnons at adjacent sites increases their exchange energy as: $E_2^{\rm EB} \simeq E_2 + J^z$. Therefore, the antiferromagnetic exchange repels magnon pairs in the saturated phase, which favors anti-bound states. Such excitations have been studied in several models, mainly dedicated to one-dimensional magnets [164, 170–172]. They have also been observed recently in a quasi-one-dimensional spin chain [173].
(iv) The single-ion bound states unfold in the same three types defined in Sec. 4.1.1, and the easy-axis single-ion anisotropy still attracts magnons to favor bound states.

The exact one-magnon energy in the fully-polarized state is given by Eq. (2.59):

$$\varepsilon_{\mathbf{k}}^T = -6S(J^z - J^\perp \gamma_{\mathbf{k}}^\triangle) + (2S-1)D + H\,. \tag{4.183}$$

Magnons have a finite gap determined by the minimum of $\gamma_{\mathbf{k}}^\triangle$, equal to[4] -1/2, satisfied at the corners K of the hexagonal Brillouin zone, see Fig. 4.12. The field at which the gap closes corresponds to the saturation field:

$$H_s = 3S(2J^z + J^\perp) - (2S-1)D\,. \tag{4.184}$$

In the following, we set $S = 1$. A two-magnon state above the ferromagnetic ground state $|\mathrm{FM}\rangle$ (of fully polarized spins along the $+z$ direction) has the form of Eq. (4.146):

$$|2\rangle = \sum_{i,j} \phi_{ij}\, S_i^- S_j^- \,|\mathrm{FM}\rangle \tag{4.185}$$

with $\phi_{ij} = \phi_{ji}$. The eigenstate condition for the state $|2\rangle$ yields again

$$\varepsilon_2\,|2\rangle = \sum_{i,j} \phi_{ij}[\hat{\mathcal{H}}, S_i^- S_j^-]\,|\mathrm{FM}\rangle\ , \tag{4.186}$$

where ε_2 is the energy of the two-magnon state. We perform calculations of the operator commutators in a way similar to Sec. 4.4.2.1, resulting in a set of linear equations in ϕ_{ij}. We use a double Fourier transformation to obtain a system of two equations on the amplitudes $\phi_{\mathbf{k},\mathbf{q}}$:

$$\begin{aligned}\Big[\varepsilon_2 - \varepsilon^T_{\mathbf{k}/2+\mathbf{q}} - \varepsilon^T_{\mathbf{k}/2-\mathbf{q}}\Big]\phi_{\mathbf{k},\mathbf{q}} &= \frac{1}{2N}\sum_{\mathbf{p}}\Big[J^z_{\mathbf{p}-\mathbf{q}} + J^z_{\mathbf{p}+\mathbf{q}} - J^\perp_{\frac{\mathbf{k}}{2}+\mathbf{q}} - J^\perp_{\frac{\mathbf{k}}{2}-\mathbf{q}}\Big]\phi_{\mathbf{k},\mathbf{p}} \\ &= 2\sum_{\boldsymbol{\delta}} \cos(\mathbf{q}\cdot\boldsymbol{\delta})\frac{1}{N}\sum_{\mathbf{p}}\Big[J^z\cos(\mathbf{p}\cdot\boldsymbol{\delta}) - J^\perp\cos\frac{\mathbf{k}\cdot\boldsymbol{\delta}}{2}\Big]\phi_{\mathbf{k},\mathbf{p}}\,,\end{aligned} \tag{4.187}$$

and

$$\frac{1}{N}\sum_{\mathbf{p}}\Big[\varepsilon_2 - \varepsilon^T_{\mathbf{k}/2+\mathbf{p}} - \varepsilon^T_{\mathbf{k}/2-\mathbf{p}} + 2D\Big]\phi_{\mathbf{k},\mathbf{p}} = 0\ . \tag{4.188}$$

[4] We have $\gamma_{\mathbf{k}}^\triangle = \frac{1}{3}\left(\cos k_x + 2\cos\frac{k_x}{2}\cos\frac{k_y\sqrt{3}}{2}\right) = \frac{2}{3}\left[(X+\frac{Y}{2})^2 - \frac{Y^2}{4} - \frac{1}{2}\right] \geq -\frac{1}{2} = \gamma^\triangle_{X=\pm1/2,Y=\mp1}$ with $X = \cos\frac{k_x}{2}$ and $Y = \cos\frac{k_y\sqrt{3}}{2}$.

The term

$$\varepsilon^T_{\mathbf{k}/2+\mathbf{p}} + \varepsilon^T_{\mathbf{k}/2-\mathbf{p}} = -12J^z + 4J^\perp \sum_{i=1}^{3} \cos\frac{\mathbf{k}\cdot\boldsymbol{\delta}_i}{2} \cos\left(\mathbf{p}\cdot\boldsymbol{\delta}_i\right) + 2D + 2H \tag{4.189}$$

gives an energy of two-magnon pairs in the continuum. Here, $\boldsymbol{\delta}_j = \exp\left[2i(j-1)\pi/3\right]$, $j =$ 1-3, are the vectors of the triangular unit cell as shown schematically in Fig. 4.12.

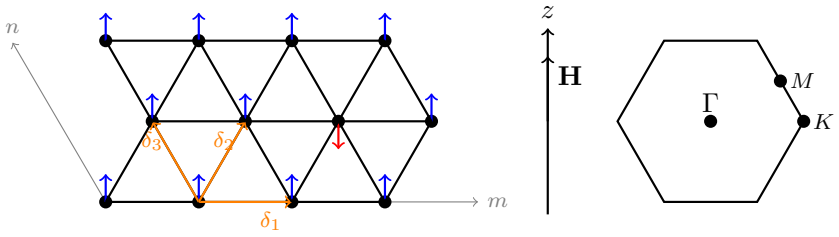

Figure 4.12: Left: Triangular antiferromagnet above saturation. The down-pointing (red) arrow depicts a reversed spin, which yields an L-magnon. Right: the Brillouin zone.

4.5.2 Exact solution

The lower boundary of the two-magnon continuum for a given total momentum $\mathbf{k}$ does not have a general analytical expression. Instead, we define the quantity

$$\mathcal{M} = \min_{\mathbf{q}} \Big\{ \sum_{i=1}^{3} c_{\boldsymbol{\delta}_i} \cos\left(\mathbf{q}\cdot\boldsymbol{\delta}_i\right) \Big\}, \tag{4.190}$$

where we use the notation $c_i = c_{\boldsymbol{\delta}_i} = 4\Delta\cos(\mathbf{k}\cdot\boldsymbol{\delta}_i/2)$, along with dimensionless parameters

$$\Delta = J^\perp/J^z\,, \qquad d = D/J^z\,,$$
$$e_b = (\min_{\mathbf{q}}\{\varepsilon^T_{\mathbf{k}/2+\mathbf{q}} + \varepsilon^T_{\mathbf{k}/2-\mathbf{q}}\} - \varepsilon_2)/J^z = -12 + \mathcal{M} + 2d + 2H/J^z - \varepsilon_2/J^z\,. \tag{4.191}$$

Here e_b denotes the dimensionless binding energy, measured from the bottom of the two-magnon continuum. The momentum resummation in Eqs. (4.187) and (4.188) yields

$$\Big[-e_b + \mathcal{M} - \sum_{\boldsymbol{\delta}} c_{\boldsymbol{\delta}} \cos\left(\mathbf{q}\cdot\boldsymbol{\delta}\right)\Big]\phi_{\mathbf{k},\mathbf{q}} = 2\sum_{\boldsymbol{\delta}} \cos\left(\mathbf{q}\cdot\boldsymbol{\delta}\right)\big[\phi_{\mathbf{k}}(\boldsymbol{\delta}) - \frac{c_{\boldsymbol{\delta}}}{4}\phi_{\mathbf{k}}(0)\big] \tag{4.192}$$

$$\big(-e_b + \mathcal{M} + 2d\big)\phi_{\mathbf{k}}(0) = \sum_{\boldsymbol{\delta}} c_{\boldsymbol{\delta}}\phi_{\mathbf{k}}(\boldsymbol{\delta})\,. \tag{4.193}$$

Note that we used the property $\phi_{\mathbf{k}}(\mathbf{r}) = \phi_{\mathbf{k}}(-\mathbf{r})$, which follows from the condition $\phi_{ij} = \phi_{ji}$ in Eq. (4.185). Now, we specify $\mathbf{r} \neq \mathbf{0}$ and convolute both sides of Eq. (4.192) with $\cos(\mathbf{q}.\mathbf{r})$, summing up over $\mathbf{q}$ in the first Brillouin zone. This yields

$$(-e_b+\mathcal{M})\phi_{\mathbf{k}}(\mathbf{r}) - \sum_{i=1}^{3}\frac{c_{\boldsymbol{\delta}_i}}{2}\big[\phi_{\mathbf{k}}(\mathbf{r}+\boldsymbol{\delta}_i)+\phi_{\mathbf{k}}(\mathbf{r}-\boldsymbol{\delta}_i)\big] = \sum_{i=1}^{3}\delta(\mathbf{r}-\boldsymbol{\delta}_i)\big[\phi_{\mathbf{k}}(\boldsymbol{\delta}_i) - \frac{c_{\boldsymbol{\delta}_i}}{4}\phi_{\mathbf{k}}(0)\big] \tag{4.194}$$

with $\delta(.)$ denoting the 2D Kronecker delta function. Like for the square lattice, this equation is simplified by rearranging amplitudes from a two-dimensional $N_L \times N_L$ plane on a one-dimensional array of length $N = N_L \times N_L$:

$$\Phi_{\mathbf{k}} = {}^t\big(\{\phi_{\mathbf{k}}(-N_0, n)\}, ..., \{\phi_{\mathbf{k}}(0, n)\}, ..., \{\phi_{\mathbf{k}}(N_0, n)\}\big). \tag{4.195}$$

The coordinates (m, n) in this grid follow the convention drawn in Fig. 4.12: $(m, n) = m\boldsymbol{\delta}_1 + n\boldsymbol{\delta}_3$. For convenience, we set $N_L = 2N_0 + 1$. The two equations Eqs. (4.193) and (4.194) are represented in the centrosymmetric matrix form

$$\begin{pmatrix}
\mathbb{P}_0 & \mathbb{J}^T & & & & & & & \\
\mathbb{J} & \mathbb{P}_0 & \mathbb{J}^T & & & & & & \\
 & & .. & & & & & & \\
 & & \mathbb{J} & \mathbb{P}_0 & \mathbb{J}^T & & & & \\
 & & & \mathbb{J} & \mathbb{P}_1 & \mathbb{Q}^T & & & \\
 & & & & \mathbb{J} & \mathbb{P}_2 & \mathbb{J}^T & & \\
 & & & & & \mathbb{Q} & \mathbb{P}_1 & \mathbb{J}^T & \\
 & & & & & & \mathbb{J} & \mathbb{P}_0 & \mathbb{J}^T \\
 & & & & & & & .. & \\
 & & & & & & & \mathbb{J} & \mathbb{P}_0 & \mathbb{J}^T \\
 & & & & & & & & \mathbb{J} & \mathbb{P}_0
\end{pmatrix} \Phi_{\mathbf{k}} = e_b \Phi_{\mathbf{k}}. \tag{4.196}$$

Here, $\mathbb{J}$ has non-vanishing terms only on its diagonal and subdiagonal as:

$$\mathbb{J}(i,i) = -c_1/2\,, \quad \mathbb{J}(i+1,i) = -c_2/2 \tag{4.197}$$

$\mathbb{Q}$ has the form:

$$\begin{gathered}
\mathbb{Q}(N_0, N_0+1) = c_2/4\,, \quad \mathbb{Q}(N_0+2, N_0+1) = -c_2/4\,, \\
\mathbb{Q}(N_0+1, N_0+1) = -c_1/4 \\
\mathbb{Q}(i,i) = -c_1/2\,, \quad \mathbb{Q}(i+1,i) = -c_2/2\,, \quad i \neq N_0+1,
\end{gathered} \tag{4.198}$$

and $\mathbb{P}_l$, $l = 0, 1, 2$ are symmetric centrosymmetric tridiagonal matrices specified by:

$$\mathbb{P}_0(i,i) = \mathcal{M}\,, \quad \mathbb{P}_0(i, i \pm 1) = -c_3/2\,,\ i \geq 2\,. \tag{4.199}$$

$$\begin{gathered}
\mathbb{P}_1(i,j) = \mathbb{P}_0(i,j)\,, \quad (i,j) \neq \{(N_0+1, N_0+1), (N_0+1\pm 1, N_0+1\pm 1)\}\,, \\
\mathbb{P}_1(N_0, N_0) = \mathcal{M} - 1 \\
\mathbb{P}_1(N_0+1, N_0+1) = \mathcal{M} - 1 \\
\mathbb{P}_1(N_0+2, N_0+2) = \mathcal{M} - 1\,.
\end{gathered} \tag{4.200}$$

$$\begin{gathered}
\mathbb{P}_2(i,j) = \mathbb{P}_1(i,j)\,, \quad j \neq N_0+1\,, \\
\mathbb{P}_2(N_0+1\pm 1, N_0+1) = -c_3/4\,, \\
\mathbb{P}_2(N_0+1, N_0+1) = \mathcal{M} + 2d\,.
\end{gathered} \tag{4.201}$$

The resulting eigenvalue problem can be solved again for e_b using a similar standard numerical algorithm as for the square lattice. The block-tridiagonal form of the matrix

above is more involved, since the subdiagonal blocks $\mathbb{J}$ and $\mathbb{Q}$ are not diagonal matrices. Still, the algorithm is consistent for $N_L^{\max} \geq 40$.

For all values of momenta $\mathbf{k}$, there are at most three solutions: one single-ion bound state (the L-magnon) and two exchange anti-bound states. The coefficients c_i do not cancel simultaneously, therefore the tridiagonal two-magnon bound-state problem here does not reduce to a diagonal one. Nevertheless, we can apply the Gershgorin circle theorem to obtain bounds on the two-magnon energy. The centrosymmetric structure of the problem yields also the same conclusions here on the nature of the symmetry of the two-magnon states. The solutions are shown in Fig. 4.12 for a set of parameters describing $Na_2BaNi(PO_4)_2$ and a field $H = 2D$, see Ref. [129].

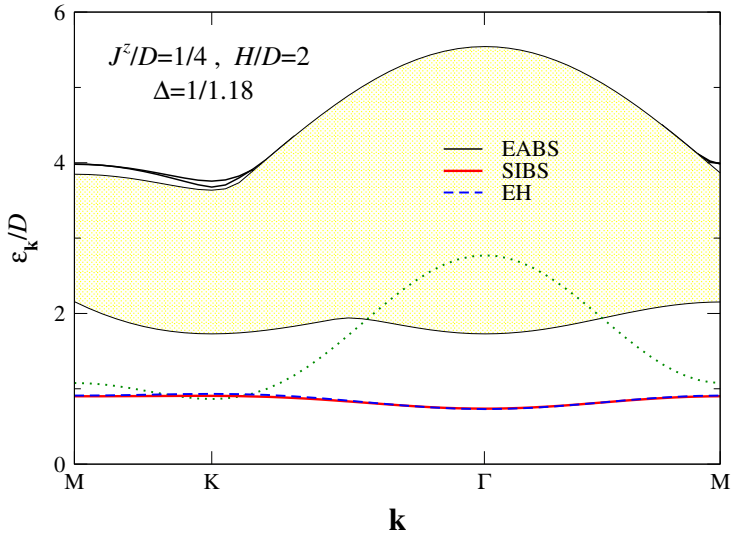

Figure 4.13: Two-magnon spectrum of the $S = 1$ polarized triangular antiferromagnet, with microscopic parameters of $Na_2BaNi(PO_4)_2$ and a calculated saturation field $H_s/D \simeq 1.15$, see Ref. [129]. We use the same acronyms as in Fig. 4.11, with EABS denoting the two exchange anti-bound states. The dotted line shows the T-magnon energy. Note that for the effective Hamiltonian (EH) we truncated the coefficients in (4.204) to the second-order, which gives slightly better agreement with the exact solution than a third-order expression.

4.5.3 Effective $s = 1/2$ Hamiltonian

In the limit of large $D > J^z$, we can still obtain a description of the longitudinal magnons as ordinary magnons in the lattice of pseudo-spins 1/2. We consider the unperturbed Hamiltonian

$$\hat{\mathcal{H}}_0 = -\sum_j \Big[H S_j^z + D(S_j^z)^2 \Big], \tag{4.202}$$

and the perturbation

$$\hat{\mathcal{V}} = J^z \sum_{\langle ij \rangle} \Big[\Delta(S_i^x S_j^x + S_i^y S_j^y) + S_i^z S_j^z \Big], \tag{4.203}$$

with $H > H_s$, $\Delta < 1$ and spin-1 operators. In the two-spin problem, we have the following unperturbed energy ladder:

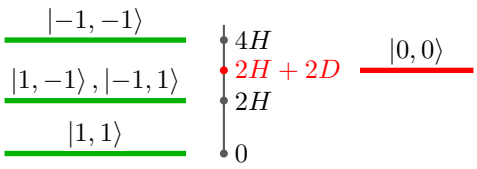

based on which we construct the effective interaction in the subspace of fully polarized spins $|\pm 1, \pm 1\rangle$. As discussed in Sec. 4.3.2, a spin flip in this subspace corresponds to a reversed spin in the spin-1 model and would describe the longitudinal magnons. We proceed accordingly with perturbation theory in the third order, similarly to Sec. 4.3.3.1. The obtained effective exchange for two spins in the spin-1/2 algebra has the form:

$$\hat{h}_J = \tilde{h}_0 + \tilde{J}_\parallel s_i^z s_j^z + \tilde{J}_\perp \left(s_i^x s_j^x + s_i^y s_j^y \right),$$

where

$$\tilde{J}_\parallel = 4J^z + \left[\frac{(J^z)^2}{D} - \frac{(J^z)^3}{2D^2} \right] \Delta^2 , \quad \tilde{J}_\perp = \left[\frac{-(J^z)^2}{D} + \frac{(J^z)^3}{2D^2} \right] \Delta^2, \tag{4.204}$$

and $\tilde{h}_0$ is a constant term. The unperturbed Hamiltonian is now non-trivial and reads:

$$\hat{h}_0 = -8D - 2H(s_i^z + s_j^z), \tag{4.205}$$

by means of the mapping (4.12). Therefore, the effective Hamiltonian in this approximation is given by

$$\hat{\mathcal{H}}_{\text{eff}}^{\triangle} = \tilde{E}_0 + \sum_{\langle i,j \rangle} \left[\tilde{J}_\perp \left(s_i^x s_j^x + s_i^y s_j^y \right) + \tilde{J}_\parallel s_i^z s_j^z \right] - 2H \sum_j s_j^z \, . \tag{4.206}$$

Note that since the perturbation $\hat{\mathcal{V}}$ commutes with the total spin S_{tot}^z, the Zeeman energy does not appear in the effective exchange interaction. Moreover, the antiferromagnetic sign of effective Ising exchange is still overcome by the strong field H, such that the ground state has ferromagnetic alignment along the z axis. Subsequently, the L-magnon dispersion is straightforward, see Tab. 4.1:

$$\varepsilon_{\mathbf{k}}^L = -3(\tilde{J}_\parallel - \tilde{J}_\perp \gamma_{\mathbf{k}}^{\triangle}) + 2H. \tag{4.207}$$

4.5.4 Conclusions

We solved here the problem of the two-magnon energy in the polarized triangular antiferromagnet exactly. To the best of our knowledge, no exact solution has been developed so far that captures both the energy and the symmetry of the bound/anti-bound states in the triangular case, see Ref. [111] for a solution with Green's functions. We also derived a simple effective model for small J/D in the polarized phase, which agrees with the exact solution, Fig. 4.13, optimally for effective coefficients truncated to the second-order.

We note that condensation of the L-magnon, which lays below the T-magnon branch for $J/D \lesssim 1/4$ here, may lead to the spin-nematic phase discussed in Ref. [129], and more

recently in Ref. [132]. The characterization of this multipolar phase may be performed using the multi-boson spin-wave theory, similar to the one elaborated in Sec. 4.4.1.2 for the square lattice. Its results for the L-magnon energy should be compared to the exact solution obtained here, which is an important step for obtaining the condensate. Carrying this calculation is an interesting open problem.

4.6 Longitudinal magnons as anti-bound states

The theory elaborated in the previous sections treated the problem of longitudinal magnons as coherent $2S$-magnon single-ion bound states in materials with strong easy-axis single-ion anisotropy. In an $S = 1$ ferromagnet, these bound states are solutions of the two-magnon problem. They satisfy an s-wave symmetry and have a wavefunction that minimizes energy by attracting two spin flips on the same site. For a different sign of the single-ion anisotropy, two spin flips on the same site would now maximize energy, which indicates a repulsive single-site potential. This is reminiscent of exchange anti-bound states, found in the polarized antiferromagnet of Sec. 4.5. For a general setting, let us consider the Hamiltonian

$$\hat{\mathcal{H}} = J \sum_{\langle ij \rangle} \mathbf{S}_i \cdot \mathbf{S}_j + \sum_i \Big[D(S_i^z)^2 - H S_i^z \Big], \tag{4.208}$$

on the square-lattice with spin-1 operators and $D > 0$. The single-ion term alone favors a disordered state with $S^z = 0$. In the field-polarized phase, this interaction is maximum and the ground-state energy per spin is

$$E_0/N = 2J + D - H. \tag{4.209}$$

The semi-classical energy estimate for two spin flips in this phase is $E_2 = 2H + 2D - 8J$, ignoring the dispersive term $O(J)$. It reaches a maximum for flips on the same site with the value $E_2^{SI} = E_2 + 2D$. Therefore, this repulsive potential occasions anti-bound states[5]. The T-magnon energy in this phase is simply

$$\varepsilon_{\mathbf{k}}^T = -4J(1 - \gamma_{\mathbf{k}}^{\square}) - D + H\,, \tag{4.210}$$

obtained in the same way as for an easy-axis anisotropy, see Sec. 2.4.2.1. The above expression holds irregardless of the sign of J, and we obtain a lower bound on magnetic field

$$H \geq \max\{D, 8J + D\} =: H_s \tag{4.211}$$

to have well defined magnons in the polarized phase. We note that a localized spin flip has energy

$$\varepsilon_0 = -4J - D + H\,, \tag{4.212}$$

which is smaller than $\varepsilon_{\mathbf{k}}^T$ around $k = 0$ for antiferromagnetic exchange.

[5]There is also the situation where spins are on two adjacent sites, which have energy $E_2^{EB} = E_2 + J$, that is favorable for ferromagnetic $J < 0$ and unfavorable for antiferromagnetic $J > 0$. This describes exchange bound and anti-bound states, respectively.

4.6.1 Exact solution

We can solve the two-magnon problem exactly, in a similar way to the solutions provided in Sec. 4.4.2.1 and Sec. 4.5.2. With the insight of the preceding work, we can write immediately the final centrosymmetric eigenvalue problem:

$$\begin{pmatrix}
\mathbb{B}_0 & \mathbb{J}^T & & & & & & & & \\
\mathbb{J} & \mathbb{B}_0 & \mathbb{J}^T & & & & & & & \\
 & & \ddots & & & & & & & \\
 & & \mathbb{J} & \mathbb{B}_0 & \mathbb{J}^T & & & & & \\
 & & & \mathbb{J} & \mathbb{B}_1 & \mathbb{Q}^T & & & & \\
 & & & & \mathbb{J} & \mathbb{B}_2 & \mathbb{J}^T & & & \\
 & & & & & \mathbb{Q} & \mathbb{B}_1 & \mathbb{J}^T & & \\
 & & & & & & \mathbb{J} & \mathbb{B}_0 & \mathbb{J}^T & \\
 & & & & & & & & \ddots & \\
 & & & & & & & \mathbb{J} & \mathbb{B}_0 & \mathbb{J}^T \\
 & & & & & & & & \mathbb{J} & \mathbb{B}_0
\end{pmatrix} \tilde{\Psi}_{\mathbf{k}} = e_a \tilde{\Psi}_{\mathbf{k}}, \tag{4.213}$$

in terms of the *anti-binding* energy e_a, counted from the top of the two-magnon continuum (in units of $|J|$). Here we used the notation of Sec. 4.4.2.1, with the blocks $\mathbb{J}$ and $\mathbb{Q}$ unchanged, and the matrices $\mathbb{B}_l$, $l = 0, 1, 2$ now specified by

$$\begin{aligned} \mathbb{B}_0(1,1) &= -c_x - c_y\,, \\ \mathbb{B}_0(i, i\pm 1) = -c_y/2\,, &\quad \mathbb{B}_0(i,i) = -c_x - c_y\,,\ i \geq 2\,. \end{aligned} \tag{4.214}$$

$$\begin{aligned} \mathbb{B}_1(i,j) &= \mathbb{B}_0(i,j)\,, \qquad (i,j) \neq (N_0+1, N_0+1)\,, \\ \mathbb{B}_1(N_0+1, N_0+1) &= -c_x - c_y + J/|J|\,. \end{aligned} \tag{4.215}$$

$$\begin{aligned} \mathbb{B}_2(i, i\pm 1) &= -c_y/2\,, \\ \mathbb{B}_2(j,j) &= -c_x - c_y\,, \quad |j - N_0 - 1| > 1\,, \\ \mathbb{B}_2(N_0, N_0) &= -c_x - c_y + J/|J|\,, \\ \mathbb{B}_2(N_0+1, N_0+1) &= -c_x - c_y - 2d\,. \\ \mathbb{B}_2(N_0+2, N_0+2) &= -c_x - c_y + J/|J| \\ \mathbb{B}_2(N_0+1\pm 1, N_0+1) &= -c_y/4\,. \end{aligned} \tag{4.216}$$

The conclusions on the s-wave symmetry of the single-ion anti-bound state hold[6], as a consequence of the symmetry of the eigenvectors. The upper bound on the binding[7] and anti-binding energies are still derived by means of the Gershgorin theorem:

$$\begin{aligned} J > 0: &\qquad e_a \leq \max\{2D, J\}, \quad e_b \leq 0 \\ J < 0: &\qquad e_a \leq 2D, \qquad\quad e_b \leq J. \end{aligned} \tag{4.217}$$

where these assertions are equalities for $\mathbf{k}_0 = (\pi, \pi)$. The two-magnon spectrum with the exact solution is shown in Fig. 4.14 for both signs of J.

[6] The s-wave and d-wave symmetries of the two exchange bound or anti-bound states also hold for the same reason: the centrosymmetric problem admits symmetric and skew-symmetric eigenvectors.

[7] Noted e_b as in the previous sections, it is the two-magnon energy measured from the bottom of the continuum downward. The eigenvalue of the problem is e_a here, and the two relate by $e_a + e_b = -2(c_x + c_y)$.

4.6.2 Effective $s = 1/2$ Hamiltonian

We can also obtain the energy of the single-ion anti-bound state from a simple spin-1/2 model, in a similar way to the previous sections. We still consider the effective interaction in the space of polarized spins with the exchange interaction as a small perturbation. We obtain the same effective exchange coupling constants, with a change now in sign of D. We proceed as in Sec. 4.5.3, assuming a strong field and small J/D, and draw the following energy ladder in the space $|\pm 1, \pm 1\rangle$:

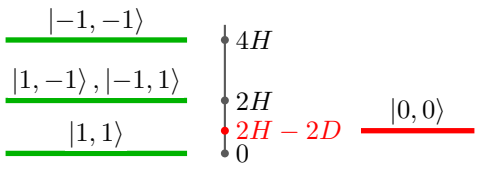

Then we mimic the derivation performed in the case of polarized triangular antiferromagnet, with few sign adjustments. This yields the effective Hamiltonian in the lattice of pseudo-spins 1/2:

$$\hat{\mathcal{H}}^{\triangle}_{\text{eff}} = \tilde{\tilde{E}}_0 + \sum_{\langle i,j \rangle} \left[\tilde{\tilde{J}}_\perp \left(s^x_i s^x_j + s^y_i s^y_j \right) + \tilde{\tilde{J}}_\parallel s^z_i s^z_j \right] - 2H \sum_j s^z_j \,, \tag{4.218}$$

with effective exchange coupling:

$$\tilde{\tilde{J}}_\parallel = 4J - \frac{J^2}{D} - \frac{J^3}{2D^2} \,, \quad \tilde{\tilde{J}}_\perp = \frac{J^2}{D} + \frac{J^3}{2D^2}. \tag{4.219}$$

Equally, we obtain the L-magnon dispersion straightforwardly from Tab. 4.1 as:

$$\varepsilon^L_{\mathbf{k}} = -2(\tilde{\tilde{J}}_\parallel - \tilde{\tilde{J}}_\perp \gamma^{\square}_{\mathbf{k}}) + 2H. \tag{4.220}$$

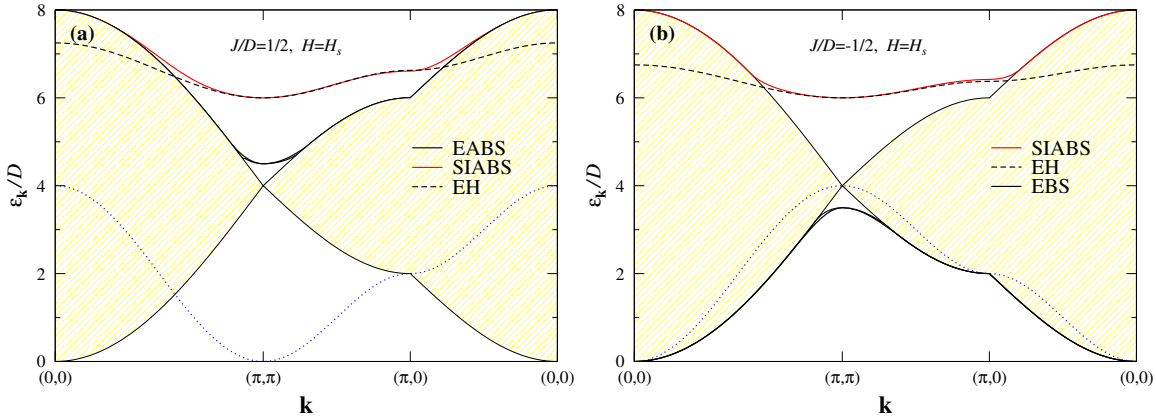

Figure 4.14: Two-magnon spectrum in easy-plane $S = 1$ square lattice for $|J|/D = 1/2$ at saturation. (a) Antiferromagnetic exchange with $H_s = D + 8J$. (b) Ferromagnetic exchange with $H_s = D$. The acronyms are similar to Fig. 4.13, with SIABS denoting the single-ion anti-bound state and EABS the two exchange anti-bound states. The dotted curve indicates the T-magnon energy.

4.6.3 Conclusions

We computed the two-magnon spectrum exactly in the fully-polarized phase of the $S = 1$ easy-plane magnet in the square lattice. We used the same method developed for the easy-axis case, Sec. 4.4.2. The most striking feature of the results obtained is mirror symmetry between the single-ion bound- and anti-bound-state pictures in ferromagnetic exchange, Fig. 4.11(b) and Fig. 4.14(b). This is implied by the special symmetry of the centrosymmetric matrix in (4.213), where the sign of anisotropy reverses the zero of the binding-energy axis from bottom to top of the two-magnon continuum. Also, the exact single-ion anti-bound-state energy is well approached by the spin-1/2 model, for the two signs of J.

Overall, the L-magnon as an anti-bound state represents a mirror image of the bound-state case, from the point of view of smooth departure from the two-magnon continuum, dispersion amplitude and symmetry of the wavefunction.

On general grounds, the appearance of single-ion anti-bound states in 1D chains was raised theoretically by Papanicolaou and Psaltakis, using the Bethe ansatz [164]. They were discussed afterwards in the context of quasi-1D antiferromagnets $Ni(C_2H_8N_2)_2Ni(CN)_4$ (commonly known as NENC) [174] and $NiCl_2$-4SC$(NH_2)_2$ (DTN) [171], both with spins $S = 1$ and large easy-plane anisotropy. Yet, compelling experimental evidence of their appearance is still lacking, to the best of our knowledge. The theory presented in our work is suited to describe them in the 1D case as well, for all ratios J/D.

Another candidate material to host the L-magnon in this context is the quasi-2D square-lattice antiferromagnet $Ba_2FeSi_2O_7$, with large easy-plane anisotropy $D/J \simeq 9$ and spins $S = 2$ [175].

4.7 Summary

Motivated by the experimental observations [116–118, 122–125, 129], we have developed in this chapter a general theory for the longitudinal magnons as a distinct type of multipolar excitations in strongly anisotropic magnetic solids. The longitudinal or L-magnons have $S^z = \pm 2S$ and can exist as coherent long-lived excitations for $D \gtrsim |J|$. Starting with the strong-coupling limit, we have presented two alternative analytical methods to compute their dispersion and other properties: the mapping to an effective spin-1/2 model and the multiboson spin-wave theory. In $S = 1$ square-lattice antiferromagnets, we presented a linked-cluster expansion, and for the ferromagnet we solved the two-magnon problem exactly and determined the symmetry of its solutions.

The approximations used in the approximate analytical methods (the multi-boson and the effective spin-1/2 approaches) can be further improved, allowing their range of applicability to be extended. Nonetheless, the multiboson spin-wave theory as is presents the only theoretical framework that allows us to compute finite lifetimes of L-magnons once their energies start to overlap with the multi-magnon continuum.

For larger spins the longitudinal magnons must disappear into the $2S$ magnon continuum. On the other hand, there are no bare decay processes for $S > 1$ that correspond to this instability in the multi-boson spin representation . Instead, an L-magnon with the quantum number $S^z = 2S$ decays into a single magnon with $S^z = 1$ and a composite excitation with $S^z = 2S - 1$. The latter can decay again with an emission of a single

magnon into an excitation with $S^z = 2S - 2$, and so on. The calculation of finite life times, as determined by such a cascade decay, is an interesting open problem. Our results provide a systematic way to describe experimentally-observed longitudinal magnons in various materials. Yet another very interesting development, in the scope of our theory, is the recent experimental observation of the condensation of the single-ion bound states (L-magnons) in a magnetic field applied to the spin-1 material $Na_2BaNi(PO_4)_2$ [129, 132]. Condensation leads to a spin-nematic phase that persists over a wide range of magnetic fields below the saturation field. The theoretical description of such condensation can be developed by a straightforward extension of our theory. The exact solution provided in Sec. 5 gives a preliminary result towards this aim. Possible condensation of longitudinal magnons in anisotropic materials with large spins, as, for example, spin-2 antiferromagnets $FePS_3$ [123] and $FePSe_3$ [124] may lead to even more exotic quantum spin phases, with high-rank spin-tensor order parameters.

5. Quantum-to-classical correspondence at finite temperature

5.1 Introduction 110
5.2 Quantum traces for powers of S^z 111
5.3 Monte Carlo simulations of realistic spin models 113
5.3.1 Thermodynamic properties 113
5.3.2 Binder cumulants 114
5.3.3 Phase transitions 115
5.4 Conclusions 121

5.1 Introduction

The Bohr-van Leeuwen theorem of classical electromagnetism states the absence of net magnetization in solids at thermal equilibrium, irregardless of external magnetic fields [32]. Magnetism in this sense is a pure quantum phenomenon, and so is ferromagnetism [176, 177]. The intrinsic spin value S is therefore a quantum quantity without classical origin. In the finite-temperature regime where thermal effects compete with, or overcome, the quantum effects, it remains nonetheless reasonable to adopt a semi-classical approach where the spin is a classical vector [178]. It remains also legitimate to search for the classical model that best describes a quantum spin system, should one such model exist. The figure of merit in this quest is the accurate transcription of thermodynamics, in terms of the free energy, the specific heat and the entropy in the high-temperature phase.

Above the transition temperature, magnetic solids are thermally populated by randomly oriented spins, which define the paramagnetic phase. The spin $\mathbf{S}$ here is a 3D classical vector of some magnitude A, leading to a classical counterpart of a quantum operator. It is widely appreciated in the literature to set $A = [S(S+1)]^{1/2}$ when performing semi-classical analyses [178–186]. This is at the root of the classical spin-wave theory in antiferromagnets [187, 188]. The quantity above is intuitively suggested by the $SU(2)$ Casimir operator $\hat{\mathbf{S}}^2 = S(S+1)$ [189]. But it also appears in other less evident contexts. Numerically, the spin-dependence of the Curie temperatures in cubic lattices was found to be an affine function of A^2 [190]. Empirically, the spin dependence of the correlation lengths at high temperatures and large S in, *e.g.* a square-lattice antiferromagnet, is also known to vary in A^2 [191].

Besides lattice problems, the use of a classical theory to study quantum spins has been relevant for instance in the path integral framework for *spinning* particles in SO(3) [192]. In lattice systems, the use of classical spins is relevant in modeling spin Hamiltonians at high temperatures, and computing spin-spin correlation functions in the classical limit [193]. Another application resides in the high-temperature series expansion in the small parameter $(k_B T)^{-1}$ [92, 94]. Using this approach, Rushbrooke remarked that the series terms for several orders are polynomials in A [102]. Oitmaa and Zheng have also investigated the magnetic susceptibility and the scaling of the transition temperatures in cubic lattices and obtained a spin-dependence that goes with A [179].

In the classical limit $S \to \infty$, one can assimilate the quantum S simply with the classical S. This has been investigated in fitting the excitation spectrum at finite T in the $S = 5/2$ antiferromagnet Rb_2MnF_4 [180]. The crossover between classical and quantum spins in different temperature regimes and spin values has also been explored in Refs. [180, 191, 194, 195].

In view of the above instances, the mapping of quantum and classical spin models has remained evasive. The question as to whether a universal substitution $S_c = \sqrt{S(S+1)}$ in semiclassical treatments of quantum spins suffices, lacks a consistent argument. In this work, we demonstrate that the above mapping is valid in high-T series expansions, and we show that it accurately describes the critical behavior of quantum magnets featuring short-range interactions. Practically, we evaluate the partition function with quantum spins for a typical spin Hamiltonian. The resulting expression recovers its classical analog in the leading order solely for the above mapping. The remainder in the quantum series is explicitly determined as a polynomial function in $S(S+1)$, which encodes quantum

corrections to the classical spin. Subsequently, we apply the above substitution in classical Monte Carlo simulations to obtain the critical temperature in various realistic models.

5.2 Quantum traces for powers of S^z

We showed in Chapter 3, Sec. 3.2.2.3, that the building block for computing the partition function in high-temperature series expansions, is to trace even powers of S^z over the paramagnetic phase. All traces of the form $Tr\{(S^x)^\alpha (S^y)^\beta (S^z)^q\}$ reduce to traces of $(S^+)^p (S^-)^p (S^z)^q$, which can be expressed as traces of polynomials in S^z, namely:

$$Tr\{(S^+)^p (S^y)^p (S^z)^q\} = Tr\{\mathcal{P}(S^z)\}. \tag{5.1}$$

Here $\mathcal{P}$ denotes a polynomial of degree $2p+q$, whose coefficients are polynomials in $S(S+1)$, see Eq. (3.81). We will map in the following the result from classical spins to the one from quantum spins. We note accordingly

$$I_n(S) = \frac{1}{Z} Tr\{(S^z)^n\} \tag{5.2}$$

with n even. In the classical picture, tracing $(S^z)^n$ over the paramagnetic phase is given by simple integration of the z component of the vector $\mathbf{S} = S_c(\cos\alpha \sin\theta, \sin\alpha \sin\theta, \cos\theta)$ over the unit sphere:

$$I_n^{\rm cl}(S_c) = \frac{1}{2} S_c^n \int_0^\pi \cos^n(\theta) \sin(\theta)\, d\theta = \frac{1}{n+1} S_c^n. \tag{5.3}$$

In the quantum picture, the trace amounts to computing expectation values over a basis of states for the spin Hamiltonian as discussed above. In the Hilbert space spanned by $|S^z = m\rangle$, one has:

$$I_n(S) = \frac{1}{2S+1} \sum_{m=-S}^{S} m^n = \frac{1}{2S+1} \sum_{k=0}^{2S} (k-S)^n. \tag{5.4}$$

For integer S, the above sum can be evaluated using the Faulhabert formulae [196]. Below, we present an alternative approach, which treats on equal footing integer and half-integer values of spin.

The expression in Eq. (5.4) can be resummed using the discrete antiderivative of x^n, defined as:

$$x^n = F_{n+1}(x+1) - F_{n+1}(x). \tag{5.5}$$

If the function F_{n+1} is known, then Eq. (5.4) transforms into a telescoping sum of the form:

$$I_n(S) = \frac{F_{n+1}(S+1) - F_{n+1}(-S)}{2S+1}. \tag{5.6}$$

In order to construct the antiderivative F_{n+1}, we first express a monomial x^n as a sum of the Newton polynomials defined by [197]:

$$\varphi_j(x) = x(x-1)...(x-j+1). \tag{5.7}$$

These polynomials satisfy the special property:

$$\varphi_{j+1}(x+1) - \varphi_{j+1}(x) = (j+1)\varphi_j(x)\,, \tag{5.8}$$

which is straightforward from their definition. Using the Newton polynomials as a basis, one writes

$$x^n = \sum_{j=1}^{n} a_j \varphi_j(x)\,, \tag{5.9}$$

where the coefficients a_j are iteratively obtained by successive substitutions $x = 1, 2, ...$ in this formula. Still, one can immediately see that $a_n = 1$.. Using the property (5.8) in Eqs. (5.5) and (5.9), one can obtain the antiderivative indirectly as

$$F_{n+1}(x) = \sum_{j=1}^{n} \frac{a_j}{j+1} \varphi_{j+1}(x)\,. \tag{5.10}$$

This is a polynomial of degree $n+1$ with leading coefficient $1/(n+1)$, defined up to a constant. The polynomial nature of F_{n+1} allows one to simplify the expression of the trace, Eq. (5.6), as follows. Its numerator is symmetrized as:

$$F_{n+1}(S+1) - F_{n+1}(-S) = F_{n+1}\Big(\big[S+1/2\big] + 1/2\Big) - F_{n+1}\Big(-\big[S+1/2\big] + 1/2\Big)\,, \tag{5.11}$$

which is a characterization of an odd polynomial in $S+1/2$, of degree $n+1$ with leading coefficient $2/(n+1)$. Therefore, the trace I_n in Eq. (5.6) is an even polynomial of degree n in $S+1/2$ with leading coefficient $1/(n+1)$.

Further using the binomial identity $(S+1/2)^2 = S(S+1) + 1/4$, the trace I_n can be seen as a polynomial in $S(S+1)$, of degree $n/2$, with the final form

$$I_n(S) = \frac{1}{n+1}[S(S+1)]^{\frac{n}{2}} + \sum_{j=1}^{\frac{n}{2}-1} b_j [S(S+1)]^j. \tag{5.12}$$

The absence of a constant term here is a consequence of $F_{n+1}(0) = F_{n+1}(1)$, see Eq. (5.5). The leading term in $I_n(S)$ recovers the classical trace (5.3) via the correspondence

$$S_c = \sqrt{S(S+1)}. \tag{5.13}$$

The remainder encodes quantum corrections of lower orders in the spin magnitude $S(S+1)$. Using the result of Chapter 3 on the coefficients of the polynomial $\mathcal{P}$, Eq. (3.81), it results that the full series expansion also exhibits spin corrections in terms of powers of $S(S+1)$. Note that the polynomial F_{n+1} constructed above relates to the so-called Bernoulli polynomial of order $n+1$ [198], and the coefficients b_j to the Bernoulli numbers[1].

The result that the sum (5.4) for an integer S is a polynomial in $S(S+1)$ is well known [200, 201], including its application to high-temperature series expansions [95, 102]. Besides the explicit derivation of this result for a general integer or half-integer S,

[1] They were also used independently in arithmetic tables by Seki around the same year (1712) as Bernoulli, see Ref. [199].

we established via Eqs. (5.3) and (5.12) the direct mapping between the quantum and the classical expressions of the traces. This corroborates the correspondence between the quantum and the classical pictures of interacting spins.

In conclusion, the elementary terms of the high-temperature series expansion are polynomials in $S(S+1)$, and so are the different thermodynamic quantities derived using the partition function. The validity of the mapping shown above is naturally dictated by the radius of convergence of the series, beyond which a crossover between quantum and classical spins then arises.

5.3 Monte Carlo simulations of realistic spin models

Using the previous results, we obtain in this section the transition temperatures of various ferro- and antiferromagnetic materials. To this aim, we use classical Monte Carlo simulations. We compare their output, for different microscopic parameters from the existing literature, with the experimental values of the transition temperatures. The classical Hamiltonian of interest here reads

$$\hat{\mathcal{H}} = \sum_{\langle i,j \rangle} \Big[J_{ij} \mathbf{S}_i \cdot \mathbf{S}_j + K_{ij} \big(\mathbf{S}_i \cdot \mathbf{S}_j \big)^2 \Big] + \sum_i \Big[D S_i^{z2} + E \Big(S_i^{x2} - S_i^{y2} \Big) \Big] + g \mu_B H \sum_i S_i^z \,, \quad (5.14)$$

where J_{ij} and K_{ij} are quadratic and biquadratic exchange constants, D and E are single-ion constants, and H is the external magnetic field. The previous results of Sec. 5.2 translate into the following mapping in the numerical simulations:

$$\begin{aligned} \mathbf{S} &= \sqrt{S(S+1)}\, \mathbf{n} \\ g \mu_B H^{\text{phys}} &= J \sqrt{S(S+1)} H \\ T_c^{\text{phys}} &= J S(S+1) T_c \\ \langle \mathbf{M}^{\text{phys}} \rangle &= g \mu_B \sqrt{S(S+1)}\, \langle \mathbf{M} \rangle \\ \chi^{\text{phys}} &= \frac{(g \mu_B)^2 N_A}{J} \chi \,, \end{aligned} \quad (5.15)$$

where $\mathbf{S}$ is the spin vector, $\mathbf{n}$ is a unit vector, T_c is the critical temperature, $\langle \mathbf{M} \rangle$ is the average magnetization and χ is the magnetic susceptibility. The Avogadro number is noted N_A. The superscript indicates quantities in physical units.

5.3.1 Thermodynamic properties

In the course of the simulations, we are interested in computing the energy and the magnetization, and thermodynamic properties derived from their fluctuations. To this aim, we use the Boltzmann distribution in thermal equilibrium:

$$p_\mu = \frac{1}{Z} e^{-\beta E_\mu} \quad (5.16)$$

where Z is the partition function defined similarly to (3.74), and E_μ is the energy obtained from (5.14) for the spin configuration μ. In order to sample configurations, we resort to

the Metropolis algorithm. In this framework, the average magnetization is given by

$$\langle \mathbf{M} \rangle = \frac{1}{N} \sum_j \mathbf{n}_j \tag{5.17}$$

where the index j spans all spins. The average energy is given by:

$$\langle E \rangle = \frac{1}{N} \sum_j E_j. \tag{5.18}$$

From the linear response theory [202], we have the specific heat:

$$C = k_B \beta^2 \big(\langle E^2 \rangle - \langle E \rangle^2 \big), \tag{5.19}$$

and the susceptibility:

$$\chi_{\alpha\alpha} = \beta \big(\langle M^{\alpha 2} \rangle - \langle M^{\alpha} \rangle^2 \big) \tag{5.20}$$

with $\alpha = x, y, z$.

5.3.2 Binder cumulants

In various contexts, we may need to compute the fourth-order Binder cumulant for the order parameter [203]:

$$U_4 = \frac{\langle M^4 \rangle}{\langle M^2 \rangle^2}, \tag{5.21}$$

where we assume M is the order parameter, but it could also be M_{xy} for easy-plane magnets or M_z for easy-axis magnets. The cumulant U_4 accounts for finite-size scaling in identifying T_c. For different system sizes, the corresponding cumulants tend to cross at a single point, defining the critical temperature. The monotony of U_4 is also informative on the nature of the phase transition. In first-order transitions, U_4 is peaked at $T = T_c$, whereas it increases monotonically in second-order transitions [204, 205].

Another means to identify first-order phase transitions is the fourth-order energy cumulant [206]:

$$U_4^E = \frac{\langle E^4 \rangle}{\langle E^2 \rangle^2}.$$

Since first-order transitions show a discontinuity in energy at T_c, say with values $E_\pm = E \pm \delta$, the cumulant U_4^E displays a peak with amplitude:

$$U_4^E(T_c) \approx 1 + \frac{(E_+^2 - E_-^2)^2}{2(E_+^4 + E_-^4)} \approx 1 + \left(\frac{2\delta}{E} \right)^2. \tag{5.22}$$

Such a feature is illustrated for $FePSe_3$ in Fig. 5.3.

5.3.3 Phase transitions

We apply the mapping presented earlier to compute the different quantities listed in the previous sections for various anisotropic ferro- and antiferromagnets. In compounds with the easy-axis single-ion term, we apply a renormalization of the single-ion constant to the first order in $1/[S(S+1)]$, which restores the mute form of the single-ion anisotropy for $S = 1/2$:

$$D^\star = \left[1 - \frac{3}{4S(S+1)}\right] D, \tag{5.23}$$

where D is the bare single-ion constant. Results of computation are synthesized in Tab. 5.1.

5.3.3.1 MnF_2

MnF_2 is one of the best known examples of the collinear Heisenberg antiferromagnet with large spins $S = 5/2$ of Mn^{2+} ions. The material has the body-centered tetragonal crystal structure. Spins in the corners and in the center of the tetragonal unit cell become oppositely aligned below the antiferromagnetic transition temperature $T_c \simeq 67$ K. The exchange parameter for MnF_2 have been recently refined by Morano *et al.* [207] with the following values for the three principal exchanges: $J_1 = -0.0677(9)$ meV, $J_2 = 0.3022(6)$ meV, and $J_3 = -0.0044(4)$ meV. In addition, the easy-axis anisotropy constant has been determined as $D = 0.0267(6)$ meV. Magnetic anisotropy is responsible for the orientation of the magnetic sublattices along the c axis as well as the appearance of a finite magnon gap:

$$\Delta = 2S\sqrt{D(8J_2 + D)} \quad \text{or} \quad 2S\sqrt{D(J_{\text{eff}} + D)}\,, \tag{5.24}$$

where $J_{\text{eff}} = 8J_2$ is a net exchange coupling between two antiferromagnetic sublattices. With the above parameters Eq. (5.24) yields the magnon gap $\Delta = 1.277$ meV or 308.8 GHz, which is somewhat larger than the ESR gap $\Delta = 259.7$ GHz [208]. Since, the ESR technique is superior over the inelastic neutron scattering at low energies, we use the ESR gap value $\Delta = 1.074$ meV to refine the anisotropy constant to $D = 0.0189$ meV. This value of D together with the exchange parameters of Ref. [207] have been used in the Monte Carlo simulations.

5.3.3.2 MnTe

MnTe is an easy-plane collinear antiferromagnet, which has recently attracted attention due to the experimental observation of 'altermagnetic' splitting of the magnon bands [209]. It has the hexagonal crystal structure $P6_3/mmc$ and orders antiferromagnetically at $T_N \simeq 310$ K. In the antiferromagnetic state, manganese spins $S = 5/2$ become positively aligned inside triangular layers and are oppositely oriented between the adjacent layers. According to the inelastic neutron scattering measurements [209], the principal exchanges are the first neighbor exchange between layers $J_1 = 3.99$ meV, the nearest-neighbor exchange within each layer $J_2 = -0.12$ meV, and the next nearest-neighbor exchange between layers $J_3 = 0.472$ meV. In addition, the single-ion anisotropy of the easy plane is given by $D = 0.0482$ meV. An alternative set of the microscopic parameters has been put forward on the basis of the *ab-initio* calculations: $J_1 = 3.628$ meV, $J_2 = 0.078$ meV,

and $J_3 = 0.457$ meV [210]. In addition, one can use the ESR result for the magnon gap $\Delta \approx 3.5$ meV [211] to obtain a more precise estimate for the single-ion anisotropy constant from

$$\Delta = 2S\sqrt{D(2J_1 + 12J_3)} \quad \text{or} \quad 2S\sqrt{DJ_{\text{eff}}}\,, \tag{5.25}$$

where $J_{\text{eff}} = 2J_1 + 12J_3$ is again a net exchange coupling between antiferromagnetic sublattices. Using the exchange constants of [210] one obtains $D = 0.0385$ meV or 0.446 K.

5.3.3.3 $MnPSe_3$

The spin Hamiltonian for $MnPSe_3$ includes the in-plane exchanges up to the third neighbors $J_{1,2,3}$ as well as the interplane exchange J_c. The material exhibits an easy-plane magnetic anisotropy which has been assigned to the anisotropic exchange parameterized by a constant $\varepsilon < 1$ [212]:

$$\hat{\mathcal{H}} = \sum_{\langle ij \rangle} J_{ij}\left(S_i^x S_j^x + S_i^y S_j^y + \varepsilon S_i^z S_j^z\right). \tag{5.26}$$

Alternatively, a single-ion term can also be used to represent the planar anisotropy. Figure 5.1 shows variation of the in-plane magnetization as a function of temperature, along with variations of the specific heat and susceptibility.

5.3.3.4 Rb_2MnF_4

The square-lattice antiferromagnet Rb_2MnF_4 orders below $T_N = 38.4$ K [213]. It features a weak exchange anisotropy, with the nearest-neighbor Hamiltonian:

$$\hat{\mathcal{H}} = J\sum_{\langle i,j \rangle}\left[S_i^x S_j^x + S_i^y S_j^y + \varepsilon S_i^z S_j^z\right], \tag{5.27}$$

where $\varepsilon > 1$. A next-nearest-neighbor interaction has also been proposed, with a weak strength $J'/J \simeq 10^{-2}$ [180]. The ordering mechanism in this compound is due to the presence of dipolar interactions.

Classical simulations using a Metropolis algorithm with the mapping $S_c \leftrightarrow \sqrt{S(S+1)}$ have been employed to study the time-dependence of the energy spectrum and the spin dynamics in this magnet [180]. They showed a good agreement with the experimental results and an overall better accuracy than the classical model of spins S down to low temperatures. It should be noted that the transition temperature T_N of this compound is in the intermediate regime where quantum and classical effects compete: $JS = 18$ K $< k_B T_N < JS(S+1) = 64$ K, with $J = 0.63$ meV [214].

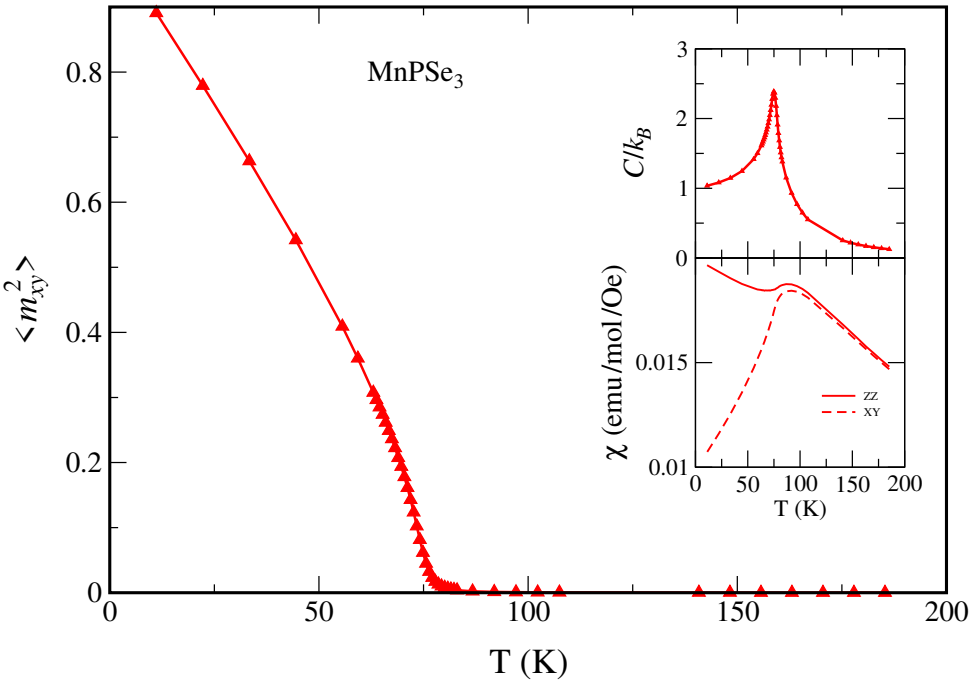

Figure 5.1: Order parameter of the quasi-2D easy-plane antiferromagnet $MnPSe_3$ by classical Monte Carlo simulations, showing a transition temperature $T_c \approx 77$ K. The computations uses the spin model of Ref. [212] with exchange anisotropy, based on a cubic cluster of linear size $L = 16$. Inset figure: Specific heat (top) and susceptibility in physical units (bottom) with $g(Mn^{2+}) = 2.08$. Continuity of the order parameter indicates a second-order transition.

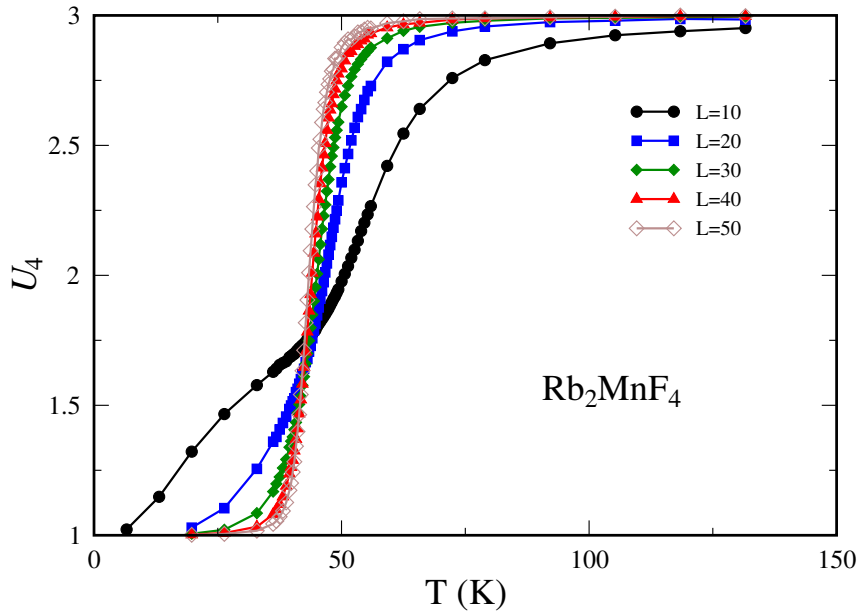

Figure 5.2: The fourth-order Binder cumulant for Rb_2MnF_4 by classical Monte Carlo simulations for different cluster sizes L^2. The monotonous variation indicates a second-order transition. The spin model used correspond to Ref. [180].

5.3.3.5 $FePS_3$

The spin Hamiltonian for $FePS_3$ with $S = 2$ spins of magnetic irons is written as:

$$\hat{\mathcal{H}} = \sum_{\langle ij \rangle} \Big[J_{ij} \mathbf{S}_i \cdot \mathbf{S}_j + K_{ij} \big(\mathbf{S}_i \cdot \mathbf{S}_j \big)^2 \Big] - D \sum_i (S_i^z)^2 \tag{5.28}$$

In Ref. [40], the magnon spectra of $FePS_3$ have been fitted using the linear spin-wave theory in order to obtain the set of macroscopic parameters including K_{ij}. This procedure amounts to simply merging the biquadratic term with the quadratic exchange interaction via an effective bond-dependent exchange coupling $J_{a,b} = J \pm 2KS^2$, for ferro- or antiferromagnetic bonds. Substituting such an anisotropic exchange in the exchange Hamiltonian yields an order parameter of lower symmetry. We find that the transition temperature is different for a pure biquadratic exchange $K \neq 0$ in comparison to an effective exchange $J_{a,b}$ for the same set.

5.3.3.6 $FePSe_3$

The compound $FePSe_3$ has a similar ordering structure to $FePS_3$, with iron ions carrying spins $S = 2$. Its spin Hamiltonian reads

$$\hat{\mathcal{H}} = \sum_{\langle ij \rangle} J_{ij} \mathbf{S}_i \cdot \mathbf{S}_j - D \sum_i (S_i^z)^2. \tag{5.29}$$

Ref. [124] has fitted the energy gaps in $FePSe_3$ at $k = 0$ for both transverse magnons at 14.5 meV and 34.6 meV, and longitudinal magnons at 52.6 meV and 55 meV. For the transverse magnons, a renormalized linear spin-wave theory has been used including the renormalized easy-axis constant $\bar{D} = D[1 - 1/(2S)]$. Whereas the longitudinal magnons are high-energy four-magnon easy-axis bound states [130], which have been approached by a strong-coupling expansion to the fifth order in J_{ij}/D.

In another work, alternative spin models have been presented featuring either an isotropic exchange, a bond-dependent exchange, or an additional biquadratic exchange similarly to $FePS_3$ [139]. Our simulations support the model of pure isotropic exchange, with a transition temperature best given by the parameter set proposed in Ref. [124].

5.3.3.7 $CoPS_3$

The Hamiltonian describing this compound involves biaxial anisotropy:

$$\hat{\mathcal{H}} = \sum_{\langle i,j \rangle} J_{ij} \mathbf{S}_i \cdot \mathbf{S}_j + \sum_i \left[D S_i^{z2} + E \left(S_i^{x2} - S_i^{y2} \right) \right] \tag{5.30}$$

with Heisenberg exchange interactions up to third nearest neighbor in the plane. Here, the magnetic cobalt ions have effective spins $S = 3/2$. The microscopic parameters have been determined in Ref. [215] from a fit of the magnon excitations in single crystals, using the linear spin-wave theory. Another fit of the magnon excitations, measured on a powdered sample, presented a spin model with an easy-plane XXZ exchange and an easy-axis single-ion anisotropy [216].

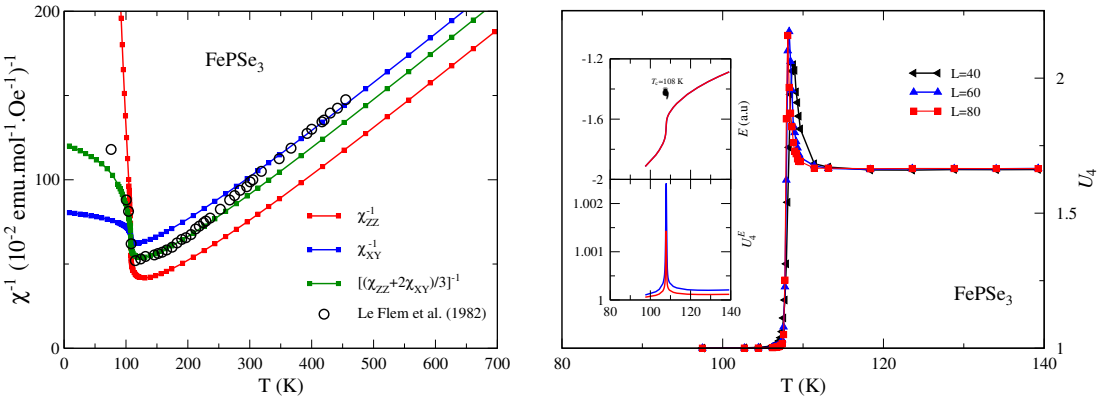

Figure 5.3: Classical Monte Carlo simulations of the spin model of Ref. [124] describing $FePSe_3$. Left: Inverse susceptibility compared to experimental measurements on a powder sample [138]. Right: Fourth-order Binder cumulant. Inset: Energy (top) and fourth-order energy cumulant (bottom). The results indicate a first-order phase transition at $T_c \approx 108$ K.

5.3.3.8 CrSBr

CrSBr is yet another example of a van der Waals magnet. It has an orthorhombic crystal structure with ferromagnetically ordered ab layers of Cr ions that are stacked antiferromagnetically along the c direction. The in-plane exchange interactions up to the eighth neighbor have been measured in the inelastic neutron scattering experiments [217]. The three dominant constants are $J_1 = -1.9$ meV, $J_2 = -3.38$ meV, and $J_3 = -1.67$ meV. The in-plane exchanges are small and do not exceed 5-10% of the dominant J_2 exchange parameter. The accuracy of the neutron experiments is insufficient to determine much weaker interlayer exchange coupling as well as the anisotropy constants. These parameters have been measured in the ESR experiments [218]. In particular, the interlayer exchange has been estimated to be $J_c = 0.0694$ K or 6.0 μeV. The bi-axial magnetic anisotropy parameters are given as $D_b = -0.3956$ K and $E_{ca} = 0.2074$ K. Here, D_b describes the easy-axis anisotropy for the b direction, while E_{ac} parametrizes anisotropy between the hard c direction and the intermediate a axis. The relevant energy scales are somewhat more transparent for a different parameterization of the bi-axial anisotropy using D_c and E_{ab}:

$$\hat{\mathcal{H}}_{\text{an}} = \sum_i D_c \big(S_i^z\big)^2 + E_{ab}\big[\big(S_i^x\big)^2 - \big(S_i^y\big)^2\big] \tag{5.31}$$

These are related with D_b and E_{ca} via $D_c = (|D_b| + 3E_{ca})/2 = 0.509$ K or 43.9 μeV and $E_{ab} = (|D_b| - E_{ca})/2 = 0.094$ K or 8.1 μeV. Thus, the magnetic anisotropy is predominantly of the easy-plane type with a weak in-plane anisotropy between a and b directions. This rather weak anisotropy together with interplane coupling J_c, which are both three orders of magnitude smaller than the principal exchange constant, play an essential role in the three-dimensional magnetic ordering in CrSBr.

Material	Reference	Model	T_c^{MC} (K)	T_c^{exp} (K)
MnF_2, $S = 5/2$ easy-axis, 3D	INS [207] and ESR [208]	$\{J_1, J_2, J_3, D\}$	69	67.7 [219]
MnTe, $S = 5/2$ easy-plane, 3D	INS [209]	$\{J_1, J_2, J_3, D\}$	359	310 [220]
	DFT [210] and ESR [211]	$\{J_1, J_2, J_3, D\}$	300	
$MnPSe_3$, $S = 5/2$ easy-plane, quasi 2D	powder INS [221]	$\{J_1, J_2, J_3, J_c\}$	73	74 [138]
	single crystal INS [212]	$\{J_1, J_2, J_3, J_c, \varepsilon \text{ or } D\}$	77	
Rb_2MnF_4, $S = 5/2$ easy-axis XXZ, 2D	INS [214]	$\{J, \varepsilon\}$	41	38.4 [213]
$FePS_3$, $S = 2$ easy-axis, 2D	INS [137]	$\{J_1, J_2, J_3, D\}$	142	118 ± 1 [135]
	INS [40]	$\{J_{1a}, J_{1b}, J_2, J_3, D\}$	130	
		$\{J_1, K_1, J_2, J_3, D\}$	95	
$FePSe_3$, $S = 2$ easy-axis, 2D	ESR [124]	$\{J_1, J_2, J_3, D\}$	108	106 ± 1 [135]
	INS [139]	$\{J_1, J_2, J_3, D\}$	134	
		$\{J_1, K_1, J_2, J_3, D\}$	120	
$CoPS_3$, $S = 3/2$ bi-axial, 2D	INS [215]	$\{J_1, J_2, J_3, D, E\}$	113	119.1 [222]
CrSBr, $S = 3/2$ bi-axial, quasi 2D	INS [217] and ESR [218]	$\{J_1, J_2, J_3, J_c, D, E\}$	166 ± 3	132 [223]

Table 5.1: Comparison of experimental T_c^{exp} and calculated T_c^{MC} transition temperatures for selected magnetic materials.

5.4 Conclusions

In this chapter we proposed a simple approach for studying quantum spin models classically. This is based on the correspondence (5.13) and the resulting substitutions for physical quantities (5.15). Whereas this seems intuitive from conservation of the spin magnitude $\mathbf{S}^2$, it is less trivial how the thermodynamic quantities computed classically in a system of interacting spins acquire quantum corrections at finite temperature, and what form these corrections eventually take. Based on the generic terms in high-temperature series expansion and the mapping of traces, we showed that the corrections are powers series of $S(S+1)$. This is for example a departure form the correction of the ground-state energy in an antiferromagnet at zero temperature in powers of S [148].

Subsequent Monte Carlo simulations of real spin models are summarized in Tab. 5.1. Its aim is not to produce a fit of the microscopic parameters, but rather to show how numerical simulations using our mapping and existing microscopic data compare to experimental measurements of the transition temperatures. The agreement is reasonably good.

6. Synthesis

This work presented two novel contributions to low-dimensional magnetism. First, we identified an exotic quasi-particle characterized by the quantum number $S^z = \pm 2S$, which appears in single-ion magnets. We termed it the longitudinal, or L-, magnon. Observed recently in $S = 2$ antiferromagnets, its properties were interpreted using a simplified version of our theory, yielding agreement with experimental measurements [124]. We developed a general theory for the L-magnon in both ferro- and antiferromagnets in two dimensions, extending prior theories limited either to ferromagnets or to small spin values. Employing diverse methods, we computed its energy -perturbatively and exactly under certain conditions-, and lifetime [130]. We demonstrated that it exists not only as a low-energy excitation driven by easy-axis anisotropy, but also in the high-energy regime with the easy-plane type above saturation. Its wavefunction satisfies an s-wave symmetry and may couple to one exchange bound or anti-bound state. We also found a mirror symmetry between the low-energy and the high-energy L-magnons.

Second, we derived a quantum-classical mapping for spin models at finite temperature, optimally representing quantum spins S in semiclassical analyses. It entails the intuitive substitution of a classical spin length S_c by $\sqrt{S(S+1)}$, consistent with the generic term in high-temperature series expansions. The quantum corrections are shown to follow a power series in $S(S+1)$. We validated this mapping through classical Monte Carlo simulations of realistic anisotropic models.

We hinted throughout this manuscript at numerous extensions of our work, and the open problems they may address. We highlight several here: the condensation of L-magnons, yielding multipolar phases such as the spin nematic; the enumeration of bound/anti-bound states in an anisotropic ferromagnet for geometries other than the hypercube; the lifetime and stability of L-magnons as high-energy anti-bound states; the stability of the L-magnon above a disordered ground state; the cross-over between quantum and classical spin models at intermediate temperatures.

In summary, this study is a contribution to exotic magnetic phenomena in classically-ordered materials, with potential future fundamental and applied research.

A. Magnetism: a cartography

We present here a cartography of some magnetic materials. Figure A.1 (Table A of Ref. [5]) shows the periodic table of magnetic elements, where diamagnets refer to elements that produce a magnetization opposite to an externally applied magnetic field.

In Tab. A.1, we give a list of some magnetically active matter, and the magnitude in Tesla of the field they generate.

Matter	Magnetic Field (T)
Human Brain	10^{-13}
Tattoo ink	10^{-9}
Recommended limit (chronic exposure)	$\sim 4 \times 10^{-6}$ [224]
Smartphone	10^{-5}
Credit card	10^{-5}
Earth	$\sim 4.7 \times 10^{-5}$
Microwave oven	10^{-4}
Network antenna	10^{-4}
Electric vehicles (full throttle)	10^{-4} [224]
Sun	10^{-3}
Hair dryer	1.3×10^{-3}
Refrigerator magnet	10^{-1}
Laptop Hard Drive	10^{-1}
Magnetic Therapy Bracelets	2×10^{-1} [225]
Headphone	5×10^{-1}
MRI Scanner	7
Magnet at LHC	8.3 [226]
Magnet at IMAPEC (Irig CEA)	16
Tokamak	20 [227]
Superconducting magnet (World record)	45.5 [228]
Pulsed field in lab (Europe)	98.8 [229]
Neutron Stars	10^{8}

Table A.1: Magnetically active objects and their induced fields, see also Refs. [5, 230]. The field associated with most of the substances decays sharply with distance.

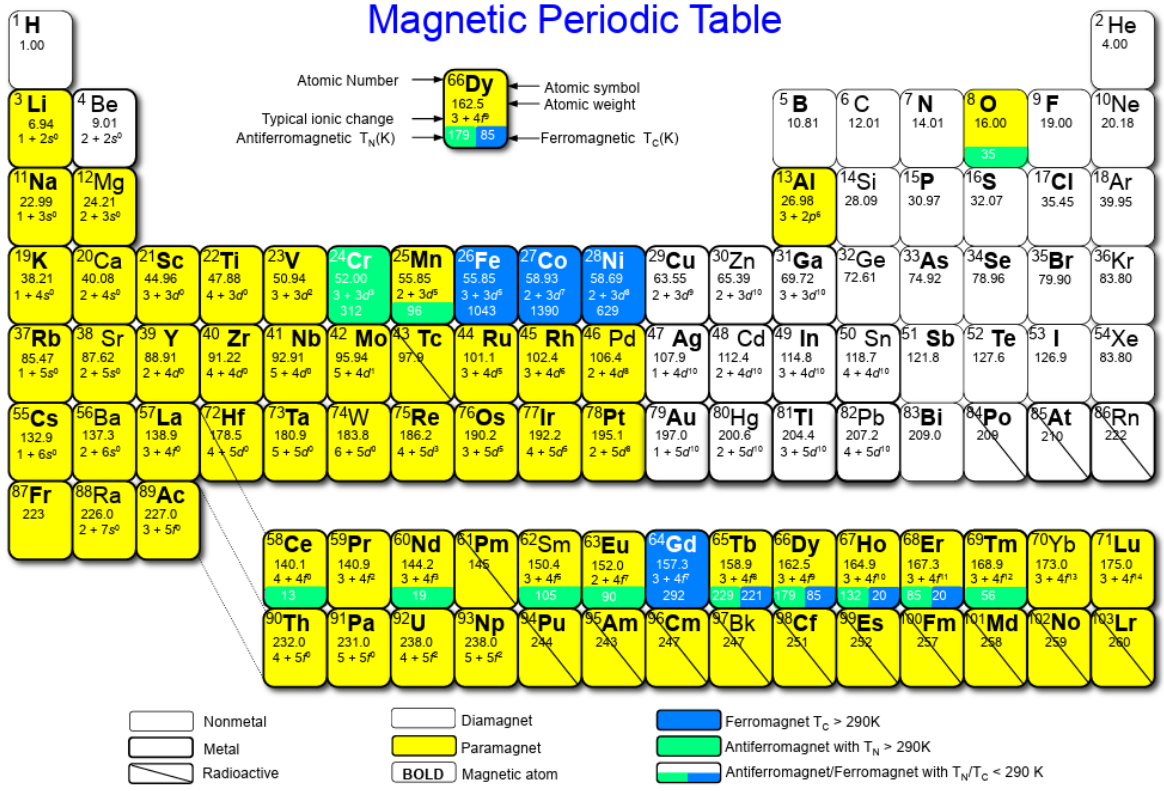

Figure A.1: Periodic Table of Magnetic Elements [5].

B. Matrix block diagonalization

The construction of effective Hamiltonians in discrete systems allows one to describe the energy of a reduced subspace amid a large (eventually infinite) Hilbert space. Such a subspace may possess a degeneracy of order $d \geq 1$. The effective Hamiltonian encodes the effect of a perturbation on lifting this degeneracy.

Here we present an algorithm to obtain an effective Hamiltonian to some finite order, describing the energy configuration of a subspace $\mathcal{E}$, if one wishes to go beyond the first non-trivial order. Practically, this approach is useful to construct an effective Hamiltonian to order n when the lower orders $j \leq n$ comprise non diagonal terms. As constructed in Chapter 3, the Hamiltonian of the discrete system is a sum of an unperturbed interaction and a perturbation:

$$\hat{\mathcal{H}} = \hat{\mathcal{H}}_0 + \hat{\mathcal{V}}. \tag{B.1}$$

We assume that the unperturbed Hamiltonian possesses a discrete part of the spectrum with energies e_i. The purpose is to derive a block-diagonal Hamiltonian $\tilde{\mathcal{H}}$ of the form:

$$\tilde{\mathcal{H}} = \begin{pmatrix} h_{\text{eff}} & & & \\ & \square & & \\ & & \square & \\ & & & .. \end{pmatrix} \tag{B.2}$$

such that h_{eff} is a $d \times d$ block, giving the effective Hamiltonian projected onto $\mathcal{E}$, and the other blocks are projections onto other subspaces. Yet, the other blocks may be merged as $\tilde{\mathcal{H}}$ only needs a two-block form[1]. This Hamiltonian relates to $\hat{\mathcal{H}}$ via the orthogonal relation:

$$\tilde{\mathcal{H}} = O^T \hat{\mathcal{H}} O \tag{B.3}$$

where O is an orthogonal matrix: $O^{-1} = O^T$. These matrices can be expanded as

$$\begin{aligned} \tilde{\mathcal{H}} &= \tilde{\mathcal{H}}^{(0)} + \tilde{\mathcal{H}}^{(1)} + \tilde{\mathcal{H}}^{(2)} + ... \\ \tilde{\mathcal{H}}^{(0)} &= \hat{\mathcal{H}}_0 \\ \tilde{\mathcal{H}}^{(1)} &= \hat{\mathcal{V}}\,, \end{aligned} \tag{B.4}$$

and

$$\begin{aligned} O &= O^{(0)} + O^{(1)} + O^{(2)} + ... \\ O^{(0)} &= \mathbb{I}\,. \end{aligned} \tag{B.5}$$

[1] Where the second diagonal block describes the whole orthogonal space to $\mathcal{E}$.

By means of Gaussian elimination, the matrix O can be chosen as block-triangular. Furthermore, it can be shown that the diagonal blocks of O are symmetric if $\tilde{\mathcal{H}}$ possesses a two-block form [231]. In this situation, we may assume this shape

$$O = \left(\begin{array}{c|c|c|c} sym & & & \\ \hline .. & sym & & \\ \hline .. & .. & sym & \\ \hline .. & .. & .. & ... \end{array}\right). \tag{B.6}$$

The condition (B.3) can be written as $O\tilde{\mathcal{H}} = \hat{\mathcal{H}}O$, which yields the sequential form after regrouping the perturbation orders:

$$\tilde{\mathcal{H}}^{(r)} + [O^{(r)}, \hat{\mathcal{H}}_0] = \hat{\mathcal{V}}O^{(r-1)} - \sum_{i=0}^{r-1} O^{(t)}\tilde{\mathcal{H}}^{(r-t)}. \tag{B.7}$$

Next, the projection on the unperturbed spaces of energies e_i, yield the matrix elements of the above operators for all orders $r \geq 1$:

$$\begin{aligned} e_i = e_j, \qquad \tilde{\mathcal{H}}^{(r)}_{ij} &= \Big(\hat{\mathcal{V}}O^{(r-1)} - \sum_{i=0}^{r-1} O^{(t)}\tilde{\mathcal{H}}^{(r-t)}\Big)_{ij} \\ O_{ij} &= -\frac{1}{2}\sum_{s=1}^{r-1} O^{T(s)}O^{r-s}, \\ e_i \neq e_j, \qquad O^{(r)}_{ij} &= \frac{1}{e_j - e_i}\Big(\hat{\mathcal{V}}O^{(r-1)} - \sum_{i=0}^{r-1} O^{(t)}\tilde{\mathcal{H}}^{(r-t)}\Big)_{ij}. \end{aligned} \tag{B.8}$$

Note that the second equation above stems from orthogonality $O^TO = \mathbb{I}$ admixed to the symmetry of the diagonal blocks in O. The purpose of the method is to obtain $\tilde{\mathcal{H}}^{(r)}$ up to a finite order. To this aim, one derives both $O^{(i)}$ and $\tilde{\mathcal{H}}^{(i)}$, $i = 1, .., r-1$. In particular, it is sufficient to obtain the columnar block O_{pq} for $1 \leq p \leq N$, $1 \leq q \leq d$.

Bibliography

[1] E. d. T. De Lacheisserie, D. Gignoux, and M. Schlenker. *Magnetism, Fundamentals*. Vol. 1. New York: Springer Science & Business Media, 2002. DOI: 10.1007/978-0-387-23062-7.

[2] M. R. Mourino. "From Thales to Lauterbur, or from the lodestone to MR imaging: magnetism and medicine." In: *Radiology* 180.3 (1991), pp. 593–612. DOI: 10.1148/radiology.180.3.1871268.

[3] L. Shu-Hua. "Origine de la boussole II. Aimant et boussole". In: *Isis* 45.2 (1954), pp. 175–196. DOI: 10.1086/348315.

[4] W. Gilbert. *De magnete*. New York: Dover Publication Inc., 1893.

[5] J. M. Coey. *Magnetism and magnetic materials*. Cambridge university press, 2010. DOI: 10.1017/CBO9780511845000.

[6] F. J. Dijksterhuis. *Lenses and waves: Christiaan Huygens and the mathematical science of optics in the seventeenth century*. Springer, 2004. DOI: 10.1007/1-4020-2698-8_2.

[7] T. Young. "II. The Bakerian Lecture. On the theory of light and colours". In: *Philosophical transactions of the Royal Society of London* 92 (1802), pp. 12–48. DOI: 10.1098/rstl.1802.0004.

[8] J.-L. Basdevant. "Famous optician: Augustin Fresnel and the wave theory of light". In: *Photoniques* (2019), pp. 18–22. DOI: 10.1051/photon/2019S418.

[9] J.-C. Boudenot. "Augustin Fresnel (1788-1827)". In: *Reflets de la physique* 7 (2007), pp. 17–18. DOI: 10.1051/refdp:2007003.

[10] H. C. Oersted. "Experiments on the effect of a current of electricity on the magnetic needle". In: *Annals of Philosophy* 16.1820 (1820), pp. 273–276.

[11] A.-M. Ampère and J. Babinet. *Exposé des nouvelles découvertes sur l'électricité et le magneétisme: de MM. Œrsted, Arago, Ampère, H. Davy, Biot, Erman, Schweiger, De La Rive, etc.;* Paris: Chez Méquignon-Marvis, Libraire, 1822.

[12] M. Faraday. *Experimental Researches in Electricity: 1852, 1*. Vol. 1852. 1. Taylor, 1852.

[13] A. Guillemin. *Electricity and Magnetism*. Macmillan and Company, 1891.

[14] J. A. Fleming. *The Alternating Current Transformer*. Vol. 1. London: The Electrician Printing and Publishing Company, 1896.

[15] V. Poulsen. *Method of recording and reproducing sounds or signals.* US Patent 661,619. Nov. 1900.

[16] A. C. Albertson. *Railway and car and magnetic appliances therefor.* US Patent 714,851. Dec. 1902. URL: https://patents.google.com/patent/US714851A/en.

[17] P. Langevin. "Sur la théorie du magnétisme". In: *J. Phys. Theor. Appl.* 4.1 (1905), pp. 678–693.

[18] P. Weiss. "L'hypothèse du champ moléculaire et la propriété ferromagnétique". In: *J. Phys. Theor. Appl.* 6.1 (1907), pp. 661–690.

[19] L. Néel. "Propriétés magnétiques des ferrites; ferrimagnétisme et antiferromagnétisme". In: *Annales de physique*. Vol. 12. 3. 1948, pp. 137–198. DOI: 10.1051/anphys/194812030137.

[20] V. A. Johnson and W. J. Whitesell. "Theory of the Magnetoresistive Effect in Semiconductors". In: *Phys. Rev.* 89 (5 Mar. 1953), pp. 941–947. DOI: 10.1103/PhysRev.89.941.

[21] R. Damadian. "Tumor detection by nuclear magnetic resonance". In: *Science* 171.3976 (1971), pp. 1151–1153. DOI: 10.1126/science.171.3976.1151.

[22] C.-W. Chen. *Magnetism and metallurgy of soft magnetic materials*. Amsterdam: North-Holland Publishing Company, 1977.

[23] D. Rugar et al. "Magnetic force microscopy: General principles and application to longitudinal recording media". In: *Journal of Applied Physics* 68.3 (1990), pp. 1169–1183. DOI: 10.1063/1.346713.

[24] C. Cohen-Tannoudji, B. Diu, and F. Laloë. *Mécanique quantique*. Vol. 2. Hermann Paris, 1973.

[25] L. D. Landau and E. M. Lifshitz. *The Classical Theory of Fields: Volume 2*. Vol. 2. Butterworth-Heinemann, 1975.

[26] B. H. Bransden and C. J. Joachain. *Physics of atoms and molecules*. Pearson Education India, 2003.

[27] C. M. Sommerfield. "The magnetic moment of the electron". In: *Annals of Physics* 5.1 (1958), pp. 26–57. DOI: 10.1016/0003-4916(58)90003-4.

[28] A. Mooser et al. "Direct high-precision measurement of the magnetic moment of the proton". In: *Nature* 509.7502 (2014), pp. 596–599. DOI: 10.1038/nature13388.

[29] J.-L. Basdevant. *Lectures on quantum mechanics*. Springer, 2007. DOI: 10.1007/978-0-387-37744-5.

[30] C. Castelnovo, R. Moessner, and S. L. Sondhi. "Spin Ice, Fractionalization, and Topological Order". In: *Annu. Rev. Condens. Matter Phys.* 3.1 (2012), pp. 35–55. DOI: 10.1146/annurev-conmatphys-020911-125058.

[31] NIST. *SI Units – Time*. URL: https://www.nist.gov/pml/owm/si-units-time.

[32] J. H. Van Vleck. *The Theory of Electric and Magnetic Susceptibilities*. New York: Oxford University Press, 1932.

[33] Y. Kuramoto, H. Kusunose, and A. Kiss. "Multipole orders and fluctuations in strongly correlated electron systems". In: *J. Phys. Soc. Japan* 78.7 (2009), p. 072001. DOI: 10.1143/JPSJ.78.072001.

[34] N. Iwahara et al. "Multipolar exchange interaction and complex order in insulating lanthanides". In: *Phys. Rev. B* 105 (14 Apr. 2022), p. 144401. DOI: 10.1103/PhysRevB.105.144401.

[35] D. Coffey, K. S. Bedell, and S. A. Trugman. "Effective spin Hamiltonian for the CuO planes in La_2CuO_4 and metamagnetism". In: *Phys. Rev. B* 42 (10 Oct. 1990), pp. 6509–6514. DOI: 10.1103/PhysRevB.42.6509.

[36] A. Kitaev. "Anyons in an exactly solved model and beyond". In: *Annals of Physics* 321.1 (2006), pp. 2–111. DOI: 10.1016/j.aop.2005.10.005.

[37] R. B. Potts. "Some generalized order-disorder transformations". In: *Mathematical proceedings of the cambridge philosophical society*. Vol. 48. 1. Cambridge University Press. 1952, pp. 106–109. DOI: 10.1017/S0305004100027419.

[38] K. Yosida. "Chapter V Magnetic Structures of Heavy Rare-Earth Metals". In: *Progress in low temperature physics*. Vol. 4. Elsevier, 1964, pp. 265–295. DOI: 10.1016/S0079-6417(08)60153-5.

[39] A. Furrer et al. "Single-ion versus two-ion anisotropy in magnetic compounds: A neutron scattering study". In: *Phys. Rev. B* 83 (2 Jan. 2011), p. 024404. DOI: 10.1103/PhysRevB.83.024404.

[40] A. R. Wildes et al. "Evidence for biquadratic exchange in the quasi-two-dimensional antiferromagnet $FePS_3$". In: *J. Appl. Phys.* 127.22 (2020), p. 223903. DOI: 10.1063/5.0009114.

[41] K. Yosida. *Theory of Magnetism*. Vol. 122. Springer Science & Business Media, 1996. ISBN: 9783540606512.

[42] J. F. Sierra et al. "Van der Waals heterostructures for spintronics and opto-spintronics". In: *Nature Nanotechnology* 16.8 (2021), pp. 856–868. DOI: 10.1002/adma.201900065.

[43] Y.-S. Meng et al. "Understanding the magnetic anisotropy toward single-ion magnets". In: *Accounts of chemical research* 49.11 (2016), pp. 2381–2389. DOI: 10.1021/acs.accounts.6b00222.

[44] A. Gaita-Ariño et al. "Molecular spins for quantum computation". In: *Nature chemistry* 11.4 (2019), pp. 301–309. DOI: 10.1038/s41557-019-0232-y.

[45] E. M. Lifshitz and L. P. Pitaevskii. *Statistical Physics, Part 2*. Oxford: Pergamon Press, 1980.

[46] D. Ter Haar. *Collected papers of LD Landau*. Elsevier, 2013. DOI: 10.1016/C2013-0-01806-3.

[47] A. R. Edmonds. *Angular momentum in quantum mechanics*. Tech. rep. Geneva: CERN, 1955. DOI: 10.5170/CERN-1955-026.

[48] F. Bloch. "Zur theorie des ferromagnetismus". In: *Z. Physik* 61.3 (1930), pp. 206–219. DOI: 10.1007/BF01339661.

[49] A. Auerbach. *Interacting Electrons and Quantum Magnetism*. New York: Springer-Verlag, 1994. DOI: 10.1007/978-1-4612-0869-3.

[50] A. Ramirez et al. "Strongly geometrically frustrated magnets". In: *Annual Review of Materials Science* 24.1 (1994), pp. 453–480. DOI: 10.1146/annurev.ms.24.080194.002321.

[51] C. Lacroix, P. Mendels, and F. Mila. *Introduction to frustrated magnetism: materials, experiments, theory*. Vol. 164. Springer Science & Business Media, 2011. DOI: 10.1007/978-3-642-10589-0.

[52] Y.-L. Wang, S. Shtrikman, and H. Callen. "Wick's Theorem for Spin-$\frac{1}{2}$ Operators, with an Application to Spin Waves in Antiferromagnets". In: *Phys. Rev.* 148 (1 Aug. 1966), pp. 419–432. DOI: 10.1103/PhysRev.148.419.

[53] E. A. Hylleraas. "Über den Grundterm der Zweielektronenprobleme von H-, He, Li+, Be++ usw." In: *Z. Phys.* 65.3 (1930), pp. 209–225. DOI: 10.1007/BF01397032.

[54] C. W. Scherr and R. E. Knight. "Two-Electron Atoms III. A Sixth-Order Perturbation Study of the 1^1S Ground State". In: *Rev. Mod. Phys.* 35 (3 July 1963), pp. 436–442. DOI: 10.1103/RevModPhys.35.436.

[55] J. Midtdal. "Perturbation-Theory Expansions Through 21st Order of the Nonrelativistic Energies of the Two-Electron Systems $(2p)^{23}P$ and $(1s)^{21}S$". In: *Phys. Rev.* 138 (4A May 1965), A1010–A1014. DOI: 10.1103/PhysRev.138.A1010.

[56] A. H. MacDonald, S. M. Girvin, and D. Yoshioka. "$\frac{t}{U}$ expansion for the Hubbard model". In: *Phys. Rev. B* 37 (16 June 1988), pp. 9753–9756. DOI: 10.1103/PhysRevB.37.9753.

[57] N. Roseveare. "Leverrier to Einstein: A review of the Mercury problem". In: *Vistas in Astronomy* 23 (1979), pp. 165–171. DOI: 10.1016/0083-6656(79)90003-5.

[58] J. W. S. B. Rayleigh. *The theory of sound*. The Macmillan Company, 1894. DOI: 10.1017/CBO9781139058087.

[59] F. Rellich. "Störungstheorie der Spektralzerlegung: I. Mitteilung. Analytische Störung der isolierten Punkteigenwerte eines beschränkten Operators". In: *Math. Ann.* 113.1 (1937), pp. 600–619. DOI: 10.1007/BF01571652.

[60] A. Einstein, L. Infeld, and B. Hoffmann. "The gravitational equations and the problem of motion". In: *Ann. Math.* 39.1 (1938), pp. 65–100. DOI: 10.2307/1968714.

[61] N. Bloembergen. *Nuclear magnetic relaxation*. Springer Dordrecht, 1961. DOI: 10.1007/978-94-017-6073-7.

[62] F. J. Dyson. "The Radiation Theories of Tomonaga, Schwinger, and Feynman". In: *Phys. Rev.* 75 (3 Feb. 1949), pp. 486–502. DOI: 10.1103/PhysRev.75.486.

[63] M. Gell-Mann and F. E. Low. "Quantum Electrodynamics at Small Distances". In: *Phys. Rev.* 95 (5 Sept. 1954), pp. 1300–1312. DOI: 10.1103/PhysRev.95.1300.

[64] K. G. Wilson. "Renormalization Group and Strong Interactions". In: *Phys. Rev. D* 3 (8 Apr. 1971), pp. 1818–1846. DOI: 10.1103/PhysRevD.3.1818.

[65] P. Baldi and K. Hornik. "Neural networks and principal component analysis: Learning from examples without local minima". In: *Neural networks* 2.1 (1989), pp. 53–58. DOI: 10.1016/0893-6080(89)90014-2.

[66] W. Weaver Jr, S. P. Timoshenko, and D. H. Young. *Vibration problems in engineering*. John Wiley & Sons, 1991.

[67] K. L. Judd. *Numerical Methods in Economics*. MIT press, 1998.

[68] J. D. Murray. *Mathematical biology: I. An introduction*. Vol. 17. Springer Science & Business Media, 2007. DOI: 10.1007/b98868.

[69] C. M. Bender and S. A. Orszag. *Advanced mathematical methods for scientists and engineers I: Asymptotic methods and perturbation theory*. Springer Science & Business Media, 2013. DOI: 10.1007/978-1-4757-3069-2.

[70] J. E. Lennard-Jones. "Perturbation problems in quantum mechanics". In: *Proceedings of the Royal Society of London. Series A, Containing Papers of a Mathematical and Physical Character* 129.811 (1930), pp. 598–615. DOI: 10.1098/rspa.1930.0177.

[71] L. Brillouin. "Les problèmes de perturbations et les champs self-consistents". In: *Journal de Physique et le Radium* 3.9 (1932), pp. 373–389. DOI: 10.1051/jphysrad:jphysrad0193200309037300.

[72] E. P. Wigner. "On a Modification of the Rayleigh-Schrödinger Perturbation Theory". In: *Part I: Physical Chemistry. Part II: Solid State Physics*. Ed. by A. S. Wightman. Berlin, Heidelberg: Springer Berlin Heidelberg, 1997, pp. 131–136. ISBN: 978-3-642-59033-7. DOI: 10.1007/978-3-642-59033-7_12.

[73] I. Hubač and S. Wilson. "Brillouin-Wigner Methods for Many-Body Systems". In: *Brillouin-Wigner Methods for Many-Body Systems*. Dordrecht: Springer Netherlands, 2010, pp. 133–189. ISBN: 978-90-481-3373-4. DOI: 10.1007/978-90-481-3373-4_4.

[74] E. Schrödinger. "Quantisierung als Eigenwertproblem". In: *Ann. Phys.* 385.13 (1926), pp. 437–490. DOI: 10.1002/andp.19263851302.

[75] K. Gottfried and Y. Tung-Mow. *Quantum mechanics: Fundamentals*. New York: Springer-Verlag, 2003. DOI: 10.1007/978-0-387-21623-2.

[76] T. Kato. "On the convergence of the perturbation method. I". In: *Prog. Theor. Phys. C* 4.4 (1949), pp. 514–523. DOI: 10.1143/ptp/4.4.514.

[77] L. D. Landau and E. M. Lifshitz. *Quantum Mechanics: A Shorter Course of Theoretical Physics*. Vol. 2. London: Pergamon, 1974.

[78] C. Møller and M. S. Plesset. "Note on an Approximation Treatment for Many-Electron Systems". In: *Phys. Rev.* 46 (7 Oct. 1934), pp. 618–622. DOI: 10.1103/PhysRev.46.618.

[79] K. Kumar. *Perturbation theory and the nuclear many body problem*. Amsterdam: North-Holland Publishing Company, 1962.

[80] L. G. Marland. "Series Expansions for the Zero-Temperature Transverse Ising Model". In: *J. Phys. A: Math. Gen.* 14.8 (1981), pp. 2047–2058. DOI: 10.1088/0305-4470/14/8/027.

[81] M. P. Gelfand. "Series Expansions for Excited States of Quantum Lattice Models". In: *Solid State Communications* 98.1 (1996), pp. 11–15. DOI: 10.1016/0038-1098(96)00051-8.

[82] M. P. Gelfand and R. R. P. Singh. "High-order convergent expansions for quantum many particle systems". In: *Advances in Physics* 49 (2000), p. 93. DOI: 10.1080/000187300243381.

[83] J. Oitmaa, C. Hamer, and W. Zheng. *Series Expansion Methods for Strongly Interacting Lattice Models*. Cambridge: Cambridge University Press, 2006. DOI: 10.1017/CBO9780511584398.

[84] M. E. Zhitomirsky. "Real-space perturbation theory for frustrated magnets: application to magnetization plateaus". In: *J. Phys.: Conf. Ser.s* 592.1 (Mar. 2015), p. 012110. DOI: 10.1088/1742-6596/592/1/012110.

[85] B. H. Brandow. "Linked-Cluster Expansions for the Nuclear Many-Body Problem". In: *Rev. Mod. Phys.* 39 (4 Oct. 1967), pp. 771–828. DOI: 10.1103/RevModPhys.39.771.

[86] F. Coester. "Bound states of a many-particle system". In: *Nucl. Phys.* 7 (1958), pp. 421–424. DOI: 10.1016/0029-5582(58)90280-3.

[87] D. J. J. Farnell and R. F. Bishop. "The Coupled Cluster Method Applied to Quantum Magnetism". In: *Quantum Magnetism*. Springer, 2008. Chap. 7, pp. 307–348. DOI: 10.1007/BFb0119597.

[88] K. A. Brueckner. "Many-Body Problem for Strongly Interacting Particles. II. Linked Cluster Expansion". In: *Phys. Rev.* 100 (1 Oct. 1955), pp. 36–45. DOI: 10.1103/PhysRev.100.36.

[89] Z. Weihong, J. Oitmaa, and C. J. Hamer. "Square-lattice Heisenberg antiferromagnet at T=0". In: *Phys. Rev. B* 43 (10 Apr. 1991), pp. 8321–8330. DOI: 10.1103/PhysRevB.43.8321.

[90] B. Narayan Roy. *Fundamentals of Classical and Statistical Thermodynamics*. John Wiley & Sons, 2002, p. 768.

[91] H. Thirring. "Zur Theorie der Raumgitterschwingungen und der spezifischen Wärme fester Körper". In: *Phys. Z.* 14 (1913), p. 867.

[92] J. H. Van Vleck. "The Influence of Dipole-Dipole Coupling on the Specific Heat and Susceptibility of a Paramagnetic Salt". In: *J. Chem. Phys.* 5.5 (May 1937), pp. 320–337. ISSN: 0021-9606. DOI: 10.1063/1.1750032.

[93] W. Opechowski. "On the exchange interaction in magnetic crystals". In: *Physica* 4.2 (1937), p. 181. DOI: 10.1016/S0031-8914(37)80135-4.

[94] M. Wortis. "Phase Transitions and Critical Phenomena". In: *Phase Transitions and Critical Phenomena*. Ed. by C. Domb and M. S. Green. Vol. 3. New York: Academic Press, 1974. Chap. 1.

[95] H.-J. Schmidt, A. Lohmann, and J. Richter. "Eighth-order high-temperature expansion for general Heisenberg Hamiltonians". In: *Phys. Rev. B* 84 (10 Sept. 2011), p. 104443. DOI: 10.1103/PhysRevB.84.104443.

[96] J. Oitmaa et al. "Phase transition and thermal order-by-disorder in the pyrochlore antiferromagnet $Er_2Ti_2O_7$: A high-temperature series expansion study". In: *Phys. Rev. B* 88 (22 Dec. 2013), p. 220404. DOI: 10.1103/PhysRevB.88.220404.

[97] M. Rigol, T. Bryant, and R. R. P. Singh. "Numerical Linked-Cluster Approach to Quantum Lattice Models". In: *Phys. Rev. Lett.* 97 (18 Nov. 2006), p. 187202. DOI: 10.1103/PhysRevLett.97.187202.

[98] M. Rigol, T. Bryant, and R. R. P. Singh. "Numerical linked-cluster algorithms. I. Spin systems on square, triangular, and kagomé lattices". In: *Phys. Rev. E* 75 (6 June 2007), p. 061118. DOI: 10.1103/PhysRevE.75.061118.

[99] L. Pierre, B. Bernu, and L. Messio. "High temperature series expansions of S= 1/2 Heisenberg spin models: algorithm to include the magnetic field with optimized complexity". In: *SciPost Physics* 17.4 (2024), p. 105. DOI: 10.21468/SciPostPhys.17.4.105.

[100] E. Ambler, J. C. Eisenstein, and J. F. Schooley. "Traces of products of angular momentum matrices". In: *J. Math. Phys.* 3.1 (1962), p. 118. DOI: 10.1063/1.1703771.

[101] N. Dalton. "Traces of products of angular momentum matrices". In: *Phys. Lett. A* 28.3 (1968), pp. 172–173. ISSN: 0375-9601. DOI: 10.1016/0375-9601(68)90182-5.

[102] G. S. Rushbrooke, G. A. Baker Jr., and P. J. Wood. "Phase Transitions and Critical Phenomena". In: *Phase Transitions and Critical Phenomena*. Ed. by C. Domb and M. S. Green. Vol. 3. New York: Academic Press, 1974. Chap. 3.

[103] T. Giamarchi. *Quantum Physics in One Dimension*. Oxford: Clarendon Press, 2004. DOI: 10.1093/acprof:oso/9780198525004.001.0001.

[104] H.-J. Mikeska and A. K. Kolezhuk. "One-Dimensional Magnetism". In: *Lecture Notes in Physics* 645 (2004), pp. 1–83.

[105] A. Y. Kitaev. "Fault-Tolerant Quantum Computation by Anyons". In: *Annals of Physics* 303.1 (2003), pp. 2–30. DOI: 10.1016/S0003-4916(02)00018-0.

[106] M. Wortis. "Bound States of Two Spin Waves in the Heisenberg Ferromagnet". In: *Phys. Rev.* 132 (1 Oct. 1963), pp. 85–97. DOI: 10.1103/PhysRev.132.85.

[107] J. Hanus. "Bound States in the Heisenberg Ferromagnet". In: *Phys. Rev. Lett.* 11 (7 Oct. 1963), pp. 336–338. DOI: 10.1103/PhysRevLett.11.336.

[108] J. B. Torrance Jr. and M. Tinkham. "Magnon Bound States in Anisotropic Linear Chains". In: *Phys. Rev.* 187.2 (1969), pp. 587–595. DOI: 10.1103/PhysRev.187.587.

[109] D. C. Mattis. "The Few-Body Problem on a Lattice". In: *Rev. Mod. Phys.* 58.2 (1986), pp. 361–379. DOI: 10.1103/RevModPhys.58.361.

[110] J. B. Torrance Jr. and M. Tinkham. "Excitation of Multiple-Magnon Bound States in $CoCl_2 \cdot 2H_2O$". In: *Phys. Rev.* 187.2 (1969), pp. 595–602. DOI: 10.1103/PhysRev.187.595.

[111] T. Tonegawa. "Two-Magnon Bound States in the Heisenberg Ferromagnet with Anisotropic Exchange and Uniaxial Anisotropy Energies". In: *Prog. Theor. Phys. Suppl.* 46 (1970), pp. 61–75. DOI: 10.1143/PTPS.46.61.

[112] R. Silberglitt and J. B. Torrance Jr. "Effect of Single-Ion Anisotropy on Two-Spin-Wave Bound State in a Heisenberg Ferromagnet". In: *Phys. Rev. B* 2.3 (1970), pp. 772–781. DOI: 10.1103/PhysRevB.2.772.

[113] S. J. Allen Jr. and H. J. Guggenheim. "Magnetic Excitations in Antiferromagnetic CoF_2. II. Uniform Magnetic Excitations near T = 0 K". In: *Phys. Rev. B* 4.3 (1971), pp. 950–959. DOI: 10.1103/PhysRevB.4.950.

[114] T. Oguchi and T. Ishikawa. "Theory of Two-Magnon Bound States in a Two-Dimensional Antiferromagnet". In: *J. Phys. Soc. Japan* 34.6 (1973), pp. 1486–1494. DOI: 10.1143/JPSJ.34.1486.

[115] C. J. Liu and Y. Chow. "Dispersion Relations for Energy Eigenvalues of Two-Magnon Bound State". In: *Phys. Rev. B* 17.1 (1978), pp. 215–222. DOI: 10.1103/PhysRevB.17.215.

[116] A. R. Fert et al. "Excitation of Two Spin Deviations by Far Infrared Absorption in FeI_2". In: *Solid State Communications* 26.10 (1978), pp. 693–697. DOI: 10.1016/0038-1098(78)90721-4.

[117] G. C. Psaltakis et al. "One- and Two-Magnon Excitations in $FeBr_2$". In: *J. Phys. C: Solid State Phys.* 17.10 (1984), pp. 1735–1751. DOI: 10.1088/0022-3719/17/10/017.

[118] K. Katsumata et al. "Single-Ion Magnon Bound States in an Antiferromagnet with Strong Uniaxial Anisotropy". In: *Phys. Rev. B* 61.17 (2000), pp. 11632–11636. DOI: 10.1103/PhysRevB.61.11632.

[119] L. Kecke, T. Momoi, and A. Furusaki. "Multimagnon bound states in the frustrated ferromagnetic one-dimensional chain". In: *Phys. Rev. B* 76 (6 Aug. 2007), p. 060407. DOI: 10.1103/PhysRevB.76.060407.

[120] J. Oitmaa and C. J. Hamer. "Ground-State Properties and One-Particle Spectra for a Spin-1 Heisenberg Antiferromagnet from Series Expansions". In: *Phys. Rev. B* 77.22 (2008), p. 224435. DOI: 10.1103/PhysRevB.77.224435.

[121] T. Fukuhara et al. "Microscopic observation of magnon bound states and their dynamics". In: *Nature* 502.7469 (2013), pp. 76–79. DOI: 10.1038/nature12541.

[122] A. Legros et al. "Observation of 4- and 6-Magnon Bound States in the Spin-Anisotropic Frustrated Antiferromagnet FeI_2". In: *Phys. Rev. Lett.* 127.26 (2021), p. 267201. DOI: 10.1103/PhysRevLett.127.267201.

[123] J. Wyzula et al. "High-Angular Momentum Excitations in Collinear Antiferromagnet $FePS_3$". In: *Nano Letters* 22.23 (2022), pp. 9741–9747. DOI: 10.1021/acs.nanolett.2c04111.

[124] F. Le Mardelé et al. "Magneto-optical study of the Verwey transition in $FePS_3$". In: *Phys. Rev. B* 109 (2024), p. 134410. DOI: 10.1103/PhysRevB.109.134410.

[125] X. Bai et al. "Hybridized Quadrupolar Excitations in the Spin-Anisotropic Frustrated Magnet FeI_2". In: *Nature Physics* 17.4 (2021), pp. 467–472. DOI: 10.1038/s41567-020-01110-1.

[126] A. Mook et al. “Magnons, Magnon Bound Pairs, and Their Hybrid Spin-Multipolar Topology”. In: *Phys. Rev. B* 107.6 (2023), p. 064429. DOI: 10.1103/PhysRevB.107.064429.

[127] X. Bai et al. “Instabilities of Heavy Magnons in an Anisotropic Magnet”. In: *Nature Communications* 14 (2023), p. 4199. DOI: 10.1038/s41467-023-39940-1.

[128] F. Delgado, M. M. Otrokov, and A. Arnau. “Spin Wave Excitations in Low Dimensional Systems with Large Magnetic Anisotropy”. In: *J. Phys. Mater.* 7.3 (2024), p. 035005. DOI: 10.1088/2515-7639/ad558b.

[129] J. Sheng et al. “Bose-Einstein Condensation of a Two-Magnon Bound State in a Spin-1 Triangular Lattice”. In: *Nature Materials* 24.4 (2025), pp. 544–550. DOI: 10.1038/s41563-024-02071-z.

[130] A. El Mendili, T. Ziman, and M. E. Zhitomirsky. “Longitudinal magnons in large-S easy-axis magnets”. In: *Phys. Rev. B* 112 (2025), p. 174433. DOI: 10.1103/gy3k-c1w3.

[131] C. Kittel. *Quantum Theory of Solids*. New York: Wiley, 1987.

[132] J. Sheng et al. “Possible Observation of Quadrupole Waves in Spin Nematics”. In: *Phys. Rev. Lett.* 135 (15 Oct. 2025), p. 156704. DOI: 10.1103/pywx-vxfh.

[133] F. Wang et al. “New frontiers on van der Waals layered metal phosphorous trichalcogenides”. In: *Advanced Functional Materials* 28.37 (2018), p. 1802151. DOI: 10.1002/adfm.201802151.

[134] K. S. Burch, D. Mandrus, and J.-G. Park. “Magnetism in two-dimensional van der Waals materials”. In: *Nature* 563.7729 (2018), pp. 47–52. DOI: 10.1038/s41586-018-0631-z.

[135] P. Ferloni and M. Scagliotti. “Magnetic phase transitions in iron and nickel phosphorus trichalcogenides”. In: *Thermochim. Acta* 139 (1989), pp. 197–203. ISSN: 0040-6031. DOI: 10.1016/0040-6031(89)87022-4.

[136] A. R. Wildes et al. “The magnon dynamics and spin exchange parameters of $FePS_3$”. In: *J. Phys.: Condens. Matter* 24.41 (Sept. 2012), p. 416004. DOI: 10.1088/0953-8984/24/41/416004.

[137] D. Lançon et al. “Magnetic structure and magnon dynamics of the quasi-two-dimensional antiferromagnet $FePS_3$”. In: *Phys. Rev. B* 94 (2016), p. 214407. DOI: 10.1103/PhysRevB.94.214407.

[138] G. Le Flem et al. “Magnetic interactions in the layer compounds MPX_3 (M=Mn, Fe, Ni; X=S, Se)”. In: *J. Phys. Chem. Solids* 43 (1982), p. 455. DOI: 10.1016/0022-3697(82)90156-1.

[139] L. Chen et al. “Thermal evolution of spin excitations in honeycomb Ising antiferromagnetic $FePSe_3$”. In: *NPJ Quantum Mater.* 9 (2024), p. 40. DOI: 10.1038/s41535-024-00651-5.

[140] K. Damle and T. Senthil. “Spin Nematics and Magnetization Plateau Transition in Anisotropic Kagome Magnets”. In: *Phys. Rev. Lett.* 97.6 (2006), p. 067202. DOI: 10.1103/PhysRevLett.97.067202.

[141] K. Wierschem et al. "Magnetic and Nematic Orderings in Spin-1 Antiferromagnets with Single-Ion Anisotropy". In: *Phys. Rev. B* 86.20 (2012). (R), p. 201108. DOI: 10.1103/PhysRevB.86.201108.

[142] E. Rastelli and A. Tassi. "Normal modes in an anisotropic antiferromagnet". In: *Phys. Rev. B* 11 (11 June 1975), pp. 4711–4716. DOI: 10.1103/PhysRevB.11.4711.

[143] U. Balucani, V. Tognetti, and M. Pini. "Kinematic consistency in anisotropic ferromagnets". In: *J. Phys. C* 12.24 (1979), p. 5513. DOI: 10.1088/0022-3719/12/24/023.

[144] A. R. Wildes et al. "High field magnetization of $FePS_3$". In: *Phys. Rev. B* 101 (2 Jan. 2020), p. 024415. DOI: 10.1103/PhysRevB.101.024415.

[145] I. U. Heilmann et al. "One- and Two-Magnon Excitations in a One-Dimensional Antiferromagnet in a Magnetic Field". In: *Phys. Rev. B* 24.7 (1981), pp. 3939–3952. DOI: 10.1103/PhysRevB.24.3939.

[146] C. M. Canali and M. Wallin. "Spin-Spin Correlation Functions for the Square-Lattice Heisenberg Antiferromagnet at Zero Temperature". In: *Phys. Rev. B* 48.5 (1993), pp. 3264–3276. DOI: 10.1103/PhysRevB.48.3264.

[147] M. Mourigal, M. E. Zhitomirsky, and A. L. Chernyshev. "Field-Induced Decay Dynamics in Square-Lattice Antiferromagnets". In: *Phys. Rev. B* 82.14 (2010), p. 144402. DOI: 10.1103/PhysRevB.82.144402.

[148] E. Manousakis. "The Spin-1/2 Heisenberg Antiferromagnet on a Square Lattice and Its Application to the Cuprous Oxides". In: *Rev. Mod. Phys.* 63.1 (1991), pp. 1–62. DOI: 10.1103/RevModPhys.63.1.

[149] A. B. Harris. "Alternating Linear Heisenberg Antiferromagnet: The Exciton Limit". In: *Phys. Rev. B* 7.7 (1973), pp. 3166–3177. DOI: 10.1103/PhysRevB.7.3166.

[150] S. Sachdev and R. N. Bhatt. "Bond-Operator Representation of Quantum Spins: Mean-Field Theory of Frustrated Quantum Heisenberg Antiferromagnets". In: *Phys. Rev. B* 41.13 (1990), pp. 9323–9329. DOI: doi.org/10.1103/PhysRevB.41.9323.

[151] T. Sommer, M. Vojta, and K. W. Becker. "Magnetic Properties and Spin Waves of Bilayer Magnets in a Uniform Field". In: *The European Physical Journal B* 23.3 (2001), pp. 329–339. DOI: 10.1007/s100510170052.

[152] N. Papanicolaou and P. Spathis. "Quantum Spin-1 Chains with Strong Planar Anisotropy". In: *Journal of Physics: Condensed Matter* 2.31 (1990), pp. 6575–6588. DOI: 10.1088/0953-8984/2/31/011.

[153] Y. Kohama et al. "Thermal Transport and Strong Mass Renormalization in $NiCl_2$-$4SC(NH_2)_2$". In: *Phys. Rev. Lett.* 106.3 (2011), p. 037203. DOI: 10.1103/PhysRevLett.106.037203.

[154] J. Romhányi and K. Penc. "Multiboson Spin-Wave Theory for $Ba_2CoGe_2O_7$: A Spin-3/2 Easy-Plane Néel Antiferromagnet with Strong Single-Ion Anisotropy". In: *Phys. Rev. B* 86.17 (2012), p. 174428. DOI: 10.1103/PhysRevB.86.174428.

[155] T. A. Tóth et al. "Three-Sublattice Ordering of the SU(3) Heisenberg Model of Three-Flavor Fermions on the Square and Cubic Lattices". In: *Phys. Rev. Lett.* 105.26 (2010), p. 265301. DOI: 10.1103/PhysRevLett.105.265301.

[156] J. Hubbard. "Electron Correlations in Narrow Energy Bands IV. The Atomic Representation". In: *Proceedings of the Royal Society of London A* 285.1403 (1965), pp. 542–560. DOI: 10.1098/rspa.1965.0124.

[157] M. E. Zhitomirsky and A. L. Chernyshev. "Instability of Antiferromagnetic Magnons in Strong Fields". In: *Phys. Rev. Lett.* 82.22 (1999), pp. 4536–4539. DOI: 10.1103/PhysRevLett.82.4536.

[158] A. V. Chubukov. "On the Quantum Effects in Helimagnets". In: *J. Phys. C: Solid State Phys.* 17.35 (1984), pp. L991–L995. DOI: 10.1088/0022-3719/17/36/008.

[159] D. Dalidovich et al. "Spin Structure Factor of the Frustrated Quantum Magnet Cs_2CuCl_4". In: *Phys. Rev. B* 73.18 (2006), p. 184403. DOI: 10.1103/PhysRevB.73.184403.

[160] Z. Z. Du et al. "Spin Casimir Effect in Noncollinear Quantum Antiferromagnets: Torque Equilibrium Spin Wave Approach". In: *Phys. Rev. B* 92.21 (2015), p. 214409. DOI: 10.1103/PhysRevB.92.214409.

[161] M. E. Zhitomirsky and A. L. Chernyshev. "Colloquium: Spontaneous magnon decays". In: *Rev. Mod. Phys.* 85.1 (2013), pp. 219–258. DOI: 10.1103/RevModPhys.85.219.

[162] M. E. Zhitomirsky. "Decay of Quasiparticles in Quantum Spin Liquids". In: *Phys. Rev. B* 73.10 (2006). (R), p. 100404. DOI: 10.1103/PhysRevB.73.100404.

[163] R. P. Hodgson and J. B. Parkinson. "Bethe Ansatz for Two-Deviation States in Quantum Spin Chains of Arbitrary S with Anisotropic Heisenberg Exchange". In: *J. Phys. C: Solid State Phys.* 18.34 (1985), pp. 6385–6397. DOI: 10.1088/0022-3719/18/34/009.

[164] N. Papanicolaou and G. C. Psaltakis. "Bethe Ansatz for Two-Magnon Bound States in Anisotropic Magnetic Chains of Arbitrary Spin". In: *Phys. Rev. B* 35.1 (1987), pp. 342–351. DOI: 10.1103/PhysRevB.35.342.

[165] S. R. Varga. *Geršgorin and His Circles*. Berlin: Springer-Verlag, 2004. DOI: 10.1007/978-3-642-17798-9.

[166] A. L. Andrew. "Eigenvectors of certain matrices". In: *Linear Algebra Appl.* 7.2 (1973), pp. 151–162. DOI: 10.1016/0024-3795(73)90049-9.

[167] D. C. Mattis. *The Theory of Magnetism*. New York: Harper & Row, 1965.

[168] G. D. Mahan. *Many-Particle Physics*. New York: Kluwer Academic/Plenum Publishers, 2000. DOI: 10.1007/978-1-4757-5714-9.

[169] J. L. Manson et al. "Spatially Anisotropic $S = 1$ Square-Lattice Antiferromagnet with Single-Ion Anisotropy Realized in a Ni(II) Pyrazine-n,n'-Dioxide Coordination Polymer". In: *Phys. Rev. B* 108.9 (2023), p. 094425. DOI: 10.1103/PhysRevB.108.094425.

[170] A. Angeletti. "Antibound states for a class of one-dimensional Schrödinger operators". In: *Letters in Mathematical Physics* 4.6 (1980), pp. 495–504. DOI: 10.1007/BF00943436.

[171] C. Psaroudaki et al. "Magnetic excitations in the spin-1 anisotropic antiferromagnet $NiCl_2$-4SC$(NH_2)_2$". In: *Phys. Rev. B* 85 (1 Jan. 2012), p. 014412. DOI: 10.1103/PhysRevB.85.014412.

[172] M. Nayak and F. Mila. "Possibility to detect the bound state of the Heisenberg ferromagnetic chain at intermediate temperature". In: *Phys. Rev. B* 105 (9 Mar. 2022), p. 094407. DOI: 10.1103/PhysRevB.105.094407.

[173] Z. Wang et al. "Experimental observation of repulsively bound magnons". In: *Nature* 631.8022 (2024), pp. 760–764. DOI: 10.1038/s41586-024-07599-3.

[174] N. Papanicolaou, O. A., and O. M. "Electron-spin resonance in spin-1 planar magnetic chains". In: *Phys. Rev. B* 56 (14 Oct. 1997), pp. 8786–8798. DOI: 10.1103/PhysRevB.56.8786.

[175] T.-H. Jang et al. "Physical properties of the quasi-two-dimensional square lattice antiferromagnet $Ba_2FeSi_2O_7$". In: *Phys. Rev. B* 104 (21 Dec. 2021), p. 214434. DOI: 10.1103/PhysRevB.104.214434.

[176] A. Aharoni. *Introduction to the Theory of Ferromagnetism*. Oxford: Clarendon Press, 2001. DOI: 10.1093/oso/9780198508083.001.0001.

[177] W. Nolting and A. Ramakanth. *Quantum theory of Magnetism*. Springer Science & Business Media, 2009. DOI: 10.1007/978-3-540-85416-6.

[178] H. A. Brown and J. M. Luttinger. "Ferromagnetic and Antiferromagnetic Curie Temperatures". In: *Phys. Rev.* 100.2 (1955), p. 685. DOI: 10.1103/PhysRev.100.685.

[179] J. Oitmaa and W. Zheng. "Curie and Néel temperatures of quantum magnets". In: *J. Phys.: Condens. Matter* 16 (2004), p. 8653. DOI: 10.1088/0953-8984/16/47/016.

[180] T. Huberman et al. "A study of the quantum classical crossover in the spin dynamics of the 2D $S = 5/2$ antiferromagnet Rb_2MnF_4: Neutron scattering, computer simulations, and analytic theories". In: *J. Stat. Mech.* 2008 (2008), P05017. DOI: 10.1088/1742-5468/2008/05/P05017.

[181] D. C. Johnston et al. "Magnetic exchange interactions in $BaMn_2As_2$: A case study of the $J_1 - J_2 - J_c$ Heisenberg model". In: *Phys. Rev. B* 84 (2011), p. 094445. DOI: 10.1103/PhysRevB.84.094445.

[182] A. Lohmann, H.-J. Schmidt, and J. Richter. "Tenth-order high-temperature expansion for the susceptibility and the specific heat of spin-s Heisenberg models with arbitrary exchange patterns: Application to pyrochlore and kagome magnets". In: *Phys. Rev. B* 89 (1 Jan. 2014), p. 014415. DOI: 10.1103/PhysRevB.89.014415.

[183] D. Schubert et al. "Quantum versus classical dynamics in spin models: Chains, ladders, and square lattices". In: *Phys. Rev. B* 104 (2021), p. 054415. DOI: 10.1103/PhysRevB.104.054415.

[184] K. Remund et al. "Semi-classical simulation of spin-1 magnets". In: *Phys. Rev. Res.* 4 (2022), p. 033106. DOI: 10.1103/PhysRevResearch.4.033106.

[185] P. Park et al. "Quantum and classical spin dynamics across temperature scales in the $S = 1/2$ Heisenberg antiferromagnet". In: *Phys. Rev. Res.* 6 (2024), p. 033184. DOI: 10.1103/PhysRevResearch.6.033184.

[186] B. Schneider and B. Sbierski. "Taming Spin Susceptibilities in Frustrated Quantum Magnets: Mean-Field Form and Approximate Nature of the Quantum-to-Classical Correspondence". In: *Phys. Rev. Lett.* 134 (2025), p. 176502. DOI: 10.1103/PhysRevLett.134.176502.

[187] M. J. Klein and R. S. Smith. "A Note on the Classical Spin-Wave Theory of Heller and Kramers". In: *Phys. Rev.* 80 (6 Dec. 1950), pp. 1111–1111. DOI: 10.1103/PhysRev.80.1111.

[188] P. W. Anderson. "An Approximate Quantum Theory of the Antiferromagnetic Ground State". In: *Phys. Rev.* 86 (5 June 1952), pp. 694–701. DOI: 10.1103/PhysRev.86.694.

[189] A. Zee. *Group theory in a nutshell for physicists*. Princeton: Princeton University Press, 2016.

[190] G. S. Rushbrooke and P. J. Wood. "On the Curie points and high temperature susceptibilities of Heisenberg model ferromagnetics". In: *Mol. Phys.* 1.3 (1958), p. 257. DOI: 10.1080/00268975800100321.

[191] N. Elstner et al. "Spin Dependence of Correlations in Two-Dimensional Square-Lattice Quantum Heisenberg Antiferromagnets". In: *Phys. Rev. Lett.* 75 (1995), p. 938. DOI: 10.1103/PhysRevLett.75.938.

[192] L. Schulman. "A path integral for spin". In: *Phys. Rev.* 176.5 (1968), p. 1558. DOI: 10.1103/PhysRev.176.1558.

[193] H. Zhang and C. D. Batista. "Classical spin dynamics based on SU(N) coherent states". In: *Phys. Rev. B* 104 (10 Sept. 2021), p. 104409. DOI: 10.1103/PhysRevB.104.104409.

[194] L. Engelhardt, M. Luban, and C. Schröder. "Finite quantum Heisenberg spin models and their approach to the classical limit". In: *Phys. Rev. B* 74 (5 Aug. 2006), p. 054413. DOI: 10.1103/PhysRevB.74.054413.

[195] D. Dahlbom et al. "Quantum-to-classical crossover in generalized spin systems: Temperature-dependent spin dynamics of FeI_2". In: *Phys. Rev. B* 109 (2024), p. 014427. DOI: 10.1103/PhysRevB.109.014427.

[196] D. E. Knuth. "Johann Faulhaber and sums of powers". In: *Math. Comp.* 61.203 (1993), p. 277. DOI: 10.1090/S0025-5718-1993-1197512-7.

[197] J. F. Epperson. *An Introduction to Numerical Methods and Analysis*. New Jersey: John Wiley & Sons, 2013. DOI: 10.1002/9781119604686.

[198] J. Brillhart. "On the Euler and Bernoulli polynomials". In: *J. Reine Angew. Math.* 234 (1969), p. 45. DOI: 10.1515/crll.1969.234.45.

[199] T. L. Kitagawa. "The Origin of the Bernoulli Numbers: Mathematics in Basel and Edo in the Early Eighteenth Century". In: *The Mathematical Intelligencer* 44.1 (2022), pp. 46–56. DOI: 10.1007/s00283-021-10072-y.

[200] T. J. I. Bromwich. *An Introduction to The Theory of Infinite Series*. London: Macmillan and Company, 1947.

[201] A. F. Beardon. "Sums of Powers of Integers". In: *Am. Math. Mon.* 103.3 (1996), p. 201. DOI: 10.1080/00029890.1996.12004725.

[202] M. E. J. Newman and G. T. Barkema. *Monte Carlo methods in statistical physics*. Oxford: Clarendon Press, 1999. DOI: 10.1093/oso/9780198517962.001.0001.

[203] K. Binder. "Finite size scaling analysis of Ising model block distribution functions". In: *Z. Phys. B Condens. Matter* 43.2 (1981), pp. 119–140. DOI: 10.1007/BF01293604.

[204] K. Vollmayr et al. "Finite size effects at thermally-driven first order phase transitions: A phenomenological theory of the order parameter distribution". In: *Z. Phys. B Condens. Matter* 91.1 (1993), pp. 113–125. DOI: 10.1007/BF01316713.

[205] S. Jin, A. Sen, and A. W. Sandvik. "Ashkin-Teller Criticality and Pseudo-First-Order Behavior in a Frustrated Ising Model on the Square Lattice". In: *Phys. Rev. Lett.* 108 (4 Jan. 2012), p. 045702. DOI: 10.1103/PhysRevLett.108.045702.

[206] M. S. S. Challa, D. P. Landau, and K. Binder. "Finite-size effects at temperature-driven first-order transitions". In: *Phys. Rev. B* 34 (3 Aug. 1986), pp. 1841–1852. DOI: 10.1103/PhysRevB.34.1841.

[207] V. C. Morano et al. "Absence of altermagnetic magnon band splitting in MnF_2". In: *Phys. Rev. Lett.* 134 (2025), p. 226702. DOI: 10.1103/PhysRevLett.134.226702.

[208] M. Hagiwara et al. "Antiferromagnetic resonance in MnF_2 over wide ranges of frequency and magnetic field". In: *J. Phys.: Condens. Matter* 8 (1996), p. 7349. DOI: 10.1088/0953-8984/8/39/011.

[209] Z. Liu et al. "Chiral split magnon in altermagnetic MnTe". In: *Phys. Rev. Lett.* 133 (2024), p. 156702. DOI: 10.1103/PhysRevLett.133.156702.

[210] I. I. Mazin. "Altermagnetism in MnTe: Origin, predicted manifestations, and routes to detwinning". In: *Phys. Rev. B* 107 (2023), p. L100418. DOI: 10.1103/PhysRevB.107.L100418.

[211] J. Dzian et al. "Antiferromagnetic resonance in α-MnTe". In: *Phys. Rev. B* 112 (2025), p. 024433. DOI: 10.1103/bb6r-2nwz.

[212] J. Liao et al. "Spin and lattice dynamics in the van der Waals antiferromagnet $MnPSe_3$". In: *Phys. Rev. B* 109 (2024), p. 224411. DOI: 10.1103/PhysRevB.109.224411.

[213] R. J. Birgeneau, H. J. Guggenheim, and G. Shirane. "Neutron Scattering Investigation of Phase Transitions and Magnetic Correlations in the Two-Dimensional Antiferromagnets K_2NiF_4, Rb_2MnF_4, Rb_2FeF_4". In: *Phys. Rev. B* 1 (5 Mar. 1970), p. 2211. DOI: 10.1103/PhysRevB.1.2211.

[214] R. A. Cowley et al. "Spin fluctuations in random magnetic-nonmagnetic two-dimensional antiferromagnets. I. Dynamics". In: *Phys. Rev. B* 15 (9 May 1977), pp. 4292–4302. DOI: 10.1103/PhysRevB.15.4292.

[215] A. R. Wildes et al. "Spin wave spectra of single crystal $CoPS_3$". In: *Phys. Rev. B* 107 (2023), p. 054438. DOI: 10.1103/PhysRevB.107.054438.

[216] C. Kim et al. "Spin waves in the two-dimensional honeycomb lattice XXZ-type van der Waals antiferromagnet $CoPS_3$". In: *Phys. Rev. B* 102 (18 Nov. 2020), p. 184429. DOI: 10.1103/PhysRevB.102.184429.

[217] A. Scheie et al. "Spin Waves and Magnetic Exchange Hamiltonian in CrSBr". In: *Adv. Sci.* 9 (2022), p. 2202467. DOI: 10.1002/advs.202202467.

[218] C. W. Cho et al. "Microscopic parameters of the van der Waals CrSBr antiferromagnet from microwave absorption experiments". In: *Phys. Rev. B* 107 (2023), p. 094403. DOI: 10.1103/PhysRevB.107.094403.

[219] J. Strempfer et al. "Magnetic properties of transition metal fluorides MF_2 (M =Mn, Fe, Co, Ni) via high-energy photon diffraction". In: *Phys. Rev. B* 69 (2004), p. 014417. DOI: 10.1103/PhysRevB.69.014417.

[220] T. Komatsubara, M. Murakami, and E. Hirahara. "Magnetic properties of manganese telluride single crystals". In: *J. Phys. Soc. Jpn.* 18 (1963), p. 356. DOI: 10.1143/JPSJ.18.356.

[221] S. Calder et al. "Magnetic exchange interactions in the van der Waals layered antiferromagnet $MnPSe_3$". In: *Phys. Rev. B* 103 (2021), p. 024414. DOI: 10.1103/PhysRevB.103.024414.

[222] A. R. Wildes et al. "The magnetic properties and structure of the quasi-two-dimensional antiferromagnet $CoPS_3$". In: *J. Phys.: Condens. Matter* 29 (2017), p. 455801. DOI: 10.1088/1361-648X/aa8a43.

[223] O. Göser, W. Paul, and H. G. Kahle. "Magnetic properties of CrSBr". In: *J. Magn. Magn. Mat.* 92 (1990), p. 129. DOI: 10.1016/0304-8853(90)90689-N.

[224] BfS. *Spotlight on BfS 2025 Study: A Focus on Absolute Levels*. 2025. URL: www.carsradiation.org/info-sources/scholarly-sources/spotlight-bfs-2025-study-focus-absolute-levels/.

[225] S. J. Richmond et al. "Therapeutic effects of magnetic and copper bracelets in osteoarthritis: a randomised placebo-controlled crossover trial". In: *Complementary Therapies in Medicine* 17.5-6 (2009), pp. 249–256. DOI: 10.1016/j.ctim.2009.07.002.

[226] CERN. *Pulling together: Superconducting electromagnets*. URL: www.home.cern/science/engineering/pulling-together-superconducting-electromagnets.

[227] D. Chandler et al. "MIT-designed project achieves major advance toward fusion energy". In: *MIT News. Retrieved September* 3 (2021), p. 2023. URL: https://news.mit.edu/2021/MIT-CFS-major-advance-toward-fusion-energy-0908.

[228] D. Castelvecchi. "Superconducting magnet breaks strength world record." In: *Nature* (2019). DOI: 10.1038/d41586-019-01869-1.

[229] LNCMI-T. *New European record for non-destructive pulsed magnetic fields*. 2017. URL: https://www.lncmi.cnrs.fr/en/news/new-european-record-for-non-destructive-pulsed-magnetic-fields/.

[230] A. Farag et al. "Electromagnetic fields in the home". In: *Electric power systems research* 45.2 (1998), pp. 73–89. DOI: 10.1016/S0378-7796(97)01224-8.

[231] W. Zheng et al. "Linked cluster series expansions for two-particle bound states". In: *Phys. Rev. B* 63 (14 Mar. 2001), p. 144410. DOI: 10.1103/PhysRevB.63.144410.